

Life Extension of High Temperature Structural Alloys by Surface Engineering in Gas and Vacuum Carburizing Atmospheres

by

Anbo Wang

WORCESTER POLYTECHNIC INSTITUTE

in partial fulfillment of the requirements for the degree of

Degree of Doctor of Philosophy

in

Materials Science and Engineering

June, 2017

APPROVED:

Richard D. Sisson Jr. Advisor
George F. Fuller Professor, Mechanical Engineering
Director, Manufacturing and Materials Engineering, Worcester Polytechnic Institute

Abstract

The heat-treating industry is in need of heat-treatment furnace materials and fixtures that have a long service life and reduced heat capacity. Based on microstructural analysis of components that were used until failure in carburization furnace application, it was found that the primary reason for failure was the excessive carburization that leads to “metal dusting” and subsequent cracking. Aluminizing is widely used to increase the high temperature oxidation and carburization resistance of nickel-based alloys. In this dissertation, RA330, RA602CA, 304L/316L, Inconel 625 alloys were selected to study their performance in an industrial carburization furnace for times up to two years. These alloys were exposed in both the as-fabricated and aluminized condition. The test samples were exposed to $C_p=0.7-1.3\%$ carburizing atmosphere at approximately 900°C for 3 months, 6months, 12months, 18 months and 24months. The oxidation properties and oxide stability at high temperatures will be presented. In addition, the analysis of microstructural development during long term exposure experiments in an industrial carburizing furnace will be presented. These samples were characterized using optical and scanning electron microscope, EBSD, and x-ray diffraction. It was found that the aluminized alloys exhibited lower weight gain and carbon uptakes.

Table of Contents

Contents

Abstract.....	1
Table of Contents	1
Introduction.....	6
1. Introduction.....	6
1.1. The need of industry	6
1.2. Project goal	6
Literature Review	7
2. Literature review	7
2.1. Literature review outline	7
2.2. Metal dusting	7

2.2.1.	Metal dusting mechanisms.....	7
2.2.2.	Carburization of furnace alloys.....	9
2.2.4.	Metal dusting on iron and low alloy steels	12
2.2.5.	Metal dusting of nickel and Ni-based alloys.....	14
2.3.	Aluminizing diffusion treatment	17
Experimental Plan		18
3.	Selected alloys.....	18
3.1.	First exposure experiments.....	20
3.2.	Second exposure experiments	22
Experimental Procedure		25
4.1.	Surface finishing.....	25
4.2.	Aluminizing.....	26
4.3.	Pre-oxidization.....	27
4.4.	Weight gain measurement	28
4.5.	Exposure experiments.....	28
4.6.	Cyclic oxidations	28
4.7.	X-ray Diffraction (XRD).....	29
4.8.	OES.....	29
4.9.	Micro hardness profile.....	29
4.10.	Electron backscatter diffraction (EBSD) analysis	29
4.11.	Optical photomicrographs.....	30
4.12.	SEM photomicrographs	30
Experimental Results.....		31
5.1. Microstructure and Failure Analysis of Austenitic Fe-Ni alloys and Ni-Cr-Fe alloys for Furnace Alloys and Fixtures		31

5.1.1. Isopleth simulation of carburizing process.....	31
5.1.2. Failed Fan Blade from Bluewater (gas carburization furnace).....	32
5.1.3. Failure mode analysis of furnace part or fixture (Vacuum carburization furnace)	42
Broken racking pole.....	42
5.1.3.1. Characterization of pole	43
5.1.3.2. OES (Optical Emission Spectroscopy) analysis.....	43
5.1.3.3. Optical micrographs	46
5.1.3.4. Vickers micro-hardness profile	51
5.1.3.5. SEM (Scanning Electron Microscope) and EDS (Electron Dispersion X-ray Spectroscopy) analysis	52
5.1.3.6. XRD (X-ray Diffraction) analysis.....	56
5.1.3.7. Phase evolution prediction from computational thermodynamics	56
5.1.3.8. Discussion	58
5.1.4. Failure analysis of failed mesh belt (Gas carburization furnace)	58
5.1.4.1. New and failed mesh belts from GKN	59
5.2. Life Extension of Furnace and Fixture Alloys by aluminizing in Vacuum Carburizing Atmospheres	65
5.2.1. Aluminizing.....	65
5.2.2. Racking poles from Sikorsky	65
5.2.2.1. Characterization of as-received racking pole	67
5.2.3.1. Characterization of exposed racking poles.....	70
5.2.3.1.1. Racking poles- Unaluminized	70
5.2.3.1.1.1. Preliminary metallographical analysis.....	72
5.2.3.1.1.2. Cross section and surface analysis.....	72
5.2.3.1.2. Racking poles – Aluminized.....	78

5.2.3.1.2.1. Preliminary metallographical analysis.....	78
5.2.3.1.3. Characterization of Flake Offs	90
5.2.3.1.3.1. Flake offs from unaluminized RA330 racking poles.....	90
5.2.3.1.3.2. Flake offs from aluminized RA330 racking poles.....	93
5.2.3.1.3.2.1. Outside surface morphology of aluminized flake offs	93
5.2.3.1.3.2.2. Inside surface morphology of aluminized flake offs	95
Racking poles exposed for 3 years	97
Conclusion.....	100
5.3. Life Extension of Furnace and Fixture Alloys by aluminizing in Gas Carburizing Atmospheres	101
5.3.1. Commercial furnace testing for first exposure experiments.....	101
5.3.1.1. Samples exposed for 3 months in gas carburization furnace.....	102
5.3.1.2. Samples exposed for 12 months in gas carburization furnace.....	103
5.3.1.3. Samples exposed for 18 months in gas carburization furnace.....	105
5.3.1.4. Samples exposed for 24 months in gas carburization furnace.....	106
5.3.2. Commercial furnace testing for second exposure experiments	110
5.3.2.1. Weight gain measurement	110
5.3.2.2. Comparison between two exposure experiments	111
References	112
5.4. The Performance of RA330 and Aluminized RA330 in an Industrial Gas Carburizing Furnace.....	116
Abstract.....	116
Introduction	116
Material and methods	117
Results and Discussion	118

Cyclic Oxidation.....	134
Weight gain measurement	139
Conclusions	140
Acknowledgements	140
References	141
5.5. Pre-oxidation treatment.....	142
References	146
5.6. Life Extension of High Temperature Structural Alloys RA602CA in Gas Carburizing Atmosphere.....	147
Abstract.....	147
Introduction	147
Materials and methods.....	148
Exposure experiment.....	149
Experiment result.....	151
Conclusion.....	178
Acknowledgements	179
References	179
6. Conclusion	180
7. Future work.....	182
8. Relevant presentations and publications	183
8.1. Publications	183
8.2. Presentation	183
8.3. List of future publications.....	184

Introduction

1. Introduction

In this dissertation, RA330, RA602CA, 304, 316, Inconel 625 alloys were selected to evaluate their performance in industrial carburizing furnaces for times up to two years. The microstructural development of alloys during the prolonged exposure in the carburizing environment will be presented and discussed.

1.1. The need of industry

According to IHEA, the sheer volume of the heat treating industry is in the range of \$65 to \$75 billion-with the sale of heat treatment equipment alone being between \$4.375 and \$5.5 billion. Any improvement of technology would have big impact on the industry. High temperature structural alloys were widely used in many applications such as aerospace turbine blades, high temperature anti-corrosion applications, and fixture inside the high temperature furnace that are supporting the products. Many of the fixtures are consumed within 1 year of exposure in high temperature carburization atmospheres. Many of these fixtures are manufactured using heat resistant alloys. Iron-nickel based and Iron-Nickel-Chromium based alloys are experiencing a variety of degradation mechanisms. The corrosion products are mainly graphite, chromium carbide, metal, and oxide particles. For iron-based alloys, the primary reason for failure was the excessive carburization that leads to “metal dusting” and subsequent cracking. In addition, metallographic analysis indicated that “flake offs” of Fe-Cr-Ni alloys were mainly graphite and chromium carbides.

Therefore, the industry was in need of alloys that have long service life. The fixtures need to have low carbon uptakes during the exposure in carburization furnaces.

1.2. Project goal

Extension of the service life for high temperature structural alloys is the goal for this project. In this research, failure modes of alloys in gas and vacuum carburization furnace were investigated. Aluminizing and pre-oxidation treatment were also studied in this project. Aluminizing is a coating that widely used in aerospace industry, especially in turbine blade applications. It is also known that carbon has very low solubility in alumina. In that case, aluminizing could be a good method for protecting high temperature structural alloys. Therefore, microstructural development during the carburizing process will be presented. And also the degradation of chromium oxide as well as alumina oxides will be identified. The weight gain of each alloys, coating, and surface treatments were measured to determine anti-corrosion properties of high temperature structural alloys.

Literature Review

2. Literature review

2.1. Literature review outline

- ❖ Metal dusting
- ❖ Metal dusting mechanism
- ❖ Carburizing of furnace alloys
- ❖ Conversion of chromium oxide in carbides
- ❖ Metal dusting of low alloy steel
- ❖ Metal dusting of Nickel and Nickel based alloys
- ❖ Aluminizing
- ❖ Pre-oxidation treatment

2.2. Metal dusting

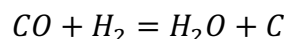
“Metal dusting (MD)” is a severe corrosion phenomenon occurring at intermediate temperatures about 400 to 900°C in strongly carburizing atmospheres at high carbon activities of $a_c > 1$ and at low oxygen pressures [1]. Heat resistance alloys were commonly used in gas carburization furnace. Iron-, nickel-, and cobalt-base alloys are susceptible; the attack leads to disintegration into fine metal particles and carbon. Flowing gas atmospheres can easily remove the loose corrosion products, this erosion leaves pits in case of local attack.

Metal dusting (MD) occurs in carburizing atmospheres, this type of corrosion is possible at any temperature [3]. The consequence of metal dusting can be a severe loss of metal from the process units, leading to high-cost maintenance and serious safety issues. Many failures have been reported by industry that MD cause expensive replacement of fixture parts, including racking poles, mash belt, fan blade and etc. Some catastrophic failures involved the disintegration of the fixtures due to metal dusting, leading to the breakdown of the furnace. Other failure, although less catastrophic but also caused a severe loss of materials, which required many repairs and replacements of various parts of the units [4].

2.2.1. Metal dusting mechanisms

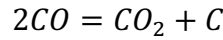
Metal dusting is caused by the tendency to graphite formation, the Gibbs free energy for the process is $\Delta G = -RT \ln a_c$

Which is zero in equilibrium with graphite ($a_c = 1$). The main reactions for carbon transfer from the atmosphere are CO-reduction:



$$(a_c)_1 = K_1 \frac{p_{CO} \cdot p_{H_2}}{p_{H_2O}} \log K_1$$

Boudouard reaction:



$$(a_c)_2 = K_1 \frac{(p_{CO})^2}{p_{CO_2}} \log K_2$$

Where K_1 and K_2 is the equilibrium constant of the corresponding reaction and P_i is the partial pressure of the corresponding gas. When a_c is greater than unity, carbon has a potential to form via the corresponding reaction, although the extent of carbon formation may be limited by the kinetics of the process. When a_c is smaller than unity, thermodynamics state that graphite should not form. It is noted from the above equations that a_c is a function of the temperature and the partial pressure of the gases involved [4].

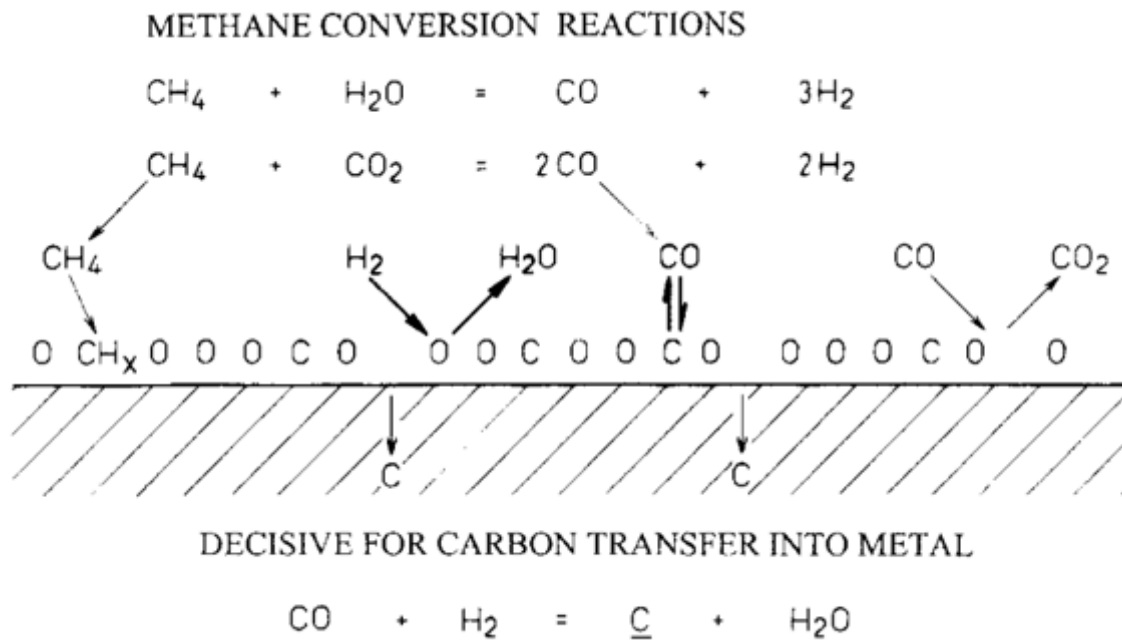
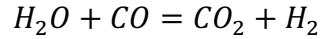
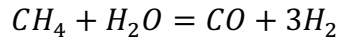


Figure 1. Schematic representation of the partial surface reactions in carburization and metal dusting in a $H_2 - CO - H_2O$ gas mixture [2].

In fact, these reactions take place on catalytically active surfaces at the temperatures of interest 400-900°C and a steady state activity of atomic oxygen is established, by reaction steps of water-gas-shift reaction.



This is generally not at equilibrium in the process. Another reaction to be considered is the oxidation of methane.



By which the synthesis and reduction gas is produced. This reaction needs catalytic acceleration and is performed generally on Ni-catalysts at temperatures $> 700^\circ\text{C}$. Its back reaction, the methanation of CO may occur when metal dusting has produced fine metal particles, catalyzing the methane already at rather low temperatures. The methane formation can indicate the occurrence of metal dusting.

2.2.2. Carburization of furnace alloys

There are two main mechanisms of high temperature corrosion caused by carbon transfer into metals and alloys: carburization and metal dusting. Internal carbides were formed during carburizing, which usually occurred at $T > 900^\circ\text{C}$. Upon carburization, the carbon activity in the metal phase stays to be $a_c < 1$, whereas metal dusting is caused by certain activities $a_c > 1$ in the atmosphere and in the metal phase. In this case, a strong tendency of graphite formation ($a_c = 1$) and in fact this leads to metal disintegration, either via intermediate formation of unstable carbides as in the case of iron and low alloy steels or by direct inward growth of graphite as in the case of Ni and Co based alloys. After carburization of high temperature alloys, the carbon activities in equilibrium with the carbides of Cr, Ti, Fe etc. would be very low. [4]

Carburization is observed in industrial processes where Fe-Ni-Cr alloys are applied in carbonaceous atmospheres at high temperature, especially in the steam cracking off hydrocarbons for ethylene production. Carbon is transferred from the atmosphere into the metal matrix, diffuses inward and causes precipitation of the carbides $M_{23}C_6$ and M_7C_3 (M=Cr, Ni, Fe). After more carbon diffuses into the matrix $M_{23}C_6$ was converted to M_7C_3 so that two zones with different precipitates are moving inward. [7] The carburization deteriorates the ductility and toughness of the materials, especially the low temperature properties; additionally stresses are generated due to the volume increase by carbide formation [7]. Due to the carburization, cracks are formed in the inner wall of cracking tubes, see Figure 2. Accordingly, the failure mainly occurred during the cooldown of furnace. In general, the effects on the high temperature properties are less dangerous, the tensile and creep strength are improved and the ductility does not decrease markedly. In most atmosphere of carburization furnace, the oxygen potential are large enough to fully oxidized so that the alloys are well protected against carburization by and oxide layer which serves as a barrier against carbon ingress.

The common alloys for carburization furnace is HK40, HP40, HP40Mod, Inconel 625, Alloy800 and RA330 etc. with 17-25% Cr and 20-35%Ni at high temperatures form an outer spinel layer $(Fe,Mn)Cr_2O_4$ and an inner Cr_2O_3 layer. The carbon permeation through grown Cr_2O_3 layers is extremely slow because the solubility of C in such oxides is almost zero. The permeation occurs by diffusion of carbon-bearing molecules, through pores, channels of cracks of the oxide layer, thus carburization is negligible in the temperature range 800-1000°C, if an adherent, continuous oxide scale had formed on the alloy.

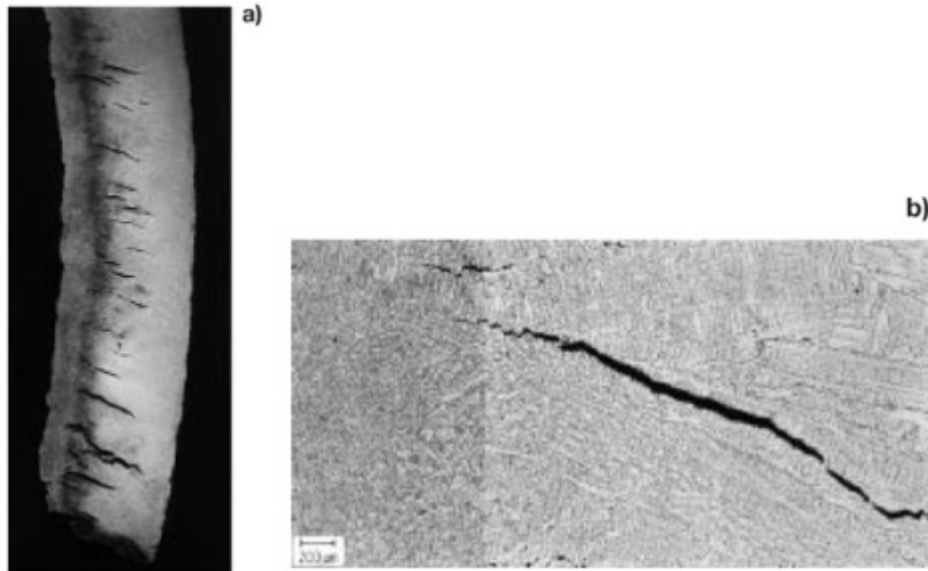


Figure 2, Carburization- section of a carburized tube from an ethylene plant; a) photo of wall section, b) internal carbide and crack formation in the inner wall [2]

2.2.3. Conversion of the chromium oxide in carbides

During the long term exposure, there are some possibilities of oxide scale failure; most frequent and momentous is the conversion of the chromium oxide in carbides. Chromia will convert to carbides at temperatures $>1050^{\circ}C$ [8]. The atmosphere in the porous carbon deposit at the oxide surface will have the carbon activity $a_c = 1$ (equilibrium with graphite) and its oxygen activity will decrease with increasing T [8]. At $>1050^{\circ}C$ the oxygen activity is so low that the equilibria of Cr_2O_3 and Cr_7C_3 or Cr_3C_2 are shifted to the stability of carbides and the conversion will start.

Cracking tubes are endangered especially during decoking, by the exothermic burning of the carbon layer with water-air mixtures. Decoking needs to be controlled at $T < 1050^{\circ}C$. On alloys with sufficient Si content $>1.7\%$ Si a sublayer of SiO_2 may be formed beneath the Cr_2O_3 .

For Ni-Cr-steels with low Si- and Al-content, the carburization at high temperatures $>1050^{\circ}\text{C}$ is not hindered by any oxide layer and its rate is just determined by the inward diffusion of carbon. The progress of internal carbide formation can be described by an equation which corresponds to the equation for internal oxidation.

$$x^2 = \frac{\varepsilon \cdot D_c \cdot c_c}{v \cdot c_M} t$$

Where D_c is the diffusivity and c_c the solubility of carbon in the metal matrix, ε is the labyrinth factor, v the stoichiometric factor for the carbide MC and c_M is the concentration of the metals involved in carbide formation [10]. The kinetic equation can describe carburization only approximately, since the variations of carbide phases and compositions and of carbon diffusivity with time and carbon activity have been neglected, however, it clearly demonstrates the main influences.

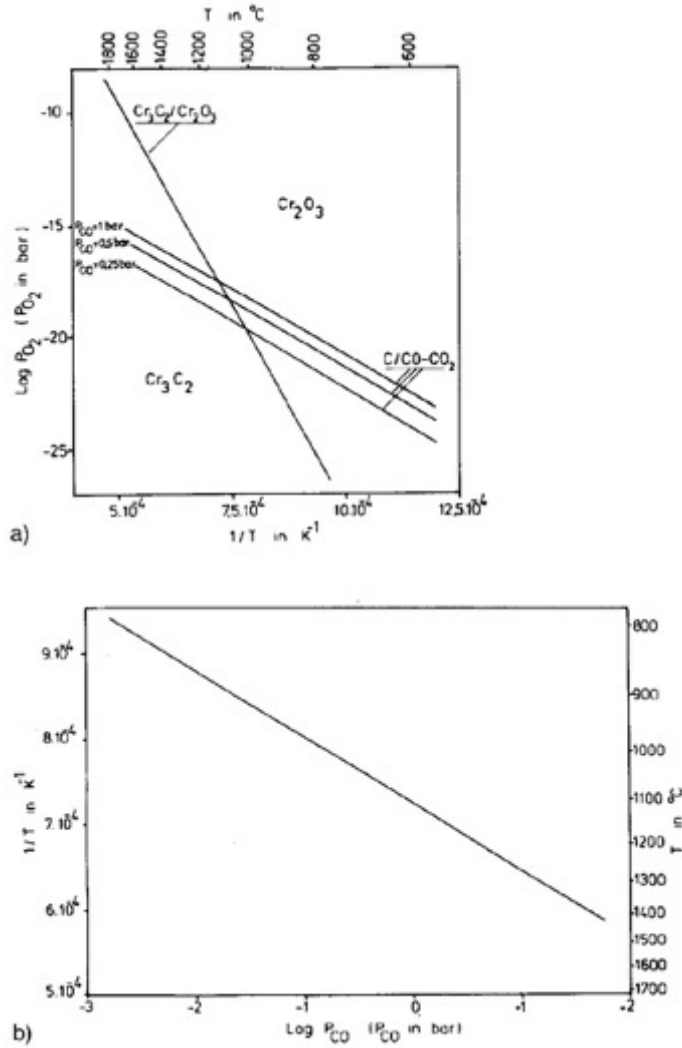


Figure 3. Thermodynamics of the conversion chromium oxide to carbide, i.e. a) equilibrium Cr_2O_3/Cr_3C_2 and Boudouard-equilibrium $C - CO_2 - CO$ at three different CO -pressures, b) influence of CO pressure on the temperature of the $Cr_2O_3 - Cr_3C_2 - C$ equilibrium [9].

2.2.4. Metal dusting on iron and low alloy steels

A mechanism was proven by thermodynamic studies, optical and electron microscopy on metallographic cross sections and high-resolution transmission microscopy. At 400 to 650°C in a $H_2 - CO - H_2O$ mixture the following reaction sequence occurs on iron and low alloy steels:

- 1) Carbon diffuse into solid solution, until oversaturation, concerning equilibrium with graphite ($a_c = 1$) and cementite a_c somewhat higher than one

- 2) Cementite nucleates and grows, mainly at the surface but also at grain boundaries. A rather irregular layer of cementite crystals grows with characteristic protrusions into the bulk metal phase. Because of very low carbon diffusivity in cementite it's a barrier against further carbon ingress, therefore the carbon activity at the surface rises and locally.
- 3) Graphite nucleates. When the carbon activity $a_c = 1$ the cementite becomes unstable.
- 4) Cementite decomposes to graphite and iron, according to $Fe_3C = 3Fe + C$, in fact by growth of graphite into the cementite. Carbon atoms from Fe_3C attach to graphite planes, growing more or less vertically into the cementite.

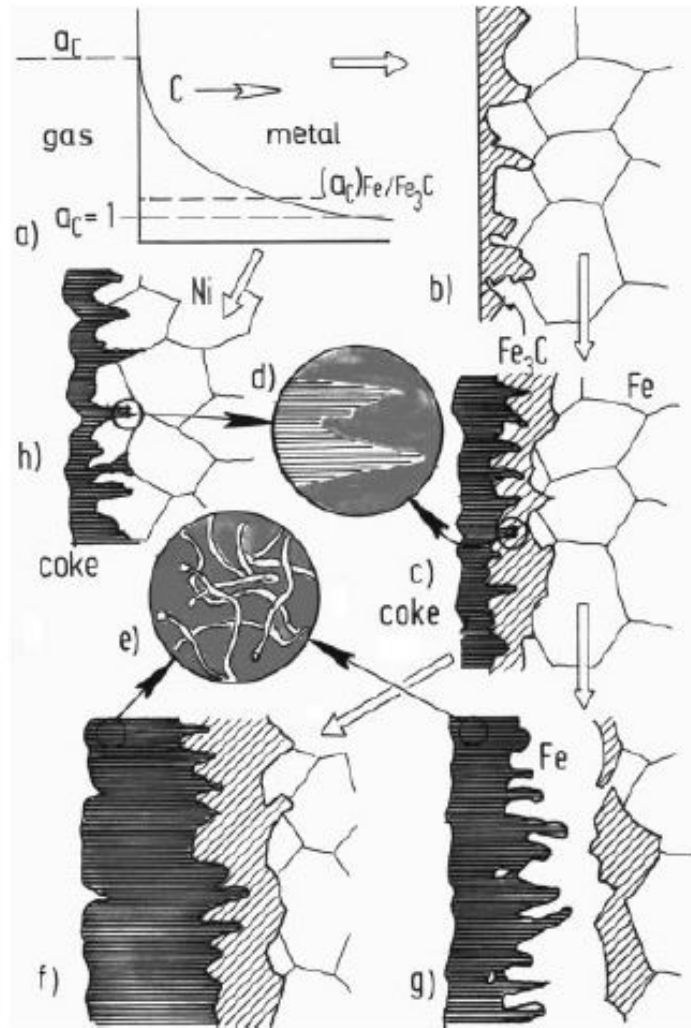


Figure 4. Schematic illustration of the processes in metal dusting of iron, low alloy steels and Ni, a) carbon transfer from the gas phase and over saturation of the metal phase, b) Nucleation and growth of cementite, Fe_3C at the surface of Fe and low alloy steels, c) Nucleation and growth of graphite into the Fe_3C , by d) C atoms attaching to the lattice planes of graphite, growing more or less perpendicular into Fe_3C , resp. Ni and high Ni-alloys, e) carbon filaments grown behind

particles detached from the metal phase by the graphite growth, f) steady state of metal dusting on Fe and low alloys steels at temperatures < 600°C, inward growth of Fe₃C which disintegrates outward under coke formation, g) Steady state of metal dusting of Fe and low alloy steels at temperatures > 700°C, formation of an iron layer between Fe₃C and coke, carbon diffusion through this layer and final disappearance of Fe₃C [9]

At higher temperature over 700°C, the morphology of the reaction products changes. The iron from the Fe₃C decomposition does not form fine particles but agglomerates to an iron layer through which the carbon must diffuse, to attach to the outer graphite layer [2]. In this case, the decomposition slowed down and metal dusting becomes controlled by carbon diffusion in ferrite, or at higher temperature in austenite. In the system: outer graphite layer, metal layer, cementite layer, metal phase, the phase boundary graphite/metal is instable, since the diffusion control causes that graphite intrusions into the metal layer grow faster, until that layer is disrupted and perturbed.

For higher temperatures, 900 and 1000°C in CH₄ – H₂ mixtures at $a_c > 1$ no cementite formation occurred, but from the oversaturated metal phase, carbon diffuses through an austenite layer to the graphite growing on the surface. Again the strong growth of graphite protrusions indicates carbon diffusion control and instable phase boundaries. After longer duration also metal disintegration is to be expected which means that metal dusting occurs also at 1000°C, but not via cementite formation.

2.2.5. Metal dusting of nickel and Ni-based alloys

The failure of nickel based alloys usually occurred above 900°C. Alloys were destroyed by direct inward growth of graphite into the oversaturated solid solution, as shown in

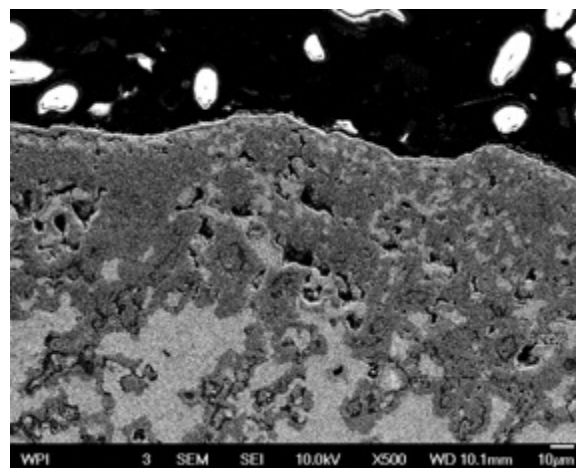


Figure 5. SEM photomicrographs at the edge of exposed RA330

The roots and filaments of graphite growing into the metal phase, separate particles from the material which are considerably bigger than in the mechanism via cementite. Therefore, the catalytic surface area generated is less and coke formation is minor compared to iron and steels [5] [6]. The mechanism of metal dusting for Ni-based alloys, $(Ni, Fe)_3C$ should be formed as an intermediate. This would need increasing carbon activities with increasing Ni-content, but actually metal dusting starts for any Ni-Fe alloy at a carbon activity $a_c > 1$.

However, the mechanism for Ni-Fe alloys with more than 40% Ni, on which no M_3C was found after metal dusting exposures. The alloys with a higher Ni content are destroyed by the mechanism valid for pure Ni which is the direct ingress of graphite. Changing the mechanism caused a decrease of carbon dissolved and deposited on the alloys and an increase of the metal content in the coke with the Ni-content in the alloys. The larger metal particles, released by metal dusting from Ni-base alloys are less catalytically active for carbon deposition than the fine particles from metal dusting of steels. In this case, the resistance of Ni is better than Fe, since the mechanism is different and much slower, coke formation is considerably less, carbon solubility and diffusivity are lower.

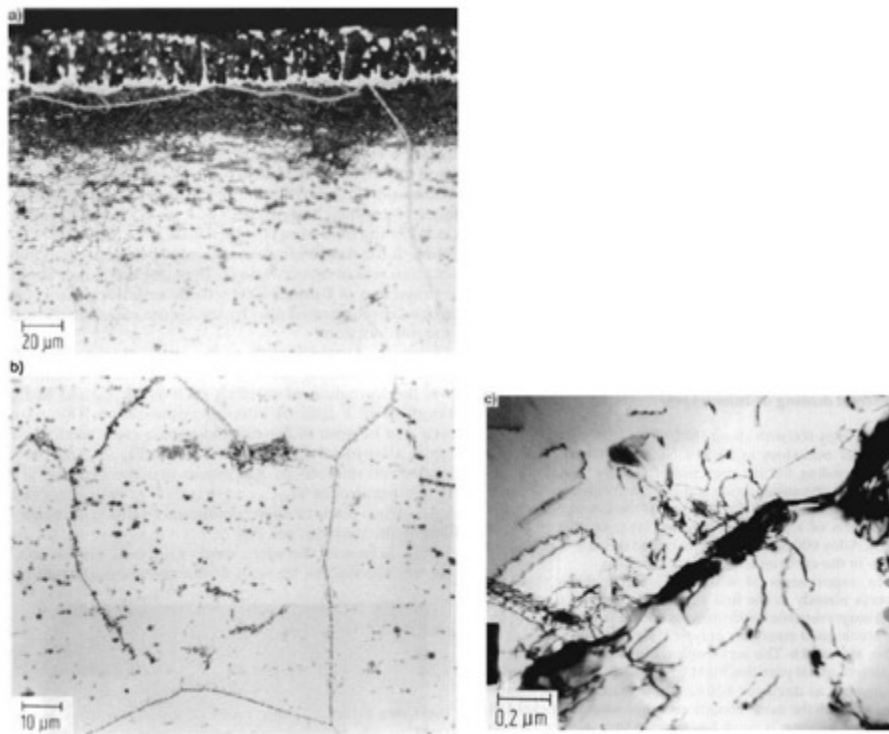


Figure 6. Metallographic cross sections of Inconel 600 after metal dusting attack for 21d at 650°C, a) Optical micrograph showing coke deposit, Cr-depleted zone(white layer) and internal carbide formation; b) internal carbides $M_{23}C_6$ and dislocations created by the internal carbide formation, also shown in c) transmission electron micrograph. [36]

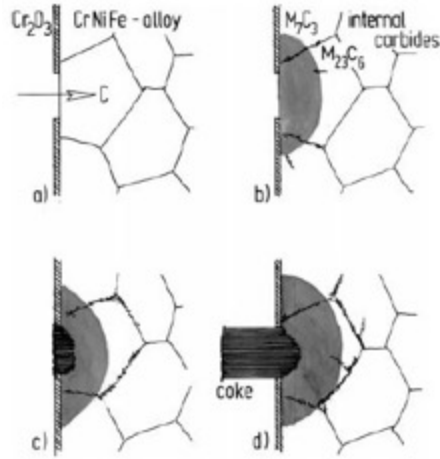


Figure 7. Schematic illustration of processes in metal dusting of chromia-forming high alloy steels and Ni base alloys, a) defect in the scale, allowing carbon ingress, b) internal carbides formation, inward moving zones with $M_{23}C_6$ and M_7C_3 , c) after oversaturation with C graphite nucleation and inward growth, d) outward growth of coke-protrusion, composed of graphite carbon filaments, metal, carbide and oxide particles. [2]

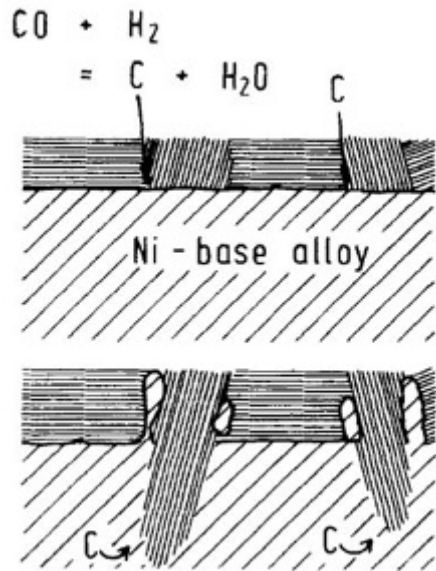


Figure 8. Schematic presentation of the metal dusting mechanism for high nickel alloys [2]

For most resistant alloys Alloy 600, Alloy 601, Alloy 625, Alloy 602CA and Alloy 690, the formation of protective scale is strongly favored, compared to initiation of metal dusting, and in fact, after the exposures the metallographic cross sections generally showed thin oxide scales [11].

2.3. Aluminizing diffusion treatment

Aluminizing has been widely used in aerospace industry for decades and is well known as one of the best coating because of its excellent anti-corrosion properties. Aluminizing is aluminum metal diffuses into the alloy to increase the aluminum concentration at the part-surface. Typically, β – $NiAl$ is formed. When the aluminized alloy is exposed to an oxidizing environmental high temperature environment, Al_2O_3 forms at the surface. This oxidation product is dense with low diffusivity and act to protect the alloy from oxidation. In addition, the Al_2O_3 oxidation products also produce an excellent barrier to carbon absorption (i.e. carburization). Alumina was carried out at 1000°C to produce NiAl intermetallic compound, which acts as a reservoir of aluminum during high-temperature oxidation so that a protective layer of alumina is maintained on the surface of the component [12]. The alumina provides good anti-corrosion properties because of its low solubility of carbon.

2.4. Pre-oxidation treatment

High temperature structural alloys suffered from two main high temperature corrosion processes, Oxidation and carburization. High temperature corrosion resistance is provided by the presence of stable, fine, dense and adhering protective oxides. The oxides which provide the best level of protection are alumina Al_2O_3 , silica SiO_2 and chromium oxide Cr_2O_3 [13].

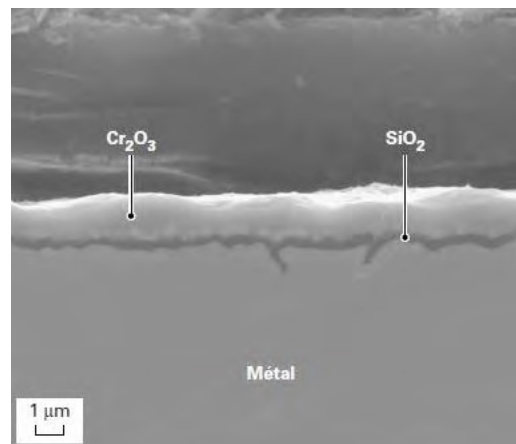


Figure 9. Protective oxide layer formed at 900°C on a ferritic stainless steel with 17%Cr and 0.5%Si content [14]

Experimental Plan

3. Selected alloys

RA330 is well known as the corrosion-resistant alloy offering an exceptional combination of strength and resistance to carburization, oxidation and thermal shock. RA330 finds wide application in high temperature industrial environments where good resistance to the combined effects of carburization and thermal cycling is prime requisite.^[15]

wt%	Cr	Ni	Mn	Si	Cu	P	S	C	Fe
MIN	18.0	34.0	-	1.0	-	-	-	0.04	-
MAX	20.0	37.0	2.0	1.5	1.0	0.03	0.03	0.08	Balance

Table 1. Chemical composition of RA330®, Supplier: Rolled Alloys

APMT is a powder metallurgical, dispersion strengthened, ferritic iron-chromium-aluminum alloy for use at tube temperatures up to 1250°C (2280°F). APMT tubes have good form stability at high temperature. APMT forms a non-scaling surface oxide (α – alumina Al_2O_3), which is thermodynamically stable and gives good protection in most furnace environments, as well as against deposits of carbon, ash, etc.^[16] Similarly, aluminizing also produce a α – alumina Al_2O_3 layer at the surface of alloys. Therefore, APMT were added as new alloy for life-time test.

wt%	Cr	Al	Si	Mo	Mn	C	Fe	Minor additions
MIN	22	5.0	-	-	-	-	-	present
MAX	22	5.0	0.7	3.0	0.4	0.05	Balance	present

Table 2. Chemical composition of KANTHAL APMT®, Supplier: Sandvik

RA 253MA is a lean austenitic heat resistant alloy with high strength and outstanding oxidation resistance. RA 253 MA control micro-alloying additions to get excellent anti-corrosion and heat resistant properties.^[17] The silicon could improve the oxidation resistance to 2000°F. Nitrogen, carbon and to some extent, rare earth and alkali metal oxides, combine to provide creep rupture strength superior to other heat resistant stainless steels.

	Cr	Ni	Mn	Si	C	N	Ce	Fe
MIN	20.0	10.0	-	1.4	0.05	0.14	0.03	-
MAX	22.0	12.0	0.8	2.0	0.1	0.2	0.08	balance

Table 3. Chemical composition of RA253MA®, Supplier: Rolled Alloys

Stainless steel 316 contains molybdenum for improved chloride pitting and general corrosion resistance. Stainless steel 304 is the original “18-8” stainless steel. Stainless steel 316 and 304 have lower price compare to Fe-Ni-Cr base alloys. These stainless steels were chosen because the performance of aluminized 316SS and 304SS were going to compare with the unaluminized super alloys such as RA330, RA253MA, APMT and so on.

	Cr	Ni	Mo	Si	C	Mn	N	Fe
MIN	16	10.0	2.0	-	-	-	-	-
MAX	18	14.0	3.0	0.75	0.08	2.0	0.1	balance

Table 4. Chemical composition of 316SS, Supplier: Peterson Steel Co.

RA 602CA is one of the most oxidation resistant high strength nickel heat resistant alloys available. High chromium, aluminum, and an yttrium addition permit it to develop a tight chromium oxide scale with an alumina subscale. RA 602CA may be considered where it is important to minimize product contamination at extreme temperatures. A nominal 0.2% carbon content contributes to high creep rupture strength. Micro-alloying with zirconium minimizes grain growth upon exposure to temperatures above 1800°F. Table 5 shows the chemical composition of RA 602CA. The density of RA 602CA is 0.285 lb/in^3 , and it melts in the temperature range from 2350 to 2550°F. The oxidation resistance is up to 2200°F.

	Cr	Ni	Cu	P	S	Fe	C	Al	Ti	Y	Zr	Si	Mn
Min (wt.%)	24	-	-	-	-	8	0.15	1.8	0.1	0.05	0.01	-	-
Max (wt.%)	26	Bal.	0.1	0.02	0.01	11	0.25	2.4	0.2	0.12	0.1	0.5	0.15

Table 5. Chemical composition of RA 602 CA® [18]

INCONEL alloy 625 is a nickel-chromium based alloy. It is used for its excellent corrosion resistance, outstanding fabricability and high strength. Strength of alloy 625 is derived from the stiffening effect of molybdenum and niobium on its nickel-chromium matrix; thus precipitation-hardening treatments are not required. High tensile, creep and rupture strength; outstanding fatigue and thermal-fatigue strength; oxidation resistance; and excellent weldability and brazeability are the properties of INCONEL alloy 625 that make it interesting to the heat treatment field.

Table 6 shows the chemical composition of INCONEL alloy 625. The density of INCONEL alloy 625 is 0.305 lb/in^3 , and it melts in the temperature range from 2250 to 2460°F. The oxidation resistance is up to 2200°F. [19]

	Ni	Cr	Fe	Al	C	Mg	Nb	Mo	Co	Si
Min (wt.%)	58.0	20.0	-	-	-	-	3.15	8.0	-	-
Max (wt.%)	-	23.0	5.0	0.4	0.1	0.5	4.15	10.0	1.0	0.5

Table 6. Chemical composition of INCONEL alloy 625

3.1. First exposure experiments

Three alloys are selected for the alloy lifetime tests, including RA 602CA, RA 330, and INCONEL alloy 625. RA 330, RA 602CA, and INCONEL alloy 625 were received from Rolled Alloys. Ten samples were prepared for each alloy. Selected samples have been aluminized by Alcoa Howmet in Branford, CT. All of the samples are engraved with the number listed below.

Figure 10, and Figure 11 show Unaluminized and aluminized, RA 330, and INCONEL alloy 625 samples.



Figure 10. Unaluminized (left) and aluminized (right) RA 330 samples



Figure 11. Unaluminized (left) and aluminized (right) INCONEL alloy 625 samples

There are 30 samples in total. These samples are divided into 10 groups. Group 1 and Group 6 were kept in WPI for characterization. The other eight groups were sent to Bluewater Thermal Solutions for the experiments in the carburizing furnace.

Group No.	RA 602CA	RA 330	INCONEL alloy 625	Surface Condition	Date Removed
1	6021	3302	6250	Unaluminized (Original)	Nov. 18 th 2013
2	6020	3310	6251	Unaluminized	Feb. 24 th 2014
3	6022	3301	6252	Unaluminized	Oct. 6 th 2014
4	6023	3303	6253	Unaluminized	April 20 th 2015
5	6024	3304	6254	Unaluminized	Dec. 7 th 2015
6	6025	3305	6255	Aluminized (Original)	Nov. 18 th 2013
7	6026	3306	6256	Aluminized	Feb. 24 th 2014
8	6027	3307	6257	Aluminized	Oct. 6 th 2014
9	6028	3308	6258	Aluminized	April 20 th 2015
10	6029	3309	6259	Aluminized	Dec. 7 th 2015

Table 7. Sample list

In the current tests, the eight groups were placed in the same carburizing furnace at Bluewater in Rockford, IL in November 2013. After three months, the Group 2 and Group 7 have been taken

out for characterization. Then after 12 months, the Group 3 and Group 8 were removed. After 18 months, the Group 4 and Group 9 were removed. Then after 24 months, the Group 5 and Group 10 were taken out and shipped back to WPI.

Samples were exposed in the batch carburizing furnace for different times. The batch furnace at Bluewater is located in Rockford, IL. These samples were placed in a batch carburizing furnace and the carbon potential of the atmosphere is approximately 0.7%. Carburizing temperature is set at 870°C to 925°C in this furnace. And the carburizing time for each cycle is depends on the size of the products, smaller parts such as gaskets will takes 1-3 hours, and the larger parts takes much longer time.

3.2. Second exposure experiments

Five alloys were selected as the additional alloys for the lifetime tests, including APMT, RA330, 316SS, 304SS, and RA253MA. RA330 were received from Rolled Alloys, KANTHAL APMT were from SANDVIK, and Stainless steel 316 and 304 were purchased from Peterson Steel, Inc.

Name of alloys	Treatments	Series number	Number of samples
RA330	Original	3301-3304	4
	Aluminized	3306-3309	4
APMT	Original	1002-1005	4
	Aluminized	N/A	
RA253MA	Original	2535-2538	4
	Aluminized	2531-2534	4
316SS	Original	1601-1604	4
	Aluminized	1605-1608	4
304SS	Original	0401-0405	5
	Aluminized	0406-0410	5

Table 8. List of second batch alloys



Figure 12 APMT No. 1001

RA253MA:

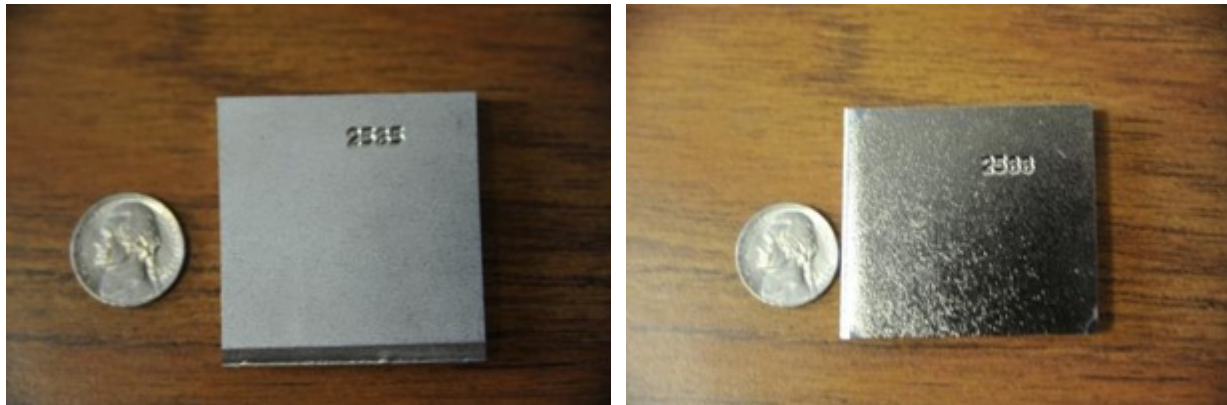


Figure 13. RA253MA (left) Aluminized RA253MA (right)

Stainless Steel 316:



Figure 14. Stainless Steel 316 (left) Aluminized Stainless Steel 316 (right)

Stainless Steel 304:

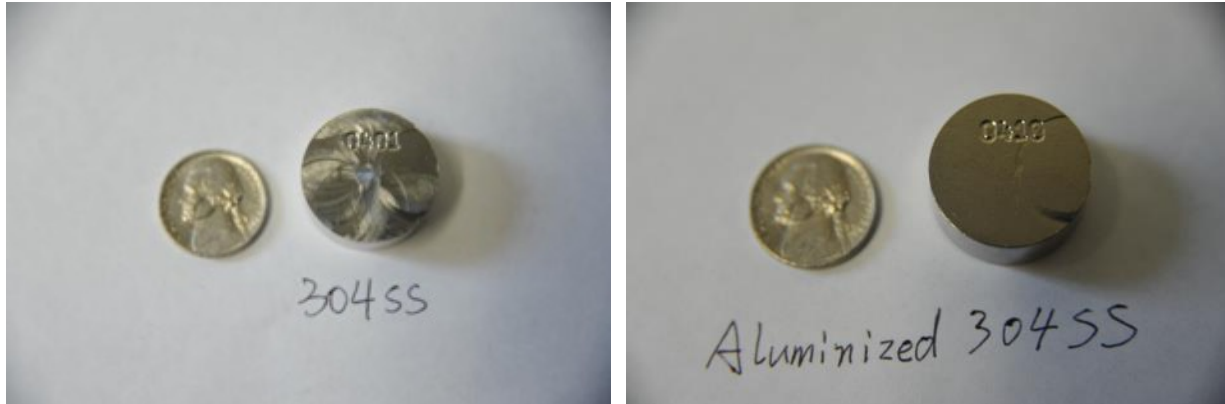


Figure 15. Stainless Steel 304 (left) Aluminized Stainless Steel 304 (right)

The second batch of samples were placed into the furnace on Oct. 6th 2014. The batch furnace at Bluewater also located in Rockford, IL. These samples were placed next to the first batch of samples in a batch carburizing furnace and the carbon potential of the atmosphere is approximately 0.7%. Carburizing temperature is set at 870°C to 925°C in this furnace. First set of samples were removed after 7 months exposure on April 20th, 2015. Then the second set of samples were removed after 14 months exposure on Dec. 7th, 2015. All the samples were collected and brought back to WPI for characterizations.

Experimental Procedure

Based on the recommendation of industry partners and literature review of alloy's properties, RA330, RA602CA, RA253MA, APMT, Inconel 625, 304SS, and 316L were selected for this research.

4.1. Surface finishing

Surface modifications were investigated as they may have beneficial effects on the degradation behavior. Surface finishing measurements were conducted on the 316SS, 304SS, APMT and RA330 samples. Washburn machine shop and other well-equipped facilities were utilized for the sample machining.



Figure 16 HASS Mini Mill for surface finish (left) HASS Lathe for cutting (right)

First, Stainless steel 316 and 304 were cut into 1'' inch diameter bar. Second, the samples were cut into discs -- 1'' inch diameter and 0.4'' in thicknesses. Finally, the surface of samples were faced with face mill and engraved with series numbers.

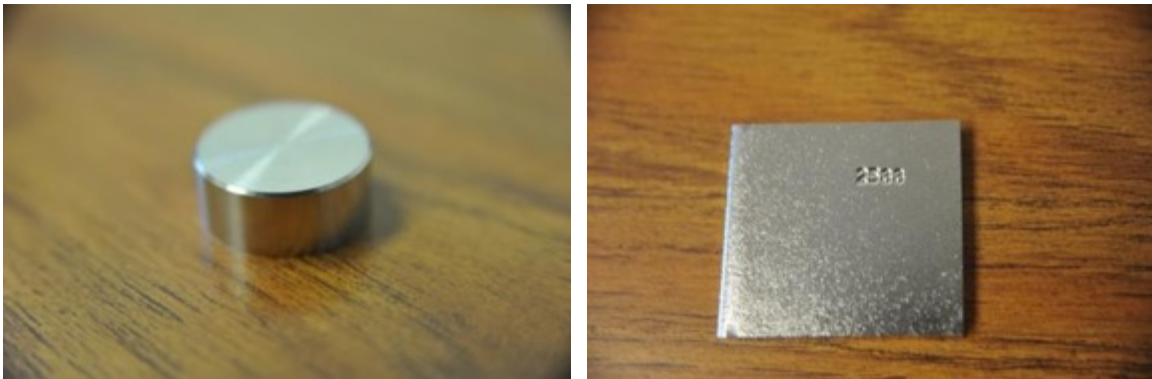


Figure 17 Stainless Steel 316 (left) Aluminumized RA253MA (right)

Surface contamination during heat treatment process can greatly affect the quality of the heat treated parts. The carburizing process can be affected by surface contamination.^[20] The cleanness of samples is important, so all the samples were cleaned by ultrasonic cleaner with ethanol before coating and any treatment.

4.2. Aluminizing

Aluminizing is widely used to increase the high temperature corrosion and oxidation resistance of nickel-based alloys. α – alumina Al_2O_3 are effective protection for high temperature and aggressive gaseous environments. Nickel aluminides formed during aluminizing act as the reservoir of aluminum for maintaining a protective Al_2O_3 scale on the material surface during high temperature services.

Selected samples were sent to Alcoa Howmet for aluminizing on December of 2013. The samples were aluminized in a static gas phase system at 1090°C for 5 hours. Chromium aluminum source material (70%Cr/30%Al) and ammonium fluoride granules were used in the system. The coating chamber was purged with argon until a dew point of -40F or better was met, then the argon is shut-off to the coating chamber (hence static system) and heating begins.

To better understand the aluminizing process, an Isopleth diagram of RA330 with mass percent Al was plotted (Aluminizing temperature is 1090°C). From the Isopleth diagram, we can see that before aluminizing RA330 has uniform single phase iron nickel austenite which is in a good agreement with SEM micrographs in Figure 18. Besides, XRD results also show single FCC phase of the unexposed RA330. However, with aluminum diffuse into sample, BCC structure Nickel aluminide will form with more than 4% aluminum at 1090°C. Then no fcc austenite will form above 8% aluminum at equilibrium, only beta Nickel aluminide were predicted.

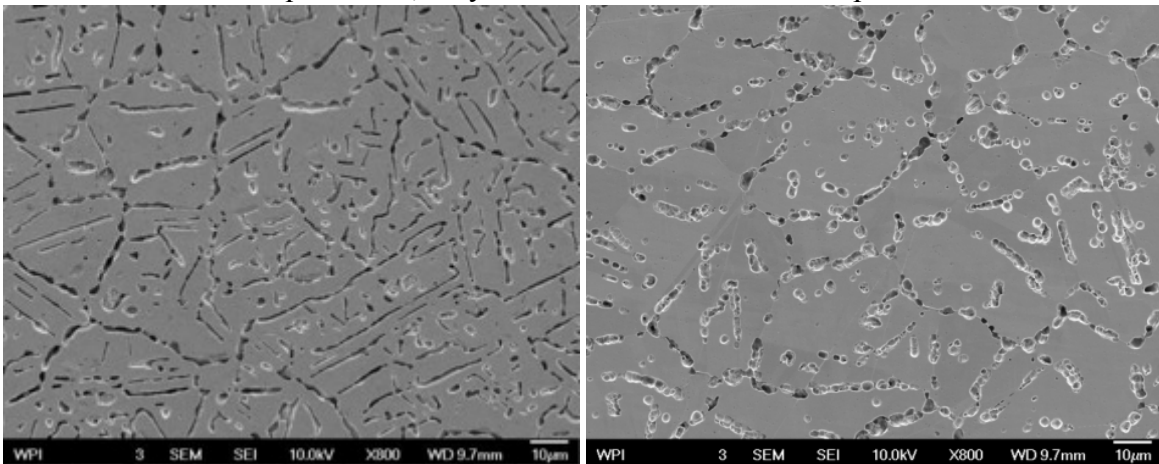
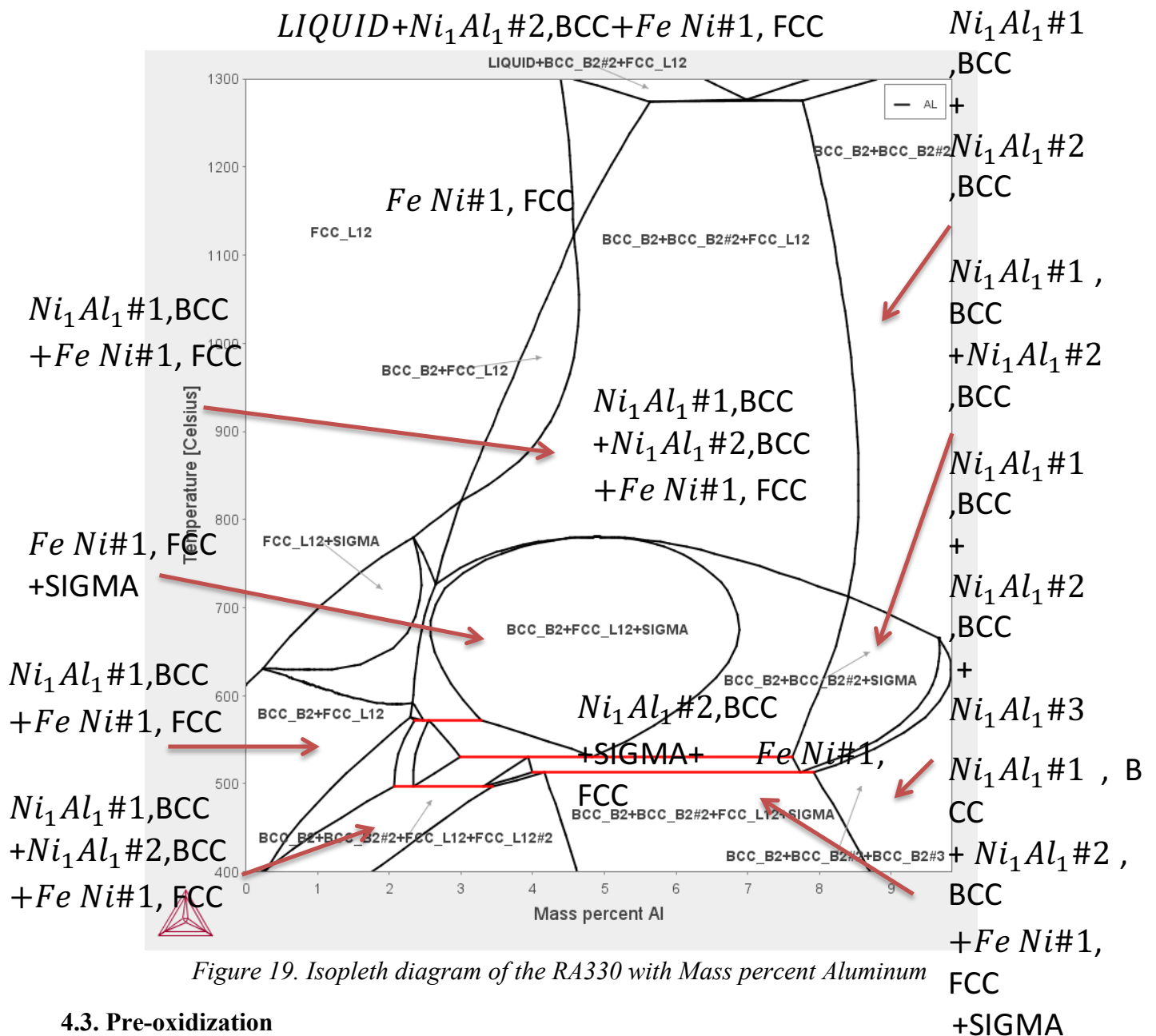


Figure 18. SEM cross section photomicrographs of RA330 at the core etched with 10% oxalic acid



4.3. Pre-oxidization

High temperature corrosion processes including carburization and oxidation are two main causes of corrosion for the alloys used in gas furnaces. High temperature corrosion resistance is provided by the presence of stable, fine, dense and adhering protective oxides.

RA330 alloys were pre-oxidized to increase the anti-corrosion properties. Sample was impregnate with 5% sodium hydroxide for 10 minutes. And then, sample was heated up in air from room temperature to 900°C and holding at 900°C for 24 hours. The atmosphere of the furnace is air. The

samples were cooled in furnace after exposure. . The layer of Cr_2O_3 and SiO_2 have grown thicker after pre-oxidized treatment. Austenite phase at the center of RA330.

4.4. Weight gain measurement

The weight of each sample has been measured by high accuracy electronic scales. Each sample was measured before every treatment. For example, the weight of RA330 samples were measured before sent for aluminizing. And then measured the weight again after the samples have been aluminized. Before each measurement, samples were cleaned in ultra-sonic machine by ethanol. The typical error range is within $\pm 0.005g$.

Weight gain was the combination of carbon uptakes and oxidation during the exposure. However, samples already formed a dense oxide layer on the surface of alloys. So, the weight gain is primarily carbon uptakes. In this case, the carbon flux could be calculated by following formula.

$$\text{Carbon flux} = \text{weight gain} / \text{surface area}$$

4.5. Exposure experiments

After the pre-treatments of sample such as aluminizing, pre-oxidation, and cleaning process, all the samples were weighted before placed into gas/vacuum carburization furnaces.

Then, two batches of samples were exposed in the same batch carburizing furnace for different times. The batch furnace at Bluewater is located in Rockford, IL. These samples were placed in a batch carburizing furnace and the carbon potential of the atmosphere is approximately 0.7%. Carburizing temperature is set at 870°C to 925°C in this furnace. The furnace only shut down three or four times during one calendar year for maintains. Samples were placed in the furnace against the production parts.

4.6. Cyclic oxidations

Cyclic oxidation experiments were conducted on the aluminized RA330 and as-fabricated RA330 to test the adherence of oxide layer (Al_2O_3 and Cr_2O_3).

Experiment Procedure:

Heat to 900°C and hold for 24h then quench in oil follow up with cleaning process, or

Heat to 900°C and hold for 24h then cooled in air follow up with cleaning process

Two cooling methods quenching in oil and air cool were used for cyclic oxidation experiments.

Weight gain was also measured for each cycle.

Each cycle last 24 hours in the furnace at 900°C, however other exposure time was also investigated

Characterizations:

4.7. X-ray Diffraction (XRD)

The outside surfaces of each sample was analyzed using X-ray Diffraction. Phase identification was conducted on the exposed samples. Crystallography and phase analysis were conducted on a PANanalytical Empyrean 2 X-ray diffractometer (XRD) with Cu-K α radiation at 45keV and 40mA. The phase percentage was also analyzed by Rietveld refinement technique.

4.8. Optical emission spectroscopy (OES)

Spectro optical emission spectroscopy (OES) analyzer was used to quantitatively measure the chemical composition of the samples. The composition of each alloys were verified by OES. The carbon profile from the surface of alloy to the core of alloy was measured by OES. The carbon content was measured for each layer, at about 20 μ m apart from each one. Three data points were collected for each layer, and the average was calculated. Then about 20 μ m of material were removed from surface by grinding machine. Continually measured the composition of next layer until the chemical composition of each element reach approximately constant. Carbon profile from the surface to the core could generate by combine the average of C% at each layer.

4.9. Micro hardness test

The Vickers hardness measurements were conducted on the as-polished specimen surface, and measured with a Micro-hardness tester at a force of 200gf. Micro hardness measurements were conducted at the cross section of exposed alloys from surface to the core area.

4.10. Electron backscatter diffraction (EBSD) analysis

EBSD analysis was widely used for obtaining structural information about materials such as phases and orientations. In this study, EBSD technology has been used for study the microstructural developments during the longer term exposure. Such as interface movement, phase transformation, precipitation, and carbon up take.

The structure and texture were studied using electron backscatter diffraction (EBSD) technique. XRD analysis was conducted at sample to identify the phases at the surface of alloys. And then, samples were cut by low speed saw and followed by mounting process. Prepared samples were grinded from 200 grit to 1200 grit. Samples were polished by 1 micrometer alumina polishing powder then 0.3 micrometer, and at end they were polished by 0.05 micrometer alumina polishing powder. The last step for samples preparation is vibration polishing; Samples have been polished for 12 hours before EBSD investigation.

4.11. Optical photomicrographs

Nikon optical microscope was used for characterization of microstructure. High temperature structural alloys have very high corrosion resistance. Therefore, electro-etching was widely used for sample preparations. For nickel iron based alloys, RA330, RA253MA, 304SS, 316L were electro etched by 10% oxalic acid for 30 seconds at 6Volt. And the nickel based alloys were electro etched by 10% oxalic acid for 60 seconds at 10Volt.

4.12. SEM photomicrographs

Secondary electron photomicrographs and back scattered photomicrographs were also obtained of samples that exposed for different times and different surface treatments. A JEOL-7000F scanning electron microscopy (SEM) was used for high magnification characterization of microstructure.

EDS point analysis indicated the chemical composition of a circle area about $1-2\mu m$ in diameter which is due to the size of electron beam. EDS mapping also shows the element distribution at the cross section of samples. Those techniques helped understanding the microstructural developed during the exposure procedure.

Experimental Results

5.1. Microstructure and Failure Analysis of Austenitic Fe-Ni alloys and Ni-Cr-Fe alloys for Furnace Alloys and Fixtures

5.1.1. Isoleth simulation of carburizing process

Thermo-Calc software was used to predict the equilibrium phases in the complex multicomponent. For RA330, Ni data base was used. Nickel, iron, and chromium Isoleth phase diagram was calculated. Carburizing process of RA330 is shown in Figure 20, following composite was used, 19 wt% Cr, 34 wt% Ni, 47 wt% Fe. Isoleth diagram was plotted with temperature as a function of 1 wt% Carbon:

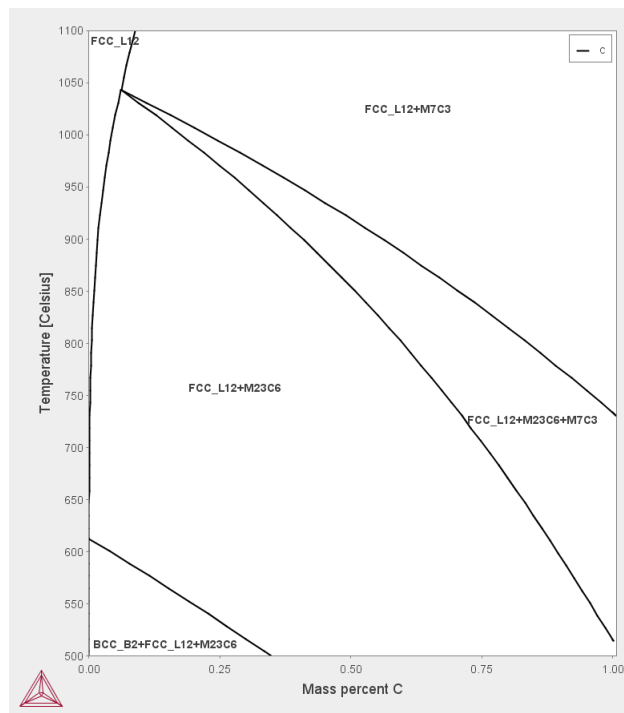


Figure 20. Isoleth simulation diagram of RA330

The microstructure development during the carburizing process can be evaluated using this diagram. Accurate simulation of this process requires knowledge of the diffusion coefficients. However, it is assumed that interstitial diffusion of carbon into the alloy is much faster than substitution diffusion.^[21] According to the diagram, FCC structure austenite phase was predicted at 900°C. When the carbon concentration reaches approximate 0.1%, M23C6 phase is predicted, and above 0.4% of carbon, M7C3 phase and M23C6 were predicted to form in the RA330. Several workers who studied carburization of stainless steel reported that $(Cr, Fe)_7C_3$ carbides formed predominantly when the carbon content was above 4 wt% and the ratio of the $(Cr, Fe)_{23}C_6$ to $(Cr, Fe)_7C_3$ phases increased as the carbon concentration of the steel decreased.^[22–25] Those

statement have good agreement with the simulation result on the Figure 20. According to their results, the near-surface zone comprises predominantly M7C3 and the zone beneath that was the phase mixed with M23C6 and M7C3.^[26] Then, with increased carbon deposition, only M7C3 is expected to form. Metal carbides (MC) have been frequently observed in austenitic steels.^[27] Many additives, such as Ti could be added to 316SS to form TiC carbide for suppressing the formation of $Cr_{23}C_6$ so that the corrosion resistance of the materials can be maintained. The thermodynamic models of M7C3 is $(Cr, Fe, Mn, Mo, Ni)_7C_3$.^[27]

5.1.2. Failed Fan Blade from Bluewater (gas carburization furnace)

Bluewater provided a section of a failed fan blade that is made of RA330. The service life of fan blade is shorter than other components due to high carbon potential environment and high stress obtained from rotation. The typical service time for a fan blade made of RA330 is 1-2 years. The failed fan blade was used in batch carburizing furnace and the carbon potential of the atmosphere is approximately 0.7%. The chemical composition of RA330 is shown in Table 9.

	Cr	Ni	Mn	Si	Cu	P	S	C	Fe
Min (wt.%)	18.0	34.0	-	1.0	-	-	-	0.04	-
Max (wt.%)	20.0	37.0	2.0	1.5	1.0	0.03	0.03	0.08	Balance

Table 9. Chemical composition% of RA330



Figure 21. Photographs of Failed fan blade

The sample was cut for metallography of the cross section. This sample was ground to 1200 grit and then polished. Unlike the unexposed RA330 alloys, this sample was easily etched by 2% Nital. Figure 22 presents optical photomicrographs at the edge of sample. And, Figure 23 presents cross section SEM photomicrographs of the failed fan blade at the edge.

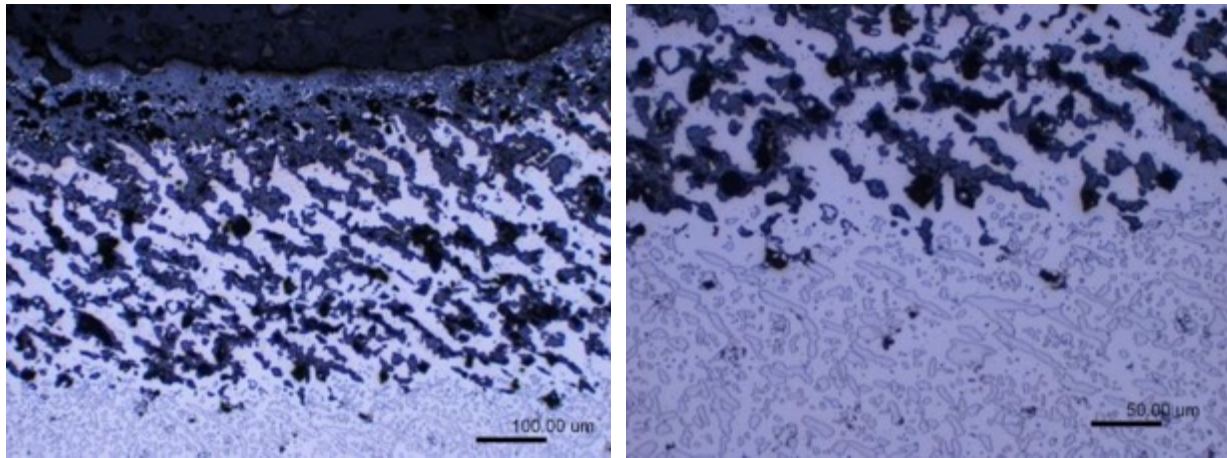


Figure 22. Optical photomicrographs of failed fan blade at the edge (etched with 2%Nital)

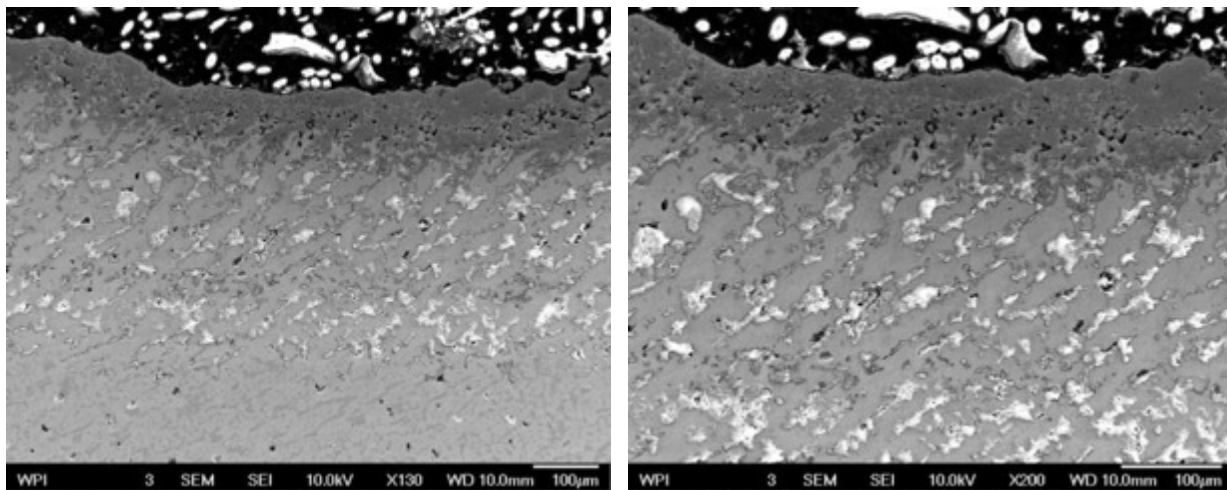


Figure 23. SEM photomicrographs of failed fan blade at the edge (etched with 2%Nital)

In surface region, the edge of RA330 fan blade was attacked. Carbon depositions associated with the pits were observed. Figure 24 and Figure 25 shows the carburizing affected region, which is combined with chromium carbides and austenite iron-nickel phase according to following EDS analysis.

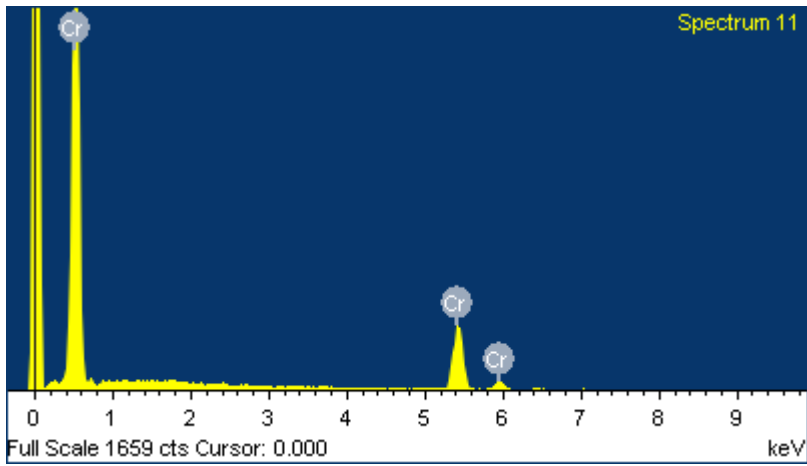
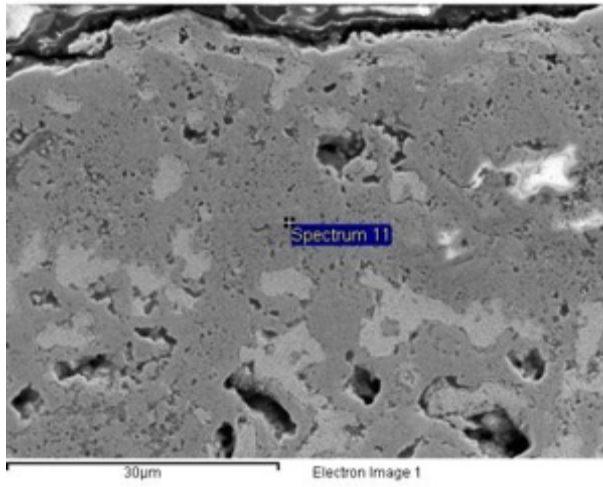


Figure 24 EDS photomicrographs and element analysis

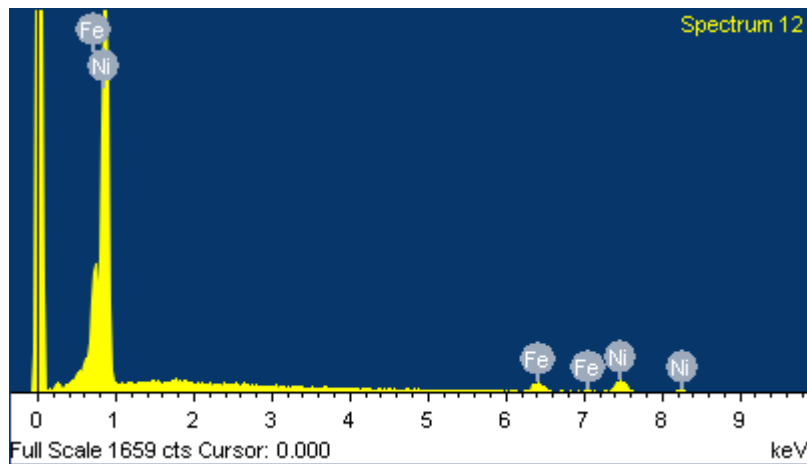
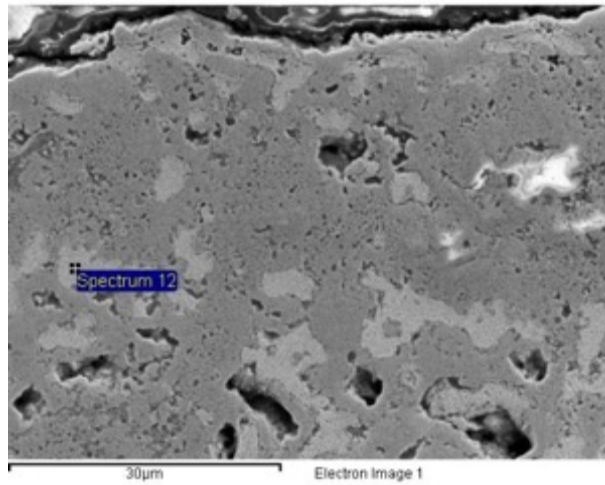


Figure 25 EDS photomicrographs and element analysis

Localized metal dusting was observed at the surface area, chromium oxide Cr_2O_3 was also identified at the edge of cross section using EDS. Figure 24 EDS photomicrographs and element analysis indicated that the dark grey area was mainly Cr_2O_3 , it also act as a protective layer from carburization. The metal dusting region was approximately $100 \mu m$ wide from the surface, which shown disintegration of the alloy. From the Figure 24, EDS result shows 40at% Cr and 60at% O indicated the dark grey area was mainly Cr_2O_3 . It was seen that the composition of the dark grey region in Figure 25 was identified as approximately 28% Cr, 13% Fe, 59% O, corresponding to spinel, $FeCr_2O_4$ plus carbon. And the grey regions also have chromium carbide according to the EDS results.

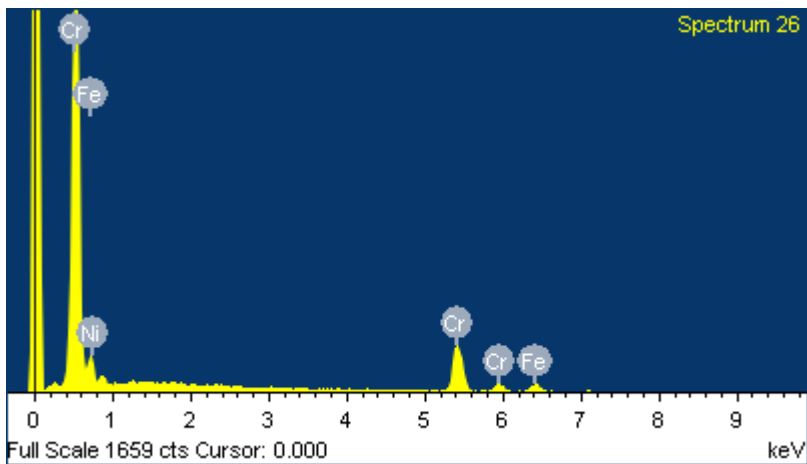
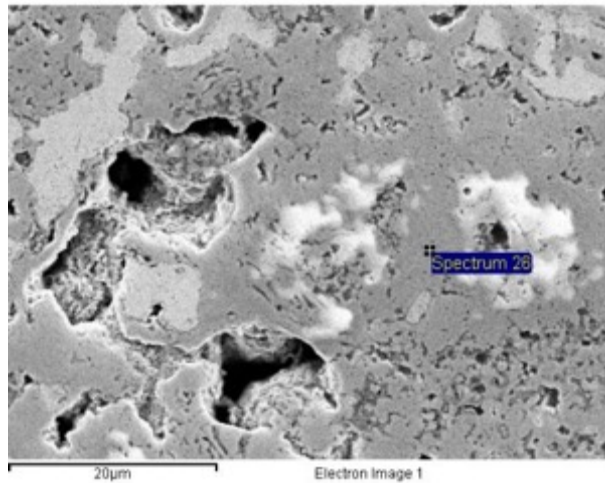


Figure 26. EDS photomicrographs and element analysis

The light grey area was identified by EDS as (Fe, Ni) austenite phase, according to Figure 26. The white areas were also identified by EDS analysis, it was qualitatively clear that they were chromium rich carbides.

Figure 27 shows the cross section SEM photomicrographs of failed fan blade. After one year service in carburizing furnace, the etched structures of RA330 are seen in Figure 27 to have undergone extensive carburization and metal dusting.

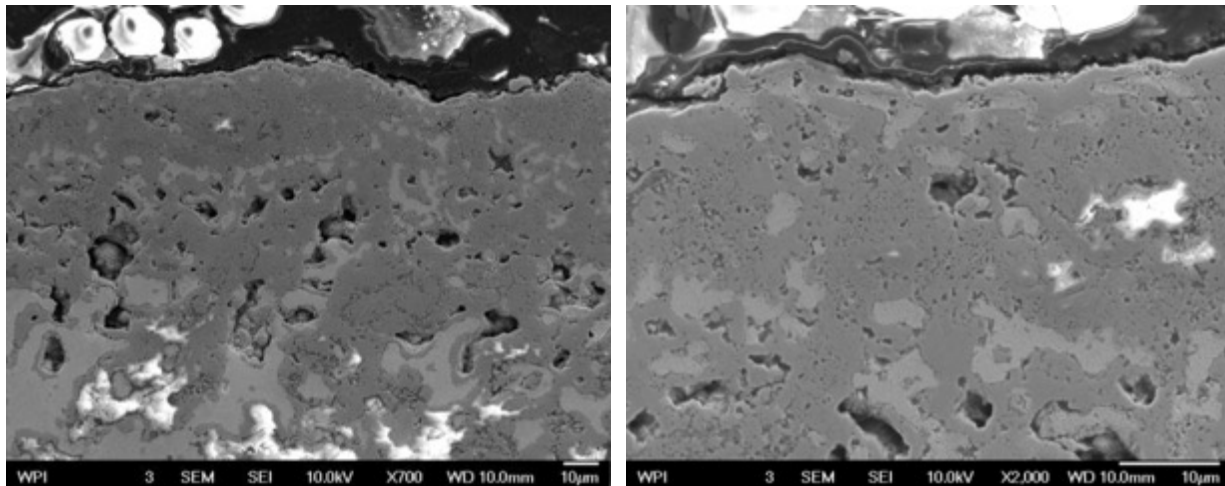


Figure 27. SEM photomicrographs of failed fan blade at the edge (etched with 2%Nital)

Figure 28 shows the cross section optical photomicrographs of RA330 fan blade etched with 2% Nital. According to isopleth simulation, the carbon concentration of RA330 is about 0.05% which could possibly form chromium carbides at the grain boundaries. And the XRD and EDS result also verified the simulation assumption.

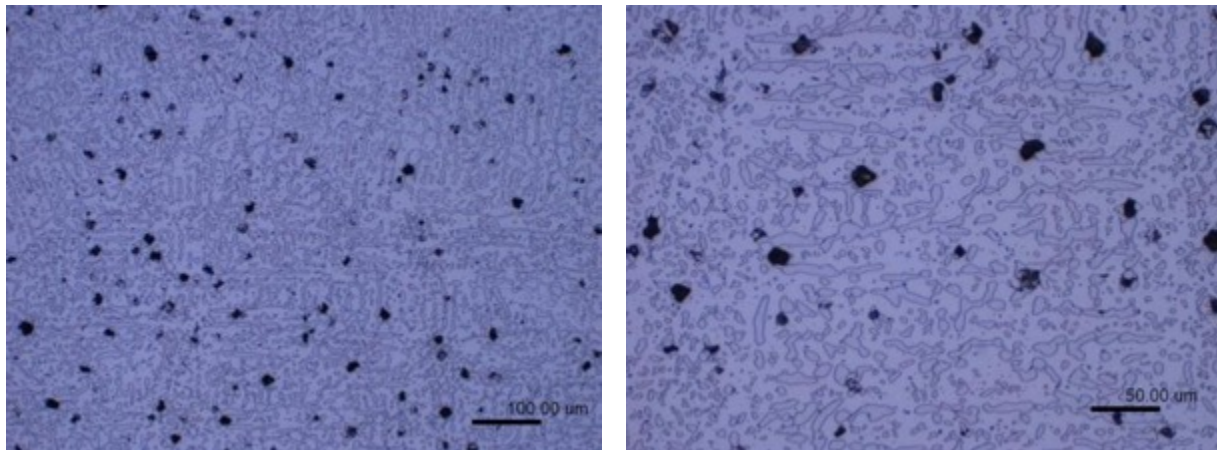


Figure 28. Optical photomicrographs of failed fan blade at the center (etched with 2%Nital)

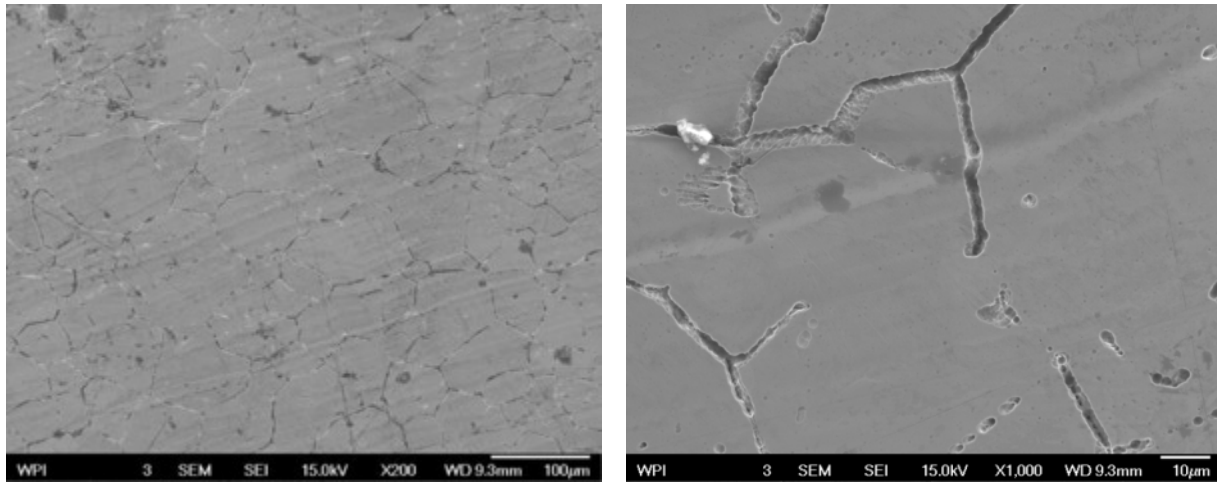


Figure 29. Cross section SEM photomicrographs of unexposed RA 330 (etched with 10%wt oxalic acid)

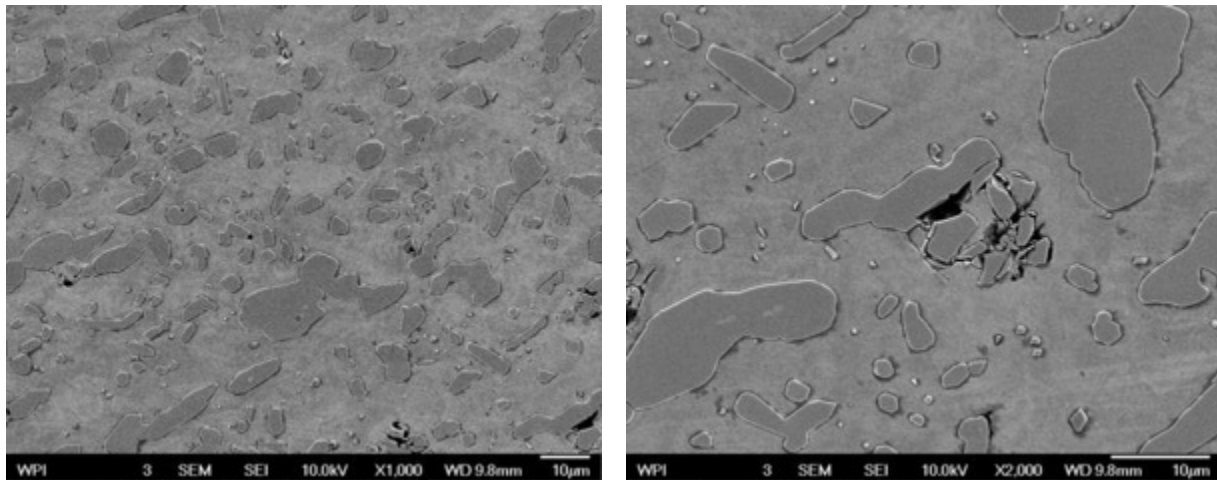


Figure 30. Cross section SEM photomicrographs of exposed RA 330 (etched with 2%Nital)

Figure 29 and Figure 30 shows the cross section SEM photomicrographs of a new RA330 and a failed RA330. It can be seen that the microstructure of the new RA330 was uniform, a secondary phase forms along the grain boundary, and within the grain (the dark grey phase in the SEM photomicrograph of failed fan blade) after exposure. The carbides precipitated at the core area were of spheroidal morphology, as shown in Figure 31 and Figure 32. The dark grey area was chromium carbides, identified by the EDS. The carbides were also found in the XRD results. In addition, the light grey area was (*Fe, Ni*) austenite.

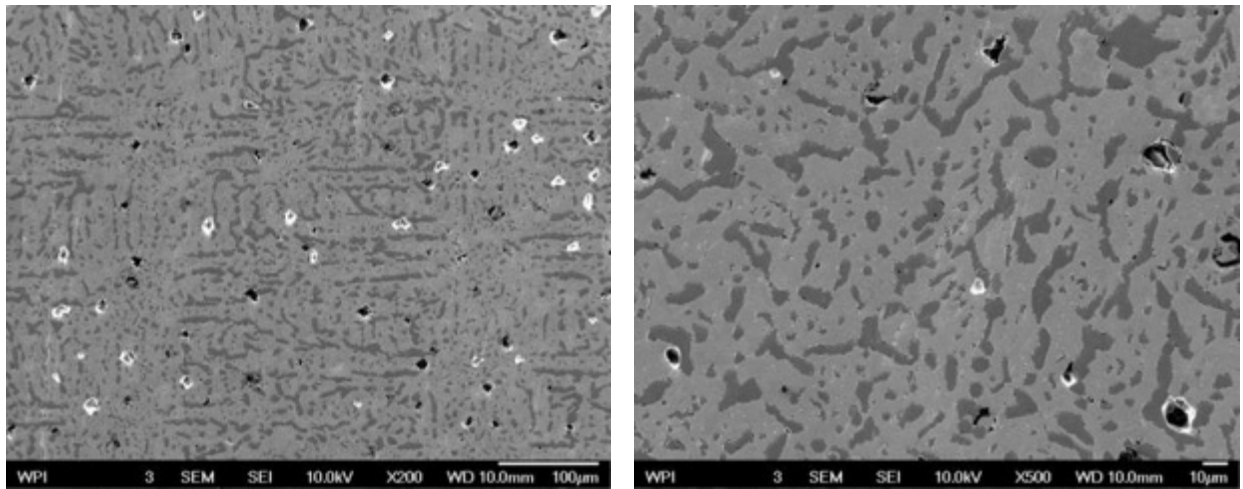


Figure 31. Cross section SEM photomicrographs of exposed RA 330 (etched with 2%Nital)

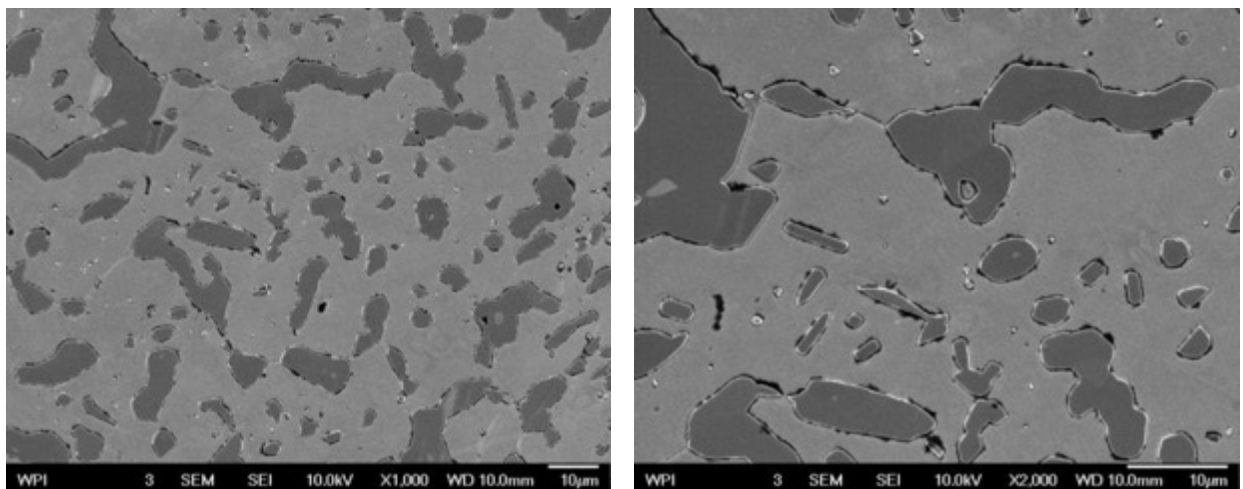


Figure 32. Cross section SEM photomicrographs of exposed RA 330 (etched with 2%Nital)

The elemental analysis by EDS was conducted on the cross section. *Figure 33* indicated that the samples contain Fe, Ni, Cr, Si, and C, which is in good agreement with the composition of RA330 (Table 9).

EDS analysis can be used to create the elemental map. *Figure 36* presents the images from the EDS maps of iron, silicon, carbon, chromium and nickel on the corresponding SEM photomicrograph of the fan blade. It can be seen that the secondary phase (dark grey phase) are rich of Cr and C, but low of Fe, Si and Ni, which indicated that the phase is a chromium carbide.

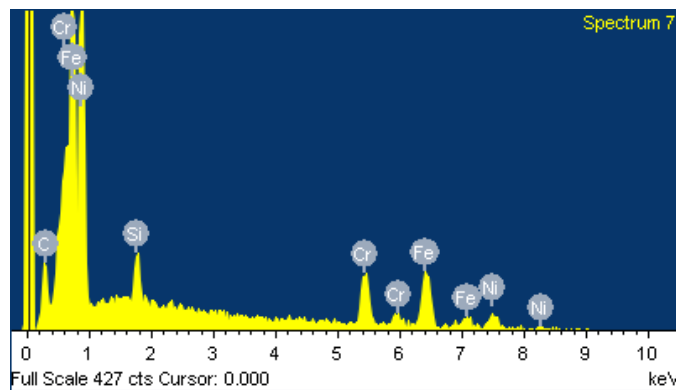
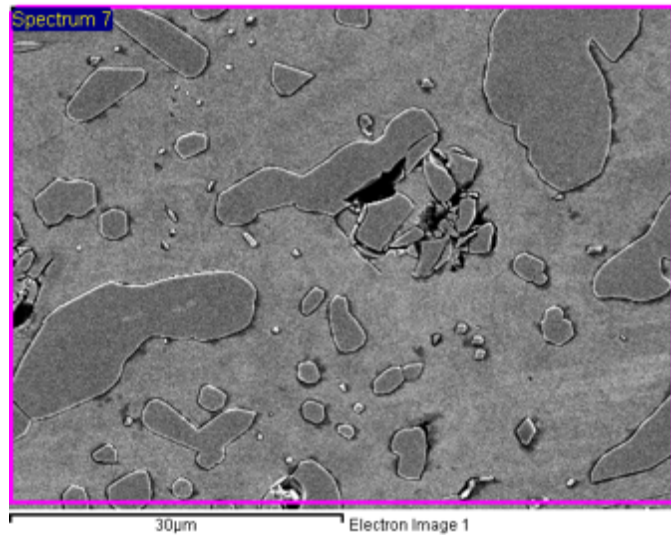


Figure 33. Elemental analysis by EDS on failed fan blade

Combined with EDS, X-ray diffraction was used to identify the phases on the surfaces of the RA330. The main phases of exposed RA330 were iron nickel with face center cubic crystal structure and secondary phase chromium carbides. Magnetite was also detected at the surface of fan blade, shows on Figure 34.

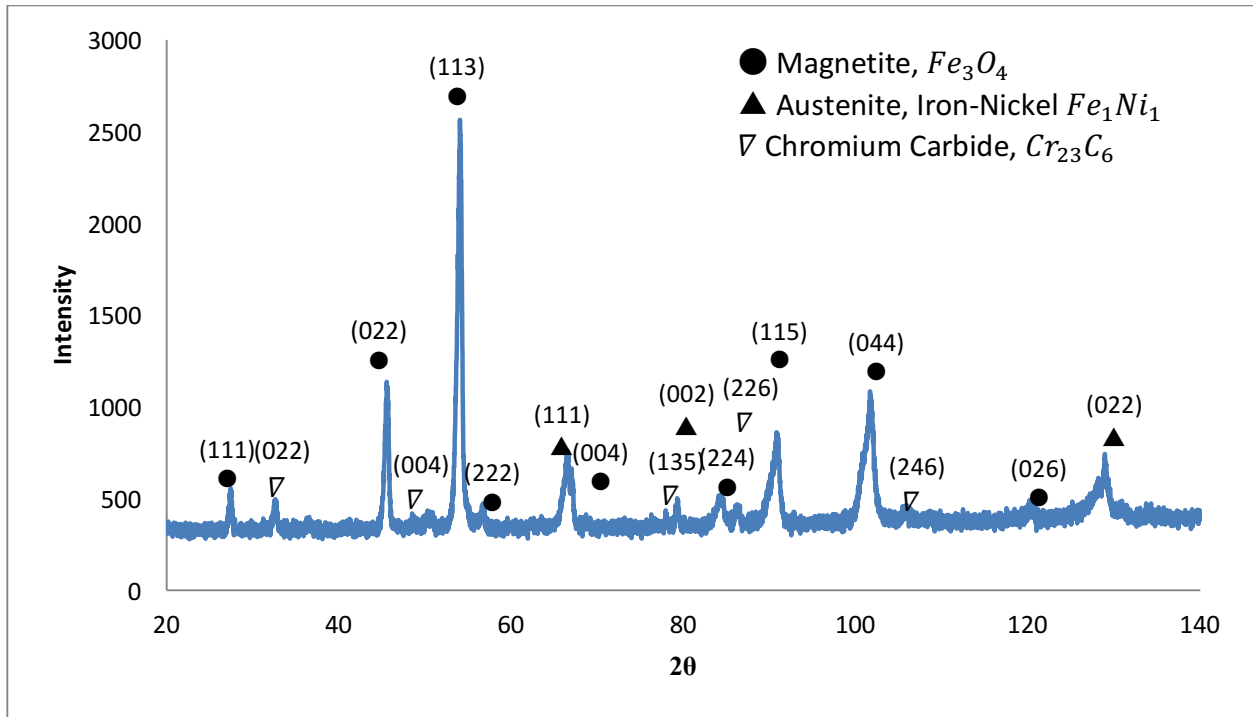


Figure 34. XRD pattern of the surface scan for fan blade (exposed 24 months) (Cu tube)

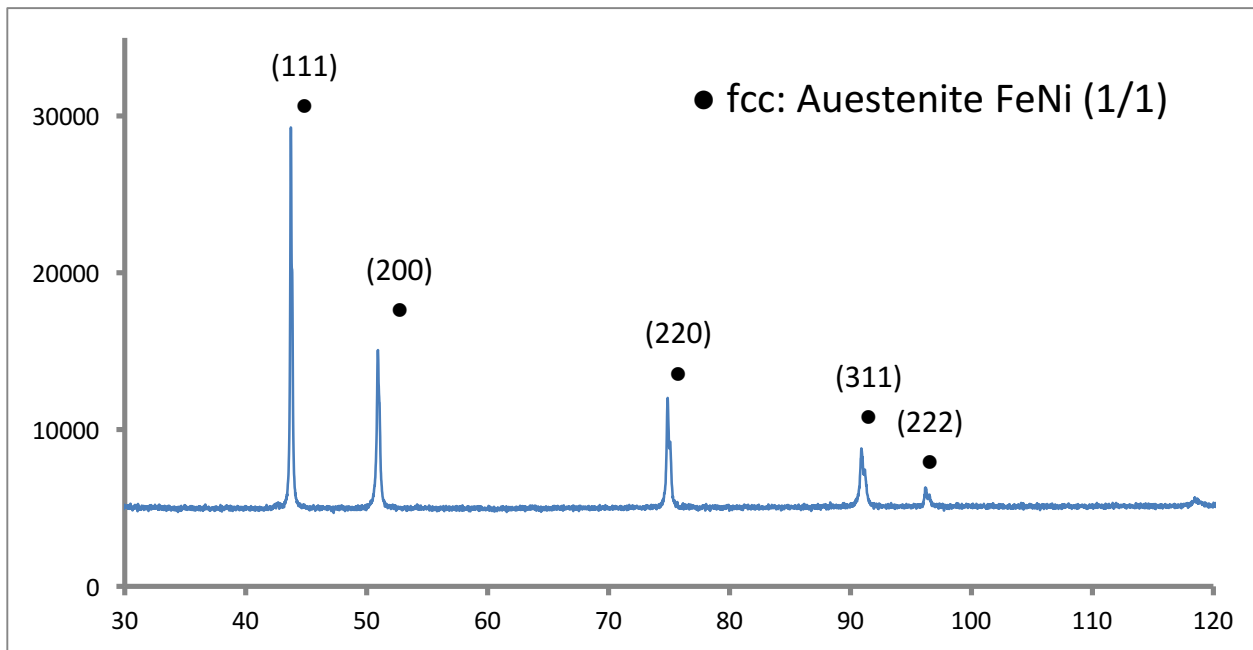


Figure 35. XRD pattern of the surface scan for as fabricated fan blade (Cu tube)

In the furnace, the oxygen levels are low when methane, propane, ethane or any other hydrocarbons are present, metal dusting occur at (425°C-900°C). Metal dusting results in pitting or thinning of material and also the formation of internal carbides in the matrix of the failed components. Internal carbides cause embrittlement, a decrease in the materials ductility and creep-rupture strengths, and a loss in most basic material properties.^[4] With the carbon diffusing into the fan blade, chromium in the steel reacts with carbon to form the chromium carbide, which decrease the corrosion resistance and increase the embrittlement of the fan blade. The failure of the fan blade was caused by extreme uptake of carbon that leads to metal dusting. As presented in the data above, the fan blade failed due to excessive carburization that lead to metal dusting and subsequent cracking.

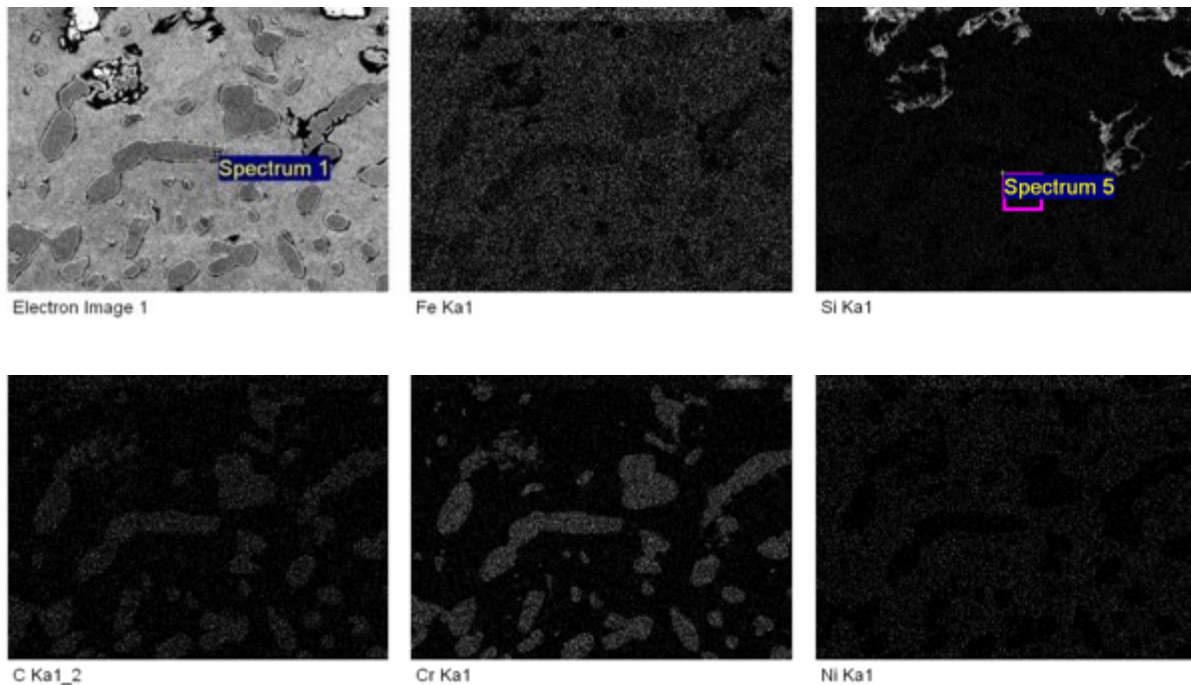


Figure 36. EDS element maps on the cross section of the fan blade

5.1.3. Failure mode analysis of furnace part or fixture (Vacuum carburization furnace)

Broken racking pole

Thank one of the members of the Center for Heat Treating Excellence, Sikorsky Aircraft, for providing a broken racking pole. Figure 37 shows three different views of the racking pole. The pole was used in vacuum carburizing furnaces at a loosely approximated time of 30 hours per week for 5 to 10 years. The vacuum carburizing operated at 925-1038°C and the endothermic carburizing furnace ran from 815°C to 925°F. The estimated number of heat treating operations is 2000-3000 or 16,000-24,000 hours.

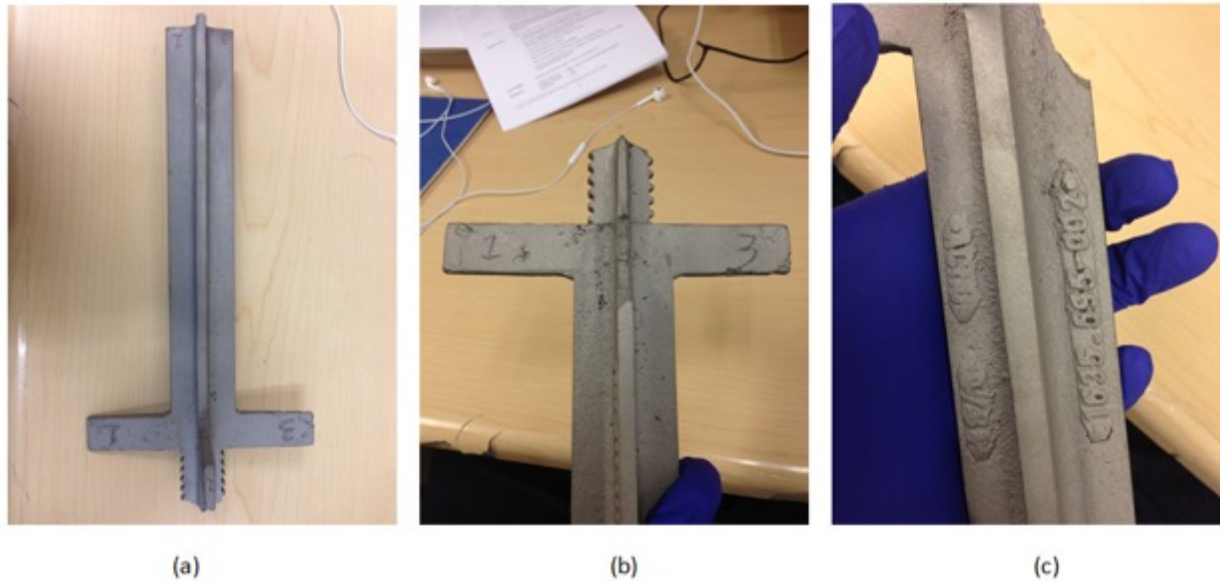


Figure 37: Failed racking pole sample from Sikorsky Aircraft carburizing furnaces. The post was labeled for reference purposes. (a) Normal view of the entire part (b) front view of broken piece (c) close-up side view of broken section.

5.1.3.1. Characterization of pole

5.1.3.2. OES (Optical Emission Spectroscopy) analysis

Spectro optical emission spectroscopy (OES) analyzer was used to quantitatively measure the chemical composition of the racking pole. A piece of sample with flat surface was cut from the pole. Figure 38 shows the sample with the sparks from the OES measurements.



Figure 38: Photo of a piece of racking pole sample after twice OES measurements

Optical Emissions Spectroscopy (OES) Results													
Racking Pole Sample													
Element	Fe	Ni	Cr	Mo	Co	Si	W	P	S	C	Mn	Nb	Cu
	wt.%												
1	45.61	32.76	17.69	0.29	0.21	1.88	0.12	0.04	0.03	0.27	0.35	0.19	0.15
2	44.14	33.83	16.53	0.29	0.21	1.99	0.11	0.03	0.02	1.86	0.32	0.20	0.15
3	44.23	33.62	16.67	0.29	0.21	1.98	0.11	0.03	0.02	1.84	0.32	0.20	0.15
4	43.68	33.91	16.28	0.29	0.21	2.03	0.11	0.04	0.01	2.47	0.30	0.18	0.25
5	43.73	33.88	16.20	0.29	0.21	1.99	0.10	0.03	0.01	2.58	0.30	0.18	0.25
7	45.58	32.55	17.86	0.30	0.22	1.92	0.12	0.04	0.03	0.29	0.36	0.19	0.16
8	42.27	35.28	16.82	0.23	0.20	2.07	0.09	0.02	0.02	2.11	0.28	0.22	0.28

9	43.11	34.93	17.17	0.22	0.20	2.04	0.09	0.03	0.02	1.27	0.30	0.21	0.17
10	43.05	34.96	17.07	0.22	0.20	2.05	0.09	0.03	0.02	1.41	0.29	0.21	0.17
11	44.61	33.89	17.84	0.22	0.21	1.90	0.10	0.02	0.02	0.26	0.31	0.19	0.17
12	44.20	34.06	17.96	0.23	0.21	1.98	0.10	0.03	0.02	0.28	0.32	0.20	0.17
Average	44.02	33.97	17.10	0.26	0.21	1.98	0.10	0.03	0.02	-	-	-	-

Table 10: Optical Emissions Spectroscopy result summary of racking pole material

The OES measurements were made on various positions on the racking pole. Table 10 presents twelve OES measurement results for each element on weight percentage and the average weight percent composition was calculated. High concentrations of iron, nickel, and chromium agree with each measurement well; approximately 44 wt.% Fe, 34 wt.%Ni, and 17 wt.% Cr was found. The carbon concentrations of these measurements varied from 0.26 – 2.58 wt.%. This variation is most probably due to carburization of the part, as it spent many hours in the carburizing furnaces. This OES measurements show similar results as the HT alloys, and based on the microstructure analysis. The racking pole was confirmed as HT alloy.

	C	Mn	Si	Cr	Ni	Mo	P	S	Fe
Min %	0.4	0.35	0.35	15	33	-	-	-	balance
Max %	0.5	2	2	19	37	0.5	0.04	0.04	balance

Table 11: Chemical composition of HT heat resistant alloy

Literature review is conducted to investigate the possible failure mode similar to this material for carburizing furnace application.

The Alloy Casting Institute designations use “H” for the alloys used in application of over 1200°F, the second letter indicates the nickel concentration increasing from A to X. [29]

HT has good resistance to thermal shocks, oxidation, and carburization at high temperatures, however is vulnerable in high-sulfur gases [30]. HT is used in load-bearing situations such as for radiant tubes, retorts, and in this particular case for fixtures [30]. In HT alloy nickel strengthens the matrix of the material and promotes austenitic growth, stabilizing the face-center cubic austenite phase [30]. Both chromium and nickel promote resistance to oxidation, whereas chromium improves creep properties and rupture strengths [30]. Figure 39 shows the microstructure of a cast HT-44 alloy from volume 9 of the ASM Handbook: Metallography and

Microstructures. HT is comprised of an austenitic face-center-cubic matrix with eutectic carbides on the boundaries [31]. The carbides on the grain-boundaries of HT help prevent the creep due to grain sliding, increase hardness, and allow for stress relaxation to occur [31].

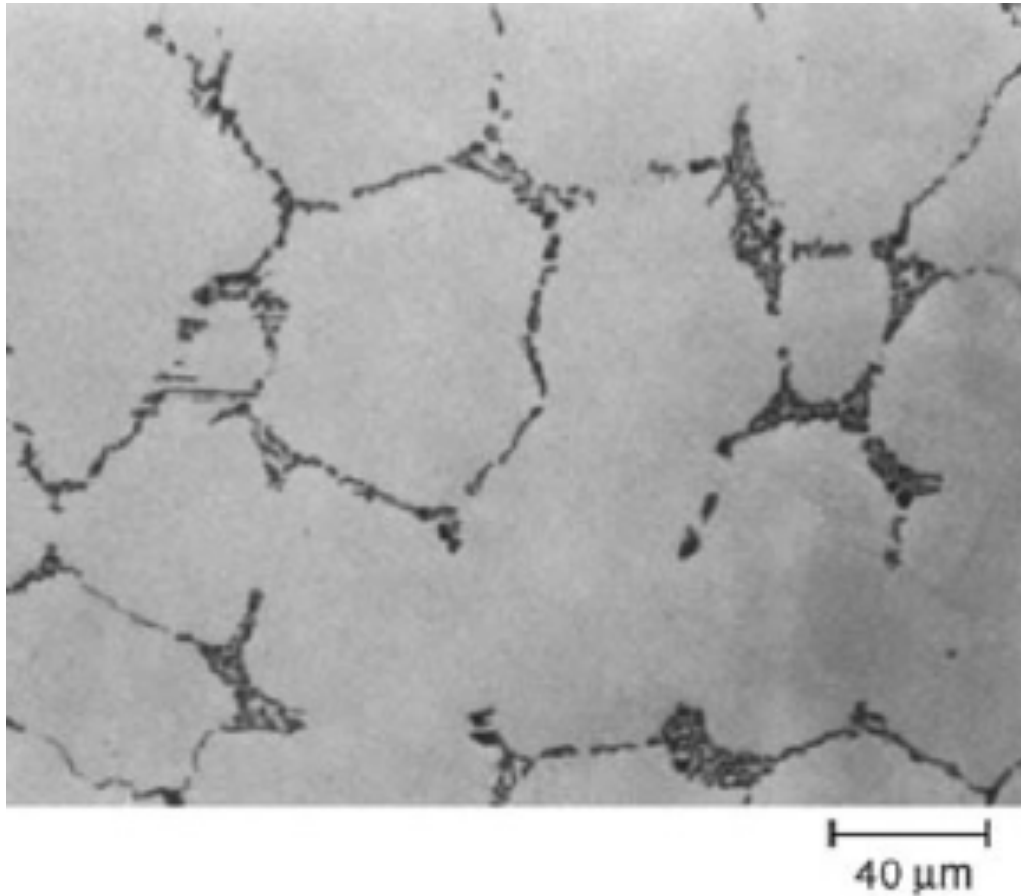


Figure 39: Cast HT-44 microstructure [31].

5.1.3.3. Optical micrographs

Figure 40 shows the sample that was cut from the bottom of the racking post, mounted, and then polished for testing purposes. It can be seen that there is a white layer on the surface of the racking pole after the sample was etched with 2 vol.% Nital (Figure 40 (c)).



(a)



(b)



(c)

Figure 40: Sample cut (a), mounted (b), and polished (c) for testing

By observing a view of the sample at a low magnification in Figure 41, it can be seen that there is a significant microstructural gradient over 1mm of the part.

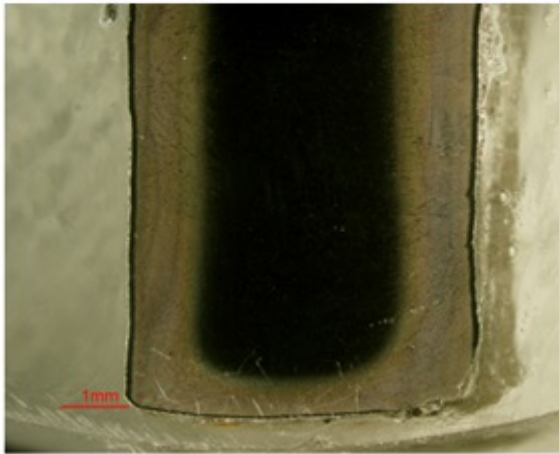
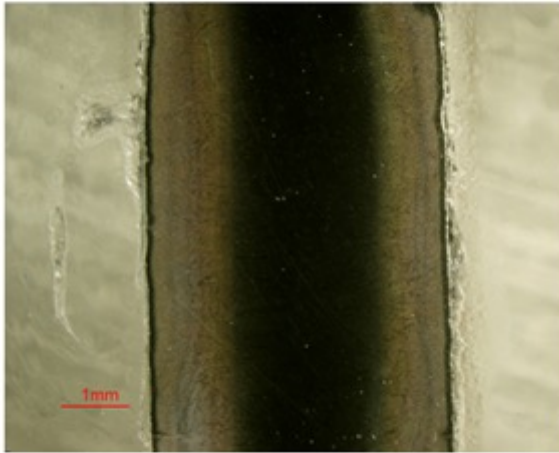
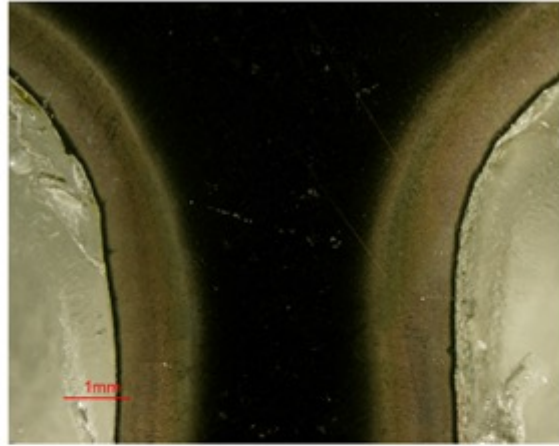


Figure 41: Diffusion zone; 1mm

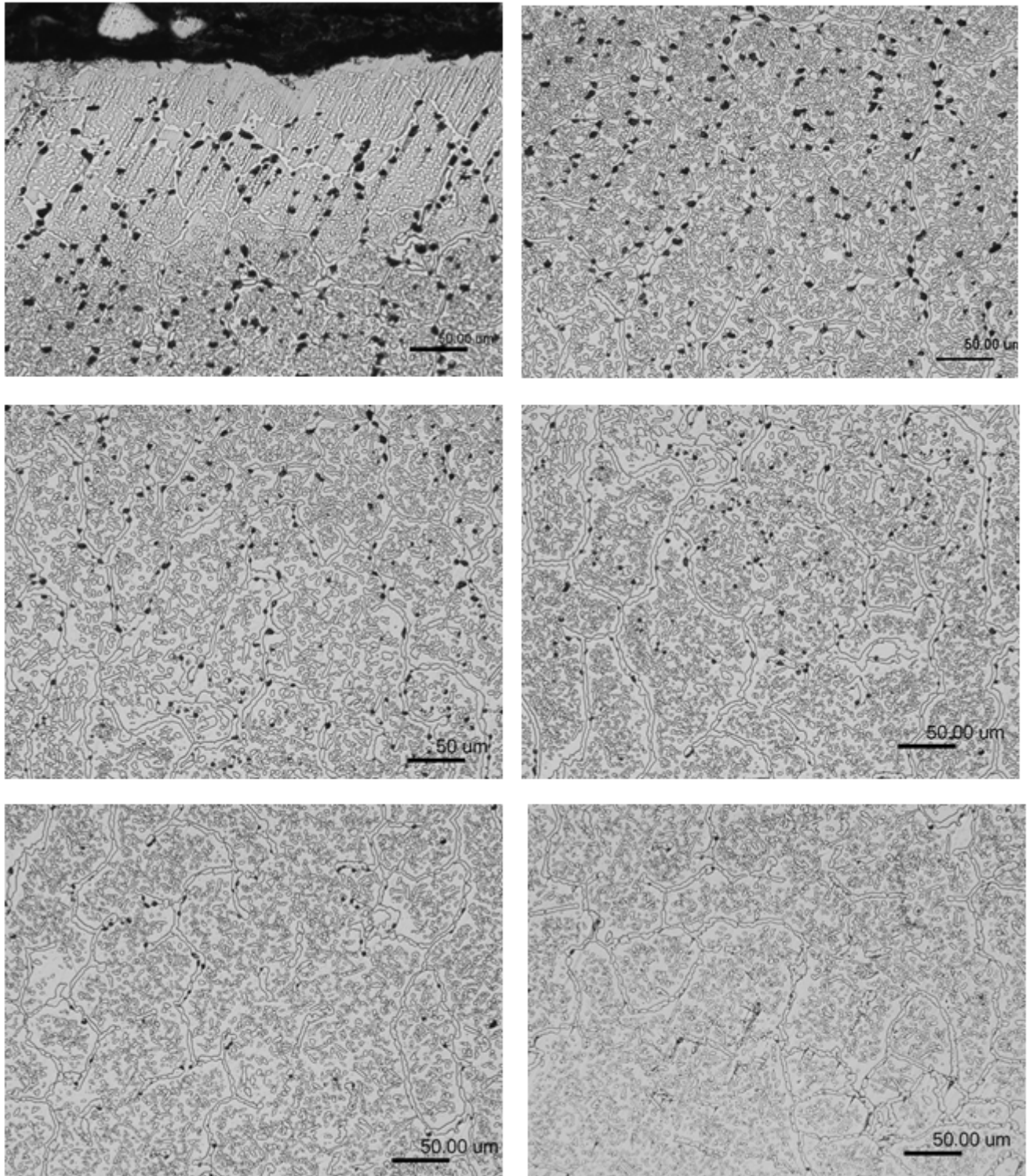


Figure 42: Optical micrographs of sample. Outermost edge (top left) to core (bottom right) of the sample (lower magnification)

Optical micrographs with lower (Figure 42) and higher magnification (Figure 43) were taken from the outward most surface of the part to the interior to observe the microstructure changes from the surface to the core of the pole. It shows that the amount of the black spots decreases from the surface to the core gradually.

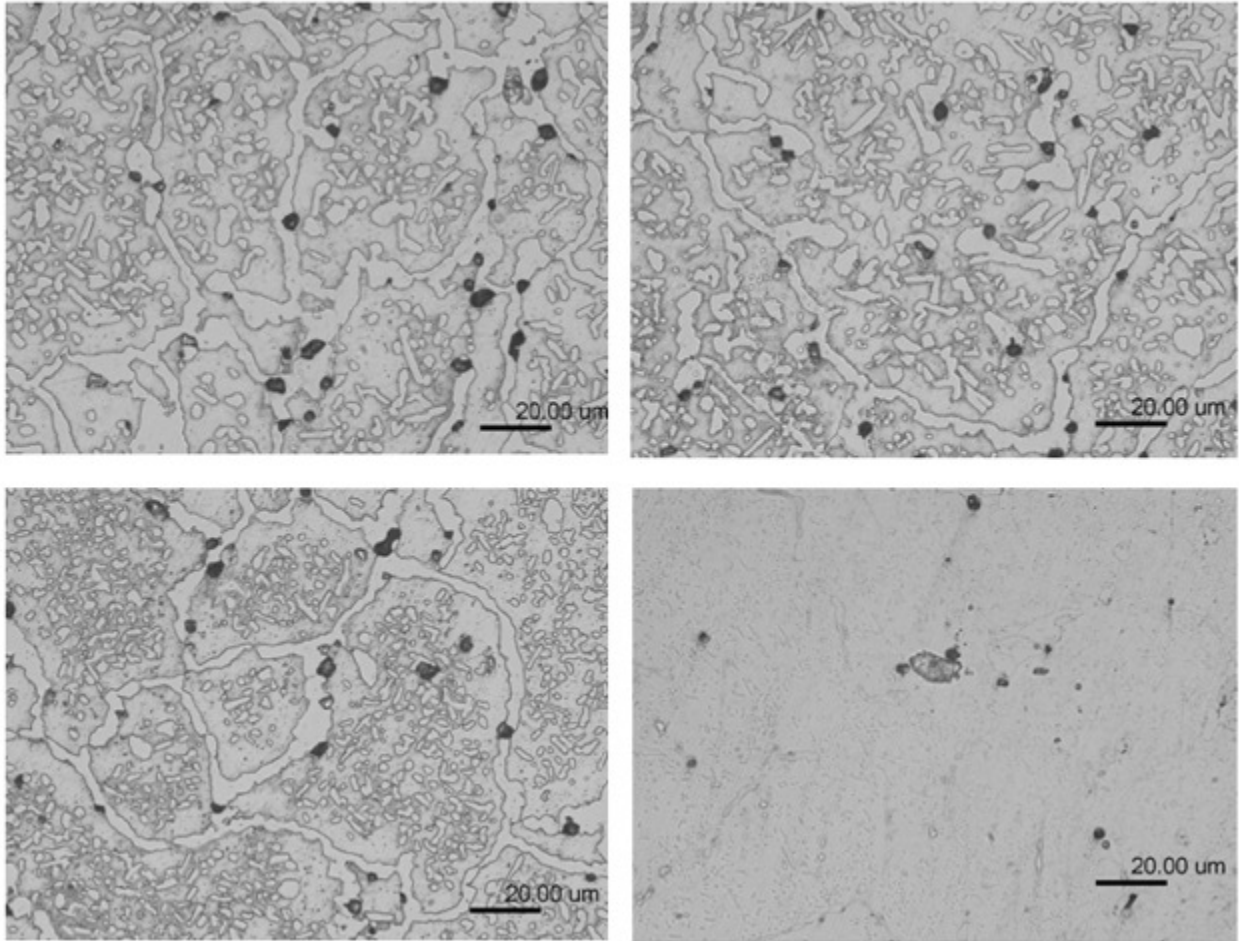


Figure 43: Optical micrographs of sample. Outermost edge (top left) to core (bottom right) of the sample (higher magnification)

Cracking is evident toward the outer surface of the pole. These defects become fewer and further between as the interior of the part is reached. Figure 44 shows one of the cracks near the surface. Based on the optical observation, it is found the surface microstructure of the pole had been changed after being used in the carburizing furnaces for a long time. And this microstructure change may be related to the failure of the pole. It is thus imperative to investigate the cause of this microstructure evolution to determine the failure mode of the racking pole.

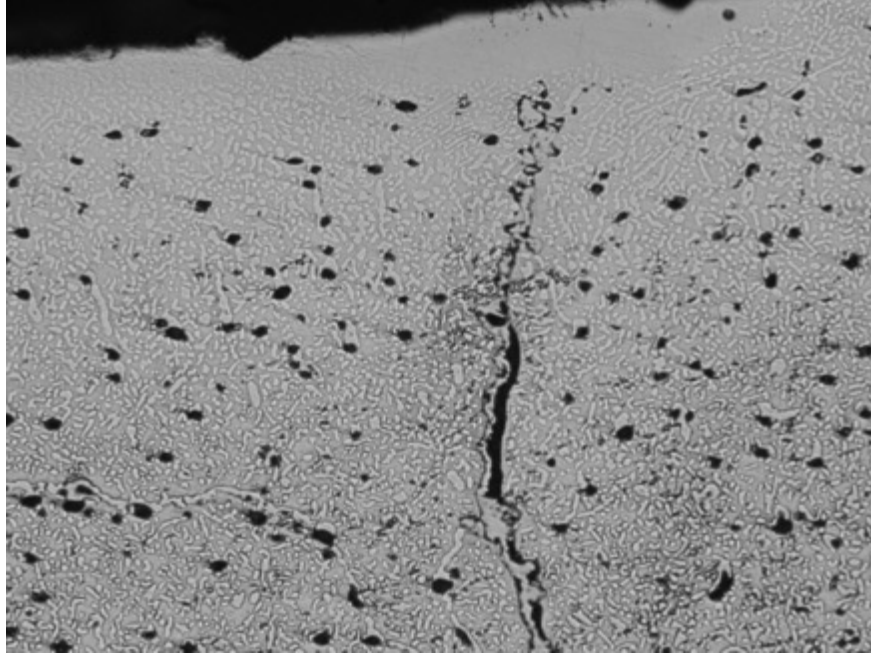


Figure 44: Crack near the surface of the pole

5.1.3.4. Vickers micro-hardness profile

The gradient shown in Figure 41 is most likely a layer due to an excess in carbon which diffused from the atmosphere into the pole during the carburizing processes. This conclusion can be confirmed by a microhardness profile. Carbon concentration in the part is related directly to the hardness of the alloy. The higher the carbon concentration the greater the hardness of the material. Figure 45 presents a significant decrease on the hardness value from the surface to the core of the racking pole.

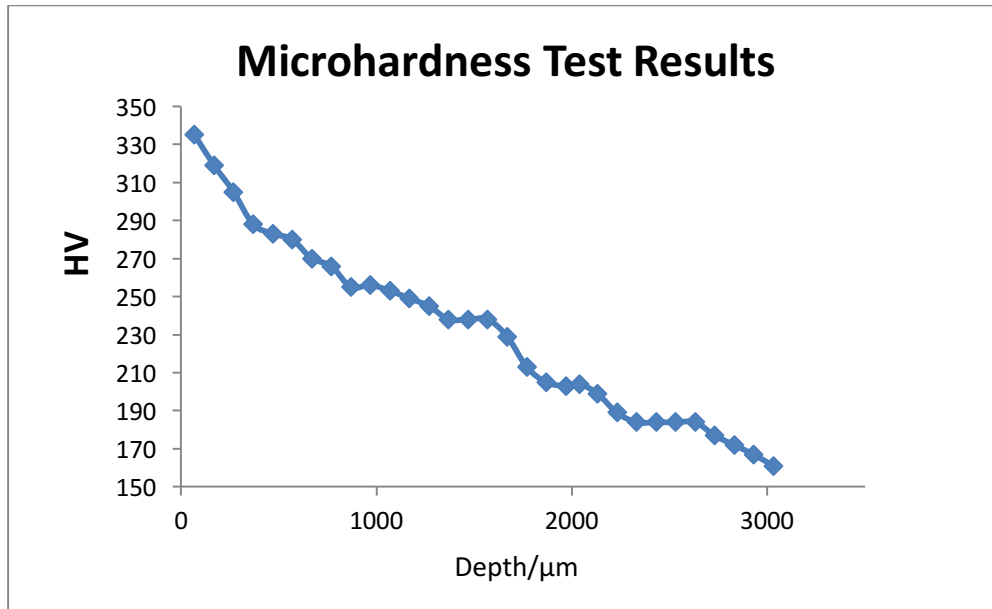


Figure 45: Vickers micro-hardness profile from the surface to the core

5.1.3.5. SEM (Scanning Electron Microscope) and EDS (Electron Dispersion X-ray Spectroscopy) analysis

Figure 46 presents the SEM micrographs from the surface of the part to the interior. Basically, the micrograph of this sample is composed of three obvious parts; the matrix (light grey phase), precipitates (dark grey phase), and black spots. It can be seen that the precipitated secondary phase along the grain boundary and within the grain (the dark grey phase) decreases from the surface to the core. The amount of the black spots also decreases gradually from the surface to the core.

EDS analysis can be used to do the element map. On the EDS map, the brighter area indicates the richer of that element. Therefore, the maps of different elements over the same area can help to determine what phases are present. Figure 47 presents the images from the EDS maps of chromium, carbon, iron, and nickel on the corresponding SEM micrograph of the sample. It can be seen that the precipitates (dark grey phase) are rich of Cr and C, but poor of Fe and Ni, which means they are probably chromium carbide. Based on these images, it is also found that the black spots are the pores.

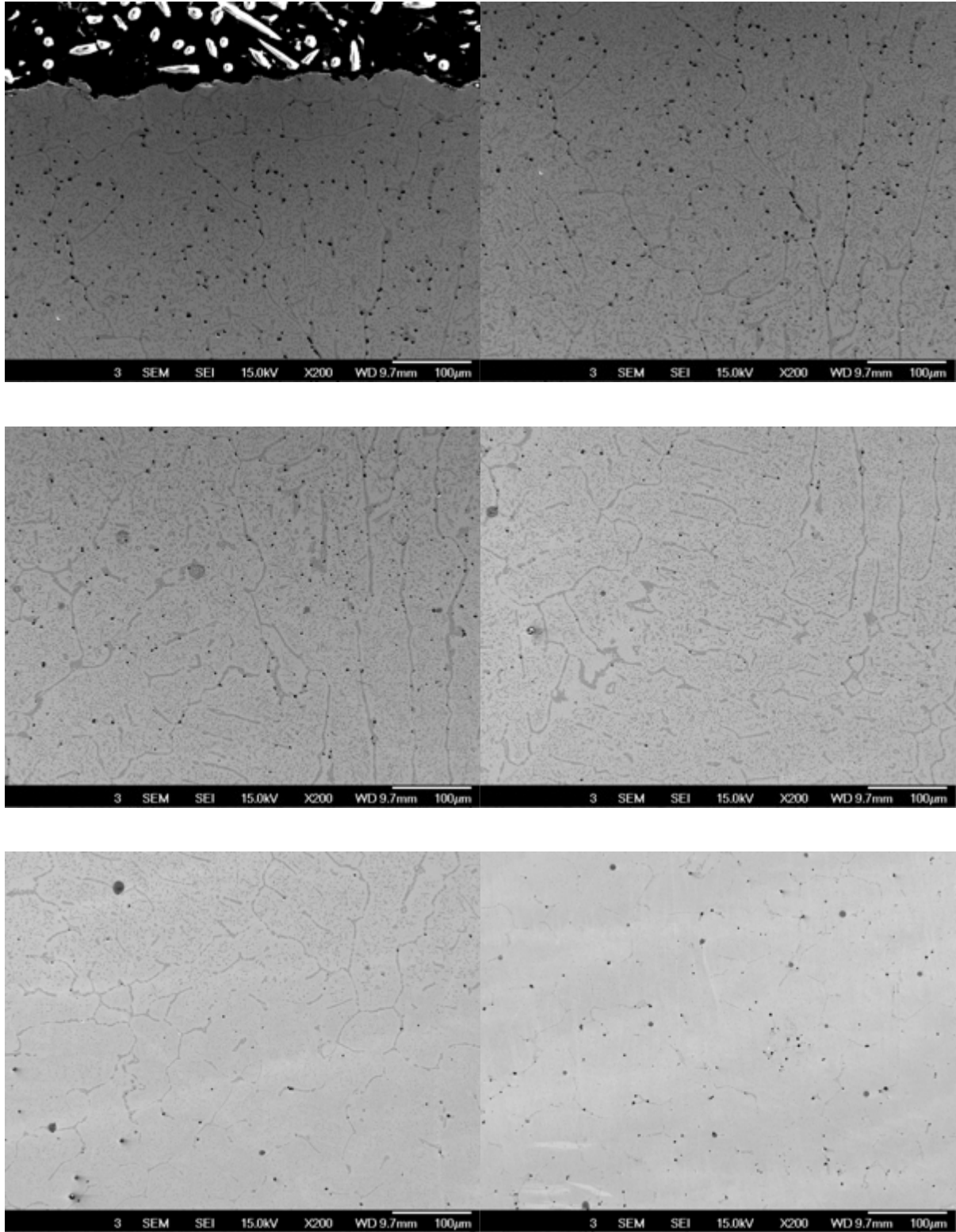
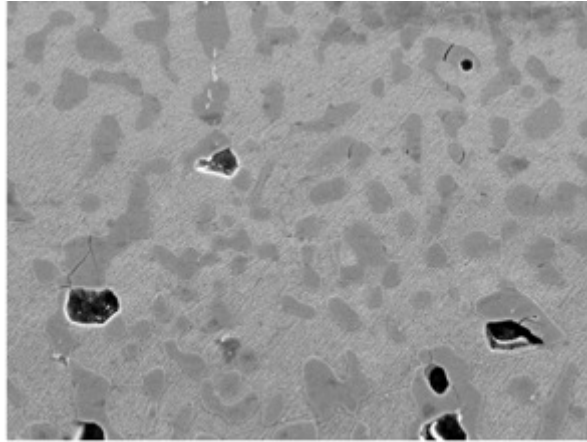
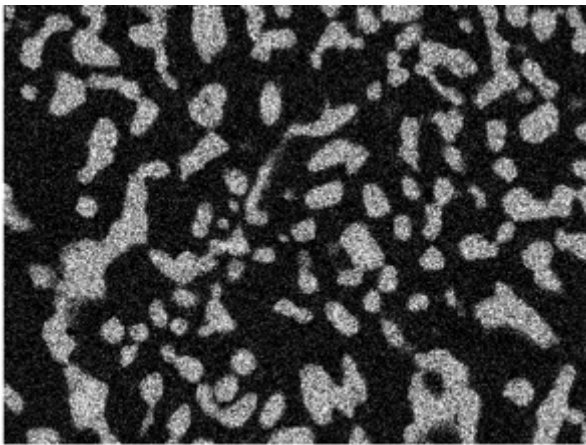


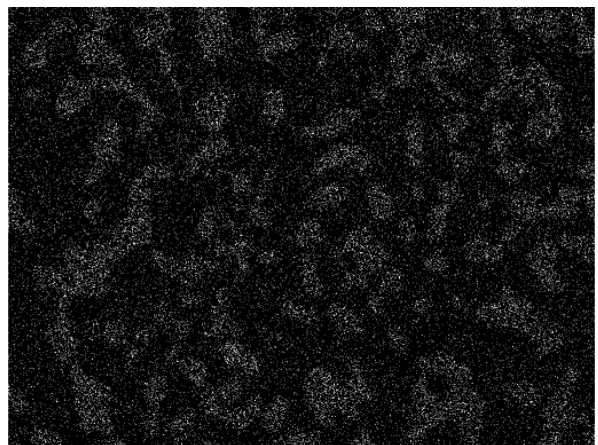
Figure 46: SEM micrographs of sample. Outermost edge (top left) to core (bottom right) of the sample



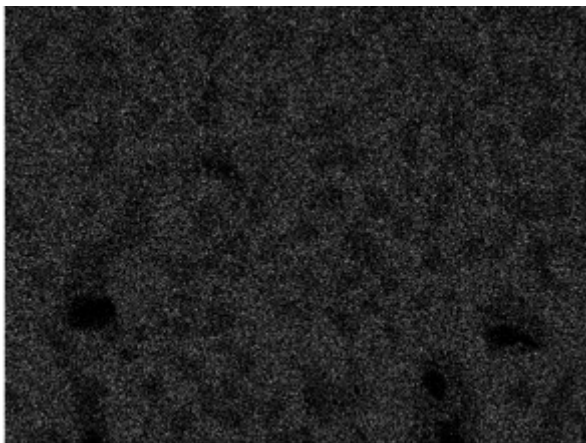
Electron Image 1



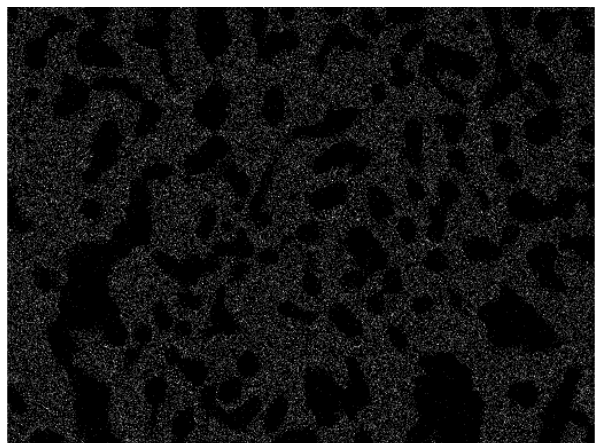
Cr Ka1



C Ka1_2

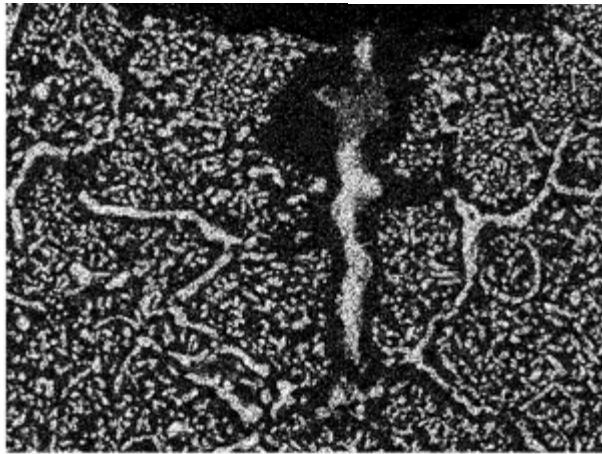
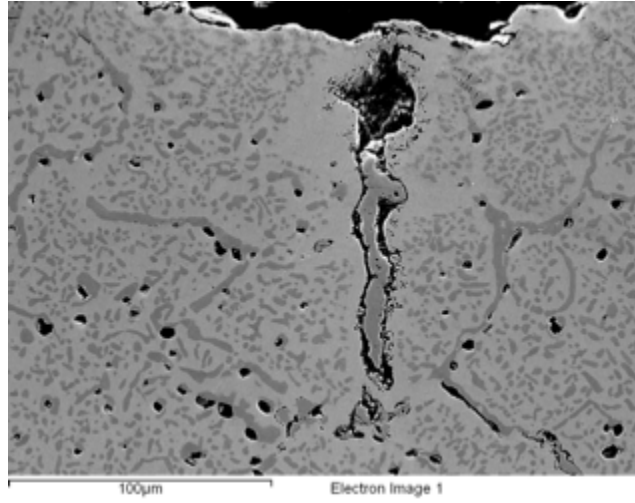


Fe Ka1

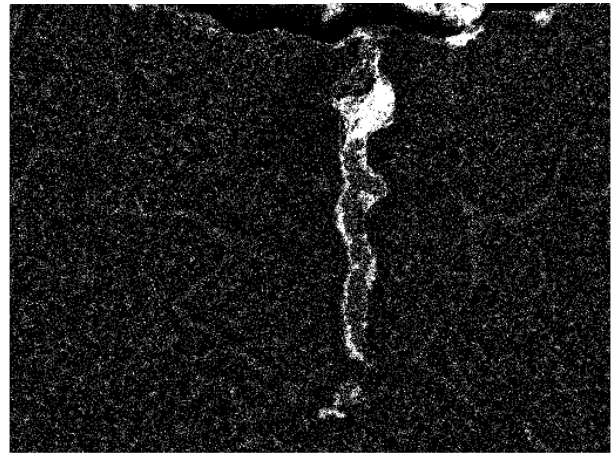


Ni Ka1

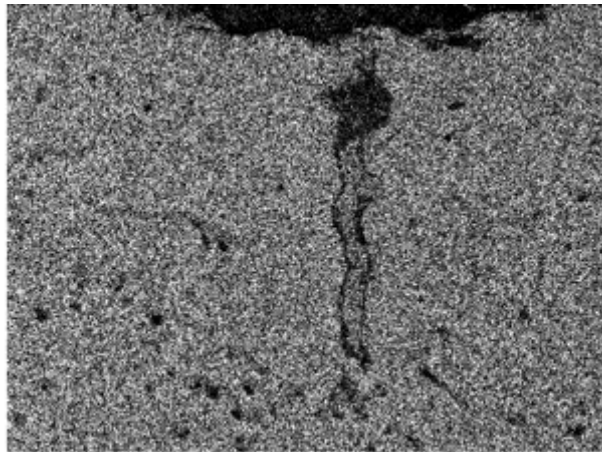
Figure 47: EDS element mapping images of the SEM micrograph without cracking



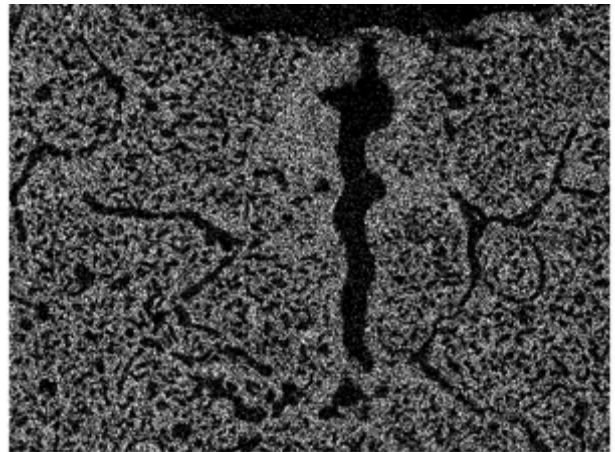
Cr Ka1



C Ka1_2



Fe Ka1



Ni Ka1

Figure 48: EDS element mapping images of the SEM micrograph with cracking

EDS element mapping is also conducted at the crack area near the surface. Figure 48 shows that the crack is formed around a big piece of chromium carbide. And carbon concentration is very high at the top of this crack, while the chromium concentration is lower than that in the typical chromium carbide of this sample.

5.1.3.6. XRD (X-ray Diffraction) analysis

XRD analysis on the surface of the racking pole is made to do the phase identification. Figure 49 shows the XRD diffraction pattern. From the pattern, (Iron Nickel) is identified, which is Fe and Ni rich austenite phase. The XRD result is in good agreement with the literature review, the matrix of RA330 alloy austenitic face-center-cubic.

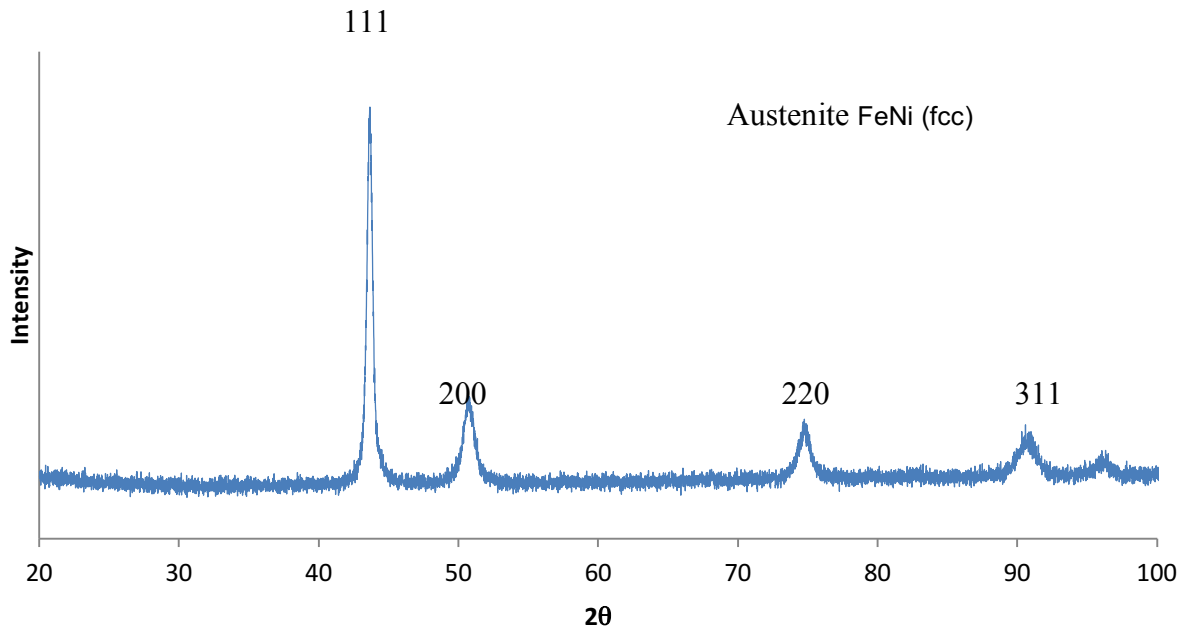


Figure 49: XRD pattern of the surface scan for the racking pole (Cu tube)

5.1.3.7. Phase evolution prediction from computational thermodynamics

Thermo-Calc [32], a powerful and flexible software package developed for performing various kinds of thermodynamic and phase diagram calculations, can be used to predict the phase evolution in racking poles with the carbon concentration increasing.

Figure 50 calculated from Thermo-Calc, which shows the mole fraction of each phase in RA330 alloy as a function of carbon concentration. It can be seen that fcc (Fe and Ni rich austenite phase) is the main phase in this alloy, which is in good agreement with the XRD result. With the carbon concentration increasing, chromium carbides form. The chromium carbide evolves from Cr₂₃C₆ to Cr₇C₃ from low carbon concentration to high carbon concentration. When the carbon concentration is high enough, Cr₇C₃ partially decomposes into graphite.

By comparing with the SEM and EDS analysis, it is evident that the chromium carbides increases from the core to the surface with the carbon concentration increasing. At the surface of the pole the carbon concentration is very high and some chromium carbides decompose to form graphite, which is the origin of the cracking. The failure mode of this racking pole is thus determined to be the metal dusting from excess carburizing.

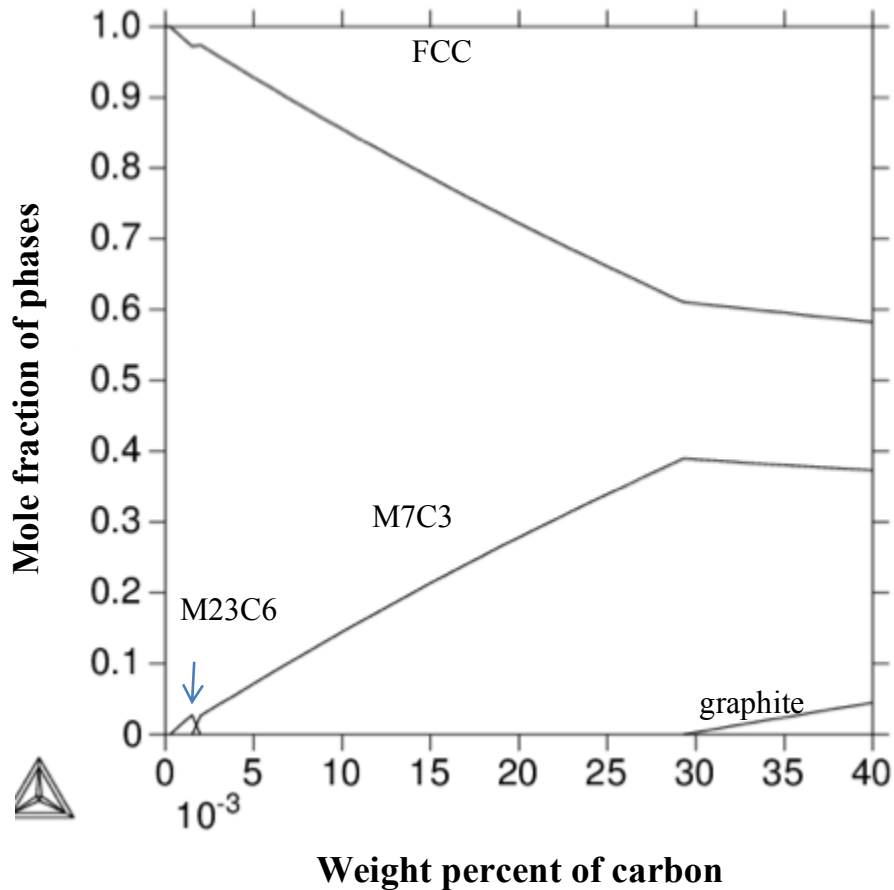


Figure 50: The phase evolution in RA330 with carbon concentration increasing at 1700°F (927°C)

5.1.3.8. Discussion

Although HT has good carburization resistance it is still evident that this particular HT sample failed due to excess carburizing. Carbon adsorbs and diffuses into the racking pole from the high carbon potential atmosphere to form the chromium carbides. These chromium carbides distribute intergranularly and within the grains, the intergranular chromium carbides are much coarser than those within the grains (Figure 46). The further adsorption and diffusion of carbon leads to the coarsening of the chromium carbides with the consumption of the matrix. And these carbides transform to graphite when the carbon concentration is high enough, which leads to the formation of the cracking. Therefore, to improve the lifetime of the racking pole the carburizing resistance of the alloy need to be enhanced.

Some research has been done to investigate the advantage of replacing the HT cast alloy by RA330® wrought alloy. It is found that the average service time is improved from 8000 hours to more than 15000 hours after using RA330® to replace HT for rotary resort in carburizing furnace [33]. Although the chemical compositions of cast HT and wrought RA330® are similar (Table 12) the physical properties of these two alloys are very different. The fine grain, smooth surface and normally free of internal and external defects in wrought alloy can greatly improve the thermal fatigue resistance of this material.

	C	Mn	Si	Cr	Ni	Fe
HT	0.5	0.9	1.7	17	35	balance
RA330®	0.05	1.5	1.2	19	35	balance

Table 12: Comparison of the nominal compositions of HT and RA330® [33]

Aluminizing the racking pole could enhance corrosion resistance, carburization resistance, and creep. Aluminizing is based on the formation of intermetallic compounds of the Ni-Al system that act as a reservoir of aluminum for maintaining a protective Al₂O₃ scale on the material surface during high temperature service. [34]

5.1.4. Failure analysis of failed mesh belt (Gas carburization furnace)

After contacting with the member companies, some failed components have been received. The characterization work started to analyze the failure mechanism of these components.

5.1.4.1. New and failed mesh belts from GKN

GKN Sinter Metals provided a section of failed mesh belt that is made of 314 stainless steel. The chemical composition of 314 stainless steel is shown in Table 13. A section of new mesh belt is also provided to compare with the failed one (Figure 51 and Figure 52). The failed mesh belt was used in the furnace whose temperature was set to 2100°F maximum steady and the atmosphere was nitrogen/endogas with some natural gas as needed.

	C	Si	P	Mn	Cr	Ni	Fe
Min (wt.%)	0.25	1.5	0.045	2.0	23.0	19.0	bal
Max (wt.%)	-	3.0	-	-	26.0	22.0	bal

Table 13: Chemical composition of 314 stainless steel

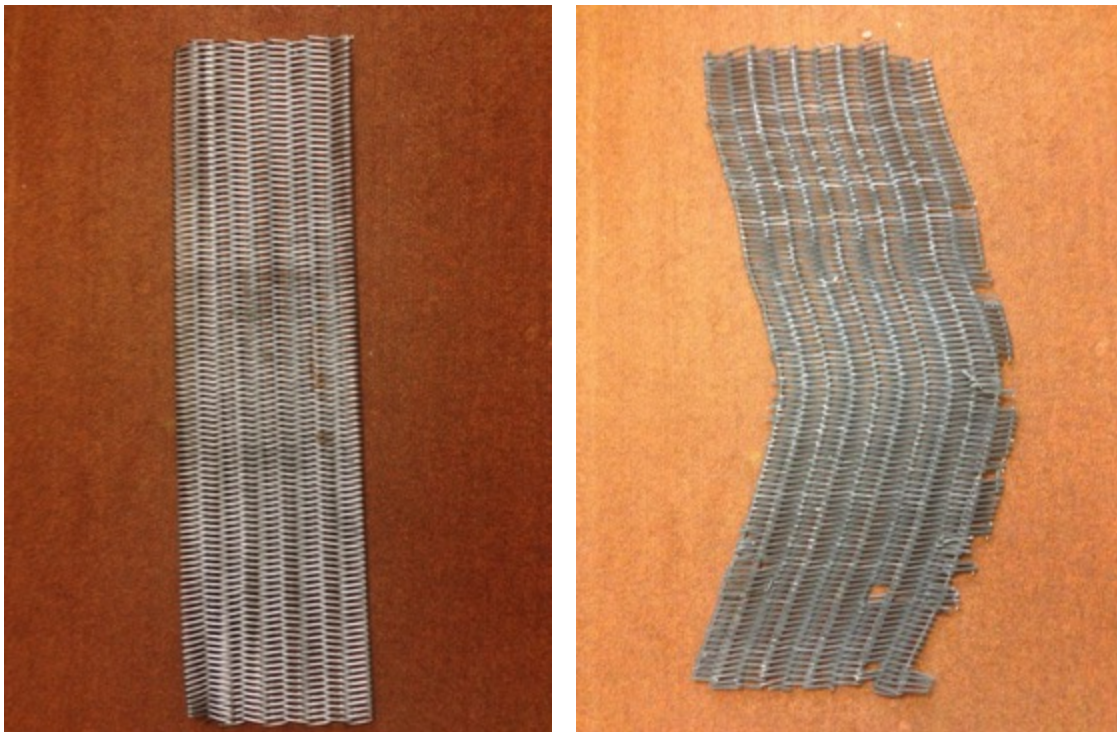


Figure 51. Received new (left) and failed (right) mesh belts from GKN

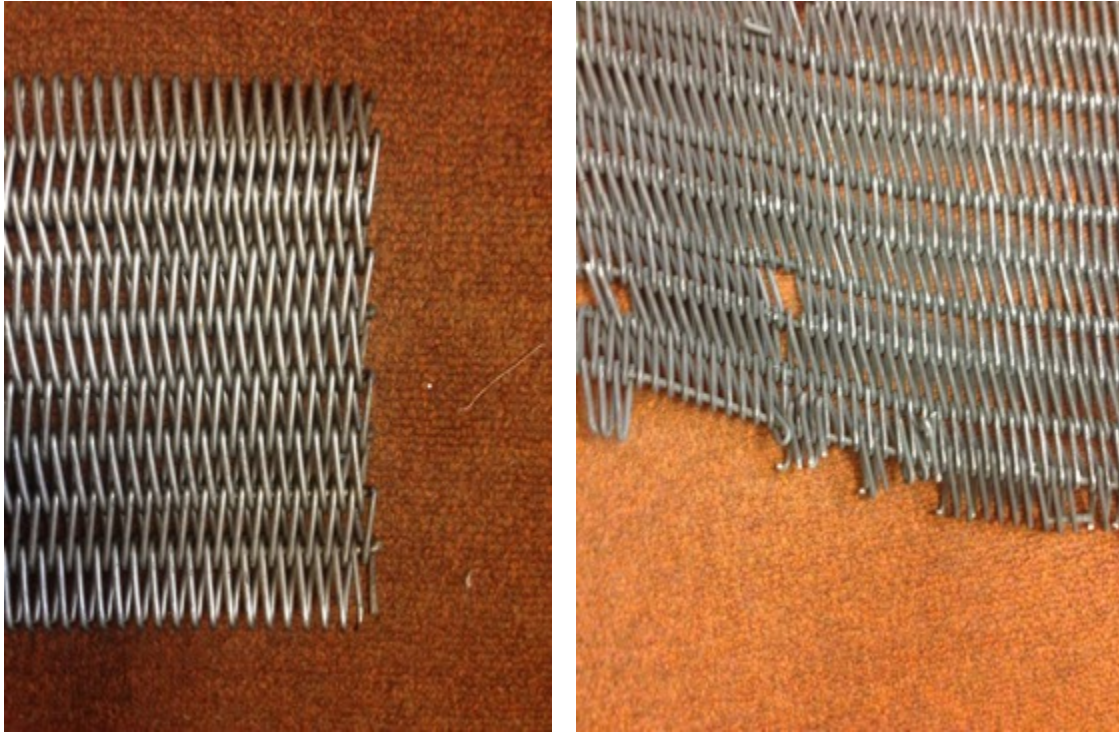


Figure 52. New (left) and failed (right) mesh belts from GKN with a closer look

Small parts of spiral were cut from the failed and new mesh belts separately and mounted in cross section to make the samples. These two samples were ground down to 1200 grit and then polished. The sample from the failed mesh belt was etched easily by 2% nital solution. However, the sample from the new mesh belt cannot be etched by nital. The electro etching with oxalic acid solution is used to etch the sample from the new mesh belt.



Figure 53. Spirals cut from new (left) and failed (right) mesh belts and mounted in cross section

Figure 54 presents cross section optical micrographs of spirals from new and failed mesh belts. And Figure 55 shows the Cross section SEM micrographs of spirals from new and failed mesh belts. It can be seen that the microstructure of the new spiral is uniform and the secondary phase forms along the grain boundary and within the grain (the dark grey phase in the SEM micrograph of failed spiral) after being used.

The elemental analysis by EDS has been done on the cross section of spirals from new and failed mesh belts. Figure 56 show that both of samples contain Fe, Ni, Cr, Si, and C, which is in good agreement with the composition of 314 stainless steel (Table 13). The Au and Pd on the spectrum of new spiral are due to the sputter coating, which covers the sample with a thin layer of conducting gold/palladium (Au/Pd) alloy by sputter deposition process. By comparing the two spectrums, the amount of Fe, Ni, Cr, and Si are similar to each other. And the amount of carbon on the spectrum of failed spiral is much higher than that on the spectrum of new spiral.

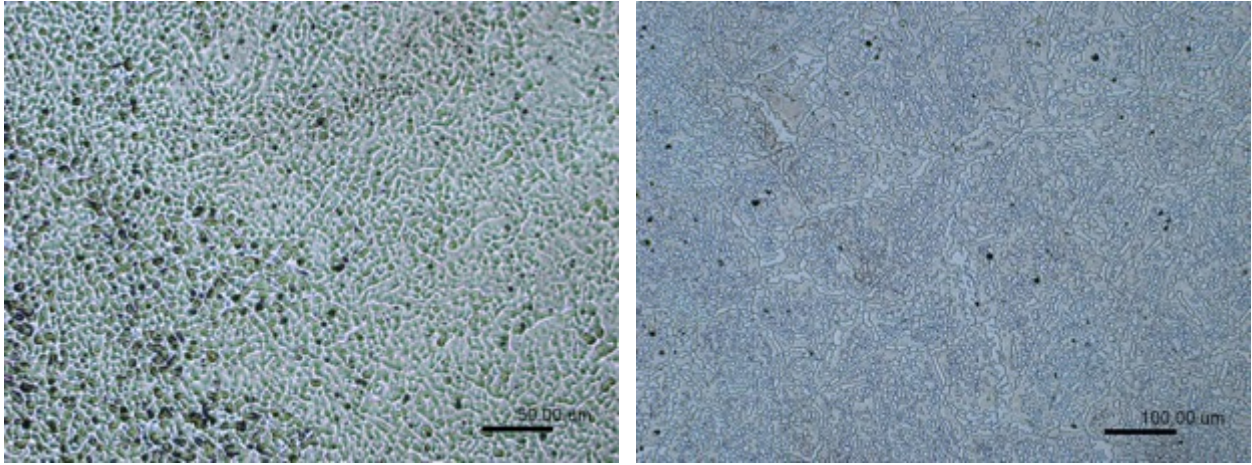


Figure 54. Cross section optical micrographs of spirals from new (left) and failed (right) mesh belts

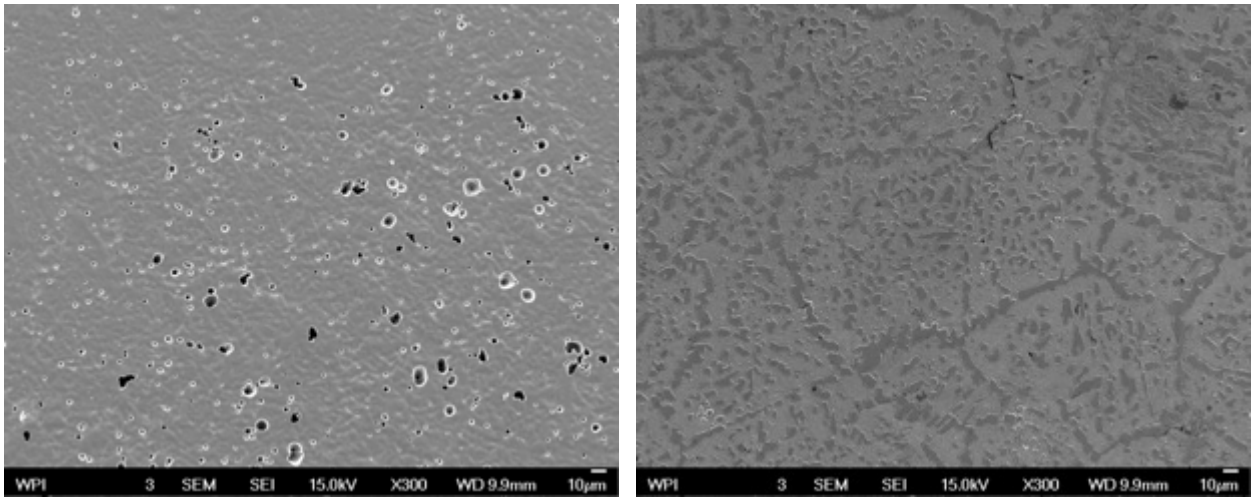


Figure 55. Cross section SEM micrographs of spirals from new (left) and failed (right) mesh belts

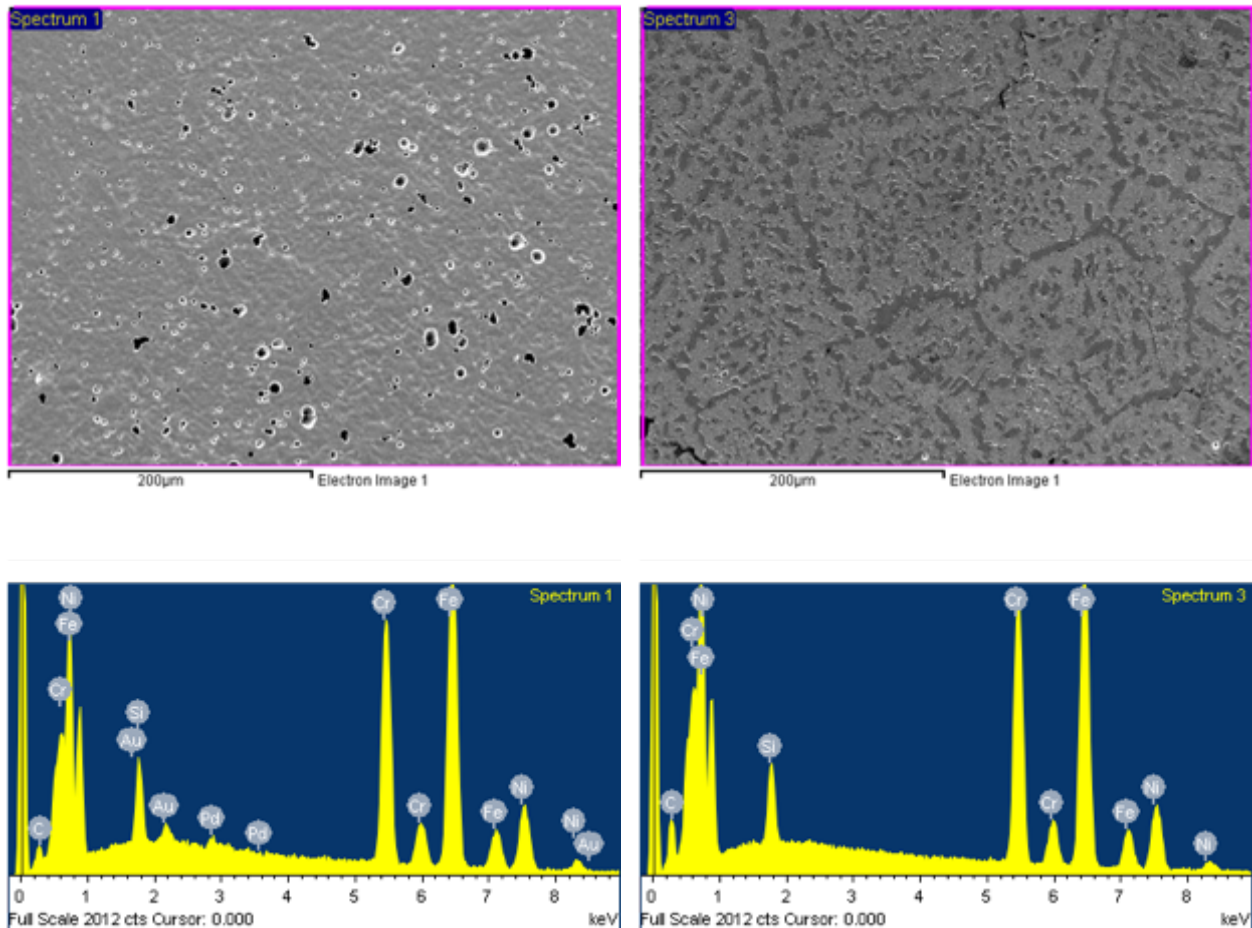
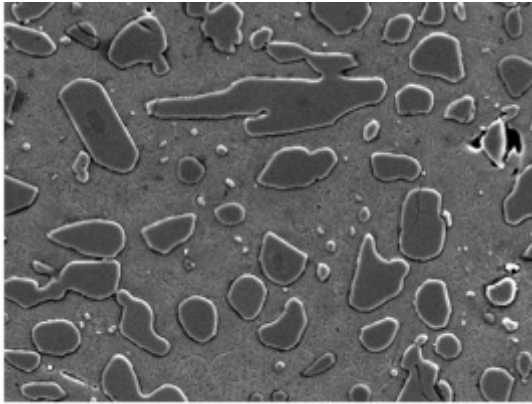


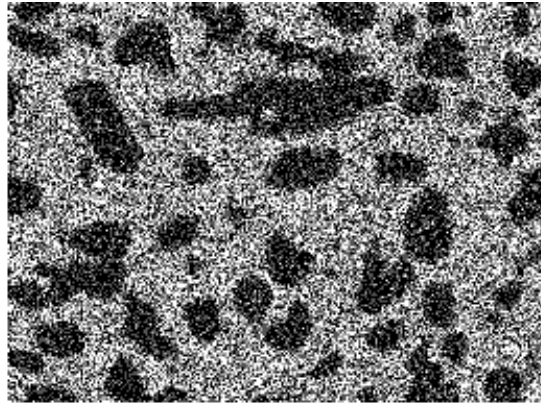
Figure 56. Elemental analysis by EDS on the spirals from new (left) and failed (right) mesh belts

EDS analysis can be used to create the elemental map. On the EDS map, the brighter area indicates the richer of that element. Therefore, the maps of different elements over the same area can help to determine what phases present there. Figure 57 presents the images from the EDS maps of silicon, chromium, carbon, iron, and nickel on the corresponding SEM micrograph of the spiral from the failed mesh belt. It can be seen that the secondary phase (dark grey phase) are rich of Cr and C, but poor of Fe, Si and Ni, which means the secondary phase is chromium carbide.

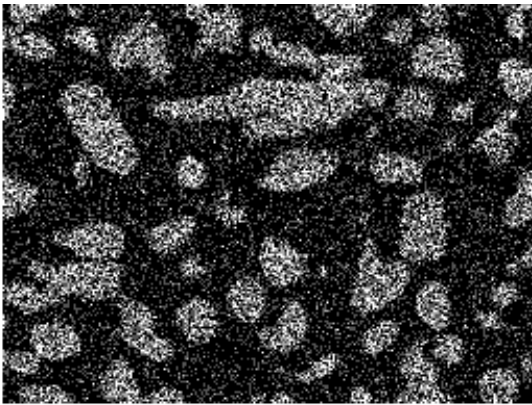
With the carbon diffusing into the mesh belt, chromium in the steel reacted with carbon to form the chromium carbide, which decreased the corrosion resistance and increased the embrittlement of the mesh belt. The failure of the mesh belt caused by the extreme uptake of carbon from the furnace atmosphere.



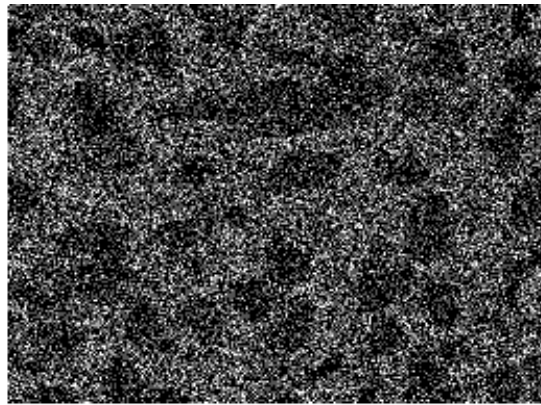
Electron Image 1



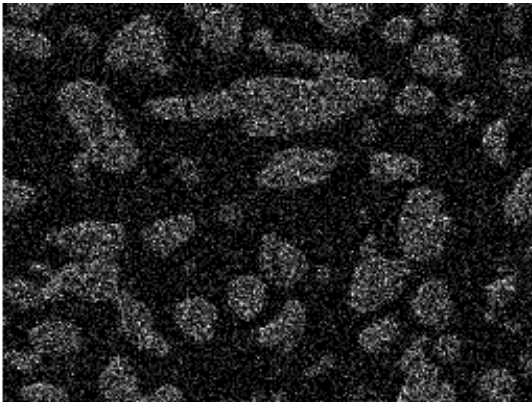
Si Ka1



Cr Ka1



Fe Ka1



C Ka1_2



Ni Ka1

Figure 57. EDS element maps on the cross section of the spiral from the failed mesh belt

5.2. Life Extension of Furnace and Fixture Alloys by aluminizing in Vacuum Carburizing Atmospheres

Anbo Wang¹, R. D. Sisson, Jr.^{1}*

¹Center for Heat Treating Excellence, Worcester Polytechnic Institute, Worcester, Massachusetts, 01609, U.S.A

**Email: sisson@wpi.edu*

To be submitted to: Journal of Materials Processing Technology

5.2.1. Aluminizing

Alcoa Howmet in Branford, CT has done the aluminizing for us. Samples were coated in a static gas phase system at 2000F for 5 hours. Chromium aluminum source material (70%Cr/30%Al) and ammonium fluoride granules were used in the system. The coating chamber was purged with argon until a dew point of -40F or better was met, then the argon is shut-off to the coating chamber (hence static system) and heating begins. The diffused aluminum-rich layer must be 0.001-0.003 inch, unless specified differently.

5.2.2. Racking poles from Sikorsky

Four new racking poles were provided by Sikorsky (Figure 58). These poles are made of RA330 and welded for assembly. Table 14 shows the Chemical composition of RA330®. Two of poles were sent out to Dirats Laboratories in Westfield, MA to cut 5mm thick slice off the top of the pole by using the wire EDM (Electric discharge machining) (Figure 59).



Figure 58. Received racking poles from Sikorsky



Figure 59. Sample cut from the racking pole by wire EDM



Figure 60 Aluminized racking poles

Table 14: Chemical composition of RA330® [15]

Ni	Cr	Fe	Si	C	Mn
35	19	43	1.25	0.05	1.5

5.2.2.1. Characterization of as-received racking pole

The cut pieces were characterized by optical microscope, SEM and XRD. The results were compared with the characterization results of aluminized, used unaluminized and used aluminized samples in the future.

The sample was cut and mounted as parallel to the surface and cross section separately (Figure 61). The samples were ground down to 1200 grit and then polished.

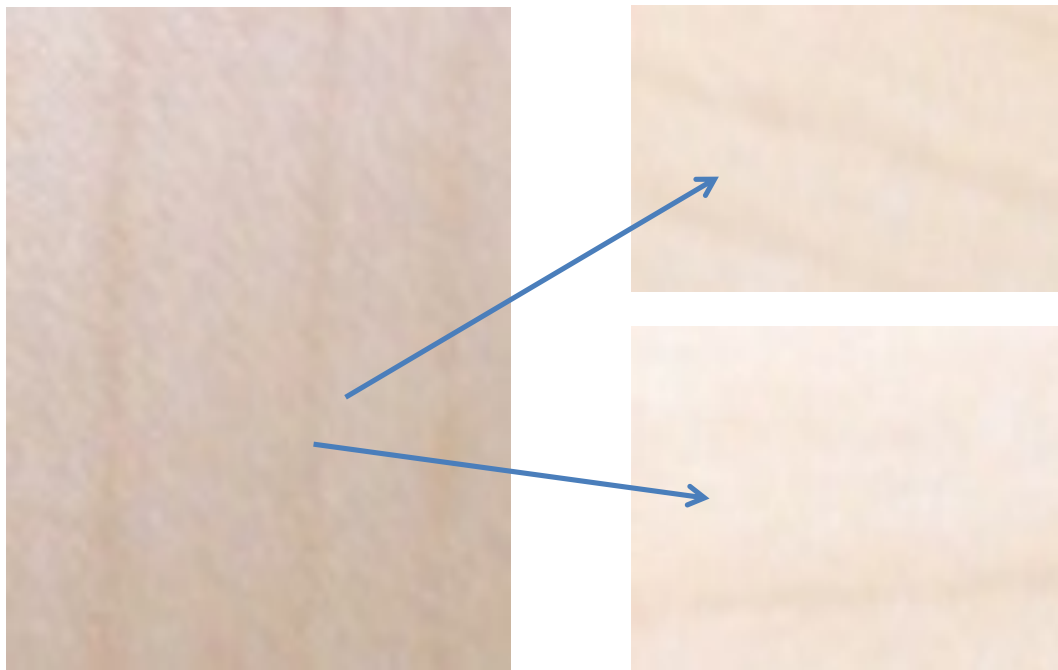


Figure 61 Cut pieces from received racking pole (left), parallel to surface mounted sample (right top), and cross section mounted sample (right bottom)

Electro-etching with oxalic acid solution is used to etch the samples. Oxalic acid is put into the water to make the solution. Keep adding oxalic acid and stirring the solution at room temperature until the solution is supersaturated (14.3g/100ml at 25°C). Then the saturated oxalic acid solution is used as electrolyte. Buehler ElectroMet® 4 (Figure 62) was used for the electro-etching, the voltage is adjusted to make the direct electric current equal 300mA. The sample was connected to the anode and etched for one minute. Figure 64 show the optical micrographs from the parallel to the surface sample and cross section sample separately.

Figure 65 shows the SEM image and EDS spectrum of the parallel to the surface sample, in which Fe, Cr, Ni, C, Si, and Mn were detected. This result is in good agreement with the alloy elements in RA 330.



Figure 62. Buehler ElectroMet® 4

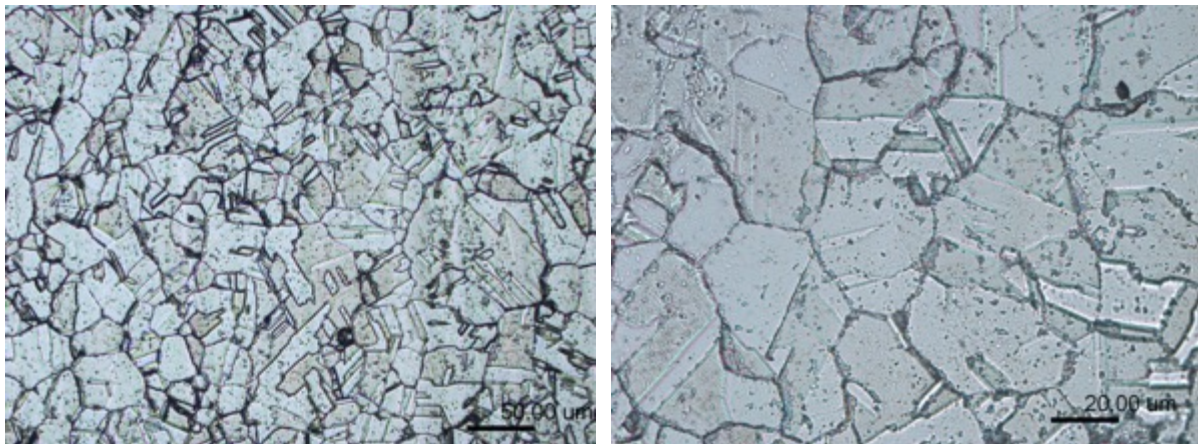


Figure 63. Parallel to surface optical micrographs RA330

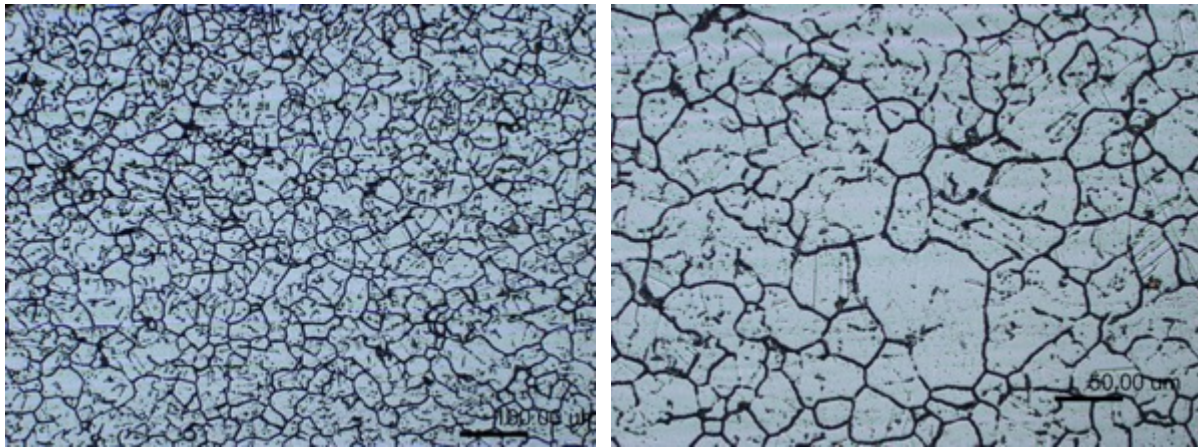


Figure 64. Cross section optical micrographs RA330

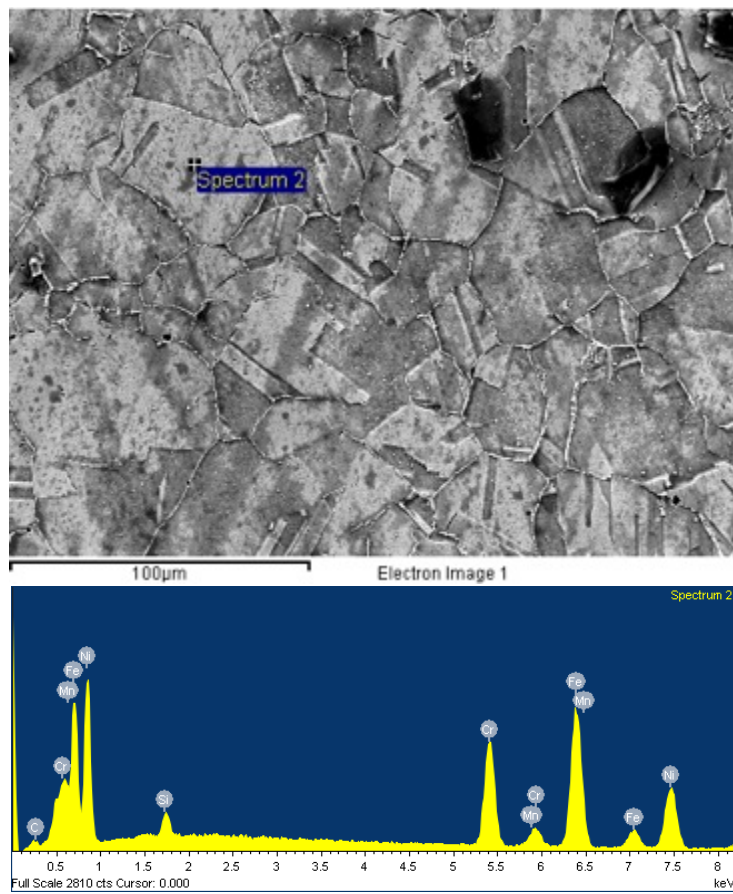


Figure 65. SEM image of parallel to the surface sample (top) and its EDS spectrum (bottom)

5.2.3.1. Characterization of exposed racking poles

5.2.3.1.1. Racking poles- Unaluminized

Racking poles are made of RA330 alloys. The aluminized and unaluminized racking poles were tested at Sikorsky from December 2nd to June 2nd. CHTE members have decided to cut ½” from all four pieces for metallographic examination. The racking poles will be returned to Sikorsky. Four new racking poles were provided by Sikorsky (Figure 58). These poles were made of RA330 and welded for assembly. Table 14 shows the Chemical composition of RA330®. Four poles were sent out to Dirats Laboratories in Westfield, MA to cut ½” thick slice off the top of the pole by using the wire EDM (Electric discharge machining) (Figure 67).



Figure 66. Received racking poles from Sikorsky



(a)



(b)



(c)



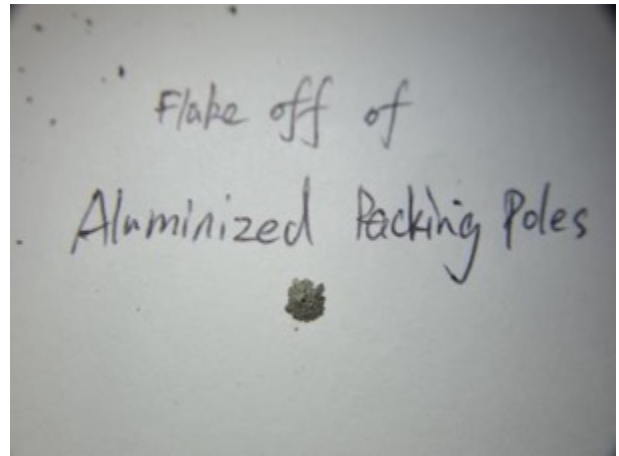
(d)

Figure 67. Exposed Aluminized Racking poles (a); Unaluminized Racking poles (b); Sample cut off from aluminized poles (c); Sample cut off from unaluminized poles (d)

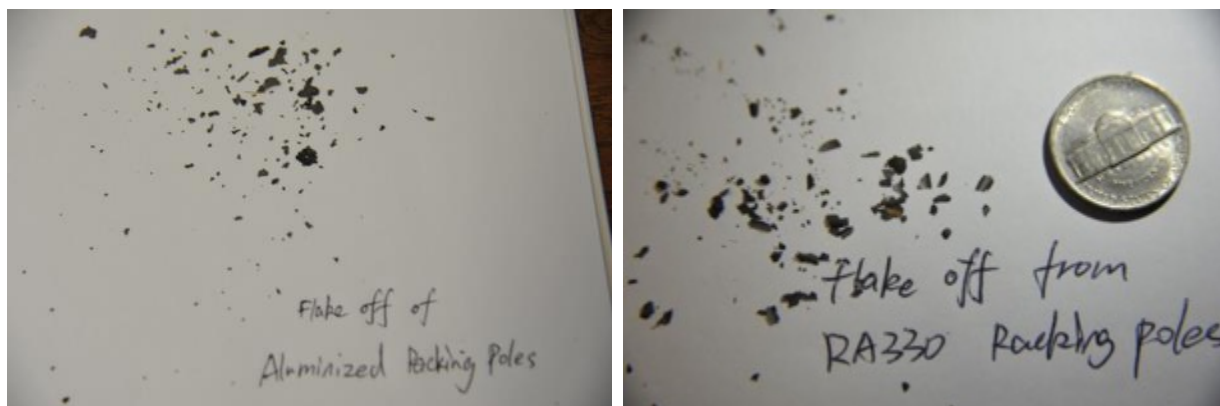
After 6 months service in the carburizing furnace, Figure 67 shows the aluminized Racking poles (a), unaluminized Racking poles (b). The “flake offs” were removed from the alloys, and analyzed by XRD and SEM. Numerous complex carbon flake offs were found on racking poles, shows on Figure 68. The result will be present on the flake off characterization chapter.



(a)



(b)



(c)

(d)

Figure 68. Photographs of aluminized racking poles (a); Flake offs removed from aluminized racking poles (b),(c); Flake offs removed from unaluminized racking poles (d)

5.2.3.1.1.1. Preliminary metallographical analysis

RA330 is a patented alloy from Rolled Alloys designed specifically for the heat treat industry. As same as fan blade, the racking poles also made of RA330 which is an austenitic heat and corrosion resisting alloy offering oxidation and carburization resistance to 1148°C. RA330 also add 1.25% Silicon to enhance the oxidation and anti-carburizing properties. The intended use of racking poles was a structural support inside a furnace. The kinetics process of racking poles is similar to fan blades. Preliminary metallographical analysis indicated that metal dusting which decrease the corrosion resistance and increase the embrittlement of the racking poles. However, further kinetics analysis is underway.

5.2.3.1.1.2. Cross section and surface analysis

Figure 69 shows a cross section surface of unaluminized racking poles in the as etched condition showing spheroidal morphology. Clearly, the cross section surface exhibited a two-phase structure in the core area i.e. austenite matrix with chromium carbides at the grain boundaries. In the core, carbides were observed only at the grain boundary.

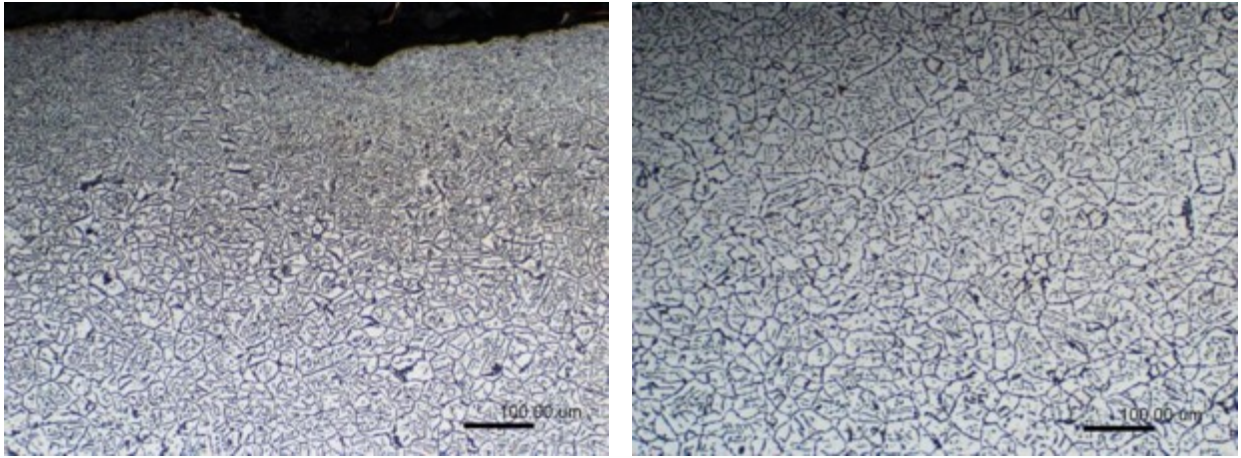


Figure 69. Optical photomicrographs of RA330 raking poles (etched with 10% oxalic acid)

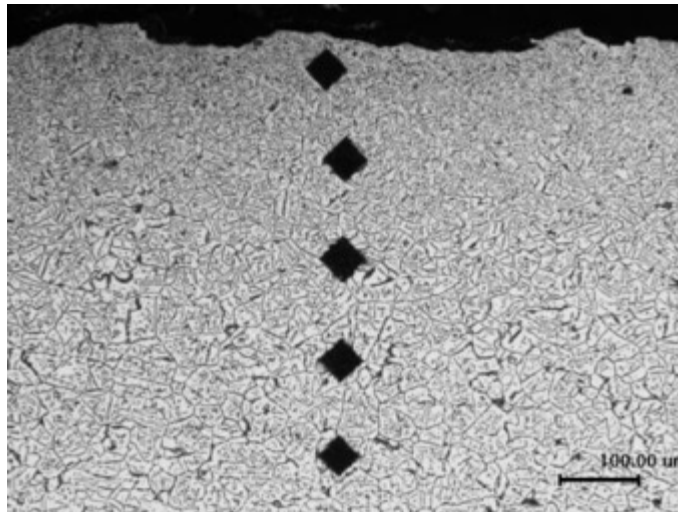


Figure 70. Optical photomicrographs of RA330 raking poles (etched with 10% oxalic acid)

A thin layer of affected region (approximately $50\mu\text{m}$) was identified at the surface. However, Table 15 shows a micro-hardness profile with relatively uniform distribution from surface to core. The reason for that might due to relatively short service time of carburizing. Although the diffusion coefficient of RA330 is still unknown, but the 6 months of carburizing are still considered as insufficient for significant difference in carbon content which could leading to hardness gradient along the cross section.

Hardness profiles:

Distance from surface	Hardness (HV)
50um	125.9
150um	106.0
200um	102.0

250um	110.3
300um	125.2

Table 15. Micro-hardness profiles of RA330 cross section

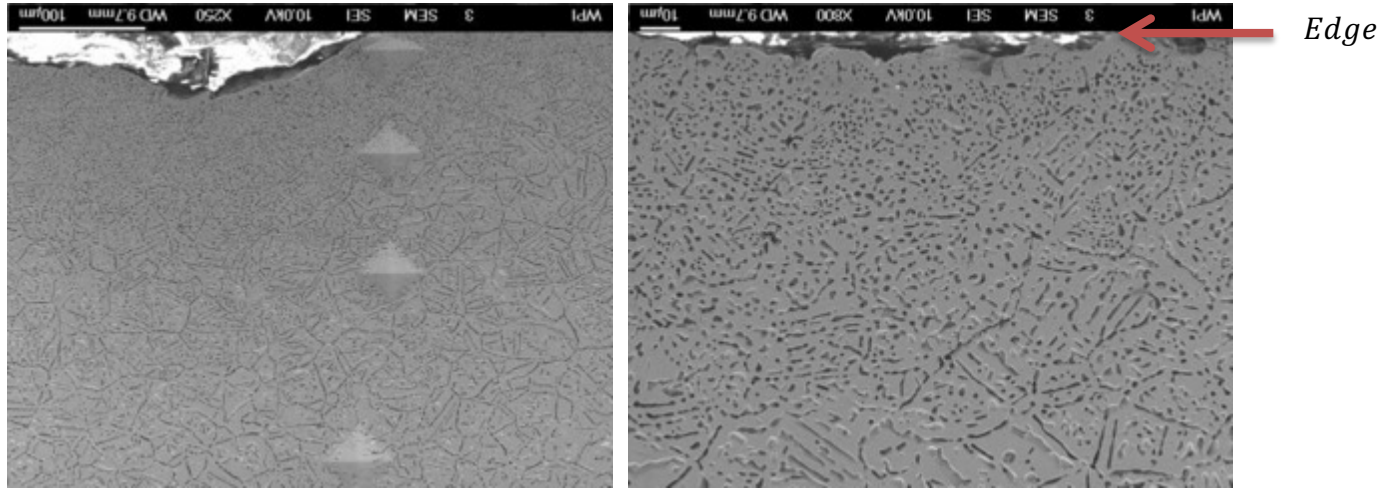


Figure 71. SEM cross section photomicrographs of RA330 at the edge etched with 10% oxalic acid

Figure 71 shows the cross section of racking poles, respectively. Sigma phase was not observed, which could cause the embrittlement of alloys. Obviously, the affected area was carburized more severely than core area.^[21] The morphology of affected area was identified as spherical. Figure 72 shows the spheroidal secondary phases within the grain boundaries on an approximately homogenous matrix.

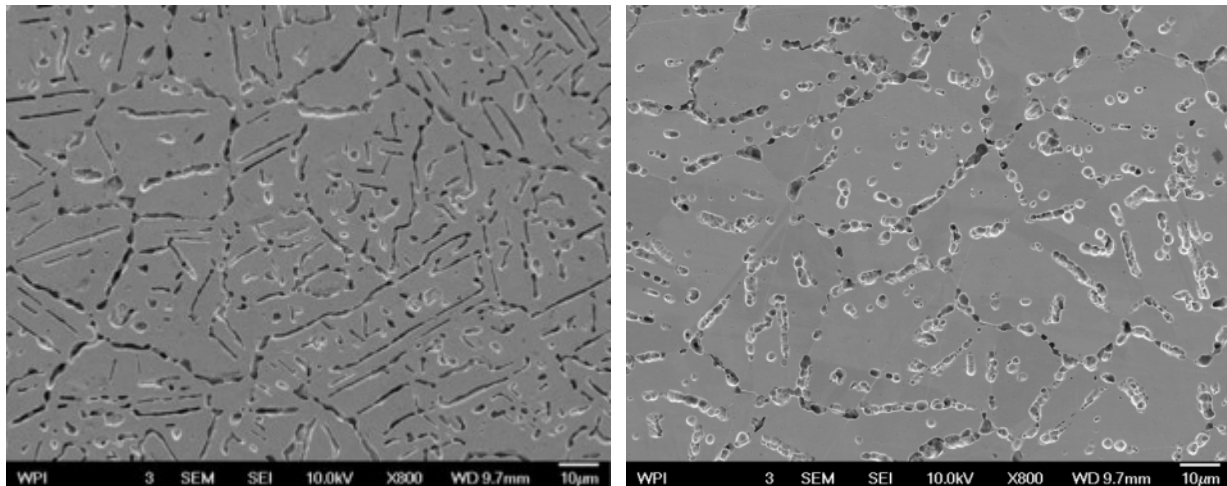


Figure 72. SEM cross section photomicrographs of RA330 at the core etched with 10% oxalic acid

Backscattered electrons photomicrographs show the secondary phase at grain boundaries. Figure 57 shows the similar morphology by secondary electrons SEM.

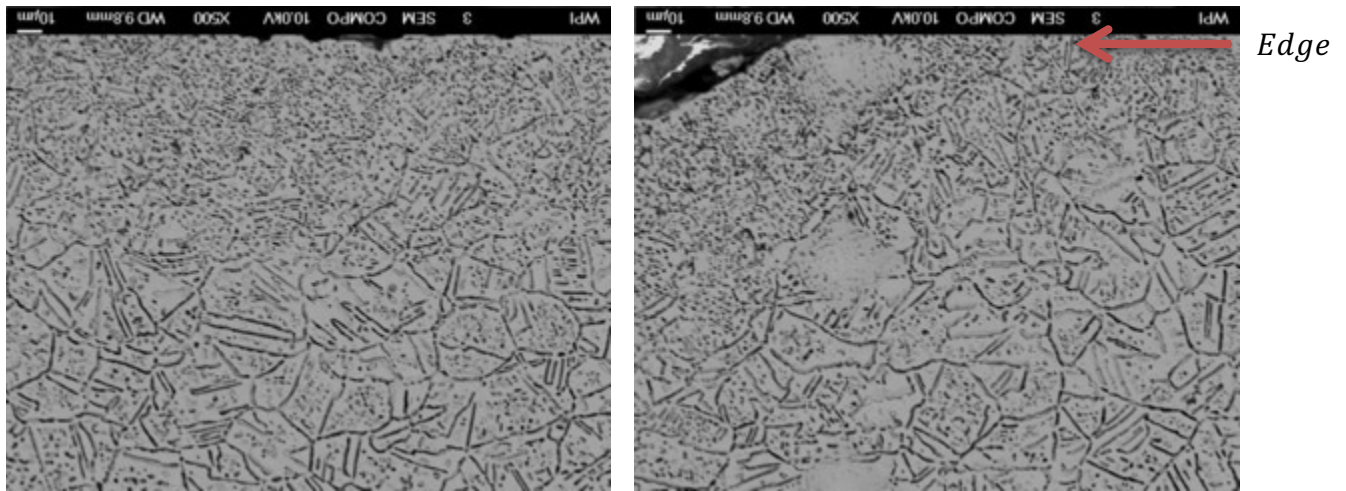


Figure 73. Backscattered electrons cross section photomicrographs of RA330 at the edge etched with 10% oxalic acid

Figure 74 shows the oriented lamellar morphology secondary phases within the grain boundaries at the core of cross section.

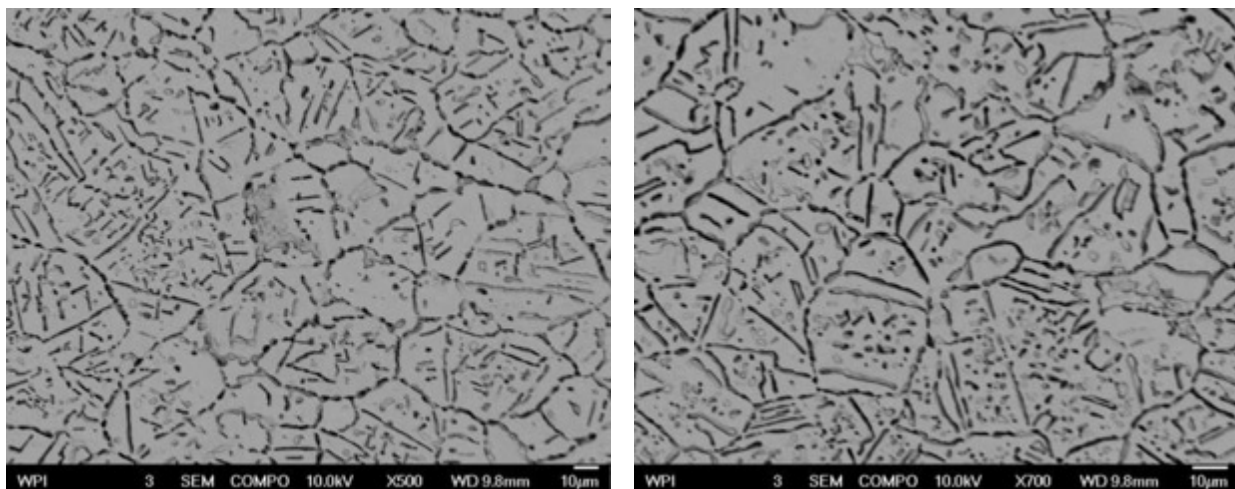


Figure 74. Backscattered electrons cross section photomicrographs of RA330 at the core etched with 10% oxalic acid

Figure 74 presents the cross section images of the racking poles. It can be seen that the matrix (light grey phase) are rich of Fe and Ni, but low of Cr and C, which indicate that the phase is an austenite.

The elemental analysis by EDS has been conducted on the cross section. Figure 75 shows that the samples contain 43.64%Fe, 48.89%Ni, 6.27%Cr, 1.19%Si, which is in good agreement with the composition of austenite phase.

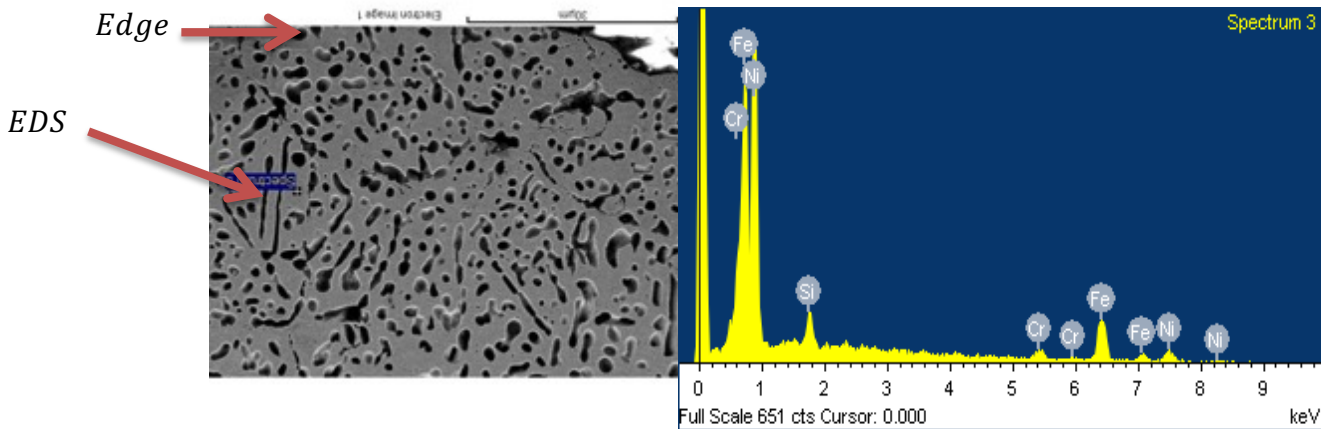


Figure 75. Elemental analysis by EDS on the edge of RA330

The elemental analysis by EDS was conducted on the secondary phase's region. Figure 76 shows that the samples contain 25.30%Fe, 17.05%Cr, 35.17%O, 22.47%C, which is in good agreement with the chromium carbides.

Figure 76 shows the cross section SEM microphotographs of the racking poles. It can be seen that the secondary phase (black phase) are rich of Cr and C, but low of Ni and Fe, which indicate that the phase is chromium carbides.

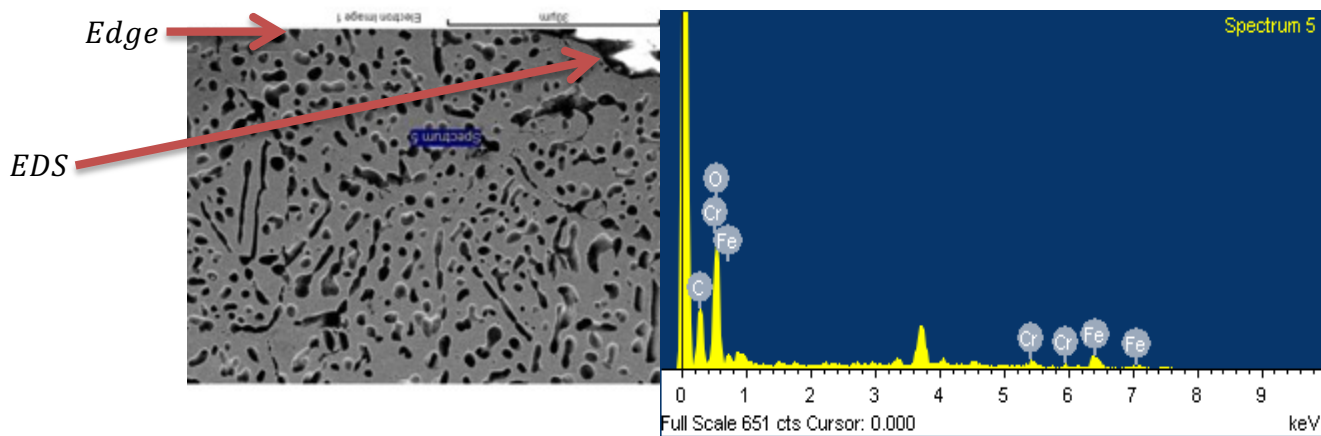


Figure 76. Elemental analysis by EDS on the edge of RA330

The result of XRD analysis of racking poles on cross section was shown in Figure 77. Austenite phase was identified. No chromium carbides were detected may due to the very low carbon concentration (0.05%) on the core area of cross section. Copper mounting material was used, so the copper phase was identified in the Figure 77. The unidentified peak was still being investigated.

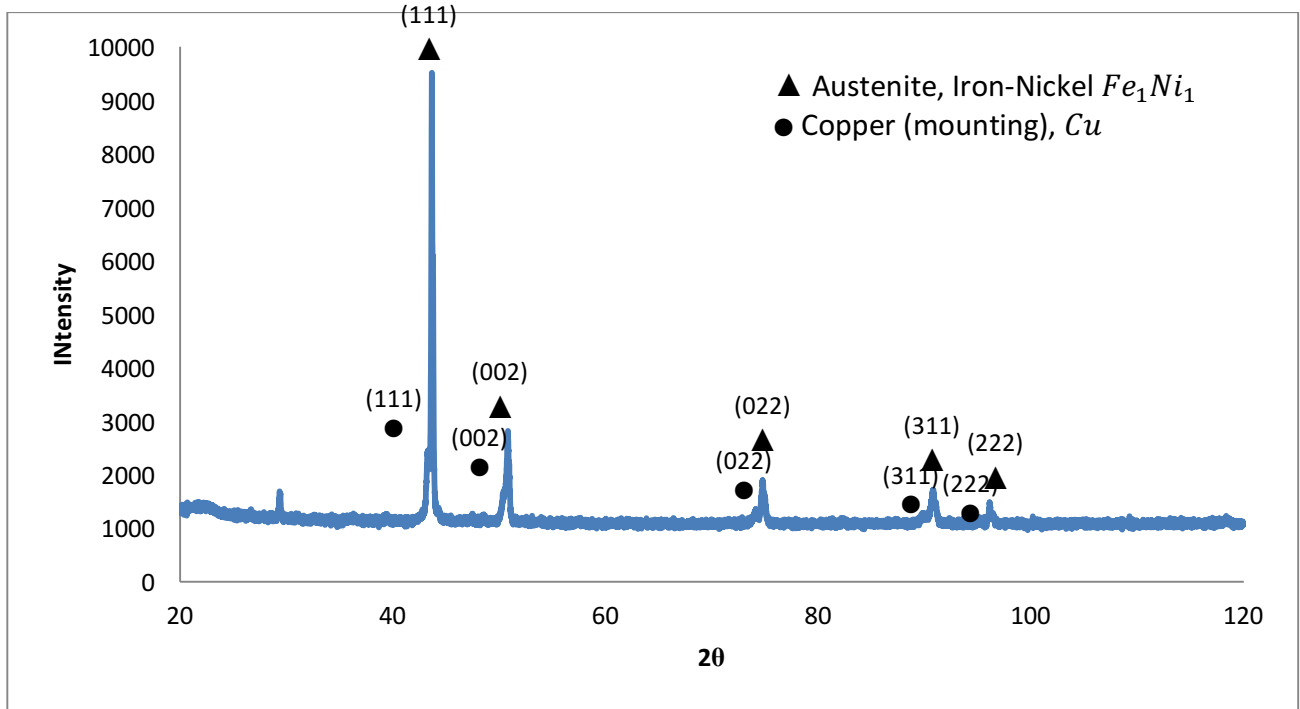


Figure 77. XRD pattern of the cross section for RA330 racking poles (exposed 6 months) (Cu tube)

XRD analysis of surface of racking poles was shown in Figure 78. Graphite and austenite phase was detected. The detection of graphite would indicate that the carbon deposited on the surface of racking poles during carburizing.

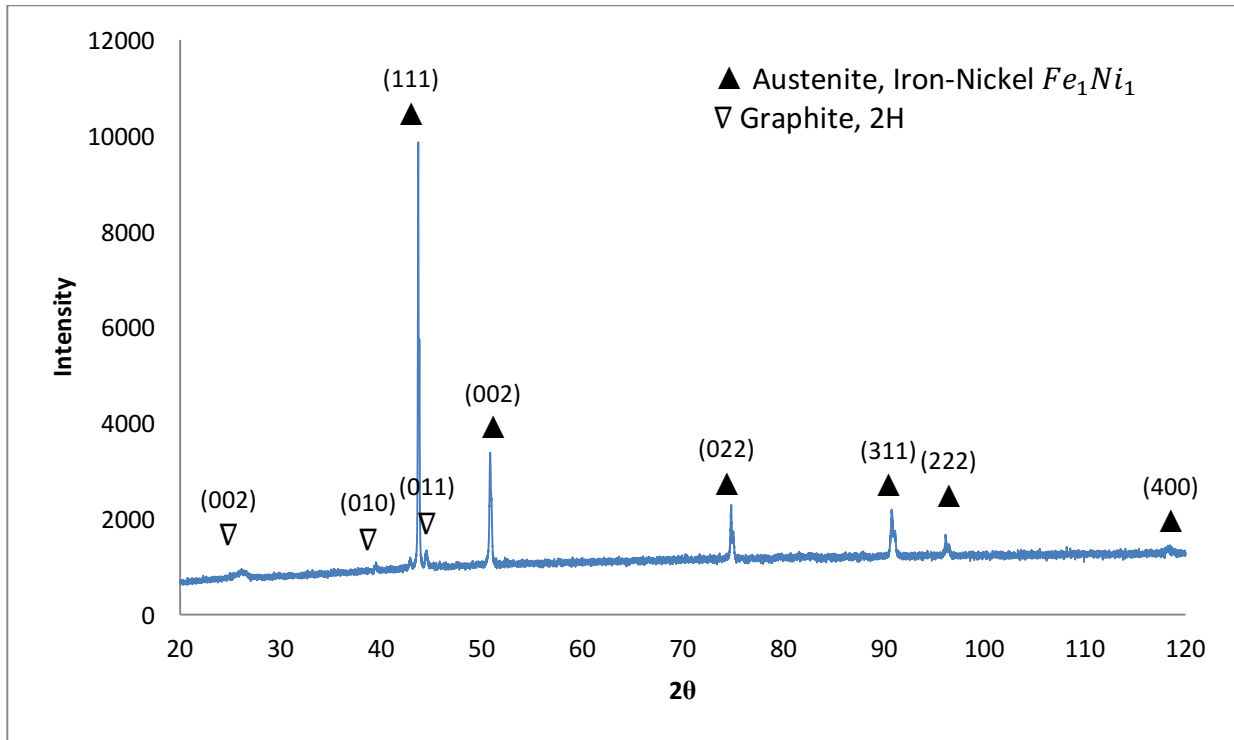


Figure 78. XRD pattern of the surface scan for RA330 racking poles (exposed 6 months) (Cu tube)

As presented in the data above, although chromium carbides and graphite were identified at the surface of racking poles, still no metal dusting was observed on the racking poles.

5.2.3.1.2. Racking poles – Aluminized

Racking poles were sent to Alcoa Howmet for aluminizing on December of 2013. The racking poles were aluminized in a static gas phase system at 1090°C for 5 hours. Chromium aluminum source material (70%Cr/30%Al) and ammonium fluoride granules were used in the system. The coating chamber was purged with argon until a dew point of -40F or better was met, then the argon is shut-off to the coating chamber (hence static system) and heating begins.

5.2.3.1.2.1. Preliminary metallographical analysis

Low magnification optical photomicrographs Figure 79 shows morphology of aluminized racking poles at edge. The cross sections were etched with oxalic acid showing spheroidal morphology. Clearly, the cross section surface exhibited a two-phase structure in the core area i.e. austenite matrix with chromium carbides at the grain boundaries.

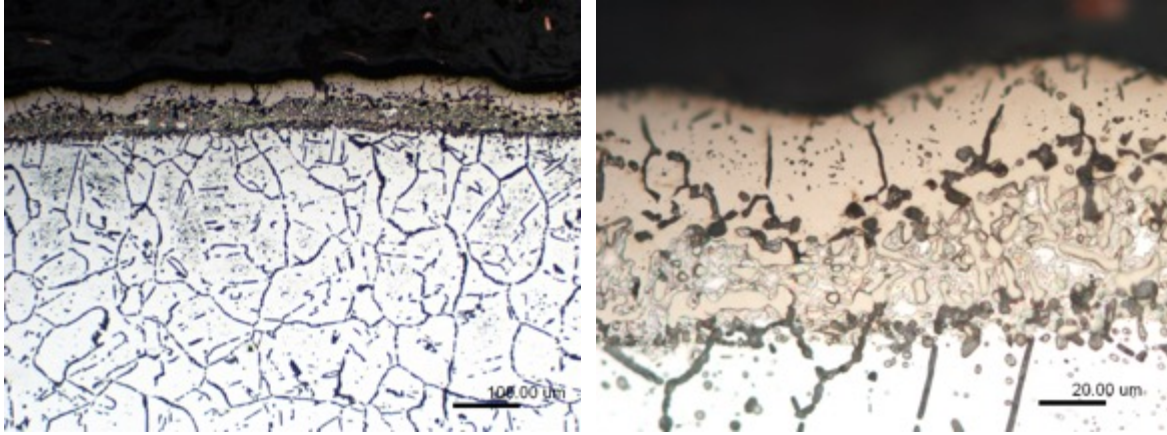


Figure 79. Optical photomicrographs of aluminized RA330 racking poles (etched with 10% oxalic acid)

Figure 80 shows the micro-hardness profile of aluminized racking poles. It can be seen that, the hardness near surface is higher than the following data points. One possible reason is that BCC structure nickel aluminide have higher hardness than FCC structure austenite.

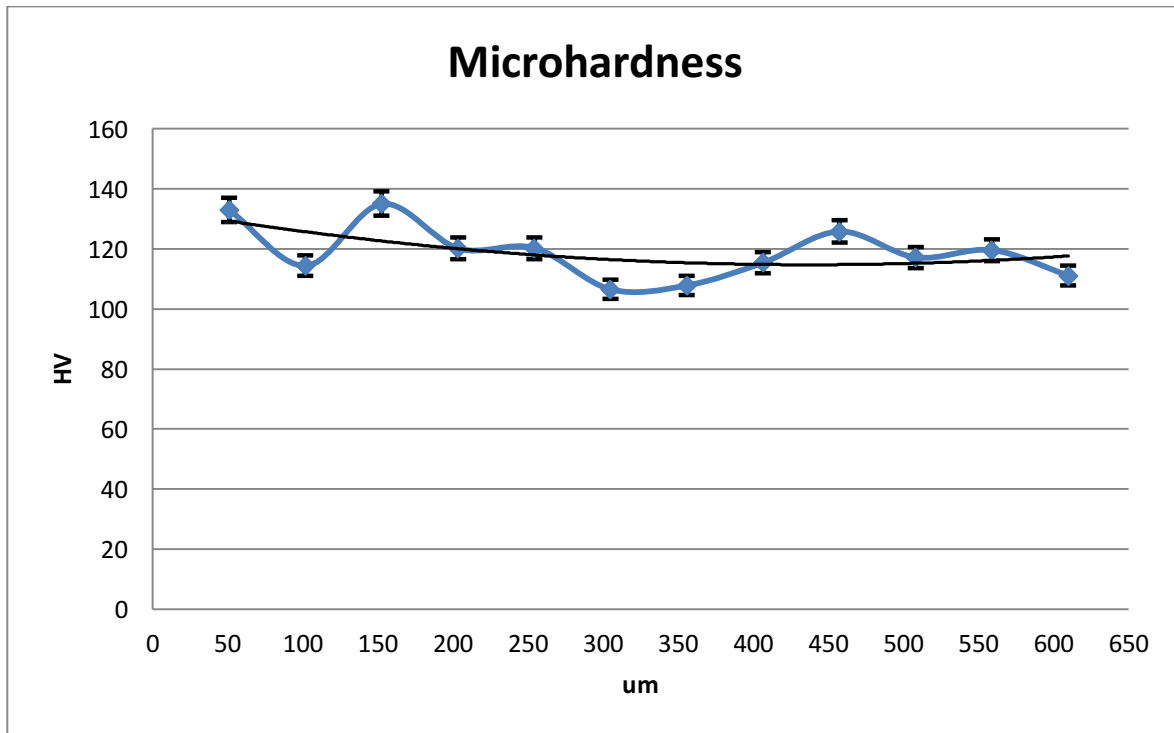


Figure 80. Microhardness profiles of aluminized racking poles

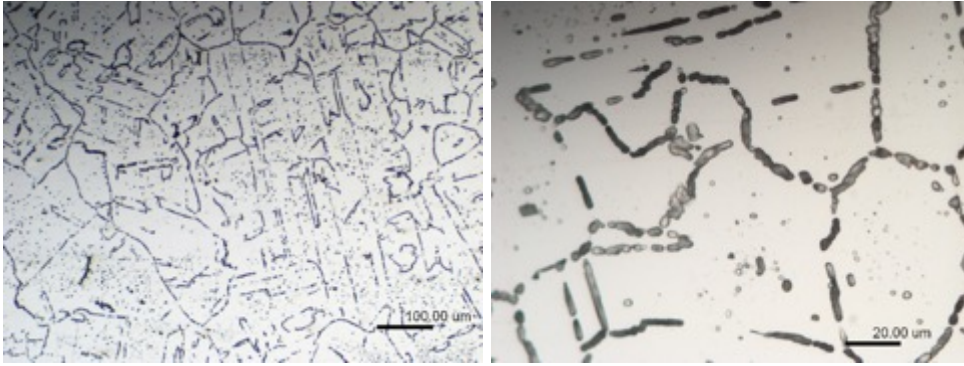


Figure 81. Optical photomicrographs of aluminized RA330 Racking poles at core Electrochemically etched with 10% oxalic acid for 30s

Figure 81 shows the optical photomicrographs of cross section area of racking poles at core area. From the optical photomicrographs, it can be seen that the chromium carbides precipitated at grain boundaries.

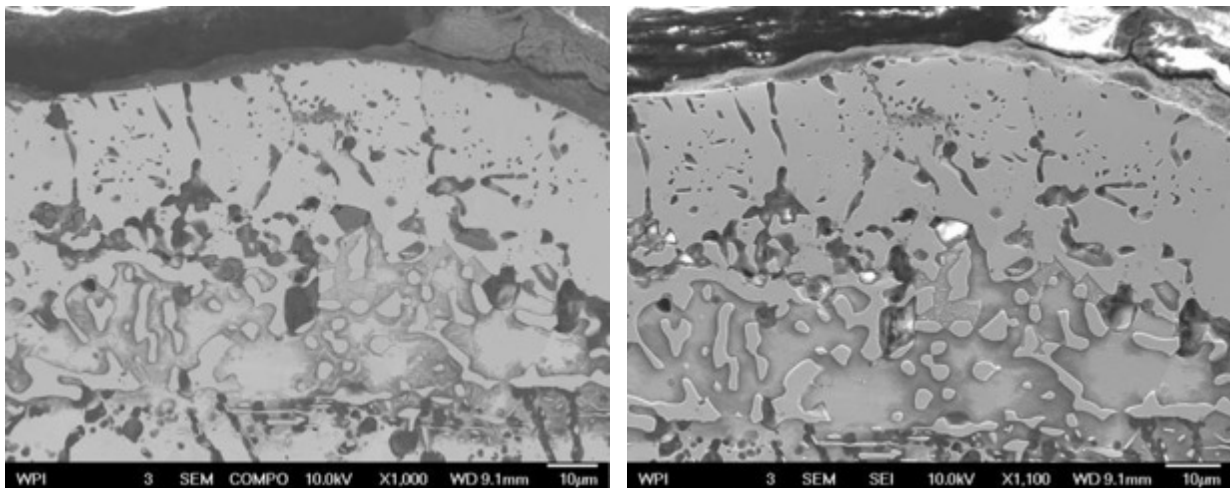


Figure 82. SEM photomicrographs of aluminized RA330 Racking poles Electrochemically etched with 10% oxalic acid for 30s; Backscattered Electron photomicrograph (left); Secondary Electron photomicrograph (right)

Figure 82 shows three to four continued or discontinued layers. The outside layer is about thirty microns wide. The surface layer was electrical etched with oxalic acid which was one possible reason for discontinuity of this layer. The etched structure of the second layer beneath the surface layer was identified as porosity structure due to etching. Again, the characterizations were also conducted on these layers. Numbers of elongated carbides were observed at the third layers beneath the surface. Finally, Figure 83 shows the fourth layer contains secondary phase at the grain boundaries.

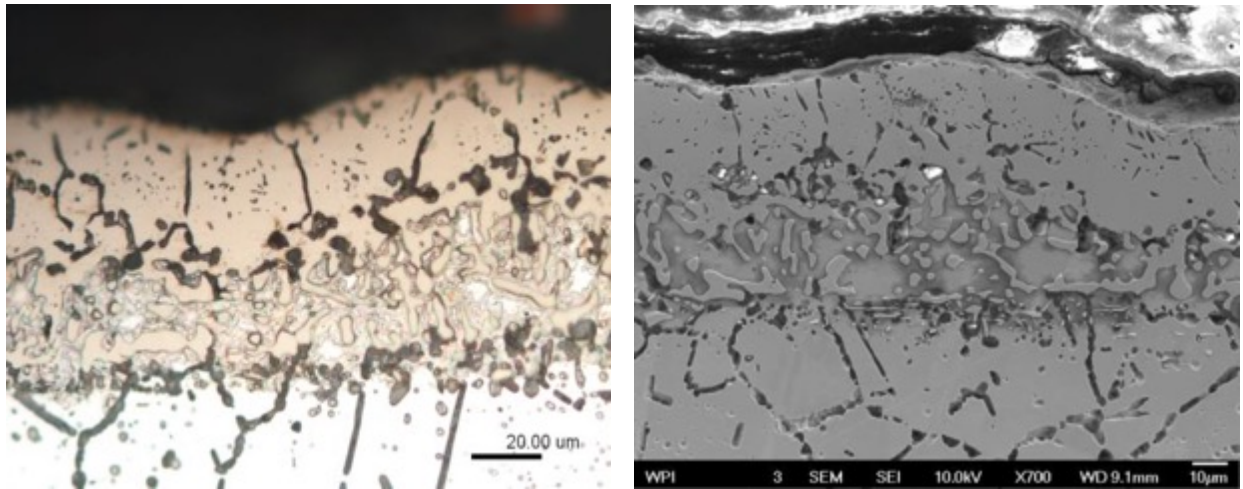


Figure 83. photomicrographs of aluminized RA330 Racking poles Electrochemically etched with 10% oxalic acid for 30s; Optical Photomicrograph (left); Secondary Electron Photomicrograph(right)

Figure 83 shows the optical photomicrographs of aluminized cross section that was etched with oxalic acid.

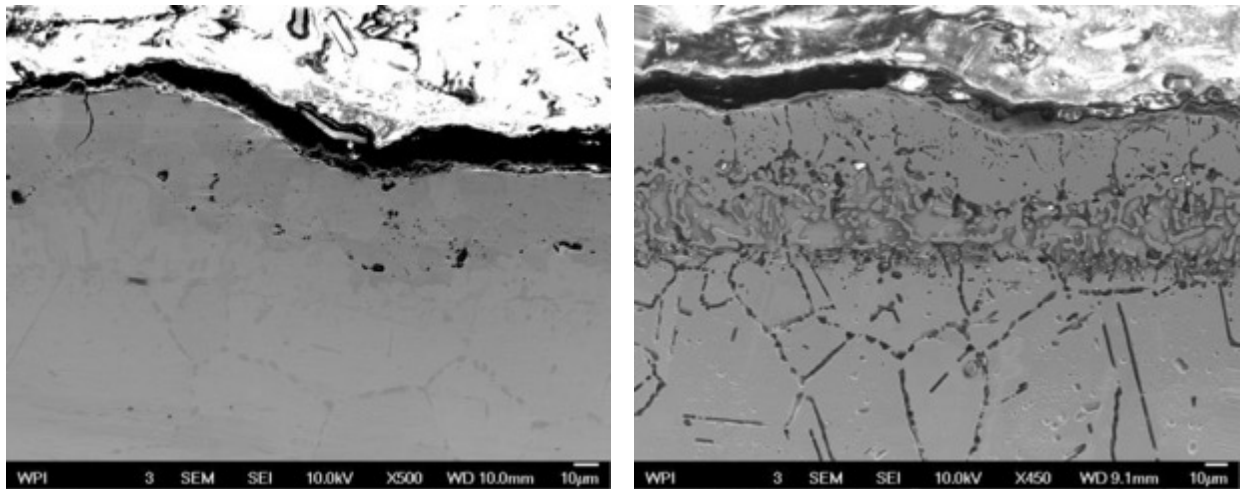


Figure 84. SEM photomicrographs of aluminized RA330 Racking poles; Unetched (left); Electrochemically etched with 10% oxalic acid for 30s (right);

Figure 84 shows the morphology before and after etching. A crack was observed on the unetched photomicrographs indicated that etching was not the only factor for discontinuity of surface layer.

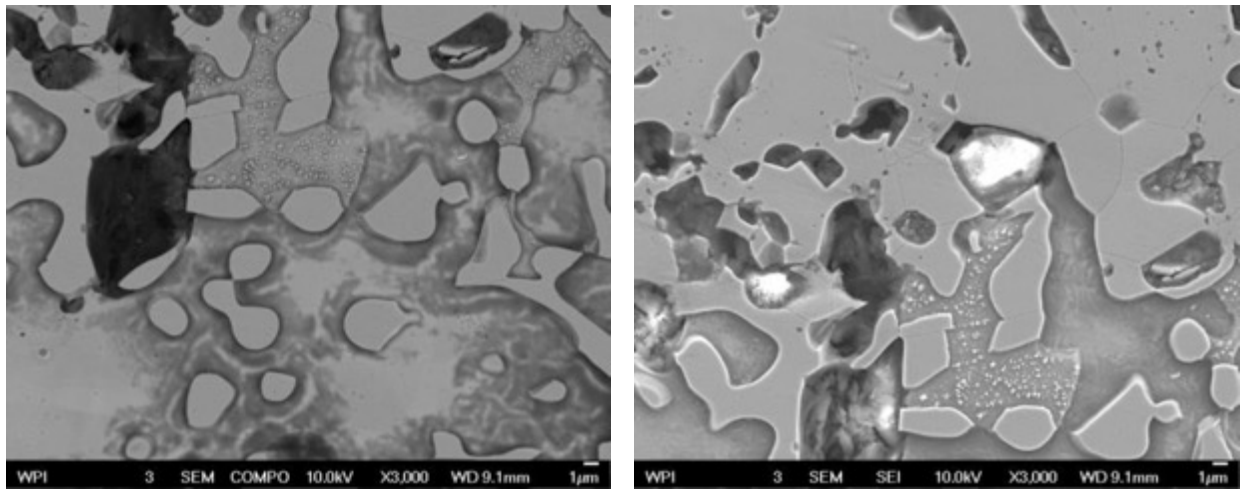


Figure 85. SEM photomicrographs of aluminized RA330 Racking poles Electro-chemically etched with 10% oxalic acid for 30s; Back-scattered electrons photomicrograph (left); Secondary electrons photomicrograph (right)

The morphology of third layer was inhomogeneous discontinued secondary phases on the matrix.

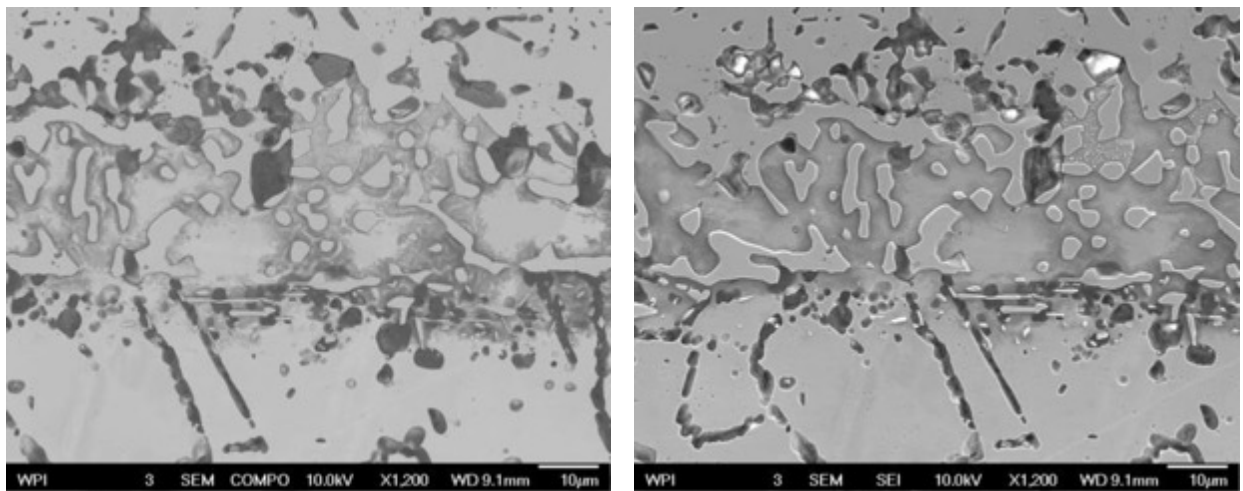


Figure 86. SEM photomicrographs of aluminized RA330 Racking poles Electrochemically etched with 10% oxalic acid for 30s; Back-scattered electrons photomicrograph (left); Secondary electrons photomicrograph (right)

In the core area of cross section, grain boundaries were clearly shown on the photomicrographs after 30s of electrical etching. The micro structure of aluminize and unaluminized RA330 are same in the core area as shown in Figure 87.

A series of photomicrographs were shown in the following two pages, relatively high magnification photos helps better identify the phases.

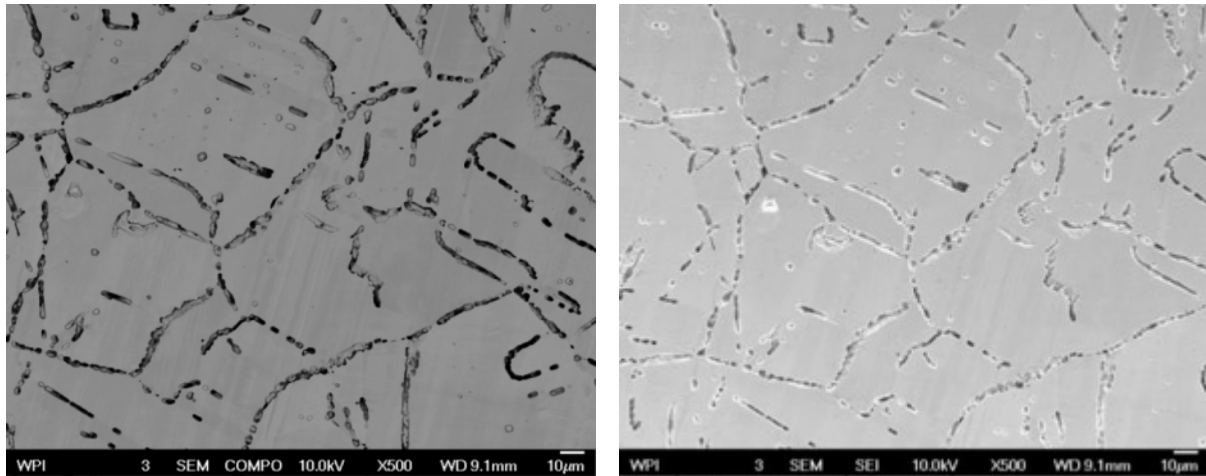


Figure 87. SEM photomicrographs of aluminized RA330 Racking poles Electrochemically etched with 10% oxalic acid for 30s; Back-scattered electrons photomicrographs (left); Secondary electrons photomicrographs (right)

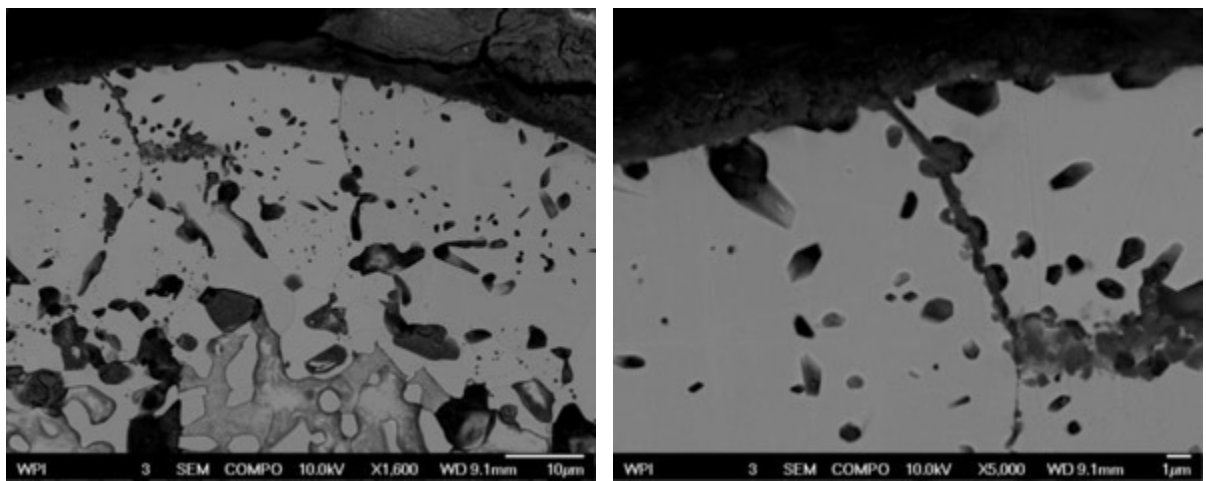


Figure 88. SEM photomicrographs of aluminized RA330 Racking poles Electrochemically etched with 10% oxalic acid for 30s; Back-scattered electrons photomicrograph (left); Secondary electrons photomicrograph (right)

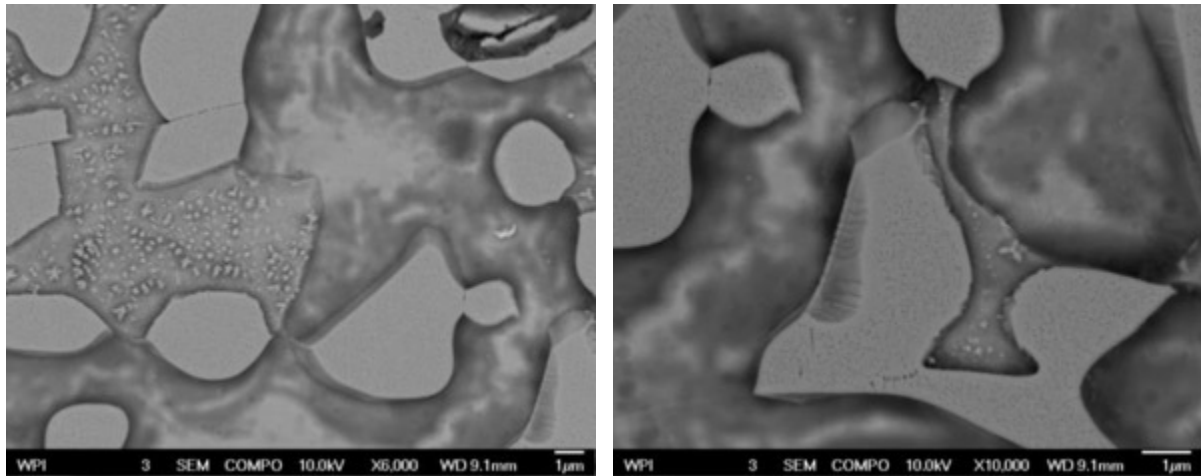


Figure 89. SEM photomicrographs of aluminized RA330 Racking poles Electrochemically etched with 10% oxalic acid for 30s; Back-scattered electrons photomicrograph (left); Secondary electrons photomicrograph (right)

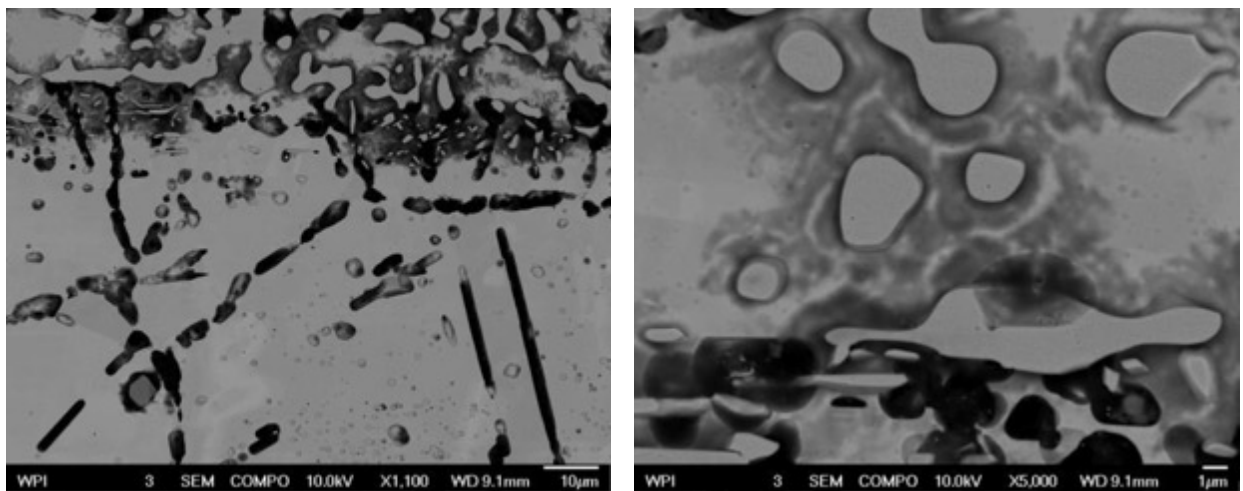


Figure 90. SEM photomicrographs of aluminized RA330 Racking poles Electrochemically etched with 10% oxalic acid for 30s; Back-scattered electrons photomicrographs (left and right)

The elemental analysis of surface layers was determined using EDS. The composition of surface layers was shown on Figure 91, in 18.26%Al, 1.35%Mn, 17.38%Fe, 63.01%Ni, indicated that β – NiAl nickel aluminide phase.

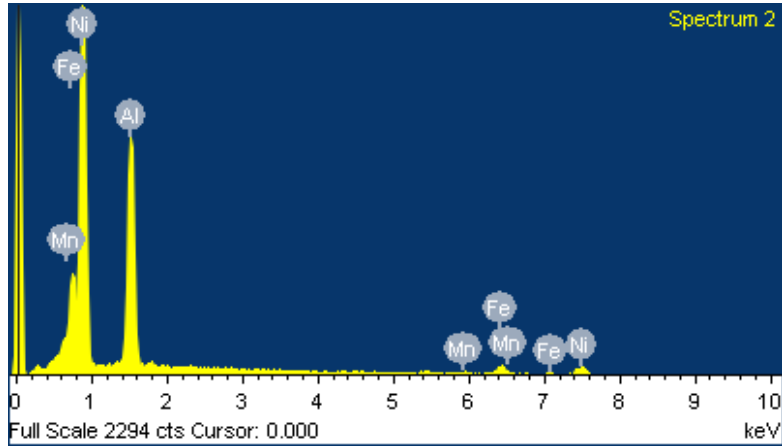
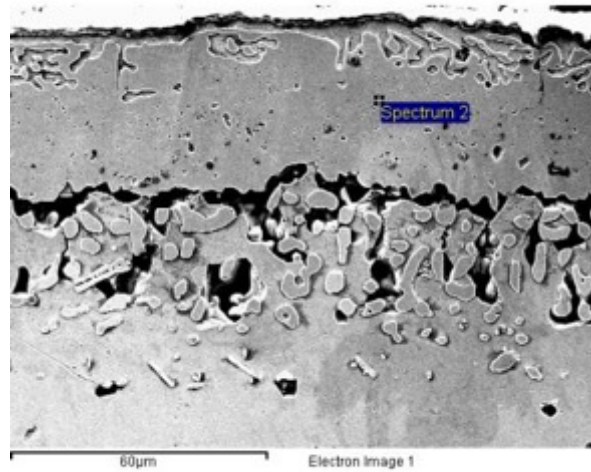


Figure 91. Elemental analysis by EDS on surface layer of Aluminized RA330

However, Figure 88, Figure 89 and Figure 90 show $\alpha - Al_2O_3$ formed on the $\beta - NiAl$ surface layer. The composition of oxide region in Figure 92 was determined using EDS, as 59.04% O, 29.86% Al, 7.69%Fe, 8.40%Ni.

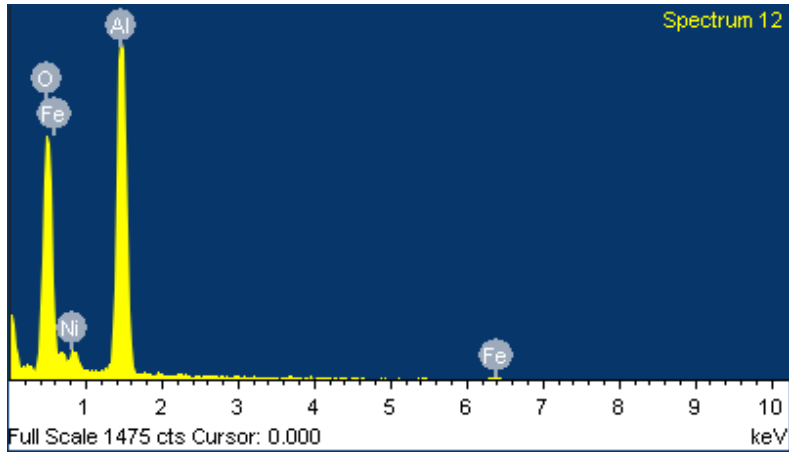


Figure 92. Elemental analysis by EDS on surface layer of Aluminized RA330

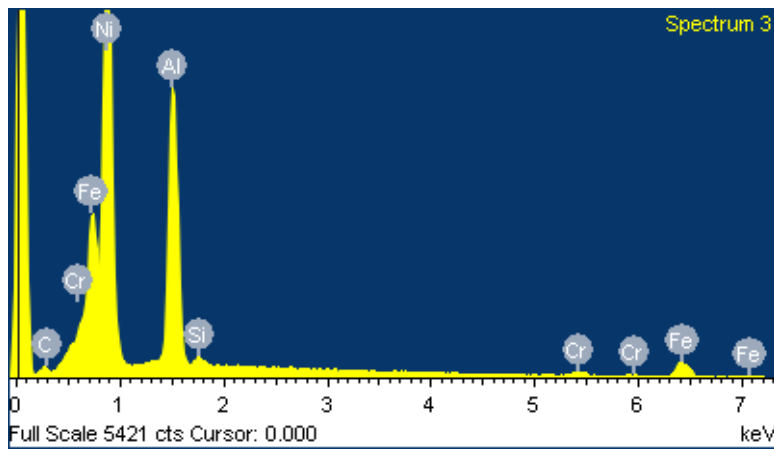
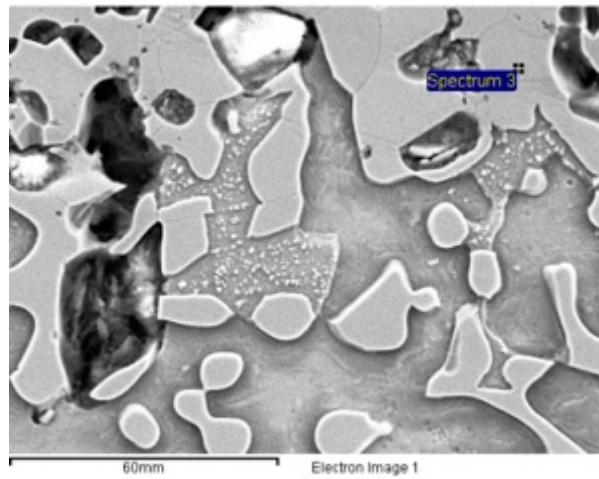


Figure 93. Elemental analysis by EDS on secondary phase on surface layer of Aluminized RA330

A different morphology was observed beneath the surface layer in Figure 88, Figure 89 and Figure 90, where elongated platelets of nickel aluminide Ni_1Al_1 were observed. Figure 93 shows the element analysis by EDS, examined that 64.30% Ni, 18.47% Al, 17.23% Fe of $\beta - Ni_1Al_1$ Nickel aluminide.

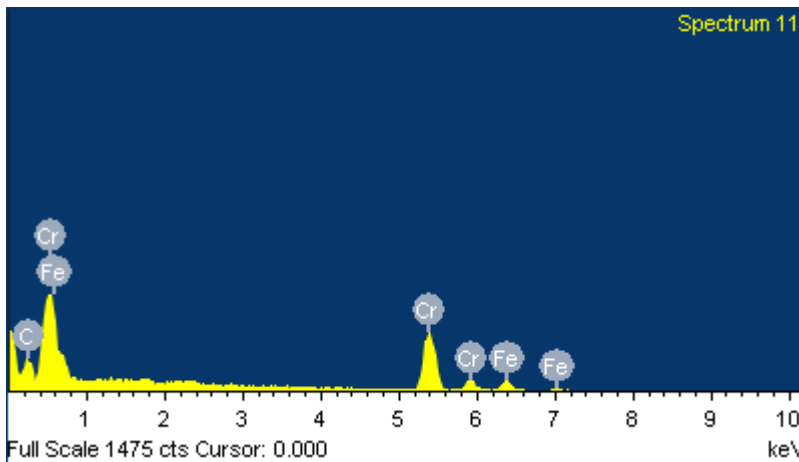
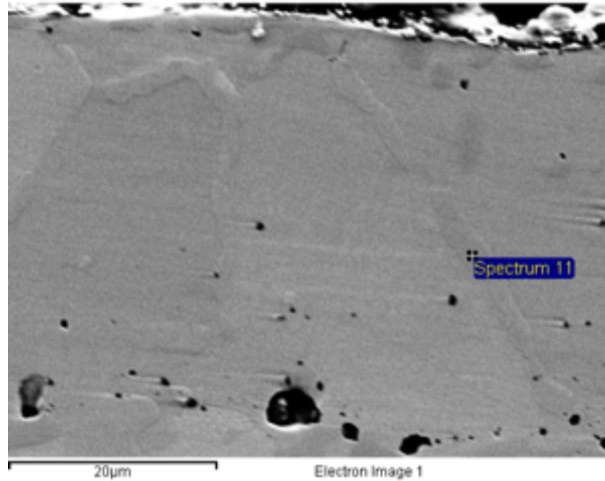


Figure 94. Elemental analysis by EDS on nickel aluminide of Aluminized RA330

Discontinued surface layer was observed after etching, on which cracks and pores were observed. However, almost no crack or pores were observed before etching except $\alpha - Al_2O_3$ participates. Therefore, EDS analyzes were conducted on unetched secondary phases, Figure 94. The composition is 19.94% C, 59.44% Cr, 20.62% Fe, which is in a good agreement with chromium carbides. The racking poles were carburized for 6 months; carbides $(Cr, Fe)_7C_3$ were identified at the $\beta - NiAl$ surface layer.

The dominate phase in aluminized RA330 is austenite iron-nickel. The composition of austenite in the matrix is 44.77% Fe, 27.98% Ni, 22.49% Cr. Figure 95 shows the EDS analysis of Fe_1Ni_1 austenite.

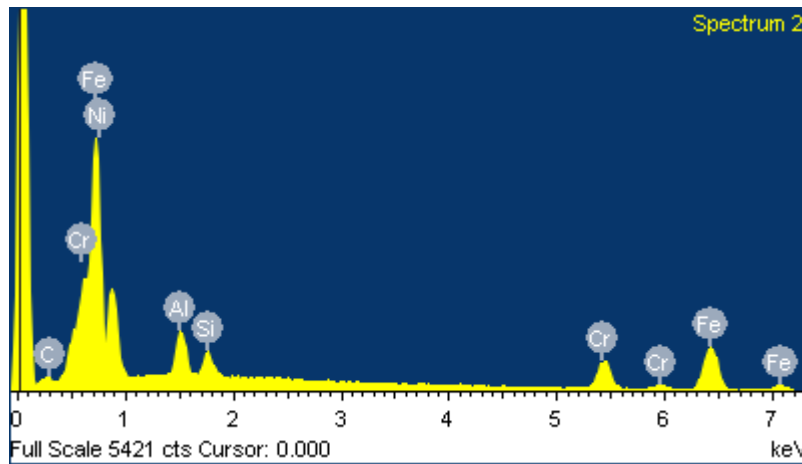
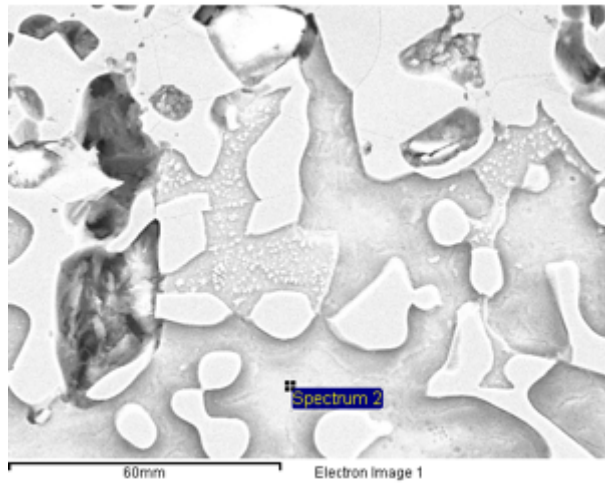


Figure 95. Elemental analysis by EDS on austenite matrix of Aluminized RA330

XRD analysis shows in Figure 96 indicated that $\alpha - Al_2O_3$ formed at the outside shell, $\beta - Ni_1Al_1$ nickel aluminide were also detected at the surface layer, graphite and chromium carbides were identified after carburizing.

EDS analysis can be used to create the element map, Figure 97 presents the images from the EDS maps of aluminum, chromium, nickel, and iron on the corresponding SEM micrograph of the aluminized racking poles, which is good agreement with the preliminary metallographical analysis above.

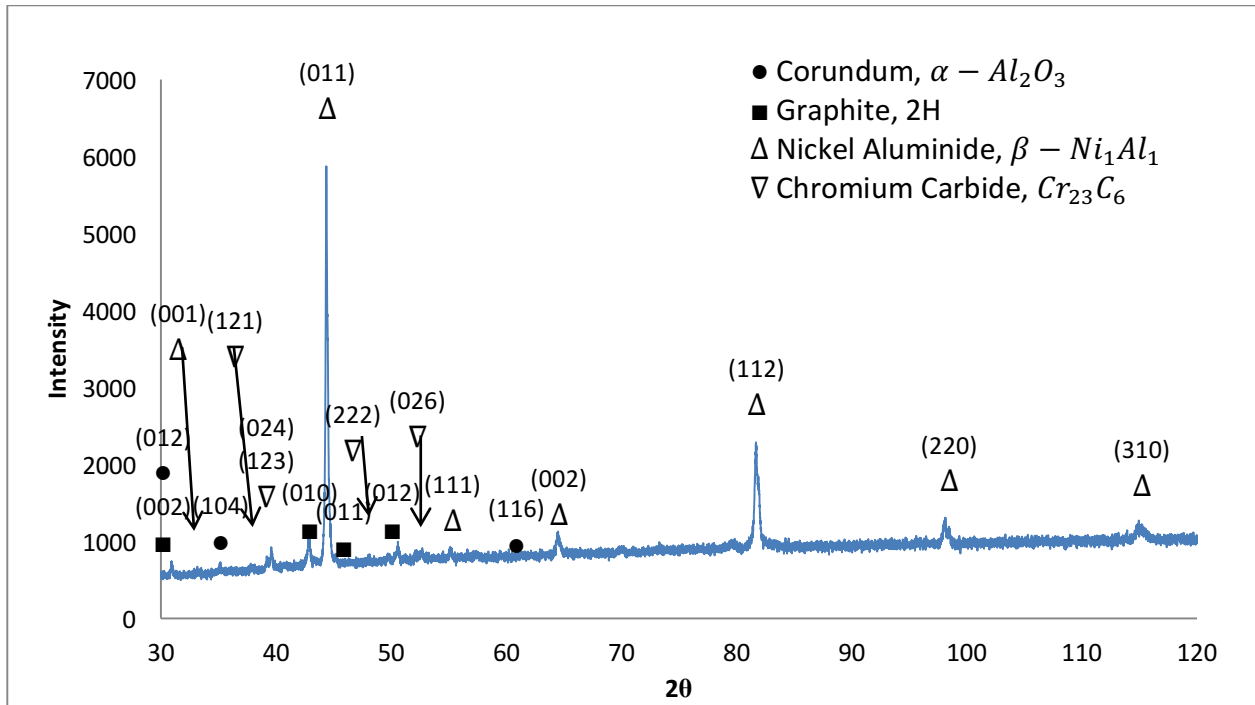


Figure 96. XRD pattern of the surface scan for aluminized RA330 racking poles (exposed 6 months) (Cu tube)

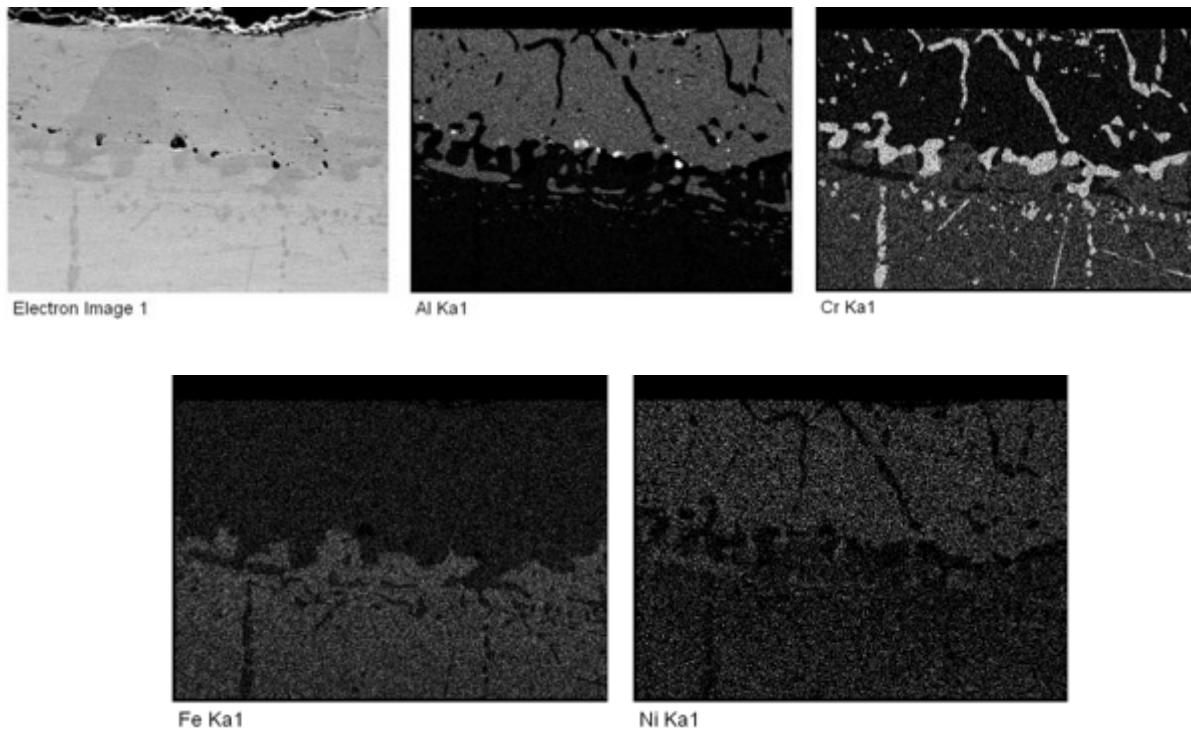


Figure 97. EDS element maps on the cross section of aluminized racking poles

As presented in the data above, no metal dusting was observed on the aluminized racking poles. As well as unaluminized racking poles, chromium carbides were also identified on the aluminized racking poles. And the flakes off from aluminized racking poles were mainly graphite and chromium carbides.

5.2.3.1.3. Characterization of Flake Offs

5.2.3.1.3.1. Flake offs from unaluminized RA330 racking poles

The flake off of unaluminized racking poles were collected and analyzed by XRD. The result shows on Figure 98. The flake offs removed from racking poles had two sides, and the morphology of two sides were significantly different. The XRD analysis were conducted on outside which was exposed in the carbon atmosphere. Figure 98 shows that graphite and chromium carbides Cr_7C_3 were identified at the outside surface of flake offs. The results show that they were mostly graphite, but chromium carbides were also detected.

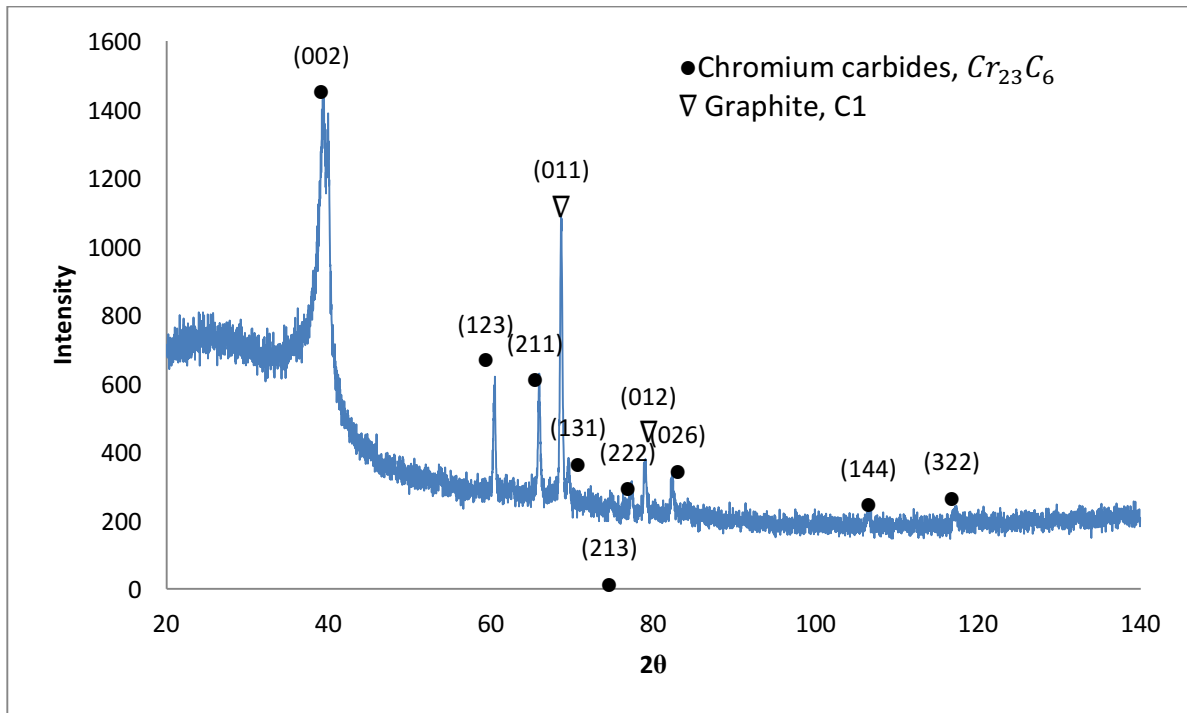


Figure 98. XRD pattern of the outside surface scan for RA330 flake offs (exposed 6 months) (Cr tube)

The morphology of two sides was different. The results of other side of flake off had the similar result to the outside. The inside of flake offs were connected to the racking poles. The results show that chromium carbides Cr_7C_3 and graphite were detected.

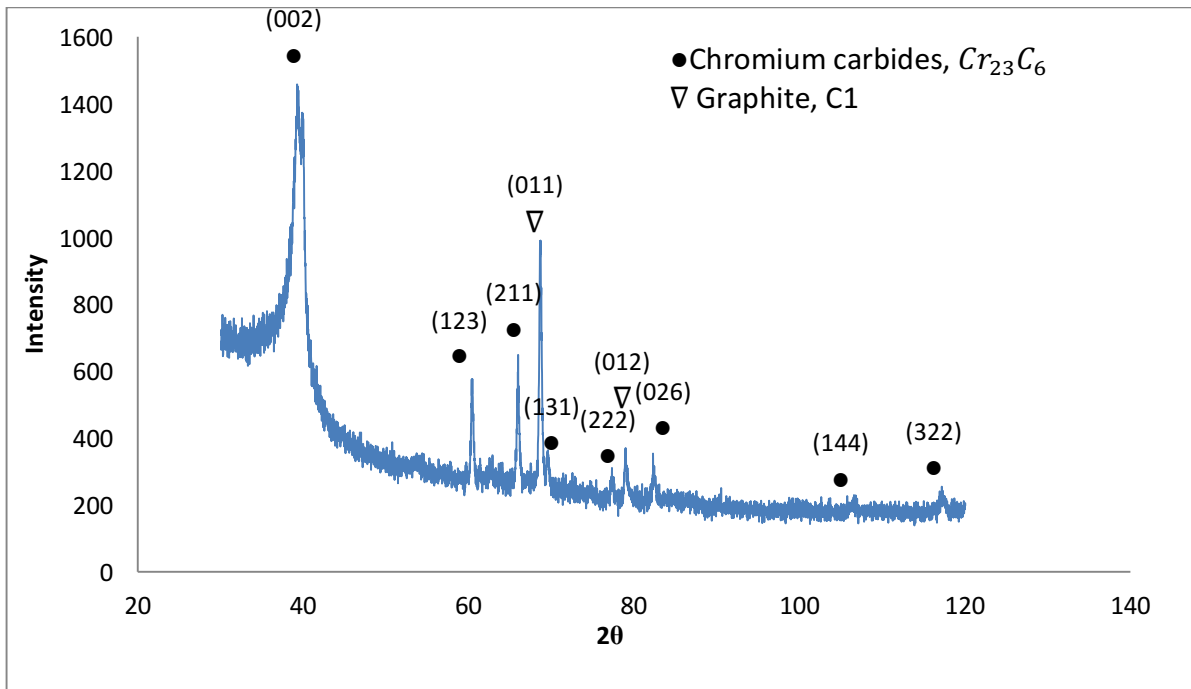


Figure 99. XRD pattern of the inside surface scan for RA330 flake offs (exposed 6 months) (Cr tube)

The outside of flake offs were examined using SEM and found to consist of filaments, tens of microns or more in length. Apparently, particles were also observed at the surface, tens of microns or less in diameter. At higher magnifications, particles of approximately 1nm were detected on the filaments and micro particles. The formation of Nano particles was still being investigated.

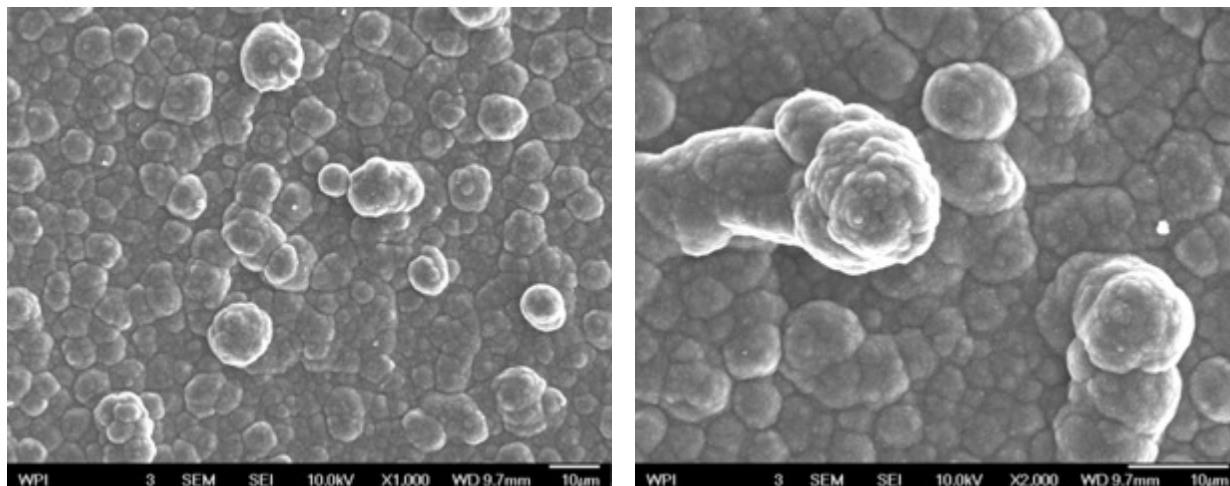


Figure 100. SEM photomicrographs of flake offs removed from racking poles (Outside)

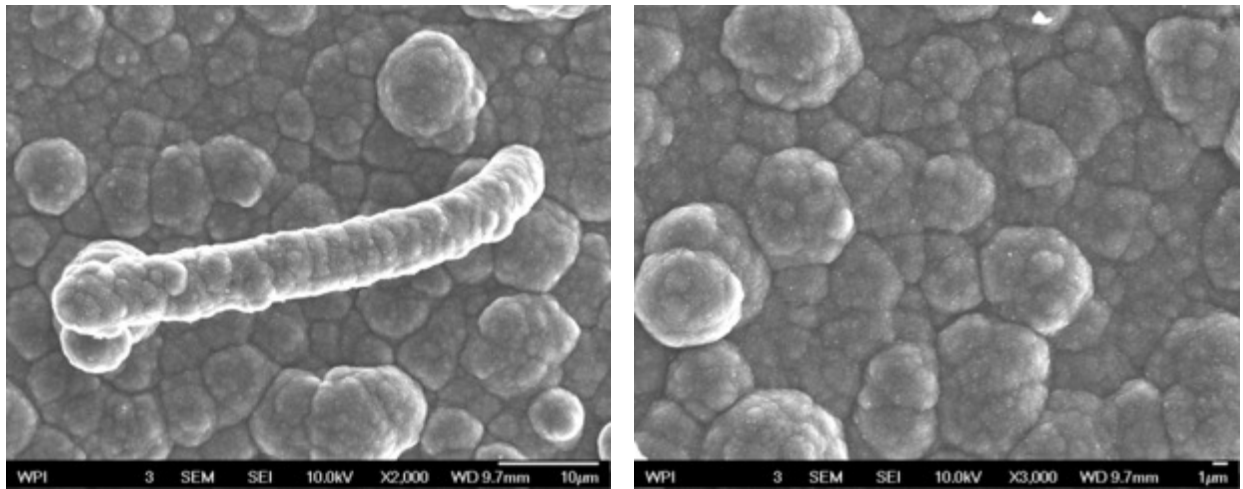


Figure 101. SEM photomicrographs of flake offs removed from racking poles (Outside)

Figure 102 shows the inside morphology of flake offs that significantly different from outside morphology. It can be seen that inside surface of flakes offs covered with inhomogeneous particles, tens of nanometers in diameter. Nano particles were also detected on the particles, which were less than 1 nanometers in diameter.

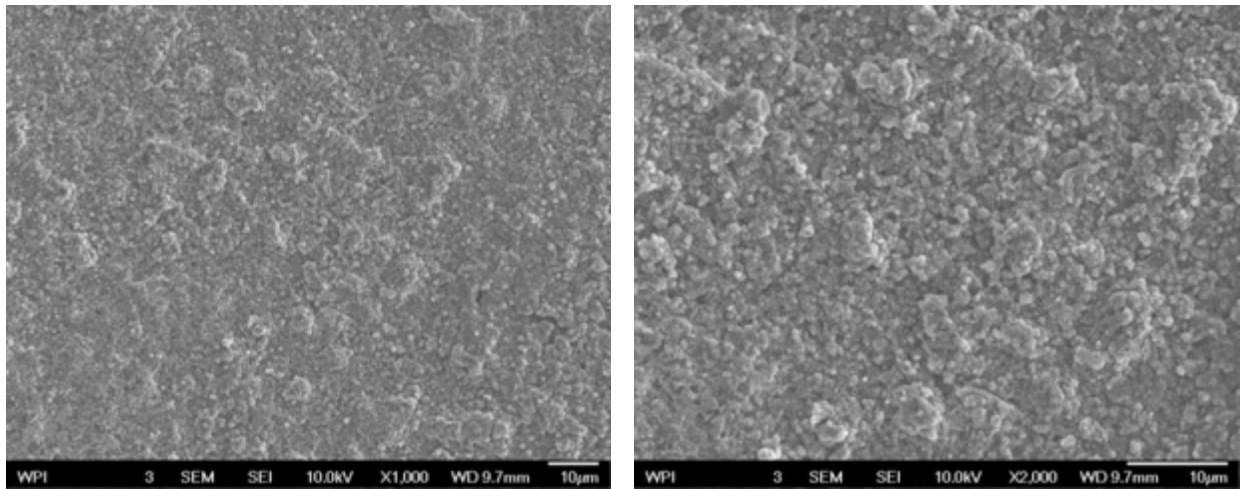


Figure 102. SEM photomicrographs of flake offs removed from racking poles (inside)

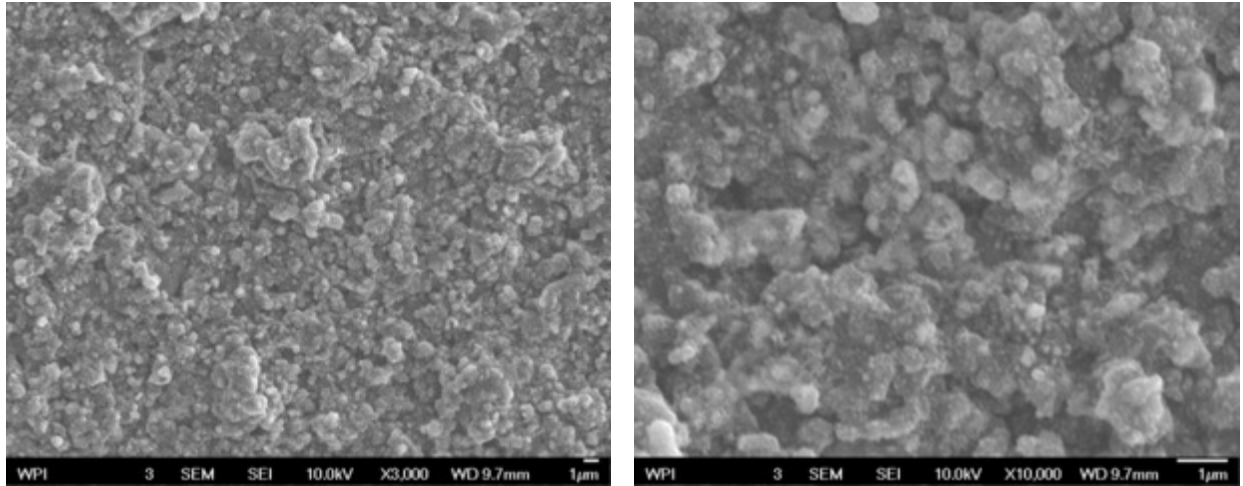


Figure 103. SEM photomicrographs of flake offs removed from racking poles (inside)

In the future, more XRD analysis will be conducted on the flake offs for structure identifications. The characterization work of carbides is still under way. Besides, the nano-particles will also be detected by SEM.

5.2.3.1.3.2. Flake offs from aluminized RA330 racking poles

5.2.3.1.3.2.1. Outside surface morphology of aluminized flake offs

After 6 months service in the carburizing furnace, carbon diffuses into the $\beta - Ni_1Al_1$ surface layer. The racking poles were aluminized before furnace testing. The XRD results of flake offs indicated that complex reactions occurred at the surface of aluminized racking poles. The results in Figure 104 show that flake offs were mostly graphite, iron oxide, and chromium carbides. This is consistent with the observation in Figure 98, which means the composition of aluminized flake offs is similar to unaluminized flake offs. Unlike the surface scan of aluminized racking poles, no $\alpha - Al_2O_3$ was identified at flake offs. In this case, it can be assumed that reaction mechanisms happened on the flake offs are similar. The influence of aluminizing on the flake offs still needs to be investigated.

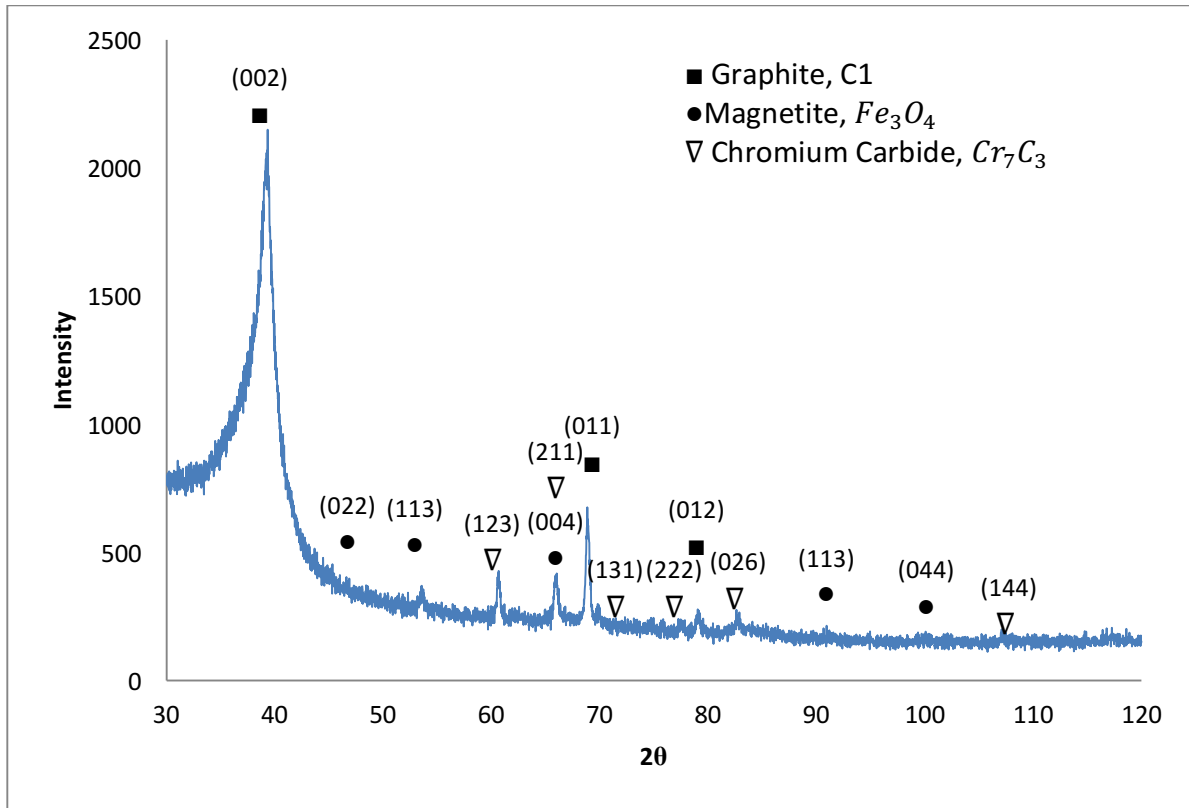


Figure 104. XRD pattern of the outside surface scan for aluminized RA330 flake offs (exposed 6 months) (Cr tube)

Figure 105 shows the spherical morphology of aluminized flake offs. Filaments were also detected on the aluminized flake offs, tens of microns or less in length. However, the length of filaments were shorter than unaluminized flake offs. In Figure 105, some particles could be seen at the surface, approximately 1 microns in the length.

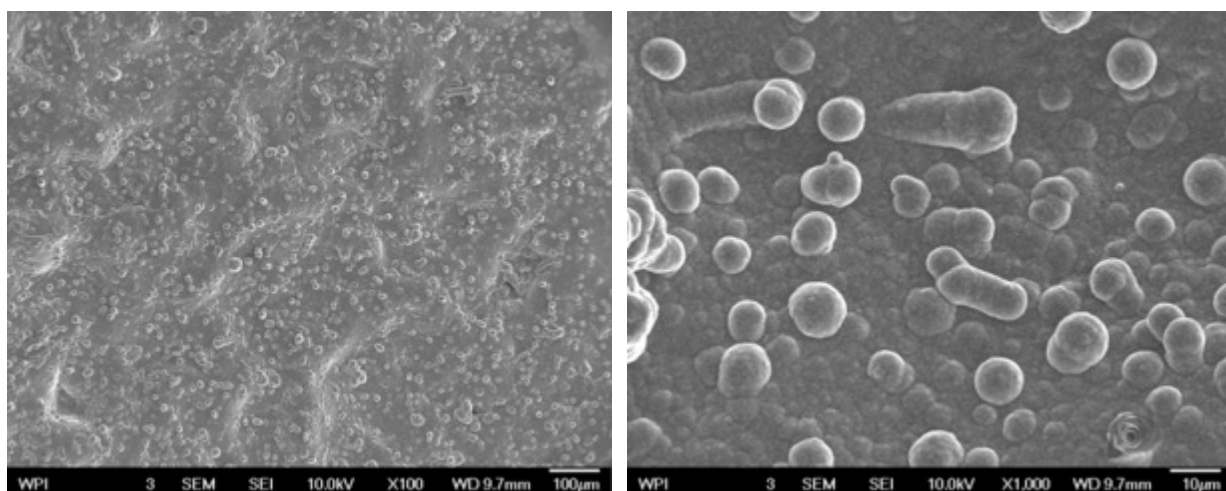


Figure 105. SEM photomicrographs of flake offs removed from aluminized racking poles (outside)

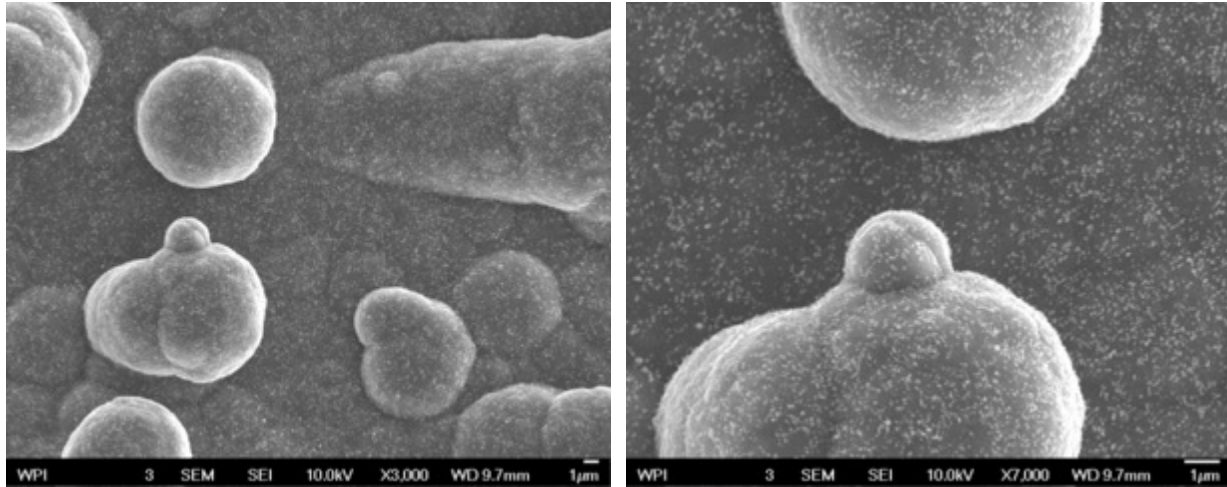


Figure 106. SEM photomicrographs of flake offs removed from aluminized racking poles (outside)

Figure 107 shows nano scale particles on the surface of micro scale particles. The identity of nano particles needs further characterization.

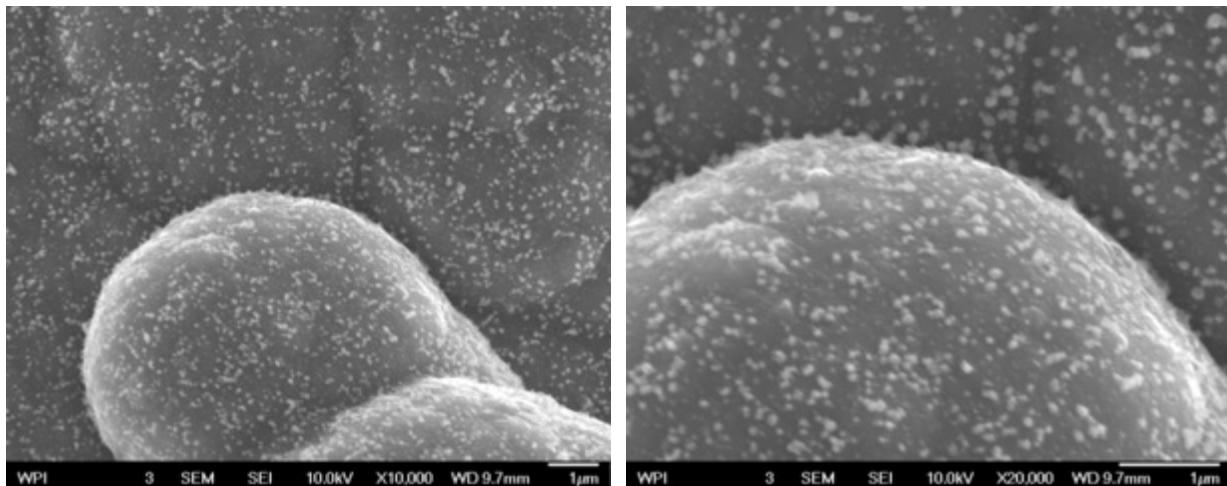


Figure 107. SEM photomicrographs of flake off removed from aluminized racking poles (outside)

5.2.3.1.3.2.2. Inside surface morphology of aluminized flake offs

The morphology of inside surface was observed by SEM. Figure 109 shows the inhomogeneous particles and filaments on the surface of aluminized flake offs. A large difference of particle size

was observed which varies approximately from $1\mu\text{m}$ to $10\mu\text{m}$ in length. It can be seen that clusters were formed by particles in the same area.

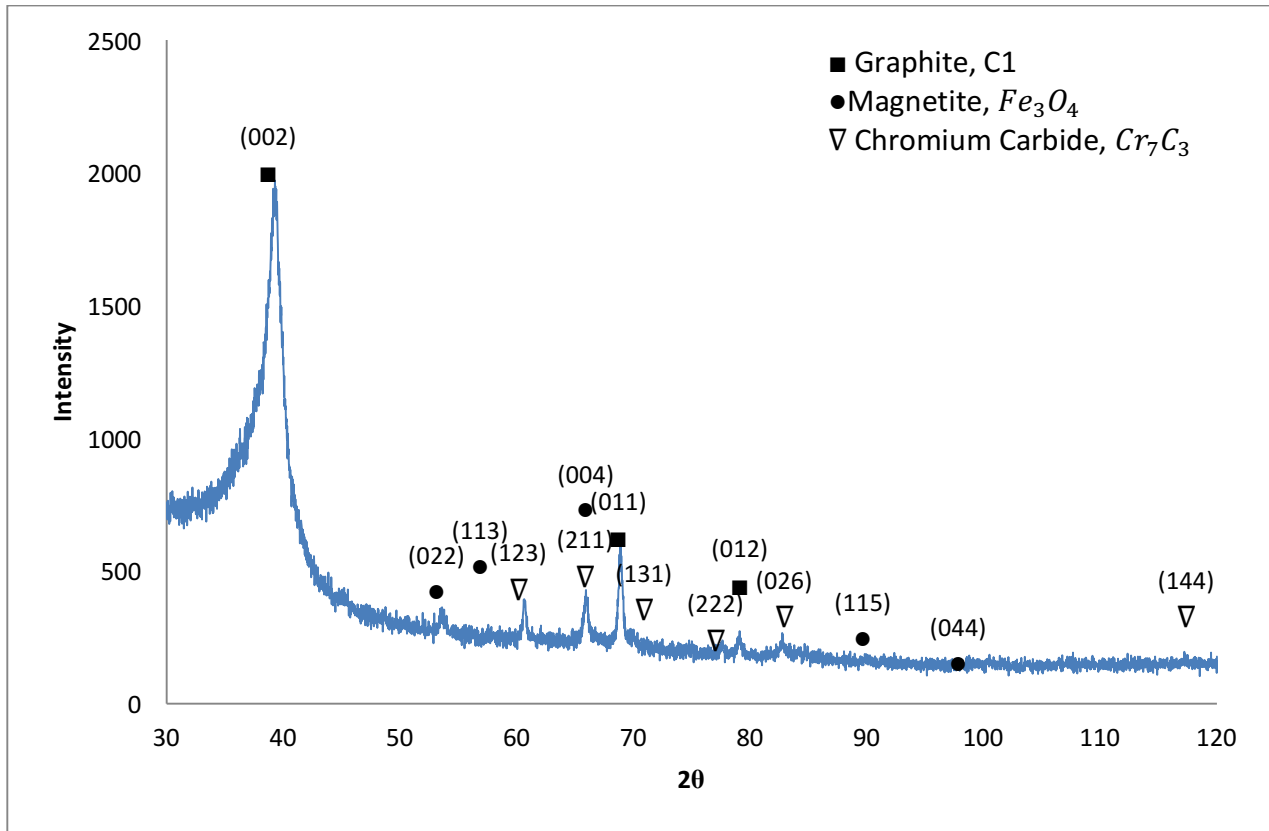


Figure 108. XRD pattern of the inside surface scan for aluminized RA330 flake offs (exposed 6 months) (Cr tube)

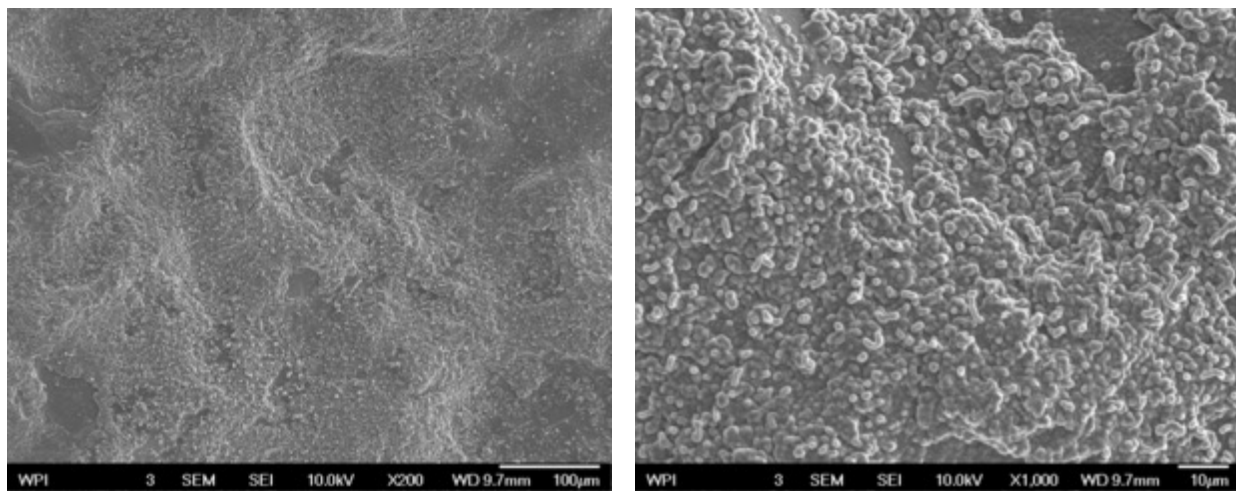


Figure 109. SEM microphotographs of flake offs removed from aluminized racking poles (inside)

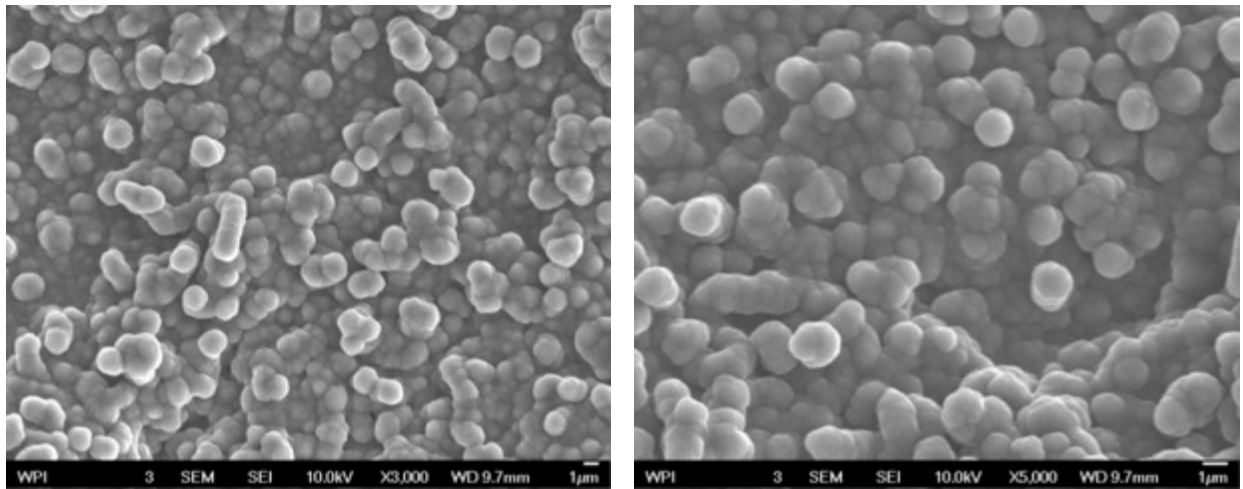


Figure 110. SEM microphotographs of flake offs removed from aluminized racking poles (inside)

Nano scale particles were not detected on the inside surface of aluminized flake offs. Preliminary metallographical analysis of aluminized flakes offs indicated that the morphology of surface is semi-spherical. The identity of flakes offs were combination of graphite and chromium carbides.

Racking poles exposed for 3 years

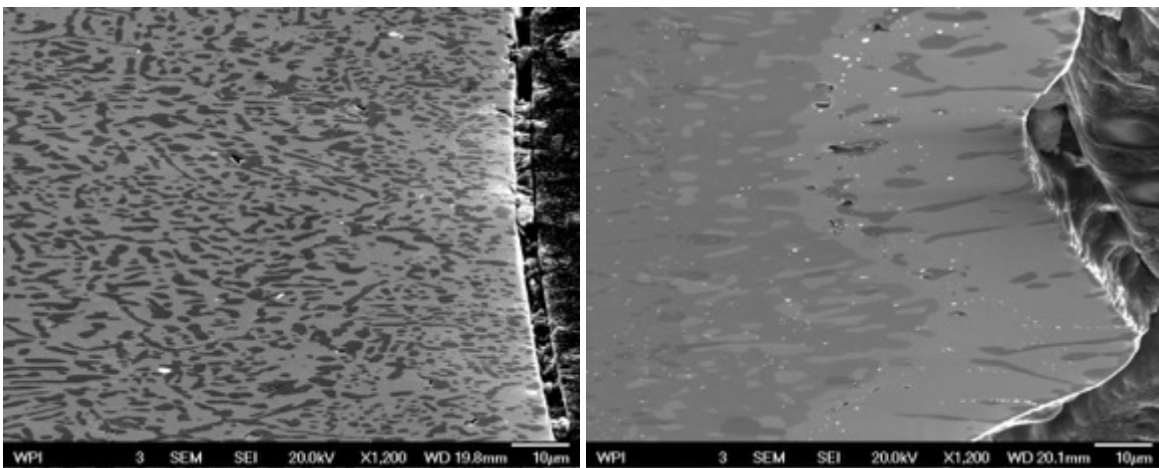


Figure 111: SEM microphotographs of as-fabricated racking poles (left) and aluminized racking poles (right) exposed for 3 years

RA330 racking poles were exposed at vacuum carburization furnace for 3 years. SEM photomicrographs of both as fabricated RA330 racking poles and aluminized racking poles indicated that chromium carbides precipitated in the matrix of alloys as shown in the Figure 111.

Phase Color 1

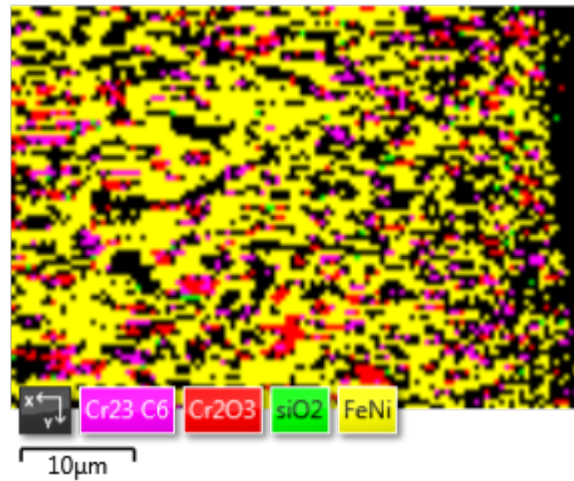


Figure 112: EBSD phase analysis of racking poles exposed for 3 years

According to EBSD analysis as presented in Figure 112, $Cr_{23}C_6$ carbides were identified in the interior of as-fabricated RA330 exposed for 3 years.

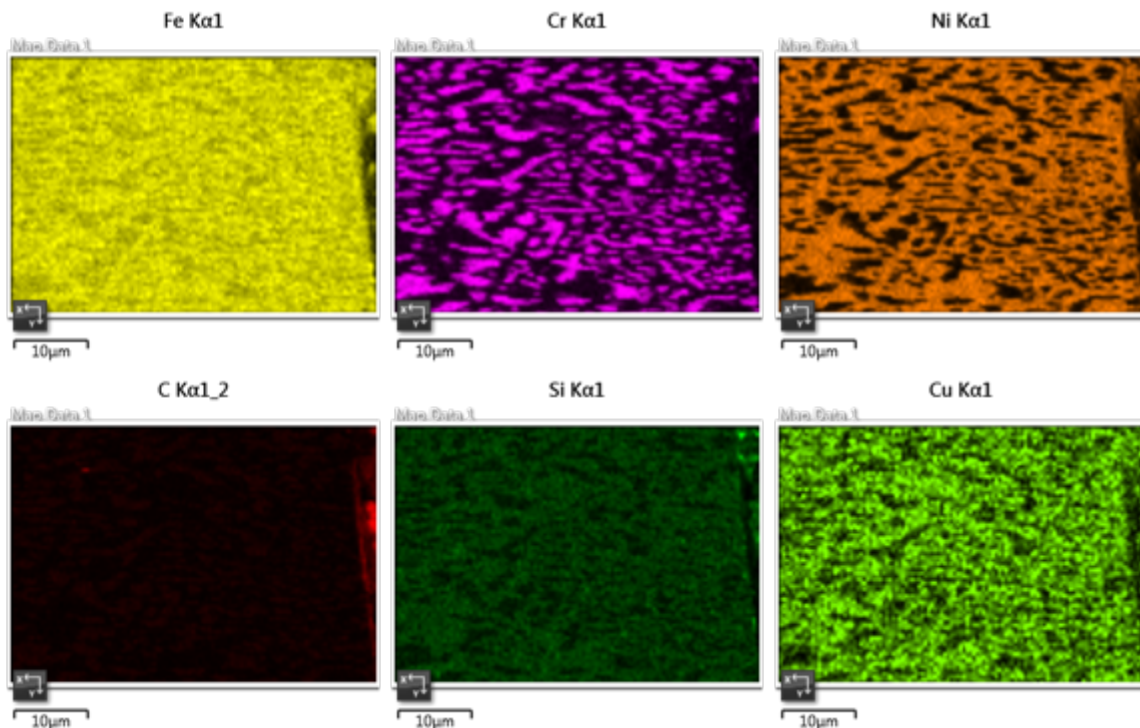


Figure 113: EDS mapping of racking poles exposed for 3 years

EDS mapping shows secondary phase chromium carbides were rich in Cr and C content as presented in Figure 113. The primary phase in the matrix of as-fabricated RA330 is austenite phase.

Phase Color 1

IPF X Color 1

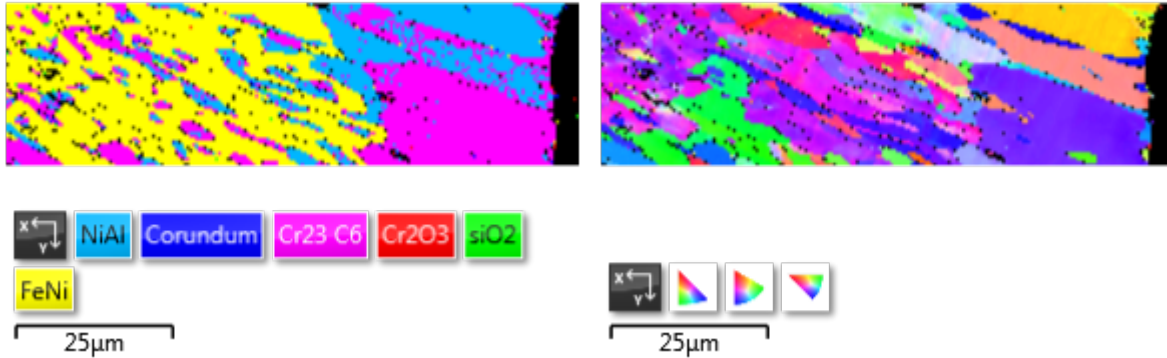


Figure 114: EBSD phase and orientation images of aluminized racking poles exposed for 3 years

Aluminized racking poles formed a layer of $\beta - NiAl$ at the surface as shown in Figure 114. However, chromium carbides $Cr_{23}C_6$ also identified in the layer of $\beta - NiAl$. A diffusion zone that contains $\beta - NiAl$, $Cr_{23}C_6$ and austenite phase was observed beneath the $\beta - NiAl$ layer as shown in Figure 114. Orientation image shows smaller grain size of diffusion zone compare to $\beta - NiAl$ layer.

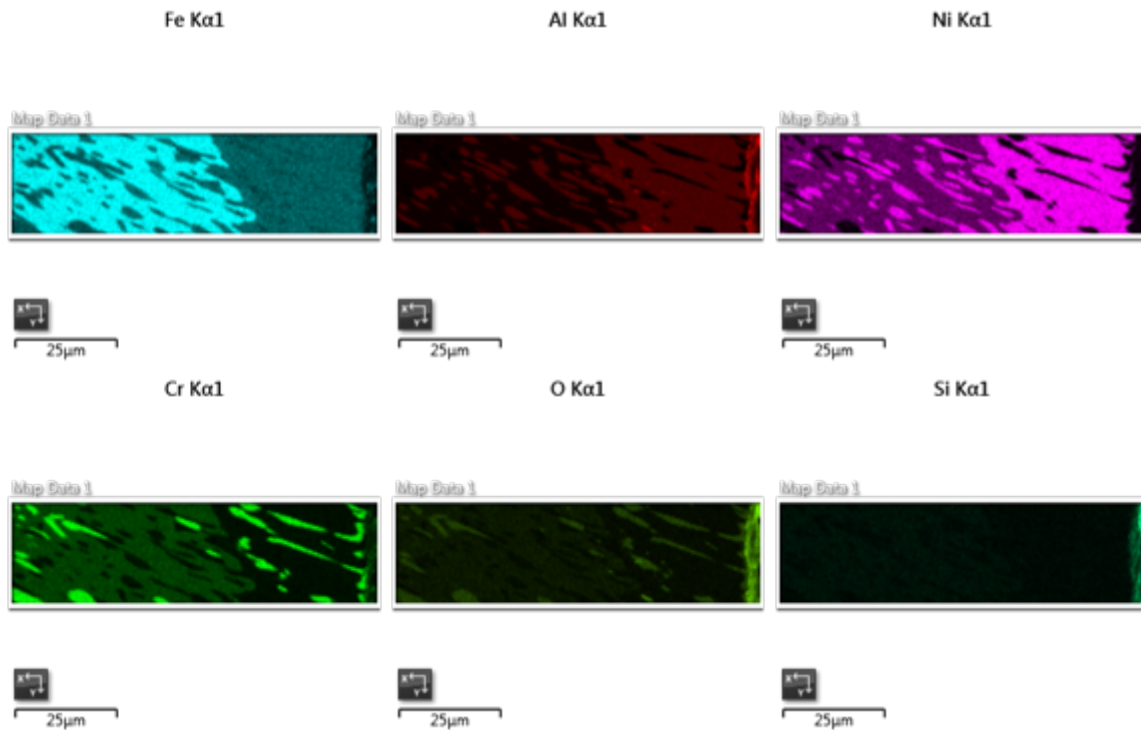


Figure 115: EDS mapping of aluminized racking poles exposed for 3 years

EDS mapping of aluminized racking poles indicated that chromium carbides precipitate at the $\beta - NiAl$ layer near the surface. More chromium carbides were found at $\beta - NiAl$ layer for vacuum carburized RA330 than gas carburized RA330. The reason may be due to vacuum carburized RA330 having relatively thin Al_2O_3 oxides at the surface of samples than gas carburized RA330. Vacuum carburization atmosphere did not have sufficient oxygen potential to form a dense oxides layer on the surface of RA330.

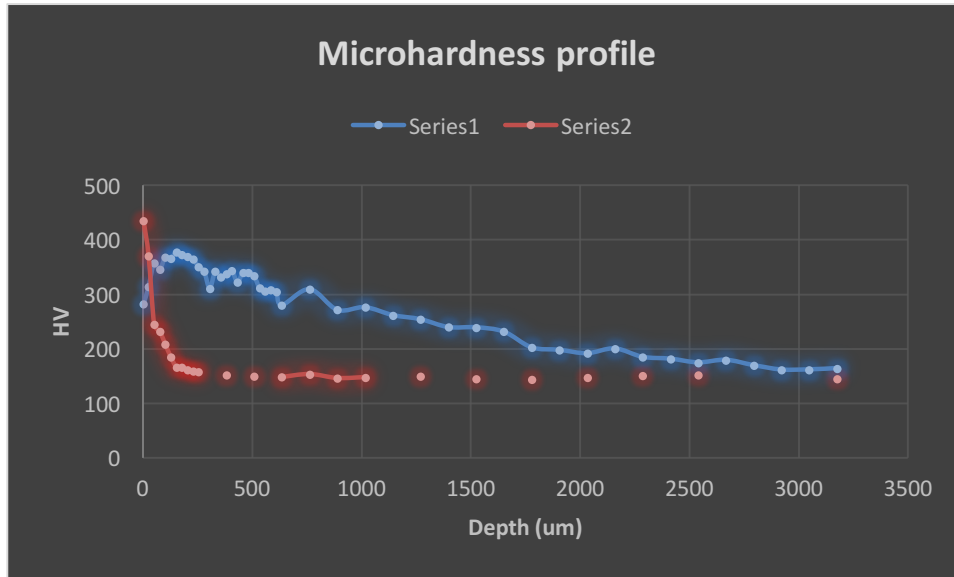


Figure 116: Cross section micro-hardness profiles of as-fabricated RA330 (series1 blue) and Aluminized RA330 (series2 red) exposed for 3 years

Micro-hardness profiles of as-fabricated RA330 racking poles exposed for 3 years shows that hardness decrease as depth increases from the surface to interior until 3mm. Micro-hardness profiles of aluminized RA330 racking poles exposed for 3 years decreased rapidly as depth increase until about $150\mu m$ from surface.

Conclusions

The micro-hardness profiles indicated that external carbon diffuse into as-fabricated racking poles formed chromium carbides precipitates from surface to 3mm depth in the matrix. However, for aluminized racking poles the depth of chromium carbides precipitates zone was only about $150\mu m$ from surface. Fewer carbon diffuses into matrix of aluminized racking poles than the as-fabricated racking poles.

In this case, aluminizing is an effective coating to reduce carburization in vacuum carburization furnaces. A dense Al_2O_3 layer was needed for aluminized alloys. Pre-oxidation of aluminized parts maybe needed for vacuum carburization.

5.3. Life Extension of Furnace and Fixture Alloys by aluminizing in Gas Carburizing Atmospheres

5.3.1. Commercial furnace testing for first exposure experiments

The alloys were selected for the alloy lifetime tests, including RA330, RA602CA, and INCONEL alloy 625. Samples have been aluminized by Alcoa Howmet in Branford, CT. These samples were divided into 10 groups. Group 1 and Group 6 were kept at WPI for microstructural characterization. The other eight groups were sent to Bluewater Thermal Solutions for extended exposure in the carburizing furnace ($T=871^{\circ}\text{C}$, $C_p = 0.8\% - 1.1\%$).

RA330, RA602CA, Inconel625 were received from Rolled Alloys.

The aluminizing was selected to improve the service life of alloys. Aluminizing is widely used to increase the high temperature oxidation and carburization resistance of nickel-based alloys. The thickness of the aluminide layer on the alloys increases with increasing aluminizing time. The intermetallic nickel aluminides that formed during aluminizing act as the reservoir of aluminum to maintain a protective Al_2O_3 layer on the material surface during high temperature services. *Alpha - alumina* Al_2O_3 provides effective protection from high temperature oxidation and carburization. Samples have been aluminized to compare the anti-corrosion properties of aluminized alloys and chromia former alloys. RA602CA, Inconel625, and RA330 were exposed in carburizing furnaces. Aluminizing coating was also conducted on these samples. These samples were exposed side by side in the furnace to compare the performances of these alloys.

After 3, 6, 12, 18, 24 months exposure, samples were removed from the furnace.

The weight gain of each sample has been measured. After exposure in the carburizing batch furnace, the weight gains were measured. The results of 6 months exposure are presented below.

Carbon potential: 0.5-1.1% average 0.7%; Temperature: $871^{\circ}\text{C} - 982^{\circ}\text{C}$ average 927°C

5.3.1.1. Samples exposed for 3 months in gas carburization furnace

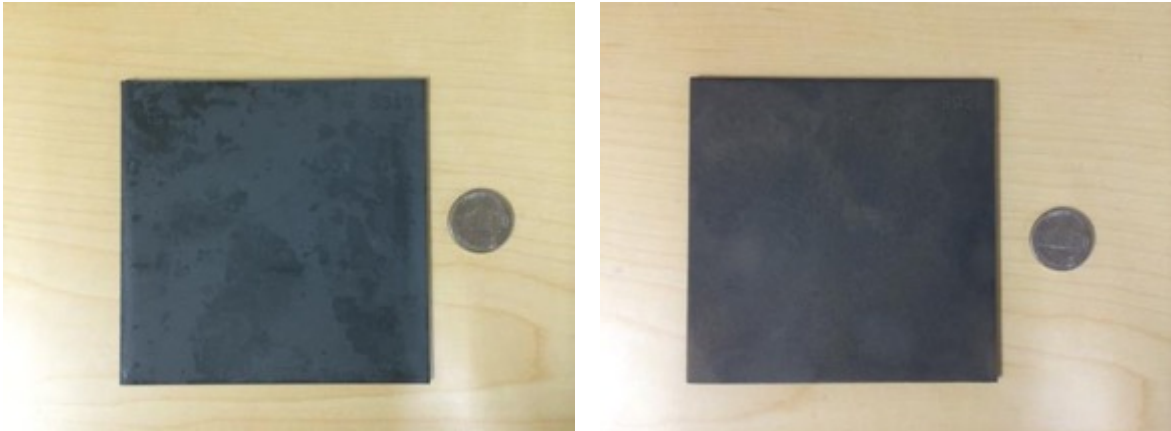


Figure 117. Exposed Unaluminized RA330 and aluminized RA330



Figure 118. Exposed Unaluminized RA602CA and aluminized RA602CA



Figure 119. Exposed Unaluminized and aluminized INCONEL alloy 625

In order to quantify the efficacy of the aluminized coating for carburization resistance, the weight gain per area has been calculated as seen in Table 16 and Table 17. Aluminized RA330 and aluminized INCONEL alloy 625 have lower weight gain than the unaluminized RA330 and INCONEL alloy 625.

Alloy	No.	Weight gain(m)	Surface area (A)	$\Delta m/A$ (g/mm^2)
RA330	3310	0.32g	21828mm ²	14.7×10^{-6}
	3306	0.20g	21828mm ²	9.16×10^{-6}
Inconel 625	6251	0.17g	21828mm ²	7.79×10^{-6}
	6256	0.11g	21828mm ²	5.04×10^{-6}
RA602CA	6020	0.12g	21828mm ²	5.50×10^{-6}
	6026	0.15g	21828mm ²	6.87×10^{-6}

Table 16. Weight gain per area for the alloys

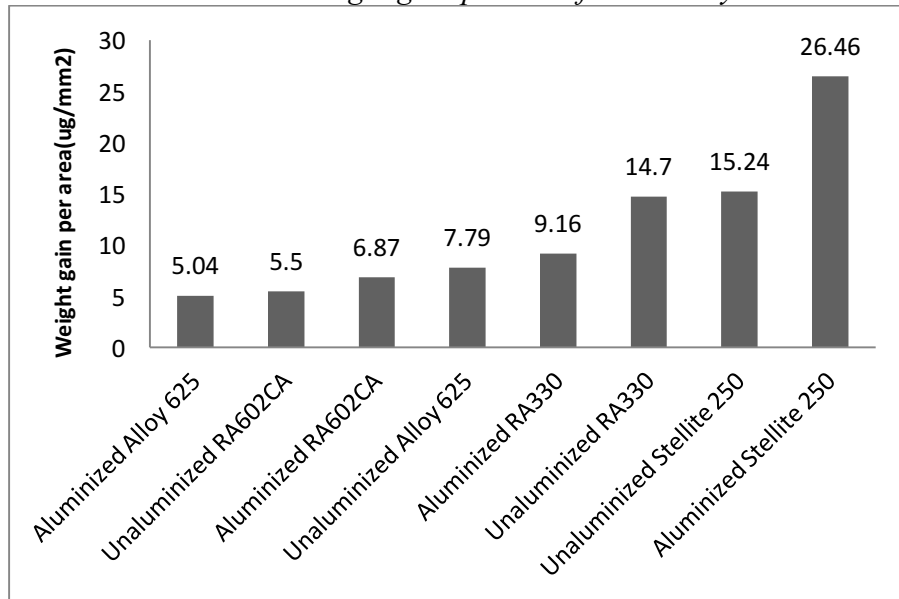


Table 17. Weight gain per area for the alloys

In general, aluminized samples have lower weight gain per area. The alumina Al_2O_3 layers coated samples have less weight gain per area than chromium oxide Cr_2O_3 coated samples.

5.3.1.2. Samples exposed for 12 months in gas carburization furnace

Samples were exposed in the batch carburizing furnace for 12 months. After 12 months furnace testing the weight gain of RA330 is listed in Table 18. After 12 months service in the carburizing batch furnace, the weight gain were measured and the results are listed below.

RA330	Weight-original	Weight-(time)	Weight gain

3301	240.97g	241.483g	0.513g
3307 aluminized	242.12g	242.290g	0.17g

Table 18. Weight gain of RA330 after 12 months exposure

RA602CA were exposed in the same carburizing atmospheres side by side with RA330 and the exposure time were also the same. RA602CA have the lowest weight gain among the 8 groups of samples which is as same as the last weight gain measurement (3 months exposure). In this case, RA602CA has the lowest carbon uptakes as shown in Table 19

RA602	Weight-original	Weight-(time)	Weight gain
6022	249.15g	249.325g	0.175g
6027 aluminized	243.60g	243.747g	0.147g

Table 19. Weight gain of RA602CA after 12 months exposure

Aluminized Inconel 625 has a relatively low weight gain compare to unaluminized Inconel 625. Consider the aluminized Inconel 625 have a continuous layer of Al_2O_3 , so the main reason for Inconel 625 take more carbon than aluminized Inconel 625 is that Al_2O_3 have better anti-carburization and oxidation resistance than Cr_2O_3 .

Inconel 625	Weight-original	Weight-(time)	Weight gain
6252	283.86g	284.14g	0.28g
6257 aluminized	286.70g	286.88g	0.18g

Table 20. Weight gain of Inconel 625 after 12 months exposure

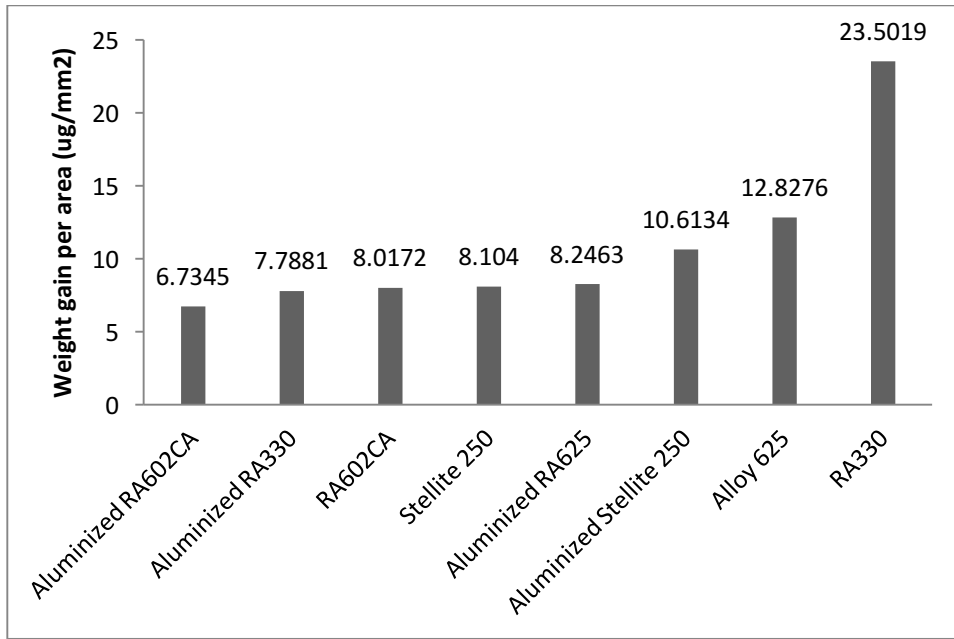


Table 21 Weight gain per area of alloys

According to the Table 21, RA330 have the highest weight gain per area compare with other alloys. However, aluminized RA330 shows relative high anti-carburizing properties according the weight gain per area. In this is case, aluminizing treatments have shown great potential for improving the life time of RA330 alloys.

5.3.1.3. Samples exposed for 18 months in gas carburization furnace

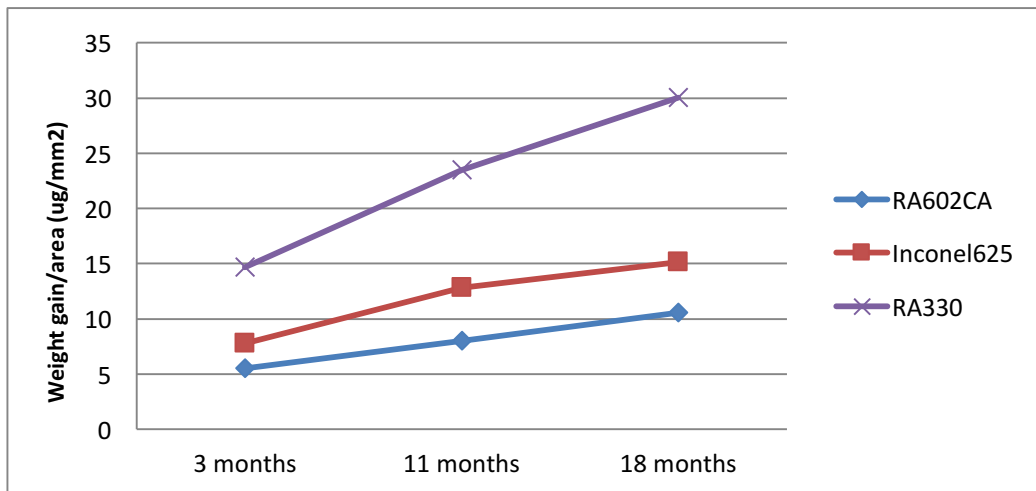


Figure 120. Weight gain per area as a function of time for unaluminized alloys

The first exposure experiments have been exposed in the carburization furnace for 18 months. Carbon continually diffuses through the oxide layer into the alloys substrate. Therefore, weight gain per area as a function of time shows the trend of weight gain. Figure 120 shows that weight gain increased for RA330, Inconel625 and RA602CA during the exposure. It was found that the coke formation may lead to metal dusting and subsequent weight lost.

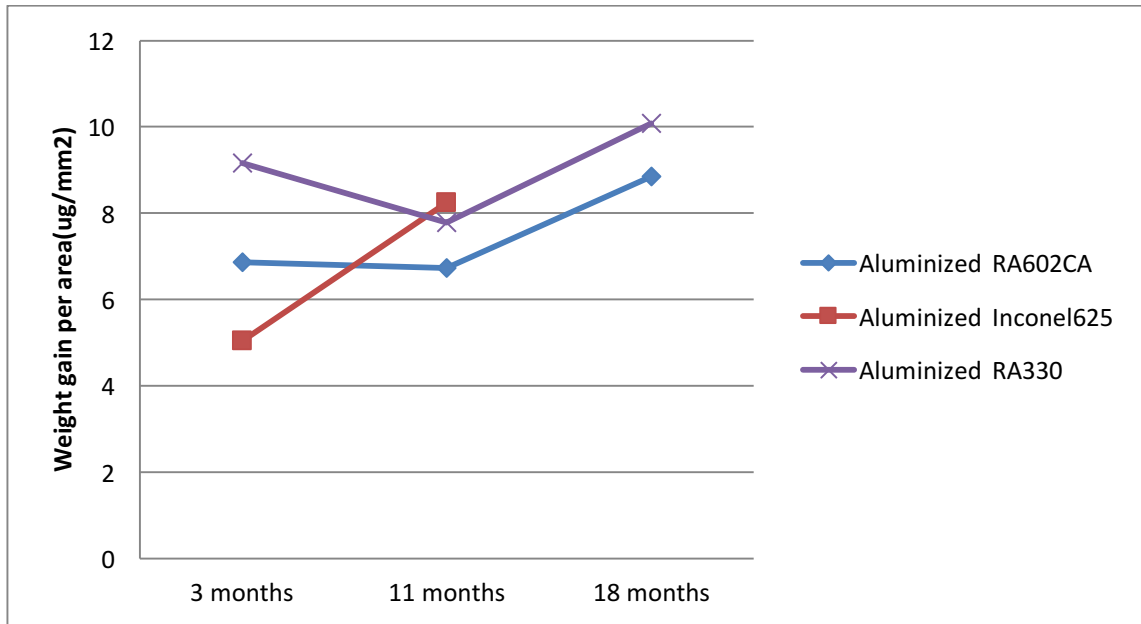


Figure 121. Weight gain per area as a function of time for aluminized alloys

For aluminized alloys, the formation of cock leads to accelerated carburization, and subsequent cracking or embrittlement may results in loss of alumina coating and possible loss of materials. According to *Figure 121* Aluminized RA330 and Aluminized RA602CA shows the similar phenomena with unaluminized exposed alloys that weight increase as the times increase.

5.3.1.4. Samples exposed for 24 months in gas carburization furnace

The weight of each sample has been measured by high accuracy electronic scales. Besides, Surface areas were also measured for RA 330, INCONEL alloy 625, RA 602CA, individually. After 24 months service in the carburizing batch furnace, the weight gain were measured and the results are listed below.

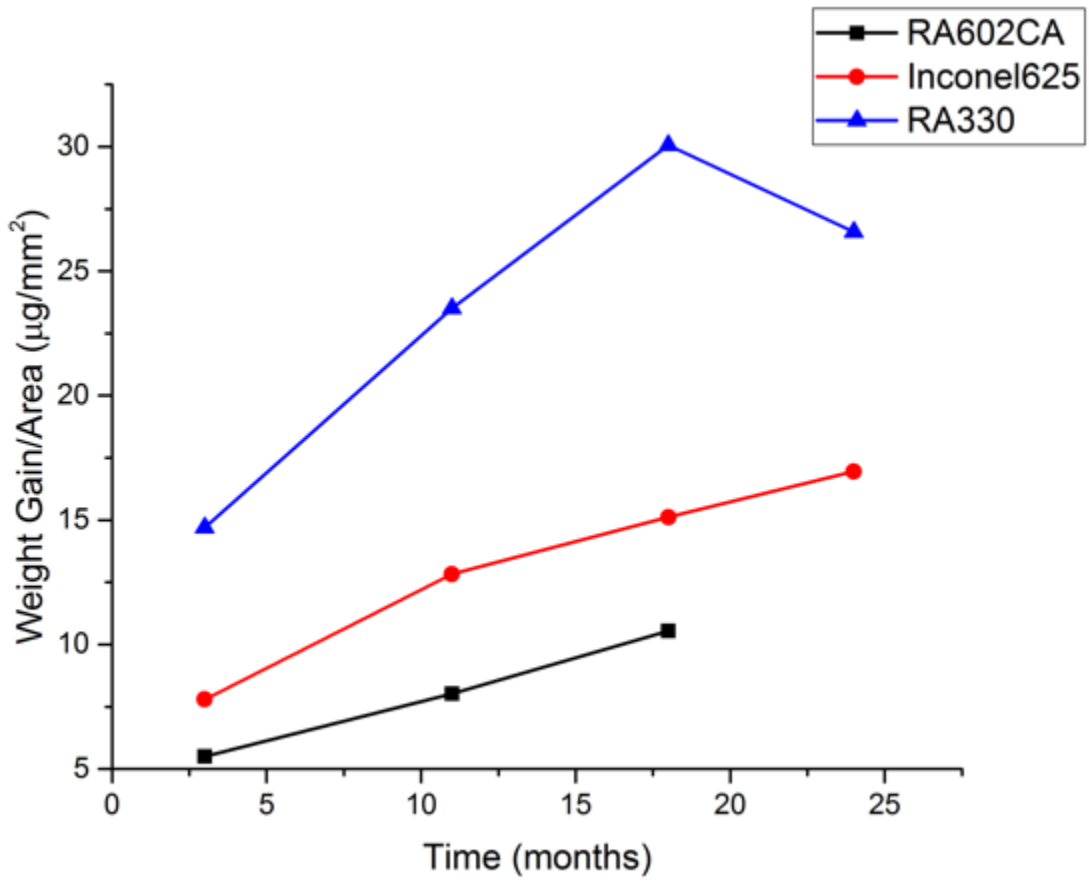


Table 22: Weight gain per area of unaluminized alloys

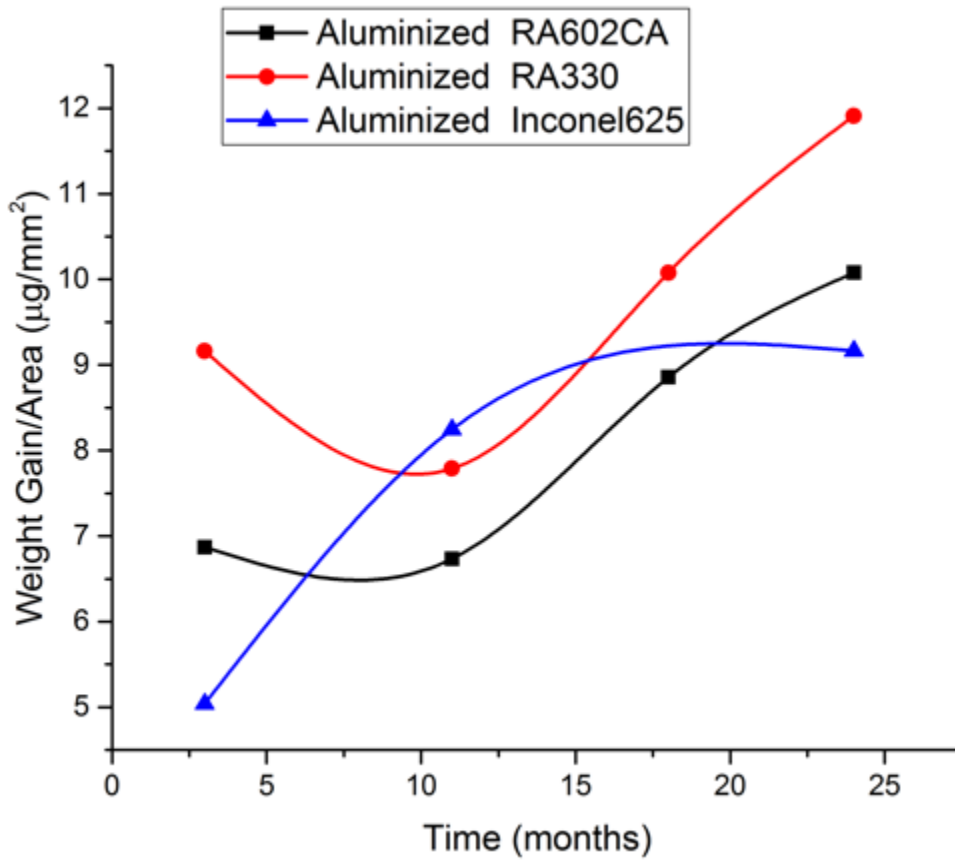


Table 23: Weight gain per area of aluminized alloys

As presented in Table 22, the weight gain is comprised of both oxidation and carburization. For RA330 alloys a reduced weight gain may be measured due to spalling of the oxides.

In general, aluminized samples have lower weight gain per area. The alumina Al_2O_3 layers coated samples have less weight gain per area than chromium oxide Cr_2O_3 coated samples. .

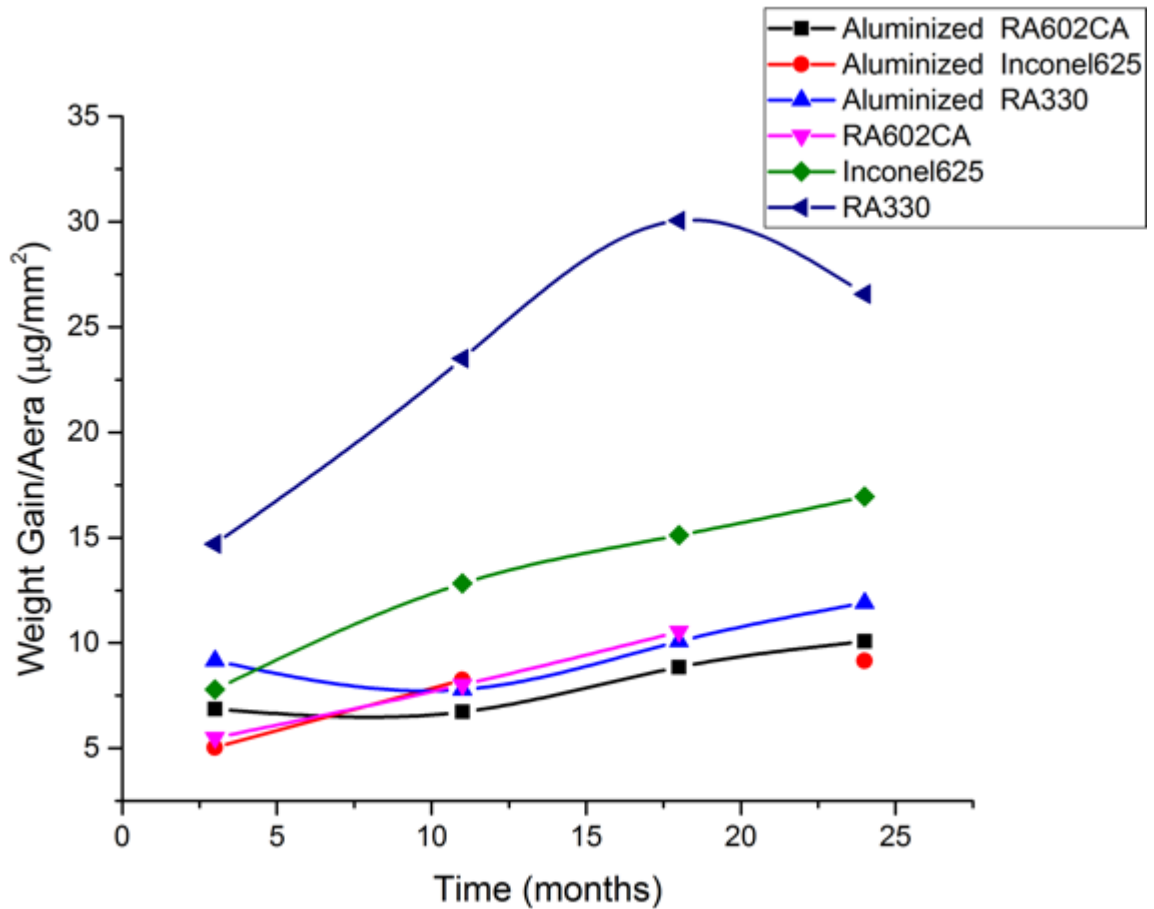


Table 24: Weight gain per area as a function of time

After aluminizing process, the anti-corrosion properties of RA330 samples increased significantly. According our weight gain analysis, aluminized samples have lower weight gain per area. The alumina Al_2O_3 layers coated samples have less weight gain per area than chromium oxide Cr_2O_3 coated samples.

As presented in Table 24, the weight gain is comprised of both oxidation and carburization. For alloys that have a reduced weight gain may be due to spalling of the oxides.

The alloys have been exposed in the carburization furnace for 24 months. Carbon continually diffuses through the oxide layer into the alloys substrate. Therefore, weight gain per area as a function of time shows that weight gain increased for RA330, Inconel625 and RA602CA during the exposure as the expose time increases.

According to Table 24, weight gain per area increases as a function of time increases. The purple line represents the weight gain for RA330, it was found that RA330 lost weight after 24 months

exposure compare to 18 months. That was because of decomposition of Cr_2O_3 layer. It was found that the weight gain for the aluminized alloys was uniformly less than the as-fabricated alloys.

5.3.2. Commercial furnace testing for second exposure experiments

After 7 months exposure, samples were removed on April 20th 2015. Samples were exposed in the batch carburizing furnace for 7 months. The batch furnace at Bluewater is located in Rockford, IL. These samples were placed in a batch carburizing furnace and the carbon potential of the atmosphere is approximately 0.7%.

5.3.2.1. Weight gain measurement

The weight of each sample has been measured by high accuracy electronic scales. Besides, Surface areas were also measured for RA 330, INCONEL alloy 625, RA 602CA, RA253MA and APMT individually. After 7 months service in the carburizing batch furnace, the weight gain were measured and the results are listed below.

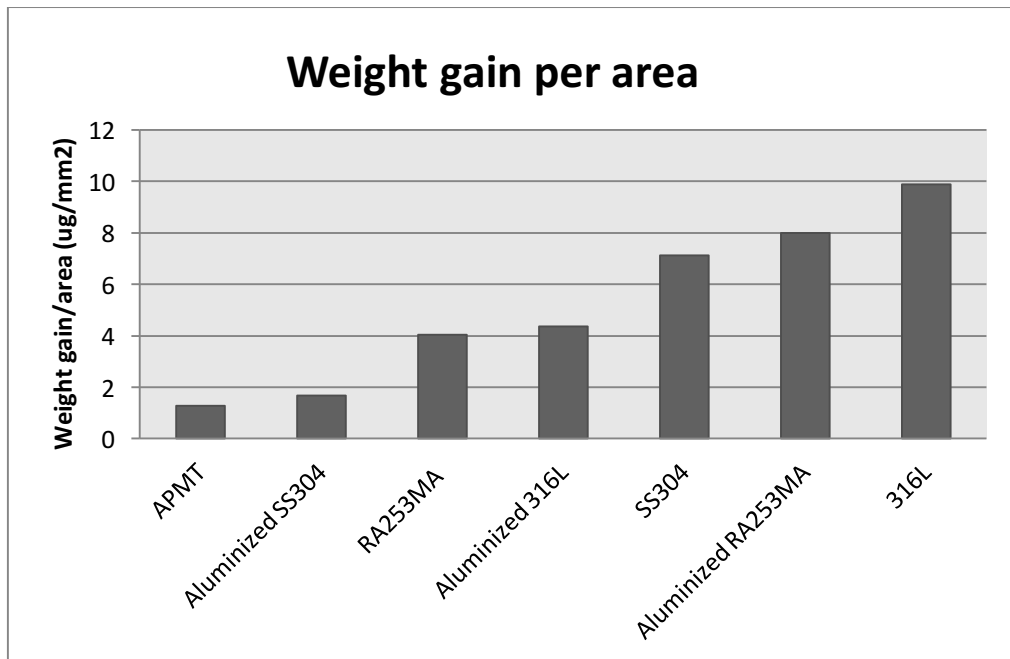


Table 25. Weight gain per areas for second exposure experiments

Exposed for 7months: APMT RA253MA 316L 304SS

Carbon potential: 0.8-1.1% average 1.0%; Temperature: 871°C -982°C average 927°C

According to Table 25 APMT have the lowest weight gain per area which indicated that APMT has the lowest carbon uptake during the carburization process. Furthermore, the weight gain was also generated because of oxidation. However, the APMT have already been fully oxidized that dense alumina were formed on the surface of APMT, in that case further oxidation during the furnace exposure would not generated sufficient weight to affect the result of weight gain measurement.

In general, aluminized samples have lower weight gain per area. The alumina Al_2O_3 layers coated samples have less weight gain per area than chromium oxide Cr_2O_3 coated samples.

5.3.2.2. Comparison between two exposure experiments

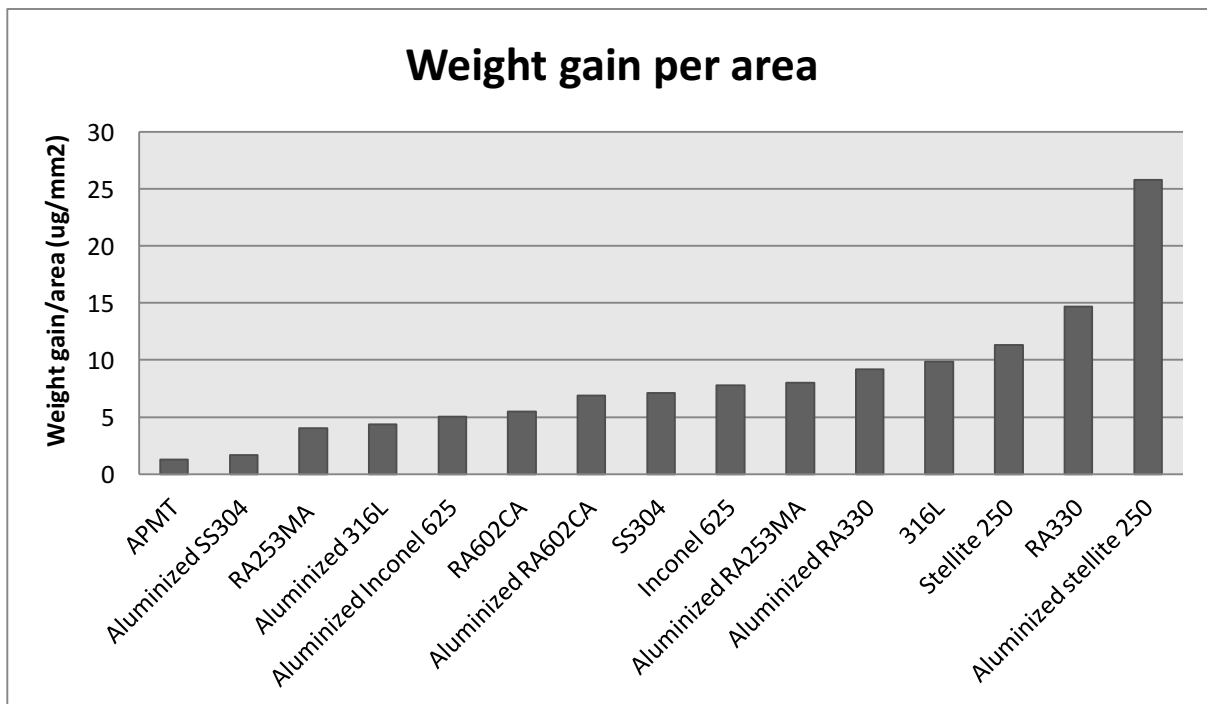


Table 26 Comparison of weight gain per area

Exposed for 3 months: RA330, RA602CA, Inconel 625

Exposed for 7months: APMT RA253MA 316L 304SS

Carbon potential: 0.8-1.1% average 1.0% ; Temperature: 871°C -982°C average 927°C

RA330, RA602CA, Inconel 625, were exposed for 7 months, and APMT RA253MA 316L 304SS were also exposed for 7 months. Alumina protected alloys are also have lower weight gain per area even the samples have been exposed for longer time. For example, APMT have the lowest weight gain per area among all the alloys.

As presented in Table 26 APMT has the lowest weight gain per area. The weight gain is comprised of both oxidation and carburization. For some alloys a reduced weight gain may be measured due to spalling of the oxides.

In general, aluminized samples have lower weight gain per area. The alumina Al_2O_3 layers coated samples have less weight gain per area than chromium oxide Cr_2O_3 coated samples.

Additionally, the alloys have been exposed in the carburization furnace for 6 months. Carbon continually diffuses through the oxide layer into the alloys substrate. Therefore, weight gain per area as a function of time shows that weight gain increased for 304L, RA330, Inconel625 and RA602CA during the exposure as the expose time increases.

References

[1]. H. J. Grabke, "On the mechanism of catastrophic carburization: metal dusting," Corrosion Science, Vol. 35, Nos 5-8, (1993) pp. 1141-1150.

[2] H. J. Grabke, "Metal dusting" Materials and Corrosion, Vol. 54, No. 10, (2003).

[3] H. J. Grabke, "Thermodynamics, mechanisms and kinetics of metal dusting," Materials and corrosion 49, 303-308 (1988)

[4] J. Zhang and D. Young, Corrosion Science 48,1496 (2006)

- [5] E. M Muller-Lorenz, H. J. Grabke, Mat. Corr. 1999, 50, 614.
- [6] S. Strauss, R. Krajak, H. J. Grabke, Mat. Corr. 1999, 50, 614.
- [7] A. Schnaas, H. J. Grabke: Werkst. Korros. 29 (1978) 635.
- [8] H. J. Grabke, U. Gravenhorst, W. Steinkusch: Werkst. Korros. 27 (1976) 291.
- [9] W. F. Chu, A. Rahmel: Oxid. Metals 15 (1981) 311.
- [10] A. Rahmel, H. J. Grabke and W. Steinkusch, Materials and Corrosion 49, 221-225(1998).
- [11] J. Klower, H. J. Grake and E. M. Muller-Lorenz., Materials and Corrosion 49, 328-329 (1998)
- [12] D.K. DAS, VAKIL SINGH, S.V. JOSHI,
- [13] Combe C., Cardey PF., “Pre-oxidation treatment to increase the service life of heat treatment furnace conveyor belts made of AISI 330Cb industrial application” International Federation of Heat Treatment and Surface Engineering 2016, Proceedings of the 23rd IFHTSE Congress
- [14] Buscail, H. & al “NaOH coatings effects on the 330Cb alloy oxidation at 900°C” Volume 25, apOxidation of metals.
- [15] RA330® vs 309/310 - Rolled Alloys. Available from:
http://content.rolledalloys.com/technical-resources/alloy-comparison/RA330vs309-310_AC_US_EN.pdf.
- [16] KANTHAL APMT, Sandvik Materials Technology. Available from:
http://netl.doe.gov/File%20Library/Events/2010/ods/Roger_Berglund.pdf
- [17] RA253MA® : <http://www.rolledalloys.com/alloys/stainless-steels/ra-253-ma/en/>
- [18] RA 602 CA® Data Sheet. Available from: http://content.rolledalloys.com/technical-resources/databooks/RA-602-CA_DB_US_EN.pdf.
- [19] Special Metals cited 2013; Available from:
<http://www.specialmetals.com/documents/Inconel%20alloy%20625.pdf>.

- [20] The Effects of Rust on the Gas Carburization of AISI 8620 Steel, Xiaolan Wang, advisor Prof. R. D. Sisson. A Thesis of the Worcester Polytechnic Institute, Degree of Master of Science.
- [21] C. H. Toh, P. R. Munroe, and D. J. Young, Metal Dusting of Fe-Cr and Fe-Ni-Cr Alloys under Cyclic Conditions, *Oxidation of Metals*, Vol. 58, Nos. ½, August 2002
- [22] J. Gwyther, M Hobdell and A. J. Hooper, Conf. Fuel Element behaviour, Metals society, London, 1972.
- [23] S. Terauchi, H. Terauchi and K. Kamei, Heat Treatment' 76, Metals Society, London, 1976, pp. 45-49.
- [24] J. P. Souchard, P. Jacquot and M. Buvron, *Mater. Sci. Eng.*, A140(1991) 454-460
- [25] I Asano, T. Araki and Y. Ikawa, *Mater. Sci. Eng.*, A140(1991) 461-468
- [26] B.-S Suh, W.-J. Lee/*Thin Solid Films* 295 (1997) 185-192
- [27] Thermodynamic modeling and kinetics simulation of precipitate phases in AISI 316 stainless steels, Y. Yang, J.T. Busby, *Journal of Nuclear Materials* 448(2014) 282-293
- [28] Lai, G.Y., *High-Temperature Corrosion and Materials Applications*, ASM International.
- [29] Institute, N.D., Heat and Corrosion Resistant Castings: Their Engineering Properties and Applications. NiDI.
- [30] Institute, N.D. Heat and Corrosion Resistant Castings: Their Engineering Properties and Applications. 2013; Available from:
http://www.nickelinstitute.org/~Media/Files/TechnicalLiterature/Heat_ResistantCastingsCorrosion_ResistantCastingsTheirEngineeringPropertiesandApplications_266_.pdf
- [31] Vander Voort, G.F., ASM Handbook, Volume 09 - Metallography and Microstructures. ASM International. p. 841.
- [32] Andersson, J.O., et al., THERMO-CALC & DICTRA, computational tools for materials science. *CALPHAD*, 2002. 26(2): p. 273-312.
- [33] Wilson, J. and J. Kelly, *Wrought Heat Resisting Alloys Provide Cost Reductions*. 1997: ASM Heat Treat Show.

[34] Yuki Matsuoka, Y.M., Kiyokazu Nakagawa, Yoshihiro Tuda and Shigeji Taniguchi, *Growth Behavior of Coatings Formed by Vapor Phase Aluminizing Using Fe-Al Pellets of Varying Composition*. Materials Transactions, 2006. 47(9): p. 2341-2347.

[35] Marc Glasser, “RA602CA: An Alloy for the Highest Temperature Processes”, 28th ASM Heat Treating Society Conference, 2015

[36] H.J. Grabke, R. Krajak, “Metal dusting of nickel-base alloys”, Materials and Corrosion 47, 495-504, (1996)

5.4. The Performance of RA330 and Aluminized RA330 in an Industrial Gas Carburizing Furnace

Anbo Wang¹, Haixuan Yu¹, R. D. Sisson, Jr.^{1}*

¹Center for Heat Treating Excellence, Worcester Polytechnic Institute, Worcester, Massachusetts, 01609, U.S.A

**Email: sisson@wpi.edu*

Submitted to: *Journal of Surface and Coating Technology*

Abstract

The high temperature corrosion resistant alloy RA330 is widely used for furnace fixtures in heat treatment furnaces. This paper focuses on the anti-carburizing and anti-oxidation properties of RA330 and aluminized RA330. Aluminizing can be used to increase the high temperature oxidation and carburization resistance of nickel-based alloys. In this paper, RA330 and aluminized RA330 were selected to study their performance in an industrial gas carburization furnace for times up to two year. The oxidation properties and oxide stability at high temperatures will be presented. In addition, the preliminary analysis of microstructural development during long-term exposure experiments in an industrial carburizing furnace will be presented. These samples were characterized using optical and scanning electron microscope, electron backscatter diffraction (EBSD), and x-ray diffraction. It was found that the aluminized alloys exhibited lower weight gain and carbon uptakes.

Introduction

The heat-treating industry is in need of heat-treatment furnace materials and fixtures that have a long service life. Stainless alloys were widely used in high temperature anti-corrosion applications such as fixtures inside the high temperature furnace. Fixtures are typically manufactured using Ni-based alloys, whose chemical composition is selected to achieve the required mechanical performance and creep resistance, even if this caused limited anti-corrosion and anti-oxidation properties [1]. As a result, without the use of protective surface treatments, these degradation mechanisms could lead to catastrophic failures, resulting in complete system shutdown. Many of the fixtures fail within one years of exposure in high temperature carburization atmospheres [2].

Furnace fixtures operate in severe environment. Iron-nickel based and Iron-Nickel-Chromium based alloys are experience a variety of degradation mechanisms [3]. The corrosion products are mainly graphite, chromium carbide, and oxides. For RA330 alloy, the primary reason for failure was the excessive carburization that leads to “metal dusting” and subsequent cracking [3-5].

An extension of the service life for high temperature structural alloys is the goal for many heat treaters. Aluminizing is a coating that has been widely used in aerospace industry, especially in turbine blade applications [6]. It is also known that carbon has very low solubility in alumina. In that case, aluminizing could be a good method for protecting high temperature structural alloys. The protection is achieved by enriching the surface layer of the aluminum through diffusion mechanisms. Aluminum element reacts with the substrate material to form secondary phases and the intermetallic that act as a reservoir of scale formers during the service life [7].

This work is focused on the development of a better understanding of the effects of carburization on these alloys and coatings.

Material and methods

In this project, RA330 is well known as the corrosion-resistant alloy offering an exceptional combination of strength and resistance to carburization, oxidation and thermal shock. RA330 finds wide applications in high temperature industrial environments where good resistance to the combined effects of carburization and thermal cycling is prime requisite [2].

RA330 was aluminized to improve the carburization resistance and oxidation resistance of this alloy. Aluminizing is widely used to increase the high temperature corrosion and oxidation resistance of nickel-based alloys. α – alumina Al_2O_3 is effective protection for high temperature and aggressive gaseous environments. Nickel aluminides formed during aluminizing act as the reservoir of aluminum for maintaining a protective Al_2O_3 scale on the material surface during high temperature services.

Selected RA330 samples were aluminized in a static gas phase system at 1090 °C for 5 hours. Chromium aluminum source material (70%Cr/30%Al) and ammonium fluoride granules

were used in the system. The coating chamber was purged with argon until a dew point of -40F or better was met, then the argon is shut-off to the coating chamber (hence static system) and heating begins.

As fabricated and aluminized samples were exposed in an industrial gas carburizing furnace. Samples were exposed in the batch carburizing furnace for 3 months, 6 months, 12 months, 18 months and 24 months. The batch furnace at Bluewater is located in Rockford, IL. These samples were placed in a batch carburizing furnace and the carbon potential of the atmosphere is approximately 0.7%. Carburizing temperature is set at 870°C to 925°C in this furnace. The furnace only shut down three or four times during one calendar year for examine. Samples were distributed in the furnace against the production parts.

The weight of each sample has been measured by high accuracy electronic scales. After exposure in the carburizing batch furnace, the weight gains was measured again. Before each measurement, samples were ultrasonically cleaned by ethanol. The typical error range is within $\pm 0.005g$.

The measured weight gain includes the carbon uptakes and oxidation. The weight gain is primarily carbon uptakes. In this case, the carbon flux could be calculated by following formula.

$$\text{Total Carbon flux} = \text{weight gain} / \text{surface area}$$

Results and Discussion

RA330 samples were provided by Rolled Alloys Co. Selected samples have been aluminized by Alcoa Howmet in Branford, CT. for characterization.

	Cr	Ni	Mn	Si	Cu
MIN%	18.0	34.0	-	1.0	-
MAX%	20.0	37.0	2.0	1.5	1.0
	P	S	C	Fe	
MIN%	-	-	0.04	-	
MAX%	0.03	0.03	0.08	Balance	

Table 27: Chemical Composition of RA330

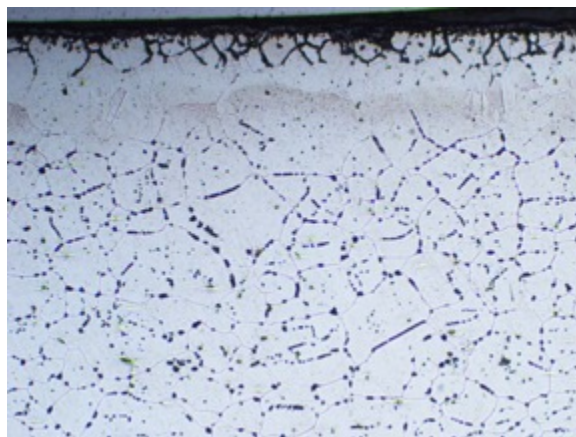
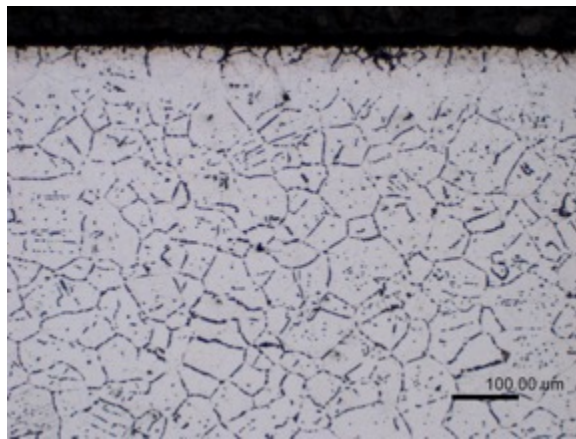
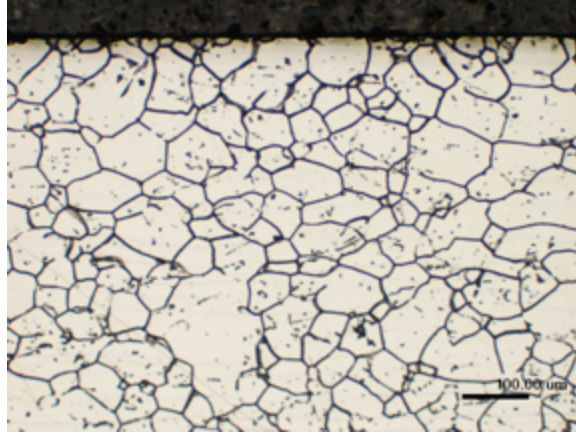
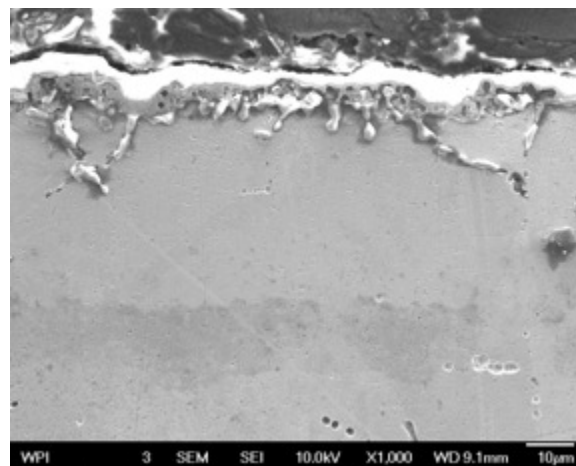
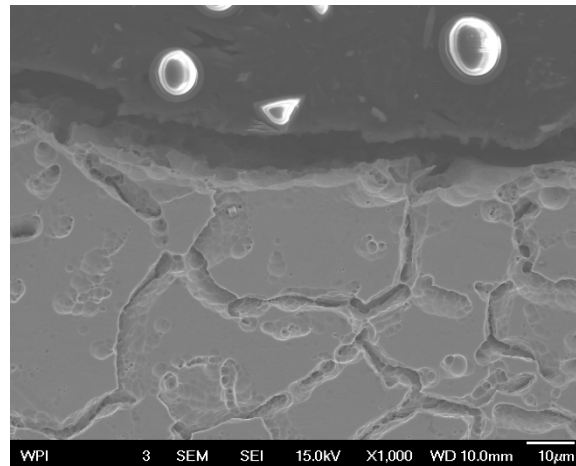


Figure 122: a) Optical photomicrographs of as fabricated RA330 b) Optical photomicrographs of RA330 exposed for 3 months c) Optical photomicrographs of RA330 exposed for 11 months

The optical photomicrographs for the unexposed and exposed cross section as presented in the Figure 122 (a,b), the single phase microstructure of unexposed (a) and exposed (b) RA330. The carburizing case and inter granule oxide (IGO) formed at the sample surface after 3 months service in carburizing furnace was seen in Figure 122. Samples were electrolytic etched with 10% Oxalic Acid at 10V for 30s.



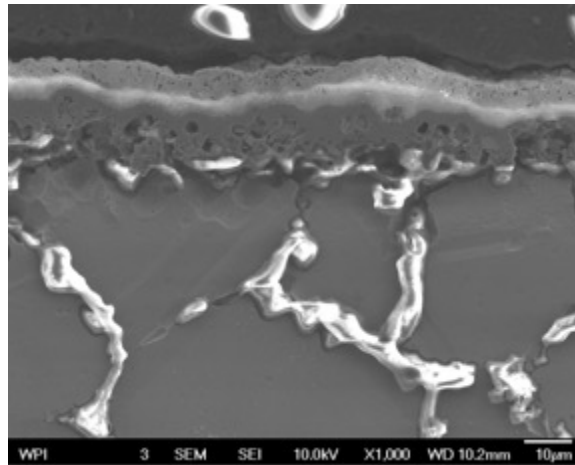
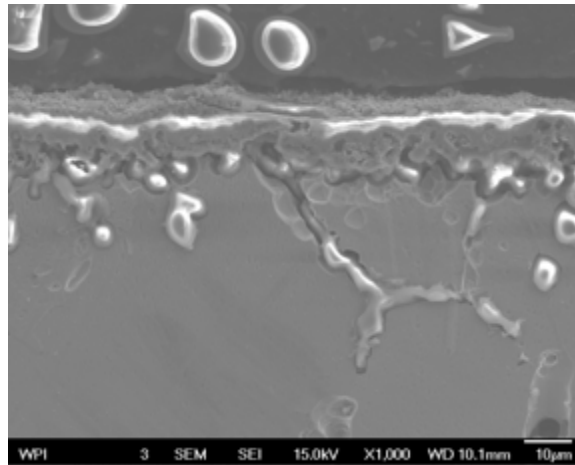


Figure 123: SEM photomicrographs of as fabricated RA330 and RA330 exposed for 3 months, 12 months and 18 months

Further investigation of RA330 exposed for 18 months were conducted. Cross-sectional photomicrographs of RA330 exposed for 18 months as presented in Figure 123 shows continuous Cr_2O_3 layer on the surface of exposed RA330. The lighter layer on the top of cross section photomicrograph is Cr_2O_3 . The SiO_2 layer was formed at the sublayer of Cr_2O_3 . The thickness of Silicon oxide distribution layer was about $50\mu m$. RA330 have been exposed for 18 months, the thickness of SiO_2 was larger than RA330 that exposed for 12 months or 3 months. In the core area of RA330, the matrix of alloy is mainly austenite phase with chromium carbides precipitate at grain boundaries.

EDS mapping of samples also indicated that oxide layers on the surface in Figure 128 are Cr_2O_3 and SiO_2 .

The structure and texture were studied using electron backscatter diffraction (EBSD) technique. Samples were cut by low speed saw and followed by mounting. Samples were ground from 200 grit to 1200 grit. Samples were polished by 1 micrometer alumina polishing powder then 0.3 micrometer, and 0.05 micrometer alumina polishing powder. The last step for samples preparation is vibratory polishing; Samples was polished for 12 hours before EBSD characterization.

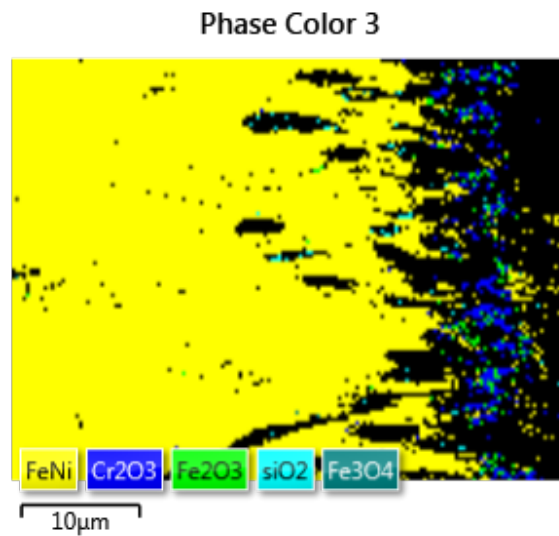


Figure 124: EBSD phase image of RA330 exposed for 12 months

EBSD phase analysis shows Austenite phase in the matrix and oxide layers at the surface of RA330. In Figure 124, yellow area on the left side represented austenite matrix phase. Blue area on the right side of Figure 124 shows the Cr_2O_3 , SiO_2 , Fe_2O_3 and Fe_3O_4 oxide layers on the surface.

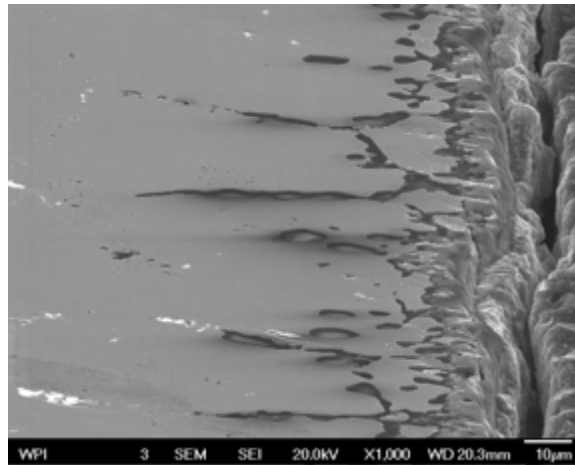


Figure 125: SEM photomicrographs of RA330 exposed for 24 months

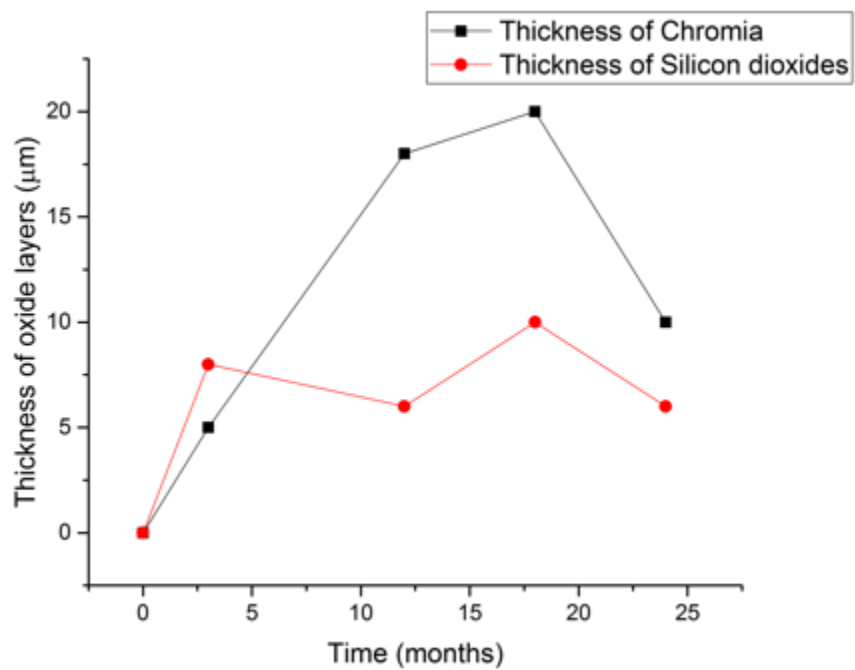


Figure 126: Thickness of oxide layers of RA330 samples

Figure 127 shows the oxides from the surface to interior, which are Fe_2O_3/Fe_3O_4 , Cr_2O_3 and SiO_2 as presented in Figure 127 from left to right.

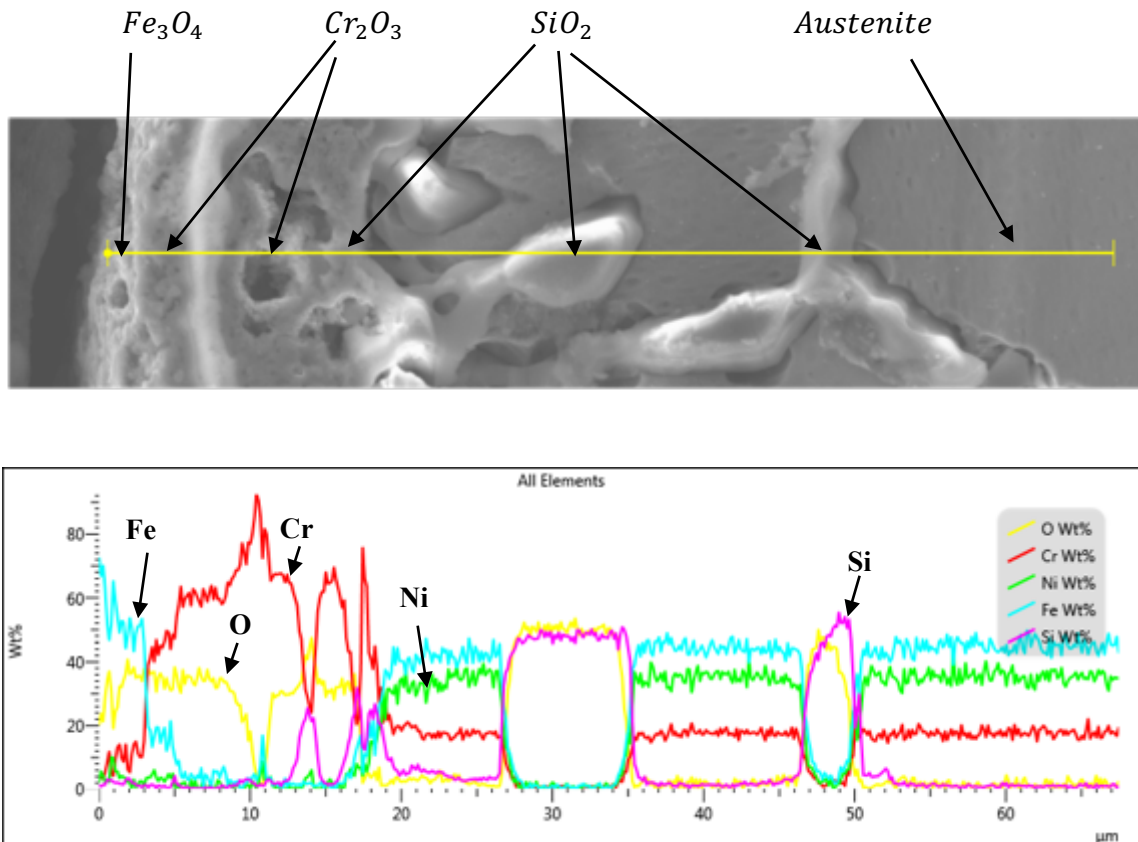
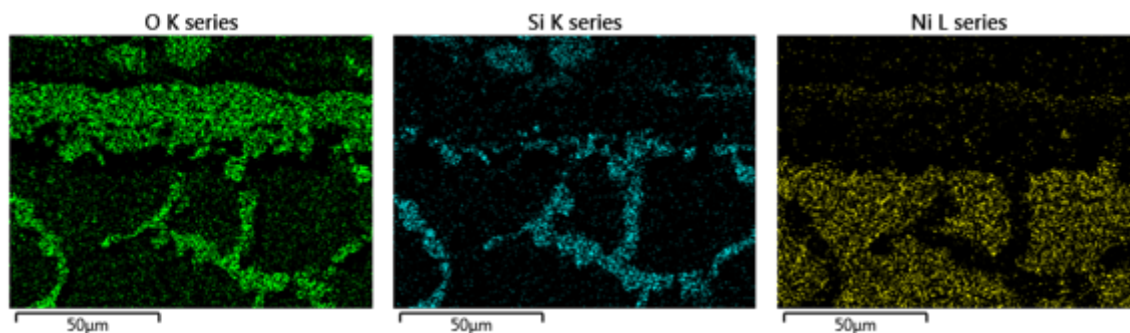


Figure 127. EDS line-scan of RA330 exposed for 12months from surface to the interior

The thickness of oxide layers increased with time before 18 months exposure as presented in Figure 126. The thickness of both Cr_2O_3 and SiO_2 decrease after exposed for 24 months, which was due to the spalling of oxides.



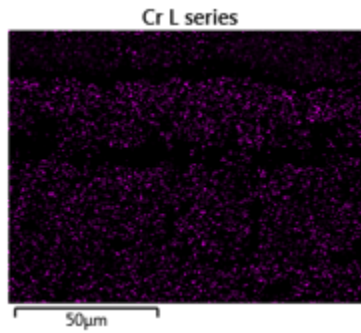
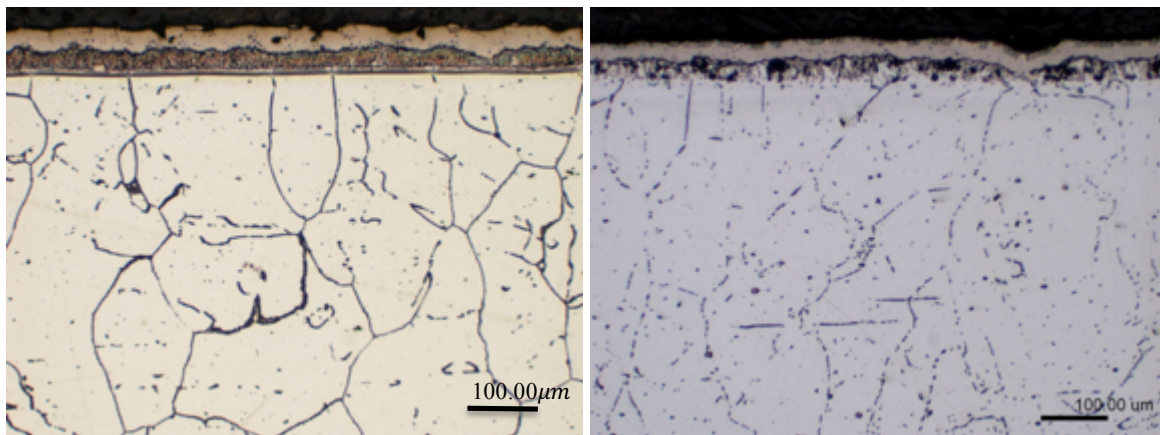


Figure 128: EDS mapping of RA330 exposed for 18 months

Aluminized RA330

The SEM photomicrographs for the unexposed and exposed cross section as presented in Figure 130. Figure 130(a) shows the SEM microstructure of polished as fabricated aluminized RA330. In Figure 130(b-d), samples were electrolytic etched with 10% Oxalic Acid at 10V for 30s. In Figure 130 (e), samples were vibratory polished and cleaned.



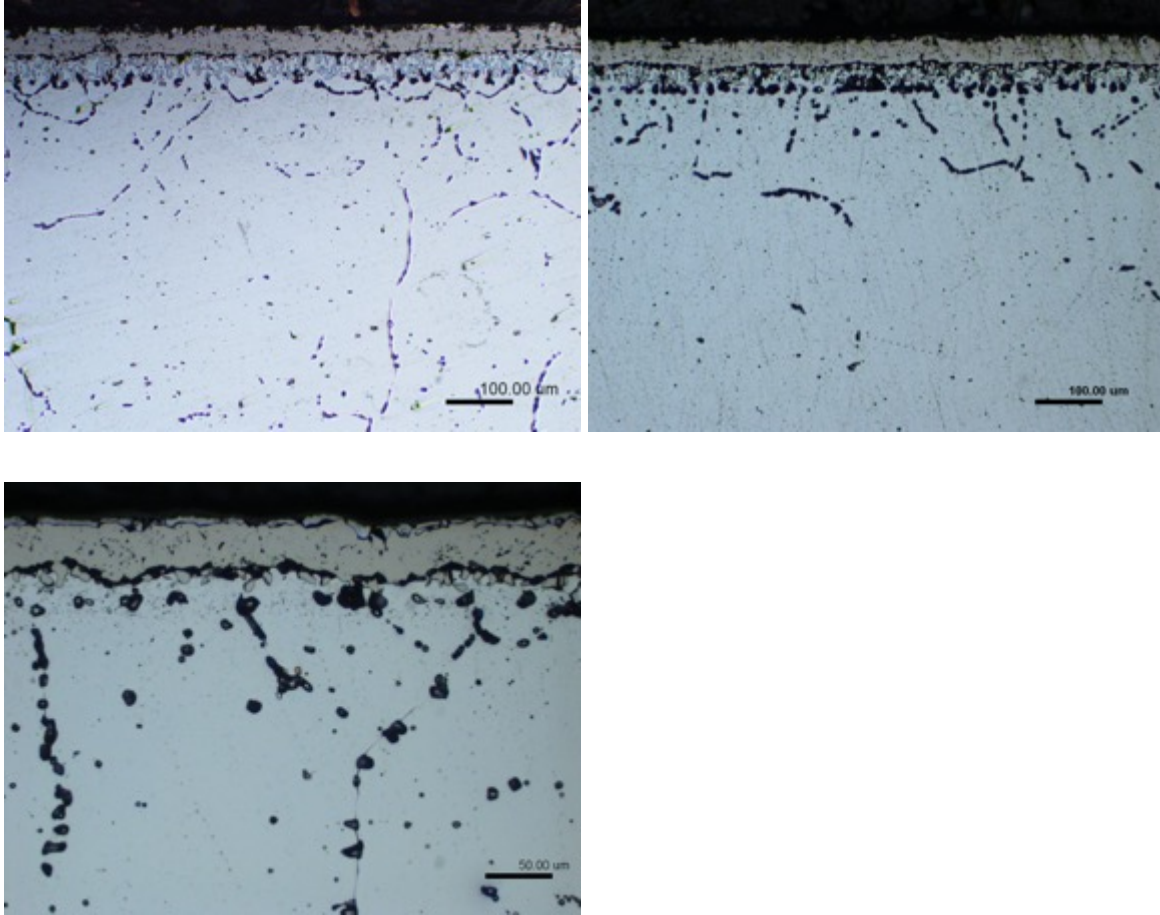
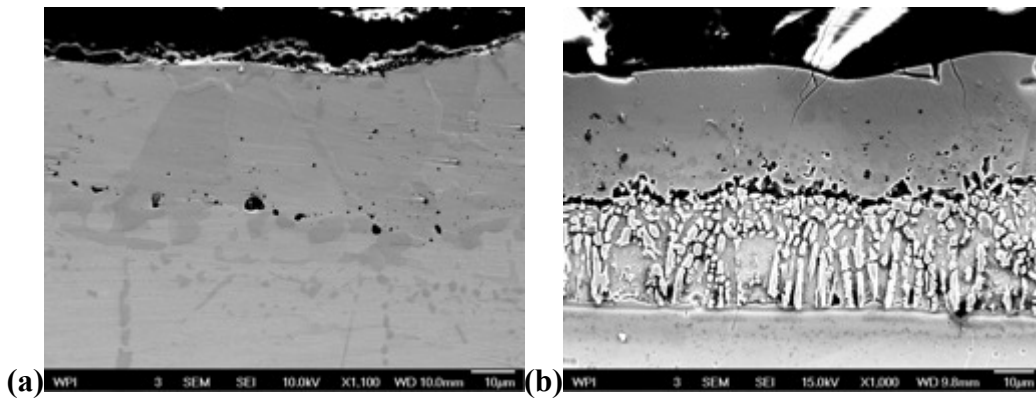


Figure 129: Optical photomicrographs of aluminized RA330, (a) original, (b) exposed for 3 months, (c) exposed for 12 months, (d) exposed for 18 months, (e) exposed for 24 months



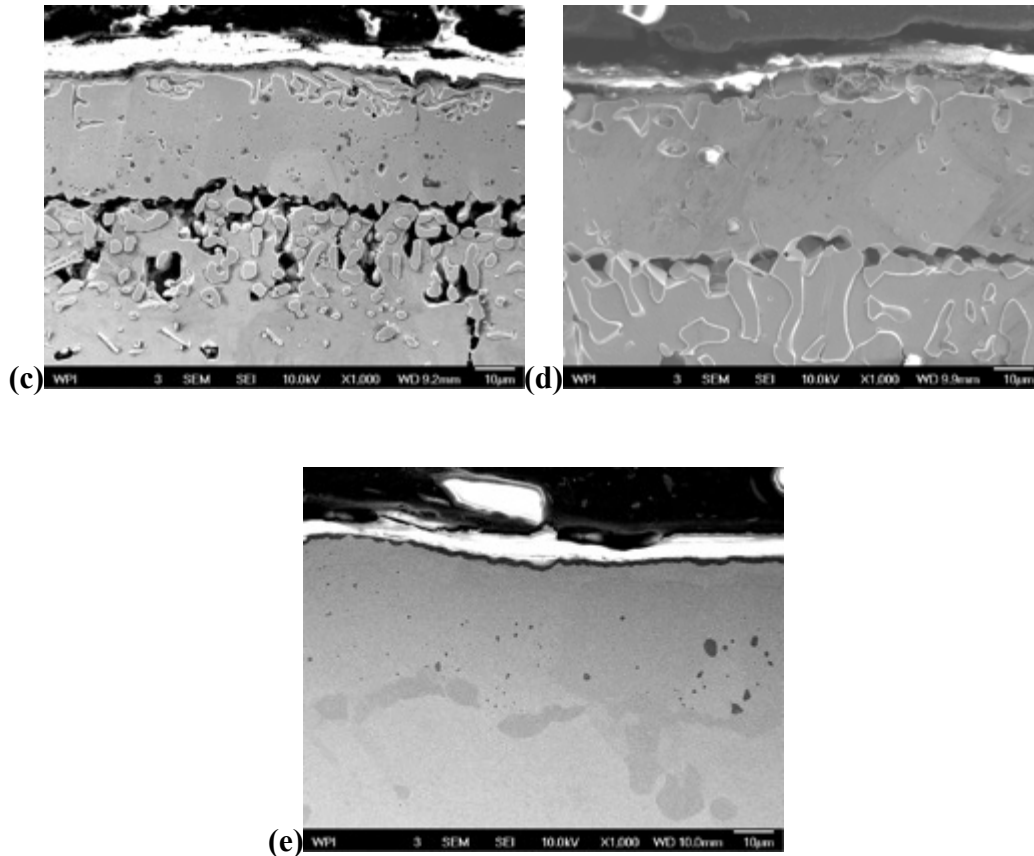


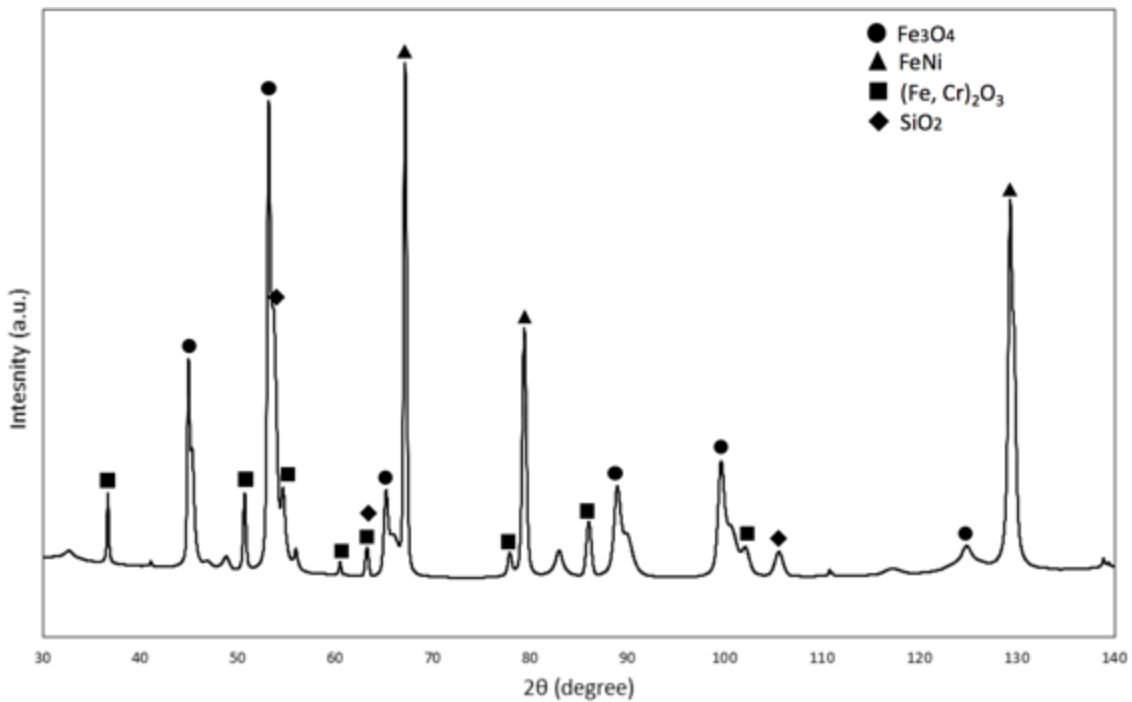
Figure 130: SEM photomicrographs of Aluminized RA330 a) As fabricated aluminized RA330 at edge, b) Electro-chemically etched as fabricated aluminized RA330, c) Electro chemical etched aluminized RA330 exposed for 3 months d) Electro-chemically etched aluminized RA330 exposed for 18 months, e) Polished aluminized RA330 exposed for 24months

Figure 130 presents the aluminized case at the surface of RA330 which is composed of two layers. The XRD pattern presents that the outer layer is mainly nickel aluminide ($\beta - Ni Al$) with aluminum oxides (Corundum, $\alpha - Al_2O_3$). And the EDS analysis presents that the inner layer is discontinuous nickel aluminide ($\beta - Ni Al$) on the austenite matrix. The alumina layer is stable and adherent to the substrate, no defect was seen. Figure 130(b-d) shows the discontinuous $\beta - Ni_1Al_1$ at depth about $35\mu m$ from the surface, the black areas were voids caused by etching.

Figure 130(e) indicated that the thickness of discontinuous $\beta - Ni_1Al_1$ decreased after 24 months exposure in gas carburization furnace. Outer layer was Alumina $\alpha - Al_2O_3$ as seen in Figure 130(e).

According to Figure 130 the thickness of $\beta - Ni_1Al_1$ decreased as the exposure time increases from 3 months to 24 months. As seen in Figure 130, after 24 months exposure $20\ \mu m$ of $\beta - Ni_1Al_1$ was still observed beneath the alumina layer of aluminized RA330.

The Alumina layer contains defects on surface. The reason for that was due to the shortage of Al content that provided by $\beta - Ni_1Al_1$. In the core, Austenite phase was identified by both XRD analysis and SEM photomicrographs.



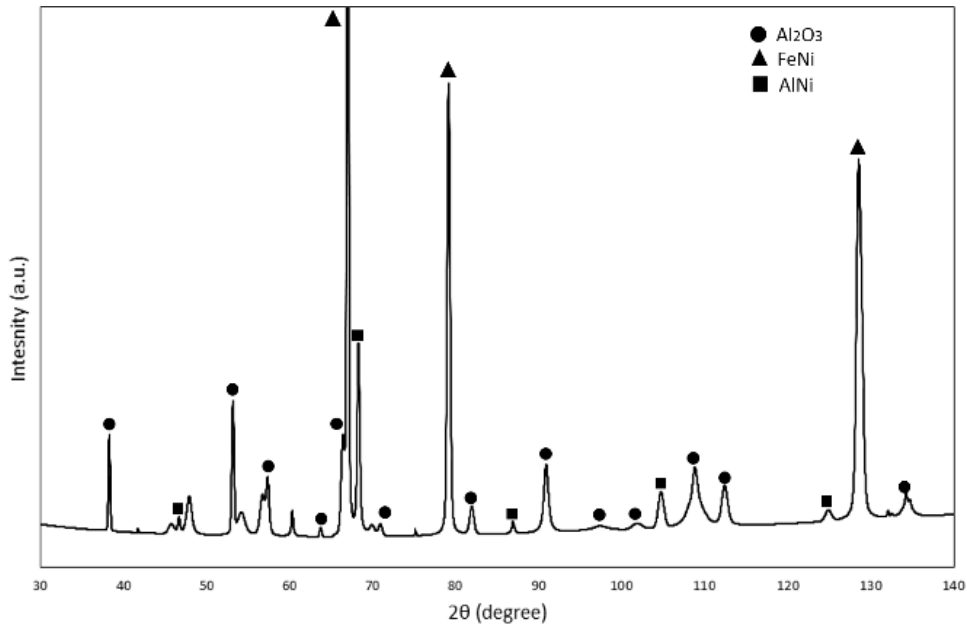


Figure 131: XRD analysis of RA330 (upper) and aluminized RA330 (bottom) exposed for 12 months

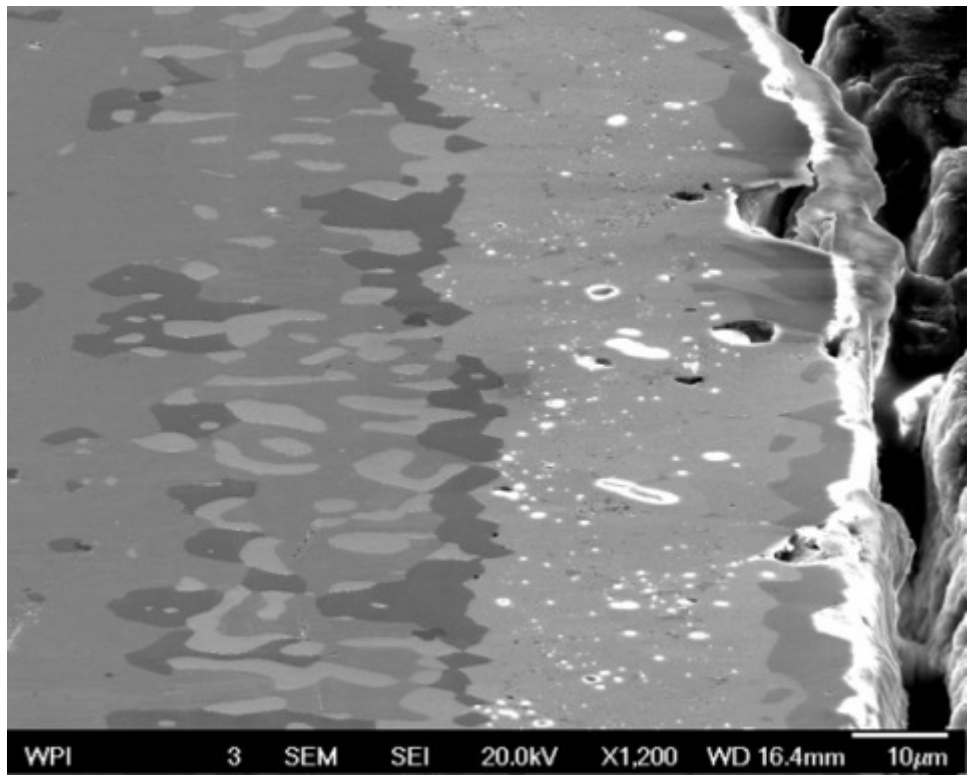


Figure 132: SEM photomicrographs of Aluminized RA330 exposed for 12 months at edge

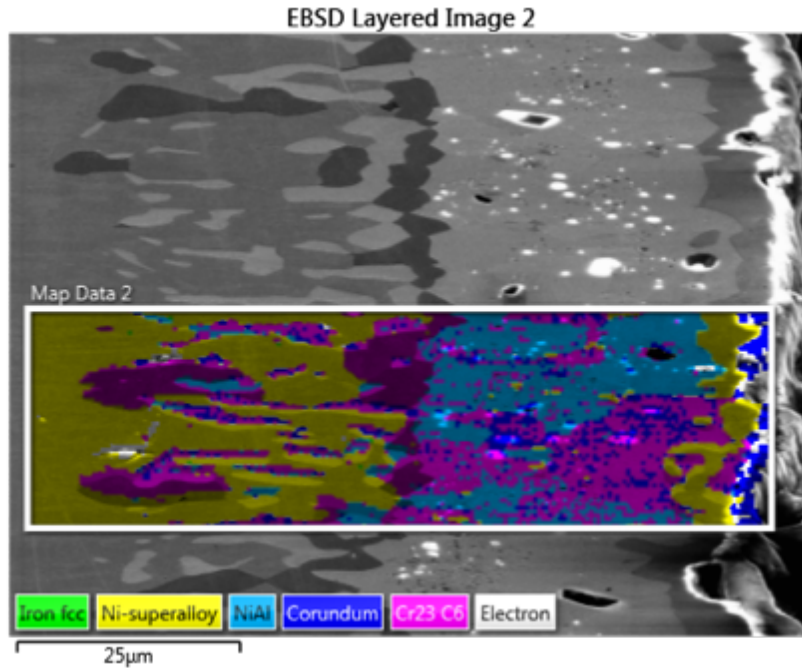


Figure 133: EBSD layered image of Aluminized RA330 exposed for 12 months at edge

Four phases were discovered by EBSD in the cross-section just below the outer surface. The yellow area on the left side of interior represents the fcc structure austenite phase. The pink area represents the chromium carbides. The light blue area close to the surface represents the $\beta - NiAl$ phase. The dark blue area on the surface represents the aluminum oxide phases. The thickness of $\beta - NiAl$ is about $35\mu m$. After 12 months exposure, the chromium carbides phase were also identified in the $\beta - NiAl$ layer and in the diffusion zone in between of austenite and nickel aluminide. However, after 12 months exposure, chromium carbides precipitated in the nickel aluminide zone. Further right of cross section image, nickel aluminide was the primary phase. Beneath the surface, a layer of austenite was identified due the outward diffusion of Al to form $\alpha - Al_2O_3$ [8]. Al content in $\beta - NiAl$ layer have been absorbed by the surface layer to form alumina. An alumina layer was observed at the surface.

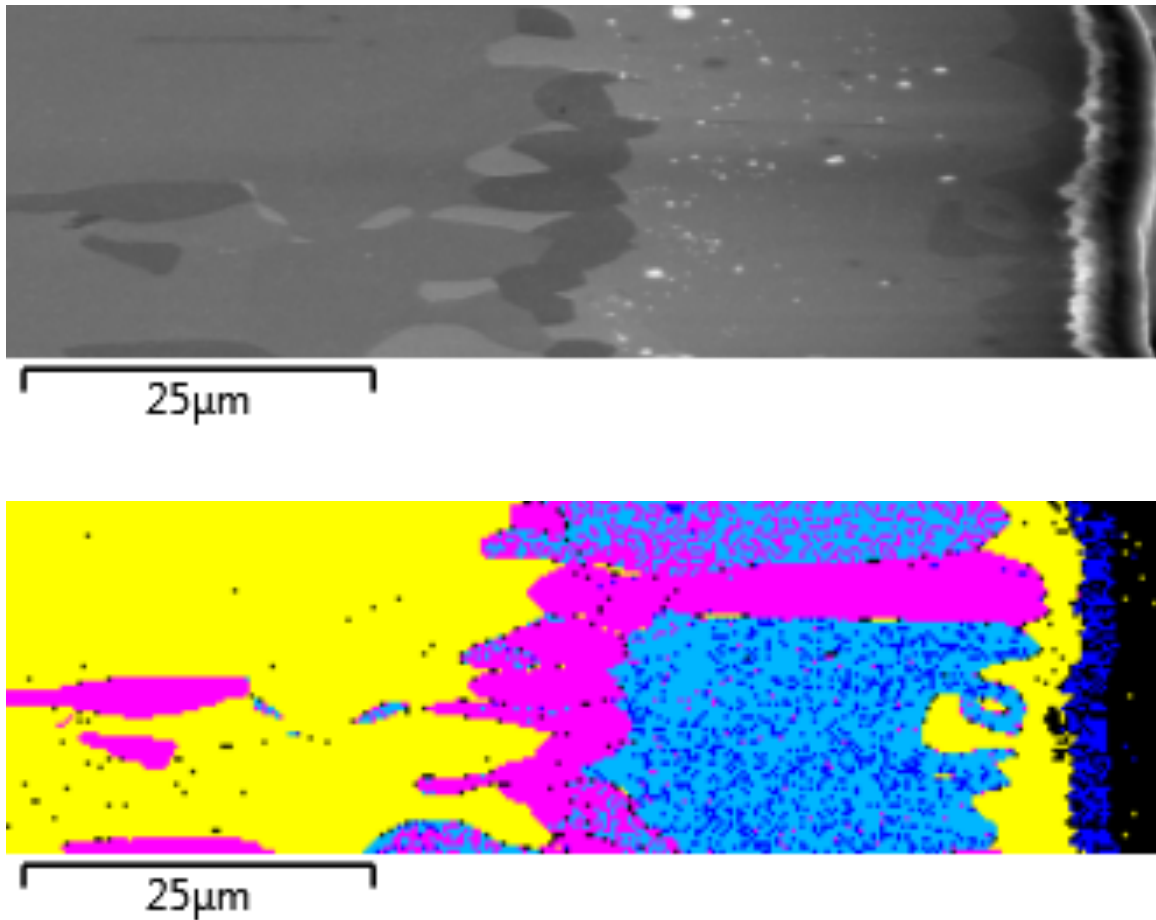


Figure 134: EBSD layered image of Aluminized RA330 exposed for 24 months at edge

During the exposure, $\beta - NiAl$ acts as the source of Al for alumina layer on the surface. Due to the concentration gradient of Al, aluminum content continues diffuse outward to form $\alpha - Al_2O_3$. The Al also diffuses inward into the matrix. In this case, the thickness of $\beta - NiAl$ decreases with time. At the same time, carbon will also pass through the $\alpha - Al_2O_3$ layer even though the diffusivity of carbon in alumina was very low, because small amount of defects in the alumina layer. As the result, chromium carbides started to precipitate at grain boundaries.

When comparing the EBSD analysis of aluminized RA330 exposed for 12 months and 24 months, interface movement and phase transformation were identified in Figure 133 and Figure 134.

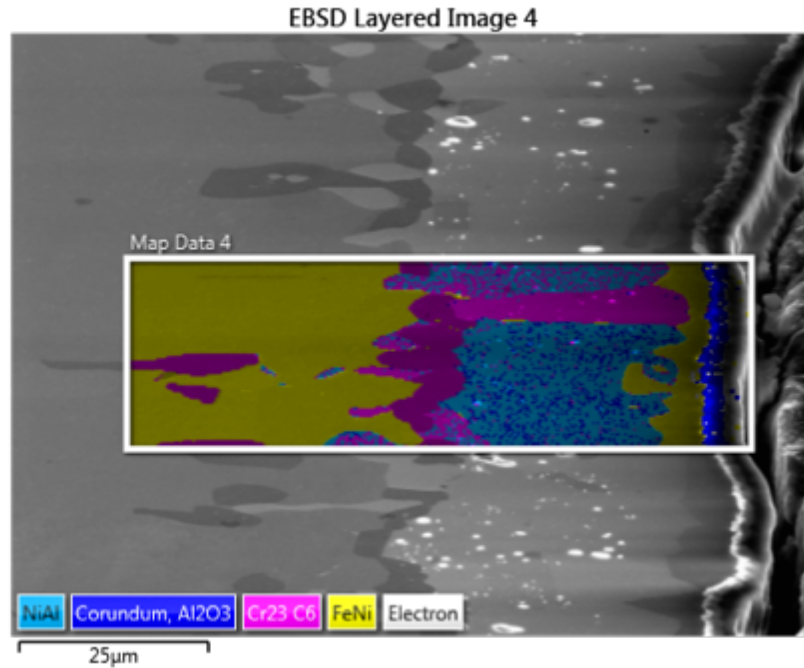


Figure 135. EBSD layered image of Aluminized RA330 exposed for 24 months at edge

On the right hand side of Figure 135, a dense layer of $\alpha - Al_2O_3$ was observed at surface of sample with a thickness was about $3\mu m$. Underneath the alumina, about $5\mu m$ of austenite layer was identified by EBSD. In addition, the RA330 that has been exposed for 24 months has thicker austenite layer beneath the alumina as shown in Figure 135. Furthermore, the width of $\beta - NiAl$ decreased from $35\mu m$ to $20\mu m$ when the sample exposed for one more year. Chromium carbides precipitated beneath the $\beta - NiAl$ layer, as seen in the middle of Figure 134 and Figure 135. Austenite and nickel aluminides, significantly decreased at carbides precipitated region according to Figure 133 and Figure 136. The thickness of diffusion zone decreases with time. $\beta - NiAl$, austenite and chromium carbides phase was identified at diffusion zone as seen in Figure 136. The interior of alloys was still FCC structure austenite phase.

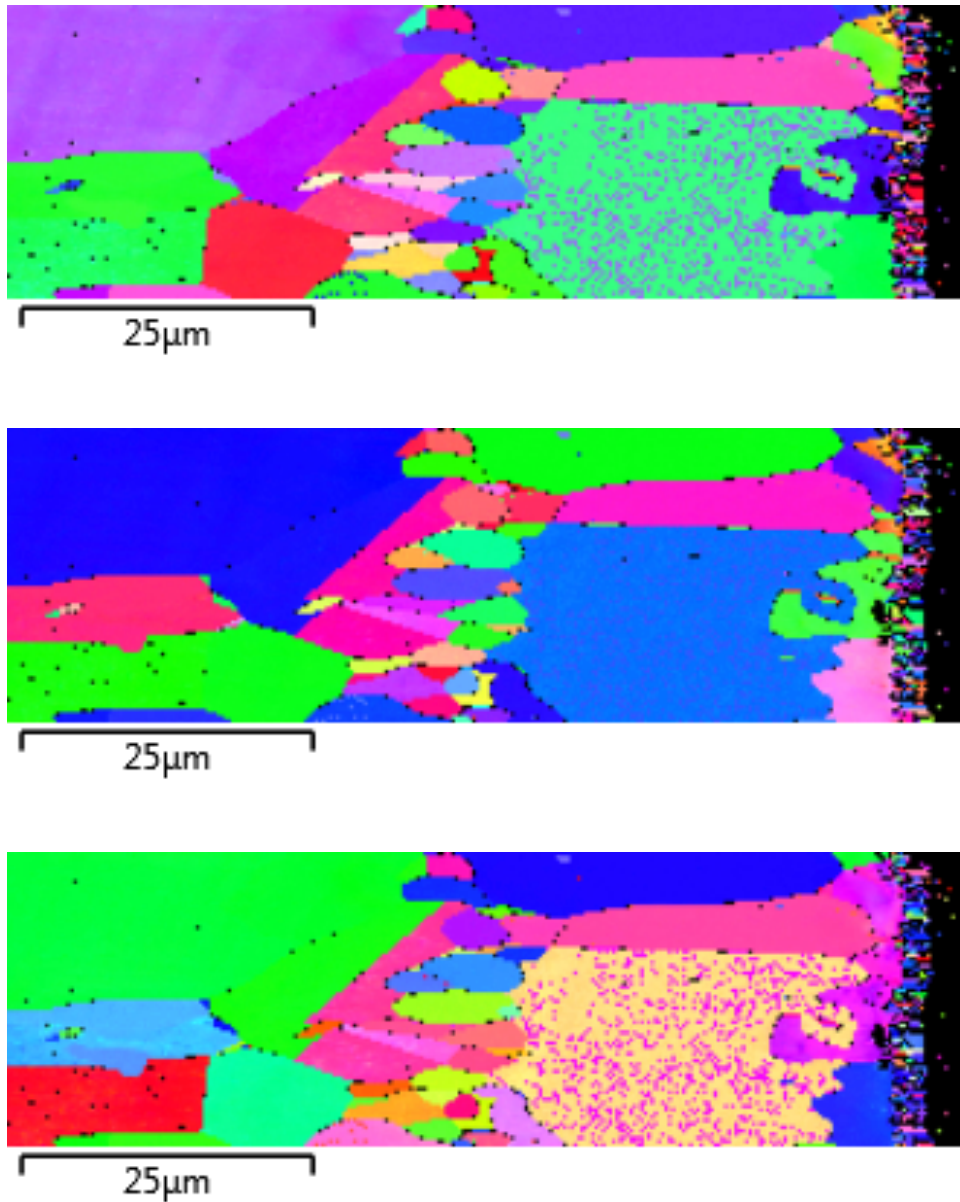


Figure 136: EBSD image of Aluminized RA330 exposed for 24 months at edge with XYZ axis orientations

However, at the $\beta - NiAl$ layer, chromium carbides precipitates $Cr_{23}C_6$ precipitated inside the $\beta - NiAl$ grain. In addition, chromium carbides also have shown preferred orientation along the diffusion path of carbon which also perpendicular to the surface. The grain size of chromium carbides were smaller than austenite and $\beta - NiAl$.

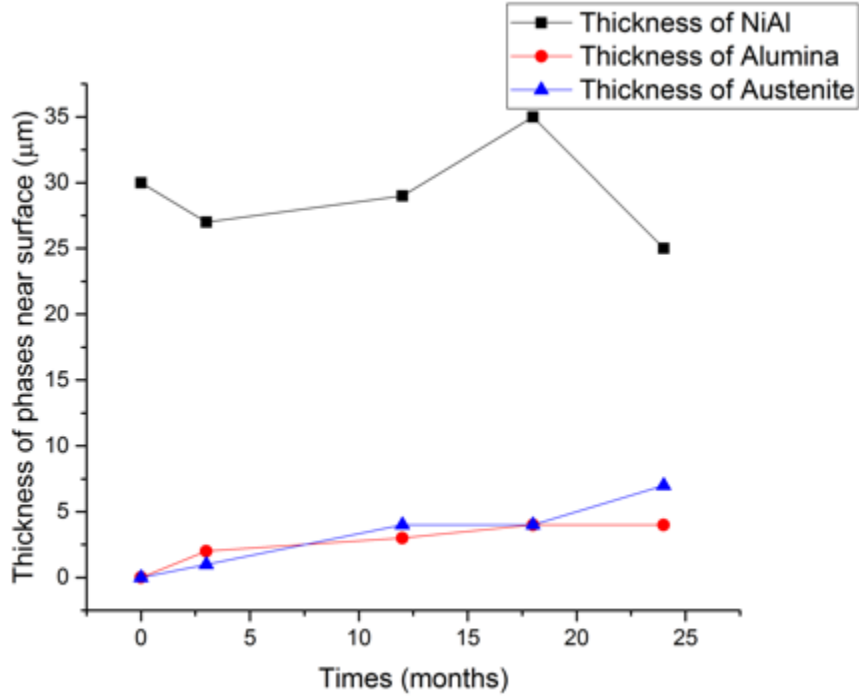


Figure 137: Thickness of β – NiAl phase, α – Al_2O_3 , and Austenite phase underneath the oxides

Cyclic Oxidation

The oxides layer of RA330 and aluminized RA330 act as protective film against oxidation and carburization in the furnaces. The thickness of Cr_2O_3 and SiO_2 oxides layer of as fabricated RA330 were less than $1\mu\text{m}$ as presented in Figure 123. Similarly, the thickness of Al_2O_3 oxide layer of as aluminized RA330 was also less than $1\mu\text{m}$ as shown in Figure 130. The thickness of oxides layer of alloys increase as exposure time. However, the thickness of Cr_2O_3 and SiO_2 oxides layer decreased after sample exposed for 24 months as seen in Figure 126: Thickness of oxide layers of RA330 samples. The oxides layer spalled off after exposed in carburization furnace for extended time.

In this case, the adherence of oxides layer was significantly affect the corrosion resistance of both as fabricated RA330 and aluminized RA330. Cyclic oxidation experiments were conducted on the as fabricated RA330 and aluminized RA330.

Experiment Process:

1. High accuracy electronic scales have measured the weight of as fabricated RA330 and aluminized RA330 samples.
2. The samples were placed into the furnace at 900C
3. Hold for 4h then air cooled follow up with cleaning process.
4. Measure the weight again and put samples back into the furnace. Another cyclic oxidation experiment was initiated.

After 18 cycle of oxidation experiment, the weight of both aluminized and as-fabricated were shown in *Figure 139* and *Figure 141*. No flake offs or spellings were found after the exposure.

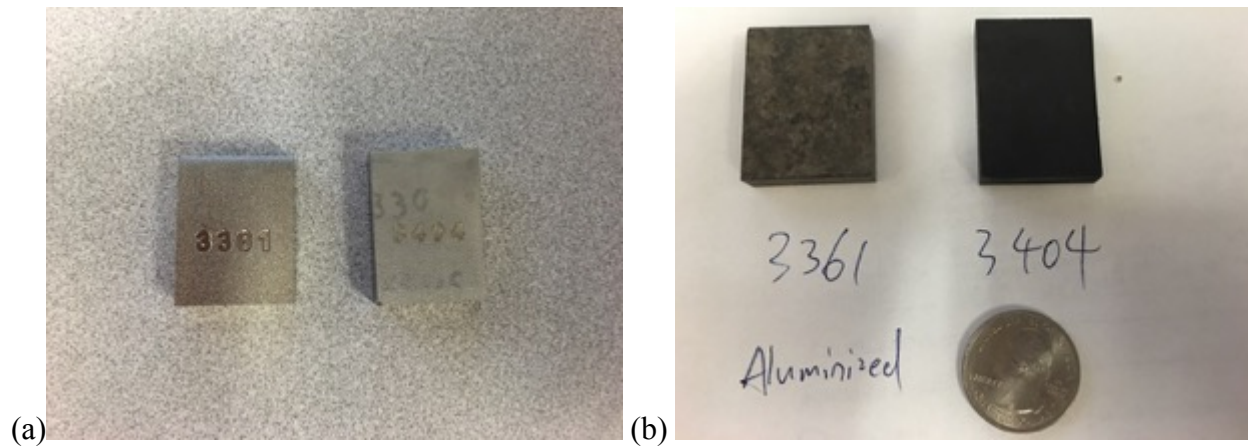


Figure 138: Cyclic oxidation samples aluminized RA330 (left) as-fabricated RA330 (right) before exposure (a) and aluminized RA330 (left) as-fabricated RA330 (right) after exposure (b)

Figure 138 shows the picture of cyclic samples before and after exposure, not spalling were found after 18 cyclic. The weight of as fabricated RA330 increase from the first cycle to the 17th cycle, and then decreased. The first cycle gain the most weight in first 18 cycles. The thickness of oxides

layer Cr_2O_3 , SiO_2 continually increased during cyclic oxidation experiment. Therefore, the weight gain of as fabricated RA330 was due to oxides layer increase. However, the total cycle number was not enough that could leads to spalling of oxides, more cycles of experiments were needed.

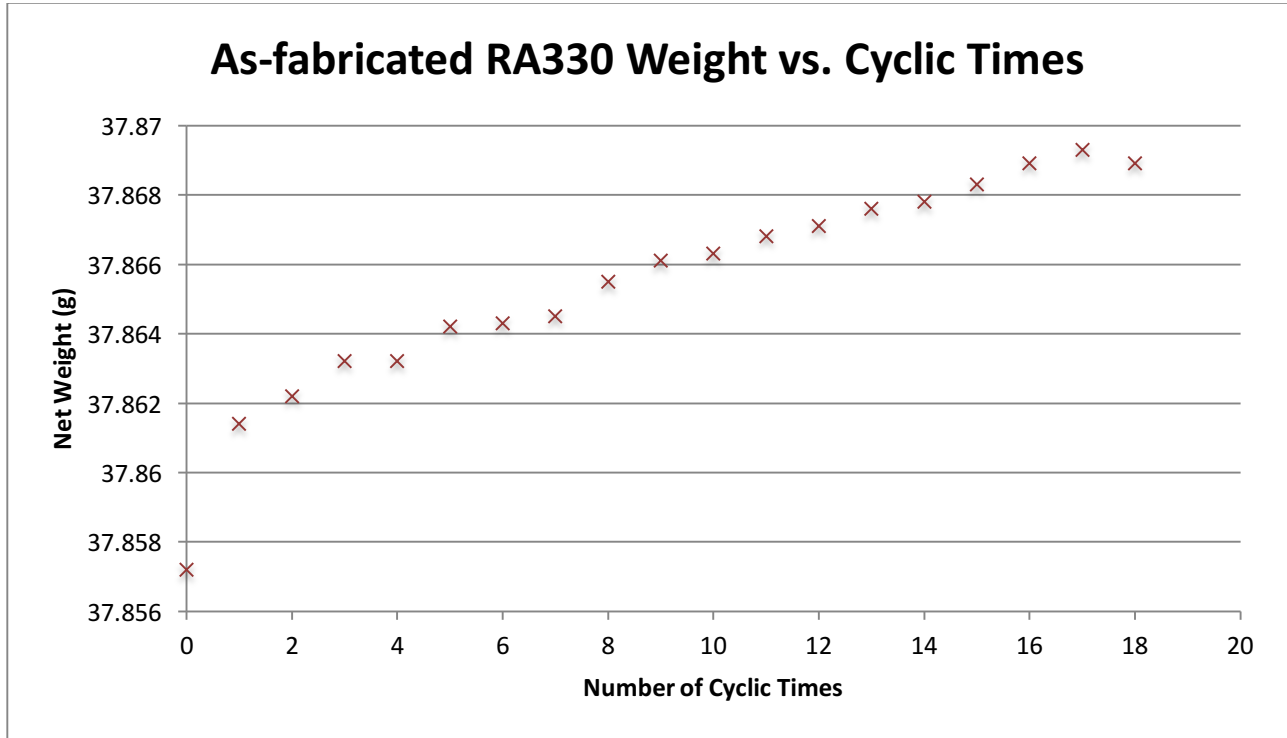


Figure 139: As-fabricated RA330 Weight vs. Cyclic Times

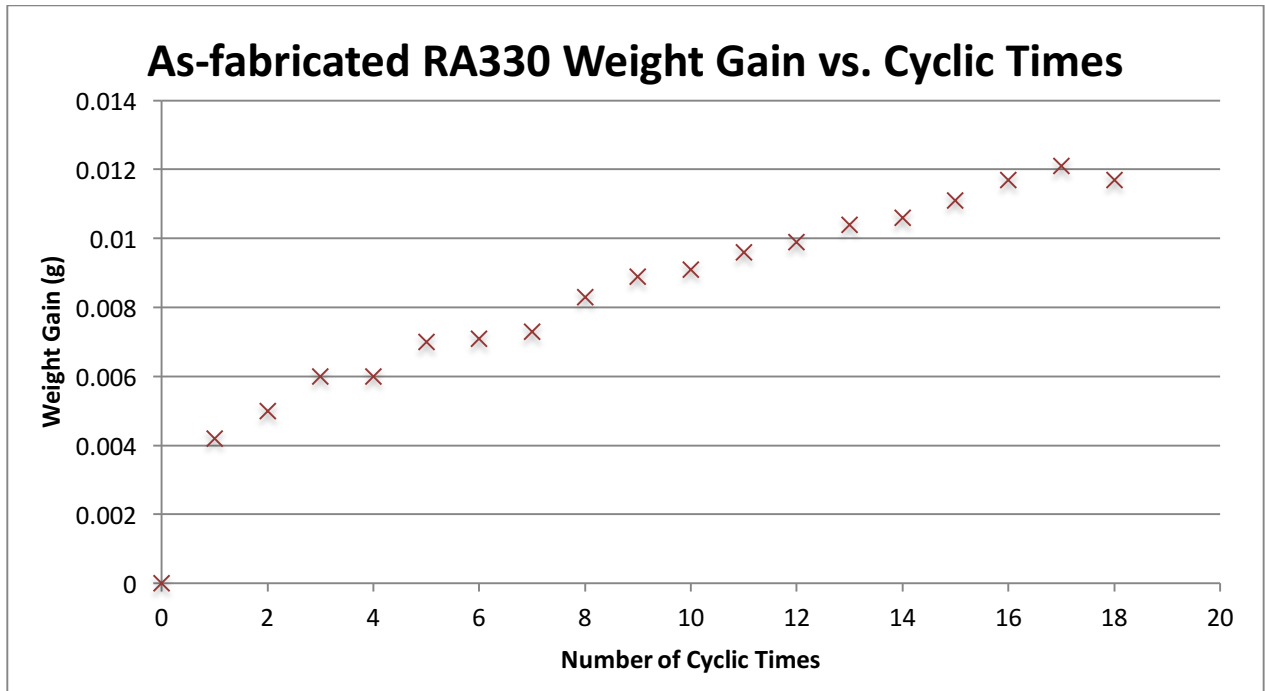


Figure 140: As-fabricated RA330 Weight Gain vs. Cyclic Times

For aluminized RA330, the weight of samples decreased at first cycle, and then continually increase from 2nd to 16th cycle as presented in *Figure 141*. The weight of aluminized sample took 14th cycles to recover from the first cycle weight lost as shown in *Figure 142*. The reason for weight lost in first cycle was still under investigation. And the thickness of Al_2O_3 oxide layer increased from second to 16th cycle. More aluminum content diffuse outward from $\beta - NiAl$ phase to form Al_2O_3 on the surface of aluminized RA330. In this case, the Al_2O_3 continues to grow until reach equilibrium.

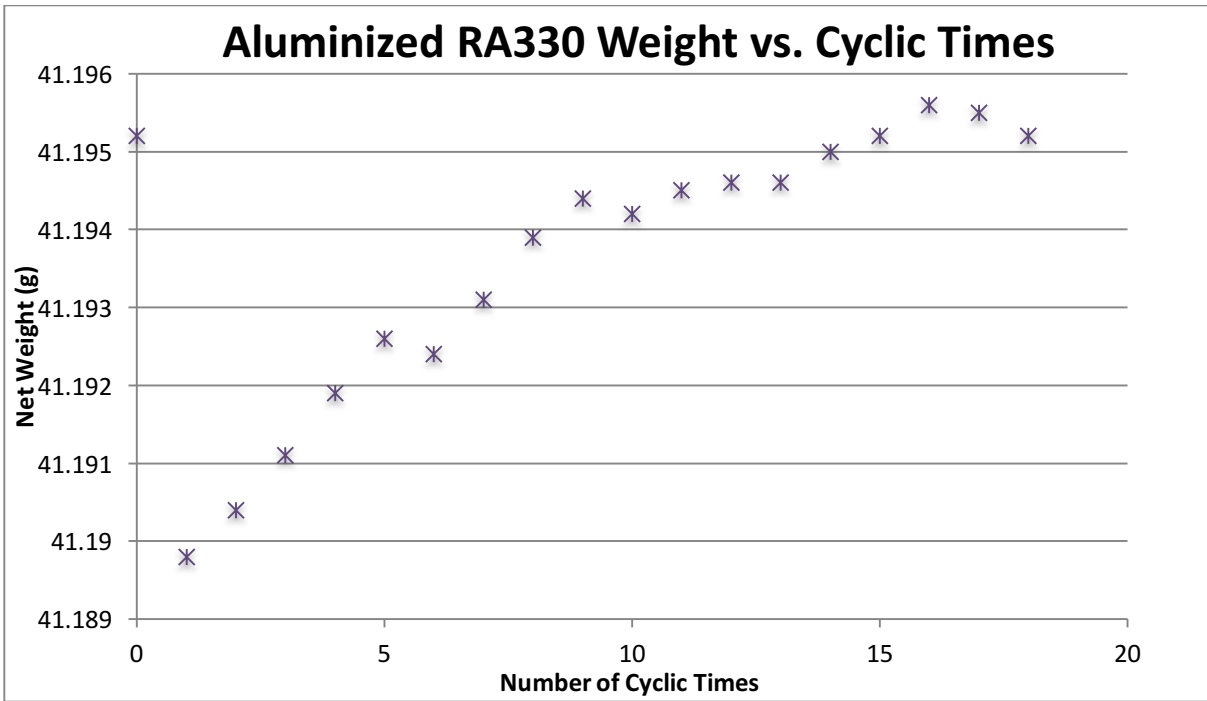


Figure 141: Aluminized RA330 Weight vs. Cyclic Times

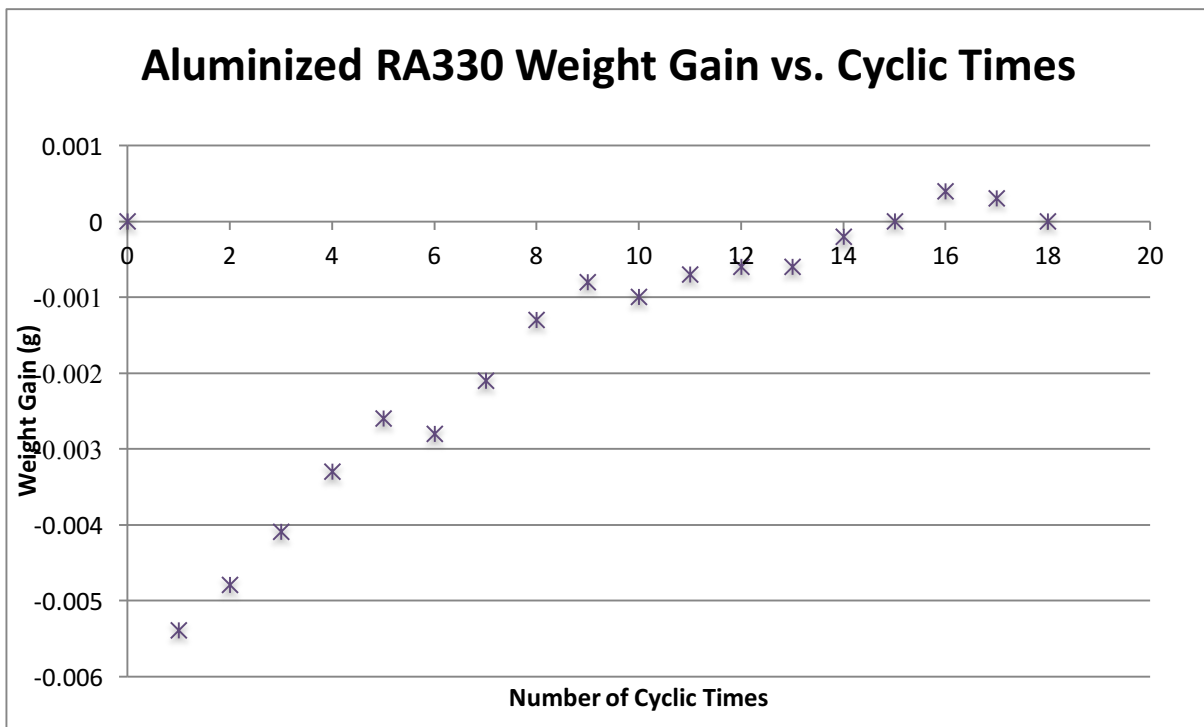


Figure 142: Aluminized RA330 Weight Gain vs. Cyclic Times

Weight gain measurement

High accuracy electronic scales have measured the weight of each sample. Surface areas of RA330 and Aluminized RA330 were calculated during 24 months service in the carburizing batch furnace, the weight gain were measured and the results are listed below.

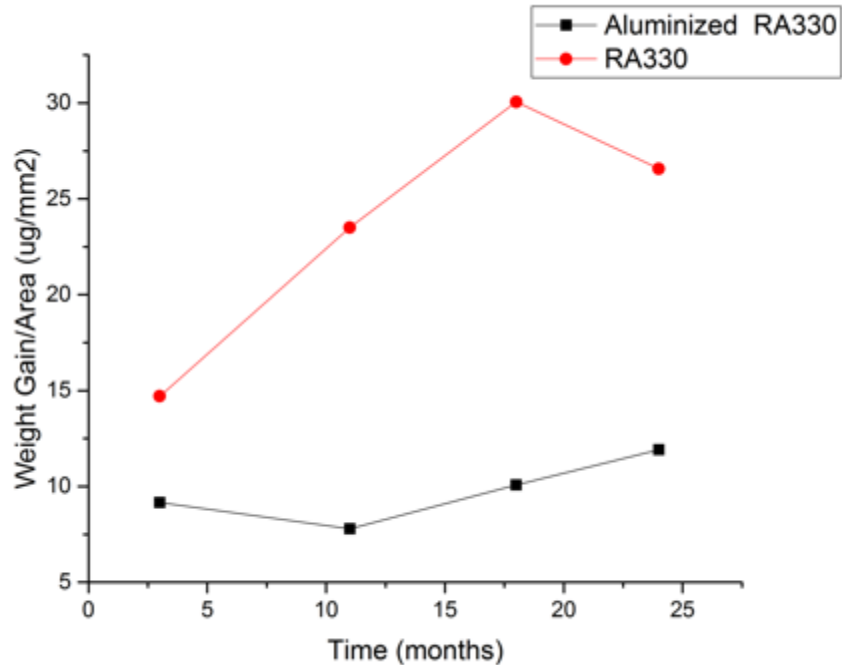


Figure 143. Weight gain per area of RA330 and Aluminized RA330

As presented in Figure 143, the weight gain is comprised of both oxidation and carburization. After the aluminizing process, oxidation resistance of RA330 samples were significantly enhanced. According our weight gain analysis, aluminized samples have lower weight gain per area. The alumina Al_2O_3 layers coated samples have less weight gain per area than chromium oxide Cr_2O_3 coated samples.

Figure 143 presents the experimentally measured weight gain for RA330 and Aluminized RA330 samples as a function of exposure time. This weight gain of the sample is due to both oxidation and carburization. For alloys that have a reduced weight gain may be due to spalling of the oxides. The alloys have been exposed in the carburization furnace for up to 24 months. Carbon continually

diffuses through the oxide layer into the alloys substrate. Therefore, weight gain per area as a function of time shows that weight gain increased for RA330 during the exposure as the exposure time increases.

According to Figure 143, weight gain per area increases as a function of time increases. The red line represents the weight gain for RA330, it was found that RA330 lost weight after 24 months exposure compare to 18 months. That was because of spalling of Cr_2O_3 layer. It was found that the weight gain for the aluminized alloys was uniformly less than the as-fabricated alloys.

Conclusions

Failure analysis indicated that the failure of fixtures in gas carburization furnace is due to the excessive carburization that leads to formation of $M_{23}C_6$ and M_7C_3 carbides in the grain boundaries, and subsequent cracking because of embrittlement of carbides [3]. In this case, the key to suppressing metal dusting is to stop the dissociation of the carbon source or subsequent carbon diffusion into the susceptible materials [4].

It was found that alloy with stable alumina layer protection on the surface have better anti-carburization properties than uncoated alloys. Continuous $\alpha - Al_2O_3$ layer on the surface of aluminized RA330 alloys was maintained after 24 months exposure in gas carburization furnace. $\beta - NiAl$ layer is important for maintaining effective protection for aluminized alloys or alloys that contain high aluminum content. The thickness of $\beta - NiAl$ decreased from $35\mu m$ to $20\mu m$ after 24 months exposure. $Cr_{23}C_6$ precipitated at the $\beta - NiAl$ region due to carbon uptake.

Aluminizing coating extended the life of RA330 in gas carburizing atmosphere. The service lifetime of RA330 fixtures increased by at least two year because of $\beta - NiAl$ kept continuous Al_2O_3 that eliminated the inward diffusion of carbon.

Acknowledgements

This work was supported by Center for Heat-treating Excellence. The authors also want to acknowledge the kindly help offered by Dr. Craig Zimmerman from Bluewater Thermal Solution, and Marc Glasser from Rolled Alloys.

References

- [1] Francesco Bozza, Diffusion mechanisms and microstructure development in pack aluminizing of Ni-based alloys, *Surface & Coating Technology* 239(2014) 147-159
- [2] A. Wang, R.D. Sisson, Jr. “*Life extension of furnace and fixture alloys by surface engineering in carburizing atmospheres*”, 23rd International Federation of Heat Treatment and Surface Engineering Congress 2016, IFHTSE 2016
- [3] H. J. Grabke, “Metal dusting,” *Materials and Corrosion*, Vol. 54, No. 10, (2003) pp. 736-746
- [4] A. Wang, R.D. Sisson, Jr. “*Microstructure and Failure Analysis of Austenitic Fe-Ni alloys and Ni-Cr-Fe alloys for Furnace Alloys and Fixtures*”, ASM International - 28th Heat Treating Society Conference, HEAT TREATING 2015
- [5] H. J. Grabke, “On the mechanism of catastrophic carburization: metal dusting,” *Corrosion Science*, Vol. 35, Nos 5-8, (1993) pp. 1141-1150.
- [6] Sohn Y, Lee E, Nagaraj B, Biederman R, Sisson R, “Microstructural characterization of thermal barrier coatings on high pressure turbine blades,” *Surface and Coating Technology*, Vol. 146-147 (2001) pp: 132-139
- [7] A. Aguero, Marcos Gutierrez, Souheil Saadi, “Metal Dusting Protective Coating. A Literature Review,” *Oxidation of Metals*, 76:23-42, (2011)
- [8] E.Y. Lee, R.D. Sisson Jr, “Modelling the microstructural evolution and degradation of M-Cr-Al-Y coatings during high temperature oxidation,” *Surface and Coatings Technology*, Vol. 32 (1987) pp. 19-39 DOI:10.1016/0257-8972(87)90095-8

5.5. Pre-oxidation treatment

Pre-oxidation treatment may be an effective way to improve the anti-carburization and anti-oxidation properties of alloys.^[1] Pre-oxidation experiments were conducted on RA330 and aluminized RA330. Experimentally optimize the Pre-oxidation process parameters such as time, temperature and pre-treatment have been done.

Pre-oxidation experiments with different conditions were conducted on RA330 and aluminized RA330.

- Dipped in 5% NaOH solution for 10 mins
- Pre-oxidized at 900C for 24 hours then quenched in oil
- Weight gain were measured for those samples
- Characterizations were conducted on the samples, including SEM, EDS, EBSD, XRD and etc.

The thickness of Cr_2O_3 layer is about $3\mu m$ according to *Figure 144*. And the combination of Cr_2O_3 and SiO_2 layer is about $10\mu m$ from the surface.

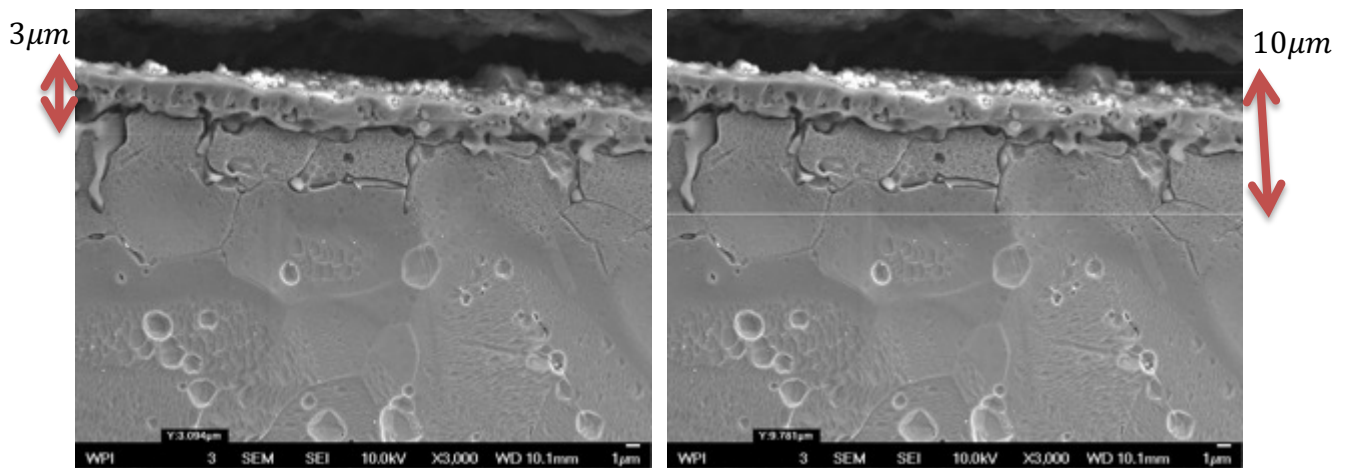


Figure 144: SEM photomicrographs of NaOH dipped RA330 pre-oxidized for 24h at edge

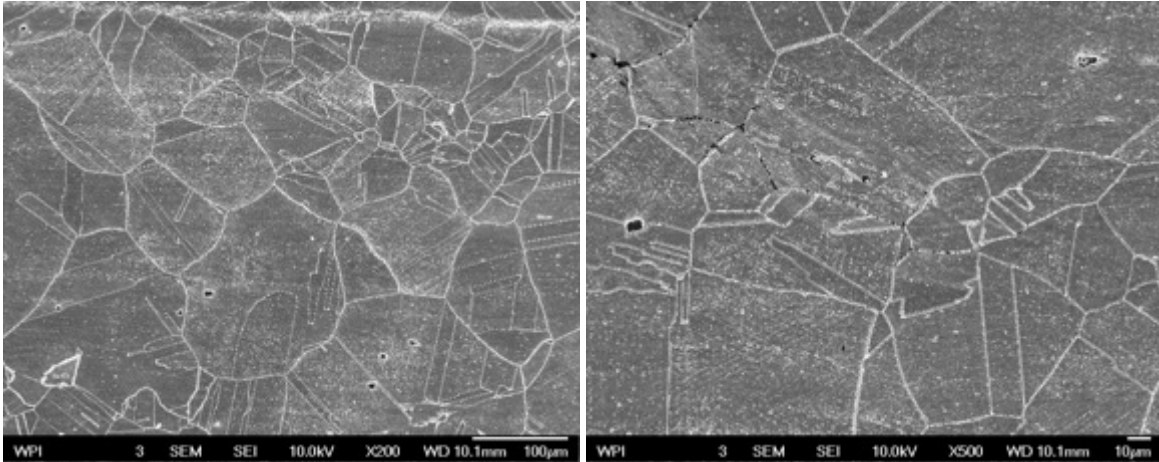


Figure 145: SEM photomicrographs of NaOH dipped RA330 pre-oxidized for 24h at core

According to Figure 143, the oxides layer was combined by Cr_2O_3 at outer layer and SiO_2 at inner layer of oxides at surface. In the matrix of pre-oxidized RA330, austenite phase was seen in Figure 145.

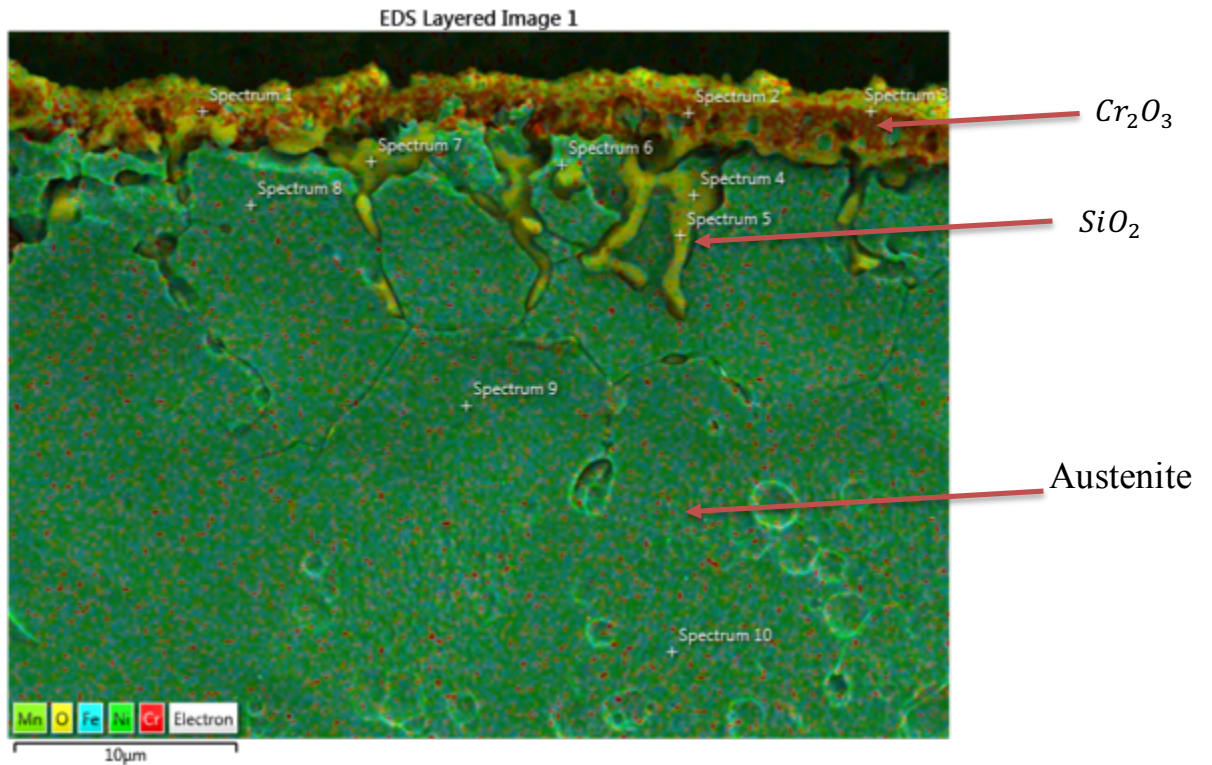


Figure 146: EDS mapping of RA330 pre-oxidized for 24 hours at 900C

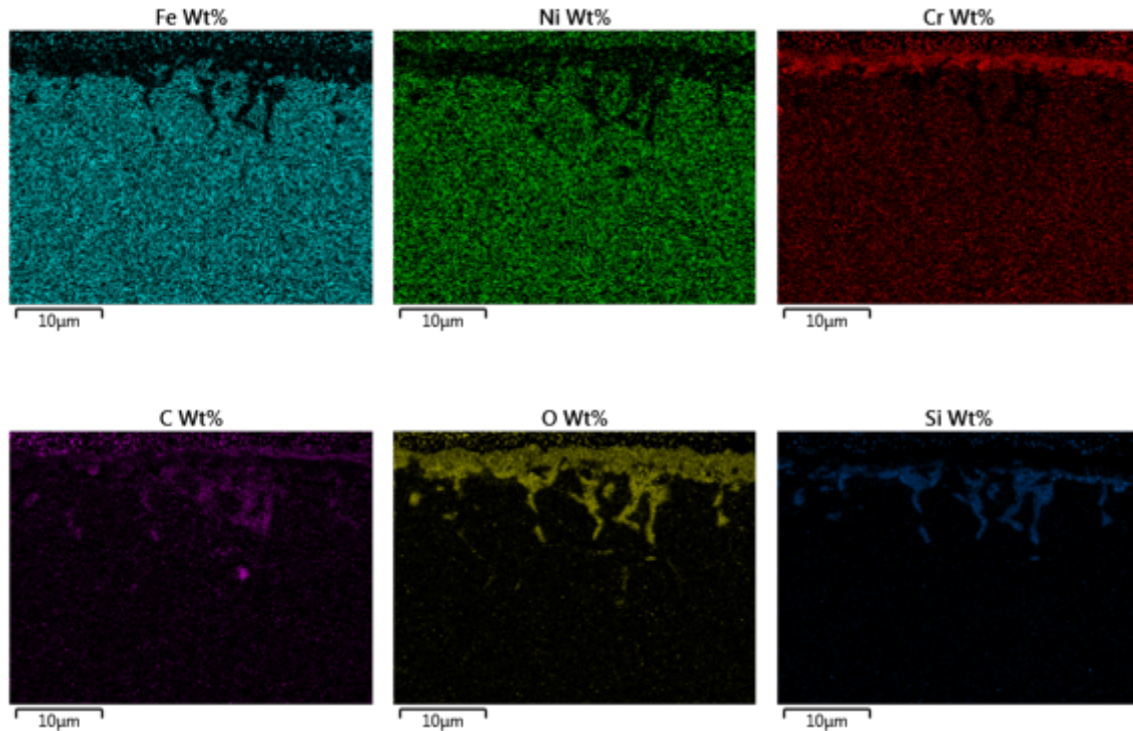


Figure 147: EDS mapping of RA330 for each element

EDS mapping were conducted on pre-oxidized RA330 as seen in *Figure 146*. The thickness of Cr_2O_3 and SiO_2 for pre-oxidized RA330 was larger than as fabricated RA330. The thickness increases from submicron for as-fabricated RA330 to $3\mu m$ Cr_2O_3 and $7\mu m$ SiO_2 for pre-oxidized RA330.

High temperature corrosion processes including carburization and oxidation are two main causes of corrosion for the alloys used in gas furnaces. High temperature corrosion resistance is provided by the presence of stable, fine, dense and adhering protective oxides. Pre-oxidation increased the thickness of oxides layer Cr_2O_3 and SiO_2 at surface of RA330. As a result, the pre-oxidation treatment enhanced the corrosion resistance of RA330 in gas carburizing furnaces.

Pre-oxidation experiment also conducted on aluminized RA330.

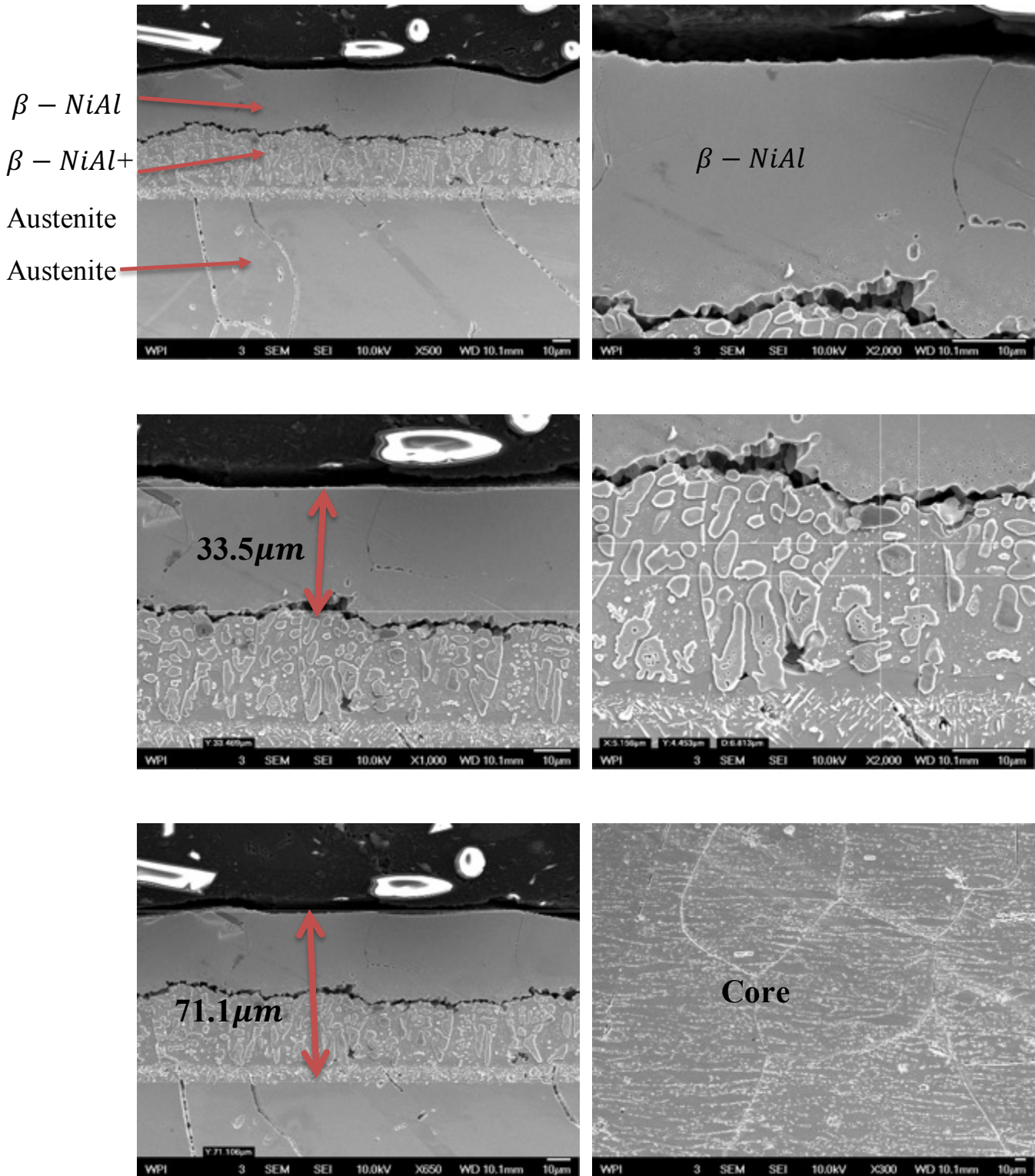


Figure 148: SEM photomicrographs of NaOH dipped aluminized RA330 pre-oxidized for 24h

Figure 148 shows the SEM photomicrographs of pre-oxidized aluminized RA330. The submicron Al_2O_3 layer was on the surface of pre-oxidized aluminized RA330. $\beta - NiAl$ was identified beneath the oxide layer which thickness was about $30\mu m$. Under the $\beta - NiAl$ layer, a mixed diffusion zone of $\beta - NiAl$ and austenite was shown in *Figure 148*. Austenite phase is in the matrix of pre-oxidized aluminized RA330.

Compare to the as aluminized RA330, pre-oxidation treatment did not change the thickness of Al_2O_3 and $\beta - NiAl$. Therefore, pre-oxidation treatment for aluminized RA330 may not as efficient as the as-fabricated RA330. However, extended pre-oxidation treatment of longer oxidation time may increase the thickness of Al_2O_3 on the surface of aluminized RA330.

References

- [1] [Combe C., Cardey PF., "Pre-oxidation treatment to increase the service life of heat treatment furnace conveyor belts made of AISI 330Cb industrial application" International Federation of Heat Treatment and Surface Engineering 2016, Proceedings of the 23rd IFHTSE Congress](#)

5.6. Life Extension of High Temperature Structural Alloys RA602CA in Gas Carburizing Atmosphere

Anbo Wang¹, R. D. Sisson, Jr.^{1}*

¹Center for Heat Treating Excellence, Worcester Polytechnic Institute, Worcester, Massachusetts, 01609, U.S.A

**Email: sisson@wpi.edu*

To be submitted to: Materials Science and Engineering A

Abstract

Extension of the service life for high temperature structural alloys RA602CA is the goal for this project. In this paper, RA602CA and Aluminized RA602CA were selected to study their performance in a gas carburization furnace for times up to two years. Aluminizing treatment were also studied in this project. Aluminizing is a coating that widely used in aerospace industry, especially in turbine blade applications. It is also known that carbon has very low solubility in alumina. In that case, aluminizing could be a good method for protecting RA602CA alloys. Therefore, microstructural development during the carburizing process will be presented. And also the degradation of chromium oxide as well as alumina oxides will be identified. The weight gain of RA602CA compare to similar alloys was presented. Coating, and surface treatments were measured to determine anti-corrosion properties of high temperature structural alloys.

Introduction

The heat treatment industry is a 40 billion dollar market; thousands of tons of high-temperature structural alloys were widely used in applications such as fixture inside the high-temperature furnaces which are supporting the products. Most fixtures were consumed within three years and it cost a significant amount of money for heat treaters to replace them.

High temperature structural alloys are usually Nickel based, Nickel-Iron-Chromium based and Nickel Chromium based alloys. Those alloys are experiencing a variety of degradation

mechanisms. The corrosion products are mainly graphite, chromium carbide, metal, and oxides. For iron-based alloys, the primary reason for failure was the excessive carburization that leads to “metal dusting” and subsequent cracking. In addition, metallographic analysis indicated that “flake offs” of Fe-Cr-Ni alloys were mainly graphite and chromium carbides. The industry was in need of alloys that have long service life. The fixtures need to have low carbon uptakes during the exposure in carburization furnaces.

RA 602CA is one of the most oxidation resistant high strength nickel heat resistant alloys available. High chromium, aluminum, and an yttrium addition permit it to develop a tight chromium oxide scale with an alumina subscale. RA 602CA may be considered where it is important to minimize product contamination at extreme temperatures. A nominal 0.2% carbon content contributes to high creep rupture strength. Micro-alloying with zirconium minimizes grain growth upon exposure to temperatures above 1800°F. Table 5 shows the chemical composition of RA 602CA. The density of RA 602CA is 0.285 lb/in³, and it melts in the temperature range from 2350 to 2550°F. The oxidation resistance is up to 2200°F.[1]

	Cr	Ni	Cu	P	S	Fe	C	Al	Ti	Y	Zr	Si	Mn
Min	24	-	-	-	-	8	0.15	1.8	0.1	0.05	0.01	-	-
Max	26	Bal.	0.1	0.02	0.01	11	0.25	2.4	0.2	0.12	0.1	0.5	0.15

Table 28. Chemical composition of RA 602 CA® [2]

Materials and methods

In this paper, the performance of RA602CA and aluminized RA602CA in an industrial carburizing furnace was investigated. RA602CA as well as similar alloys were exposed in both the as fabricated and surface treated condition to determine the corrosion resistance of RA602CA. The test samples were exposed to 0.7%C carburizing atmosphere at approximately 900°C for 3 months, 6months, 12months, 18months, and 24months. In this paper the microstructural development of alloys during the prolonged exposure in the carburizing environment will be presented and discussed.

Aluminizing is widely used to increase the high temperature corrosion and oxidation resistance of nickel-based alloys. α – alumina Al_2O_3 are effective protection for high temperature and aggressive gaseous environments. Nickel aluminides formed during aluminizing act as the reservoir of aluminum for maintaining a protective Al_2O_3 scale on the material surface during high temperature services.

Selected samples were sent to Alcoa Howmet for aluminizing. The samples were aluminized in a static gas phase system at 1090 °C for 5 hours. Chromium aluminum source material (70%Cr/30%Al) and ammonium fluoride granules were used in the system. The coating chamber was purged with argon until a dew point of -40F or better was met, then the argon is shut-off to the coating chamber (hence static system) and heating begins.

High temperature corrosion processes including carburization and oxidation are two main causes of corrosion for the alloys used in gas furnaces. High temperature corrosion resistance is provided by the presence of stable, fine, dense and adhering protective oxides.

Exposure experiment

Three alloys were selected for the alloy lifetime tests, including, RA 602CA, RA 330, and INCONEL alloy 625. Rolled Alloys provided RA 330, RA 602CA, and INCONEL alloy 625 samples. Ten samples were prepared for each alloy. Selected samples were aluminized by Alcoa Howmet in Branford, CT. Samples were engraved with the number listed below. 30 samples are divided into 10 groups. Group 1 and Group 6 were kept in WPI for characterization. The other eight groups were sent to Bluewater Thermal Solutions for the experiments in the carburizing furnace.

Group No.	RA 602CA	RA 330	INCONEL alloy 625	Surface Condition	Date Removed
1	6021	3302	6250	Unaluminized (Original)	Nov.18 th 2013
2	6020	3310	6251	Unaluminized	Feb. 24 th 2014

3	6022	3301	6252	Unaluminized	Oct. 6 th 2014
4	6023	3303	6253	Unaluminized	April 20 th 2015
5	6024	3304	6254	Unaluminized	Dec. 7 th 2015
6	6025	3305	6255	Aluminized (Original)	Nov.18 th 2013
7	6026	3306	6256	Aluminized	Feb. 24 th 2014
8	6027	3307	6257	Aluminized	Oct. 6 th 2014
9	6028	3308	6258	Aluminized	April 20 th 2015
10	6029	3309	6259	Aluminized	Dec. 7 th 2015

Table 29. Sample list

In the current tests, the eight groups were placed in the same carburizing furnace at Bluewater in Rockford, IL in November 2013. After three months, the Group 2 and Group 7 have been taken out for characterization. Then after 12 months, the Group 3 and Group 8 were removed. After 18 months, the Group 4 and Group 9 were removed. Then after 24 months, the Group 5 and Group 10 were taken out and shipped back to WPI.

Samples were exposed in the batch carburizing furnace for different times. The batch furnace at Bluewater is located in Rockford, IL. These samples were placed in a batch carburizing furnace and the carbon potential of the atmosphere is approximately 0.7%. Carburizing temperature is set at 870°C to 925°C in this furnace. And the carburizing time for each cycle is depends on the size of the products, smaller parts such as gaskets will takes 1-3 hours, and the larger parts takes much longer time.

The weight of each sample has been measured by high accuracy electronic scales. All of the sample was measured before every treatment. For example, the weight of RA330 samples were measured before sent for aluminizing. And then measured the weight again after the samples have been aluminized. Before each measurement, samples were cleaned in ultra-sonic machine by ethanol. The typical error range is within $\pm 0.005\text{g}$.

The measured weight gain includes the carbon uptakes and oxidation. The weight gain is primarily carbon uptakes. In this case, the carbon flux could be calculated by following formula.

$$\text{Carbon flux} = \text{weight gain} / \text{surface area}$$

Experiment result

I. RA602CA

RA602CA is an oxidation resistant high strength nickel heat resistant alloys. High chromium, aluminum, and an yttrium addition permit it to develop a compact chromium oxide scale with an alumina subscale.^[1] Chromium carbides precipitate at the grain boundaries due to 0.2% carbon content. Creep strength was increased by carbides precipitates during high temperature exposure. These alloys were exposed in both the as fabricated and aluminized condition. It was found that the weight gain for the aluminized alloys was uniformly less than the as-fabricated alloys.

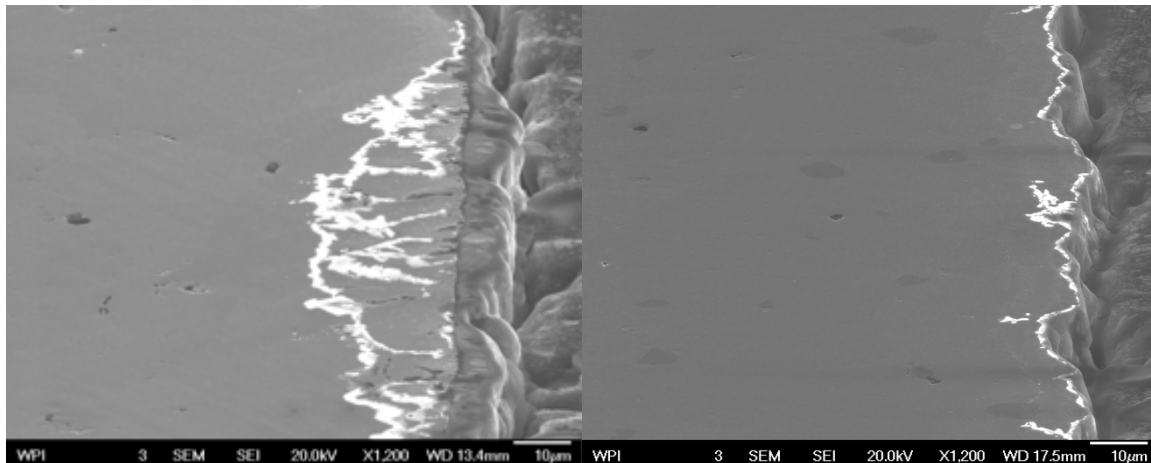


Figure 149: SEM photomicrographs of RA602CA exposed for 18 months(left) and SEM photomicrographs of RA602CA exposed for 24 months (right)

RA602CA contains about 2% of Aluminum which is much higher than regular Ni-based high temperature structural alloys. *Figure 149* shows white alumina precipitate below the surface of RA602CA after exposure for 18 months. The oxide layer on the surface of RA602CA exposed for 18 months were Cr_2O_3 , SiO_2 and Al_2O_3 . The thickness of that oxides layer is about 5-10 μm . On the right hand side of *Figure 149*, about 1 μm thickness of alumina layer was found at surface of RA602CA after 24 months exposure. The thickness of oxides layer decreases was due to spalling during long term exposure.

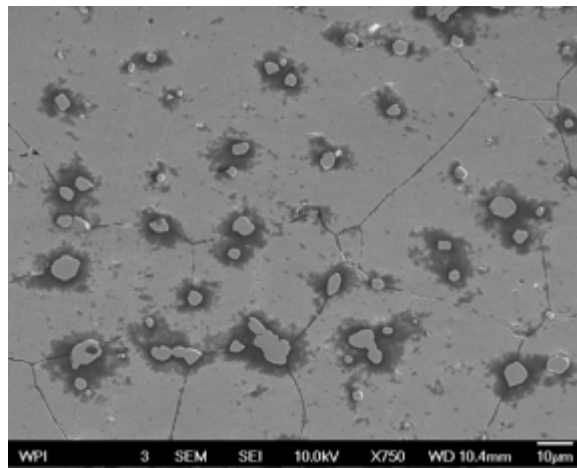


Figure 150: SEM photomicrographs of RA602CA exposed for 12 months at core

RA602CA contains about 0.2% of carbon in the matrix that is sufficient to form chromium carbides at the grain boundaries. $M_{23}C_6$ carbides also precipitated under the oxides layer.

Back scattered electron photomicrographs also indicated the chromium carbides in the grain boundaries. Besides, carbides were also discovered in the core area of cross section after exposure as seen in *Figure 150*.

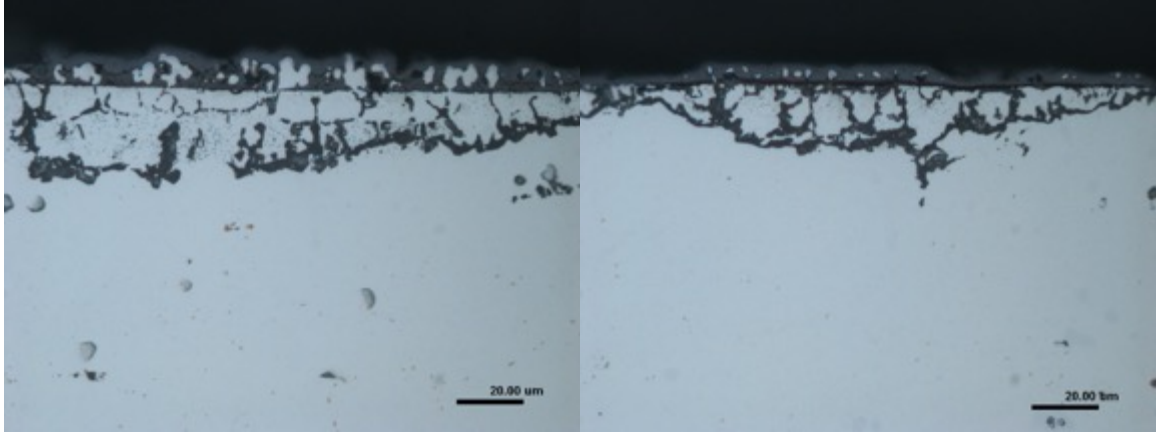


Figure 151: Optical photomicrographs of RA602CA exposed for 18 months at core

Optical photomicrographs of RA602CA shows the oxide layer contains Al_2O_3 and Cr_2O_3 . Besides, austenite phase was also found in the oxide layer as shown in *Figure 151*. EDS mapping shows Ni, Fe, Cr rich austenite particles inside the oxide layer as seen in *Figure 153*. EBSD phase identification was in good agreement with EDS mapping as presented in *Figure 152* and *Figure 153*. The Al_2O_3 oxide layer was at the bottom of oxides layer as shown in *Figure 151*. EDS mapping indicated that Al content concentrated at the bottom layer of surface oxide layer as presented in *Figure 153*. Large amount of Al_2O_3 precipitations were identified at substrate about 10-25 μm depth from surface of RA602CA exposed for 18 months as presented by EBSD and EDS mapping in *Figure 152* and *Figure 153*.

The structure and texture were studied using electron backscatter diffraction (EBSD) technique. RA602CA samples were placed into gas carburization furnace on Nov. 18th 2013. XRD analysis was conducted at sample before any characterization. And then, samples were cut by low speed saw and followed by mounting process. Prepared samples were grinded from 200 grit to 1200 grit. Samples were polished by 1 micrometer alumina polishing powder then 0.3 micrometer, and at end they were polished by 0.05 micrometer alumina polishing powder. The last step for samples preparation is vibration polishing; Samples have been polished for 12 hours before EBSD investigation.

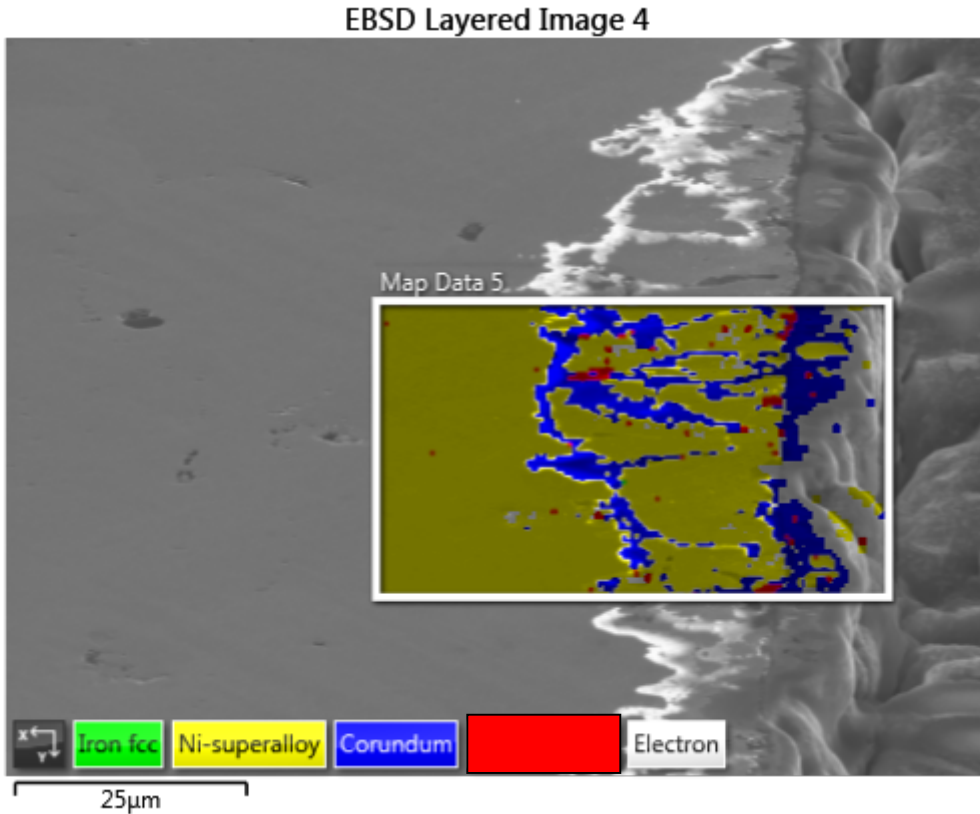
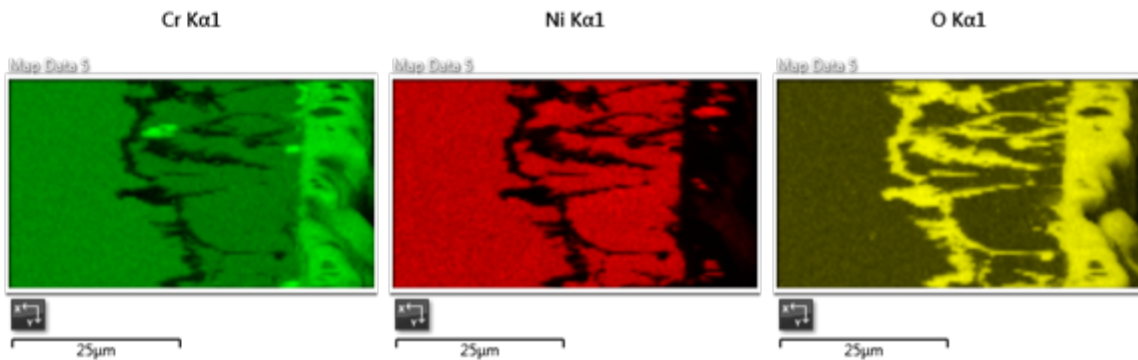


Figure 152: EBSD layered image of RA602CA exposed for 18 months at edge

Figure 152 shows that Al_2O_3 precipitate near the surface of RA602CA exposed for 18 months. According to EBSD image, alumina precipitates at the substrate after long term exposure. The thickness of Al_2O_3 precipitate layer is about 10-25µm as shown in *Figure 152*. In the interior, the light grey phase is austenite. Corundum Al_2O_3 phases also identified at the surface of alloys by EBSD.



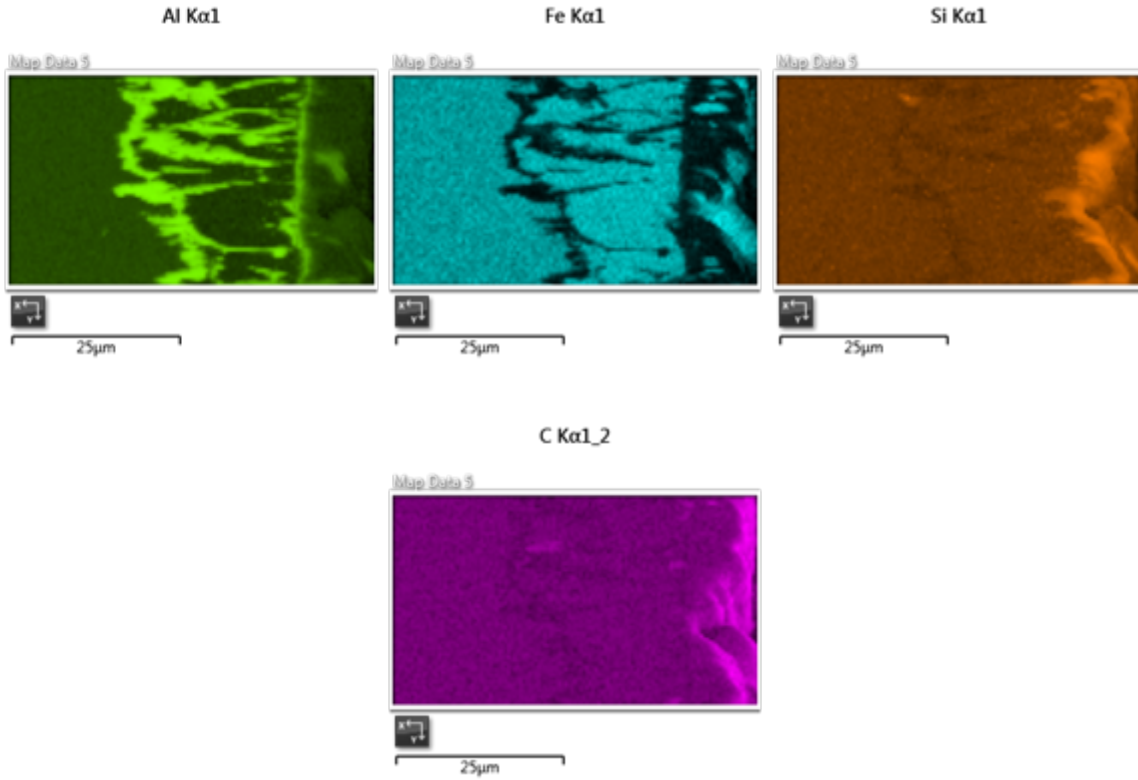


Figure 153: EDS mapping of RA602CA exposed for 18 months

Figure 153 shows the EDS mapping at surface area, about 5-10 μm of oxides layer was identified. The oxide layer contains primarily Cr_2O_3 at outer layer. SiO_2 was observed beneath the Cr_2O_3 layer. And the Al_2O_3 layer located as third layer at the surface of RA602CA.

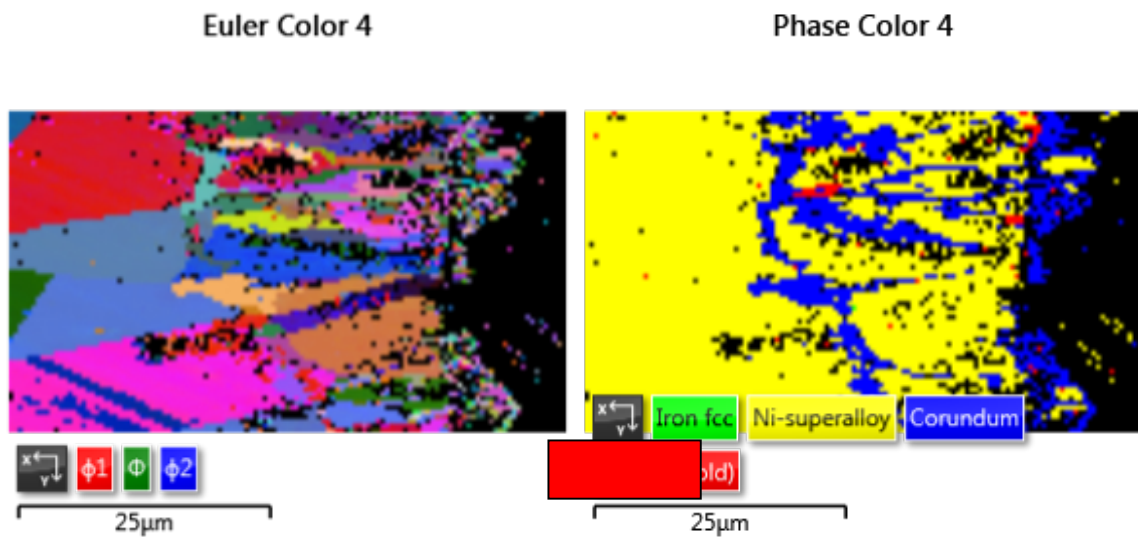


Figure 154: EBSD phase identification of RA602CA exposed for 18 months

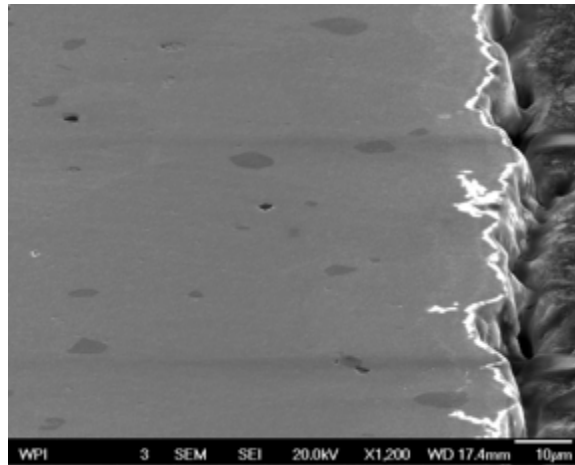


Figure 155: SEM photomicrograph of RA602CA exposed for 24 months

According to Figure 155, about $1\mu\text{m}$ thickness of alumina layer was found at surface of RA602CA after 24 months exposure. Cr_2O_3 and SiO_2 also identified at the surface. However, the thickness of oxide layer decreased compare to RA602CA exposed for 18 years. It appears that oxide layer increase at the beginning of exposure experiment which is 3 months to 12 months. When samples have been exposed for more than 18 months, the thickness of oxide layer decreased. After 24 months exposure, RA602CA still maintain $1\mu\text{m}$ of oxide layer which was significantly thinner than samples exposed for 18 months or less. So far, no chromium carbides were identified in the matrix of RA602CA after 24 months exposure. But the anti-carburization and anti-oxidation properties of thin oxide layer needs further investigation.

EDS Layered Image 1

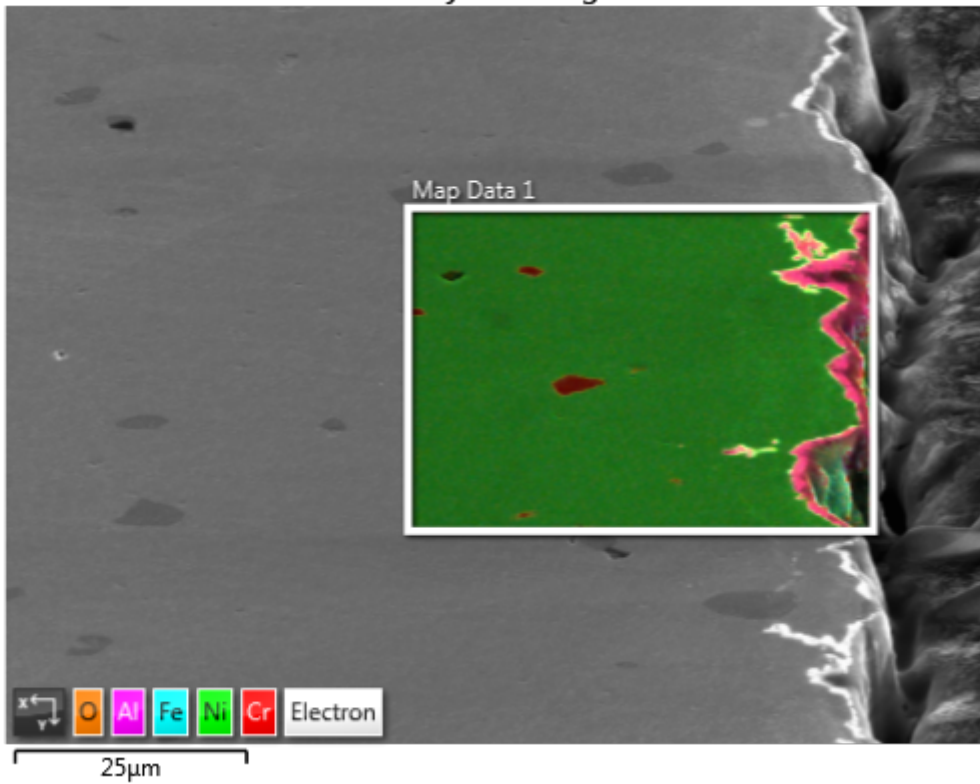
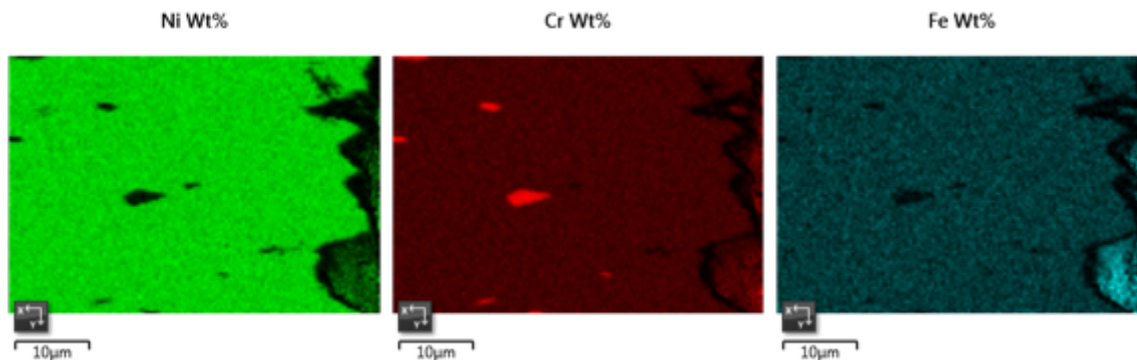


Figure 156: EDS layered image of RA602CA exposed for 24 months

EDS mapping on *Figure 156* shows the oxides layer was mainly alumina, chromina and silica. The matrix was austenite phase as shown on *Figure 156*.



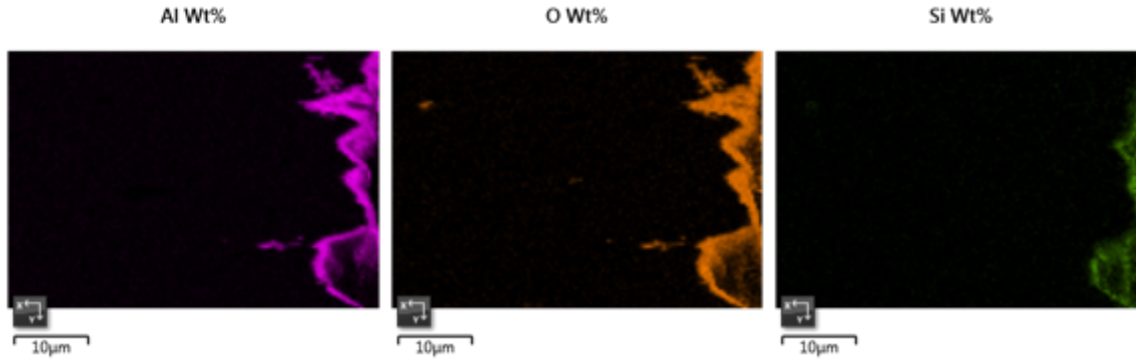


Figure 157: EDS mapping of RA602CA exposed for 24 months

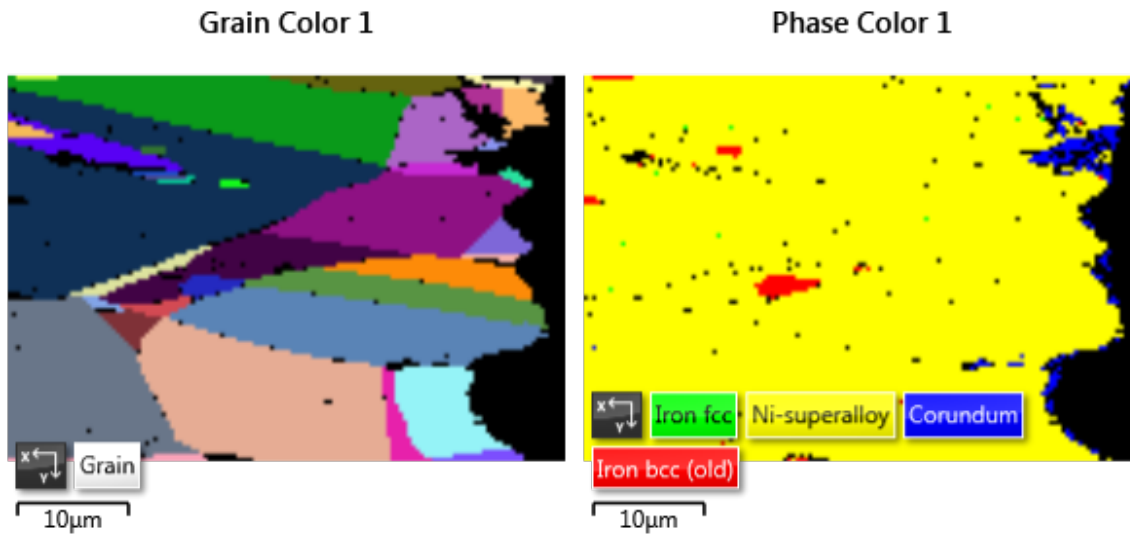


Figure 158: EBSD phase identification of RA602CA exposed for 24 months

Figure 158 shows the EBSD analysis of RA602CA exposed for 24 months. Grain size was identified on the Figure 158. Grain size of interior was larger than the grain size of surface area. EBSD analysis indicated matrix was primarily austenite as shown in yellow on Figure 158. Corundum phase was identified at surface of RA602CA exposed for 24 months.

EBSD Layered Image 2

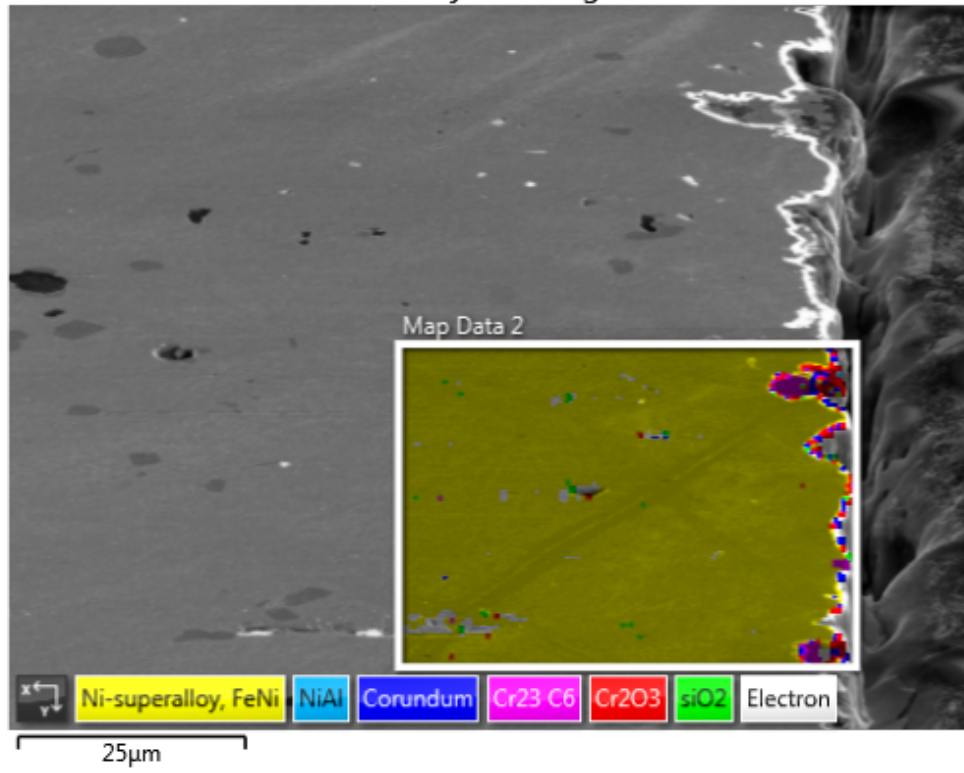
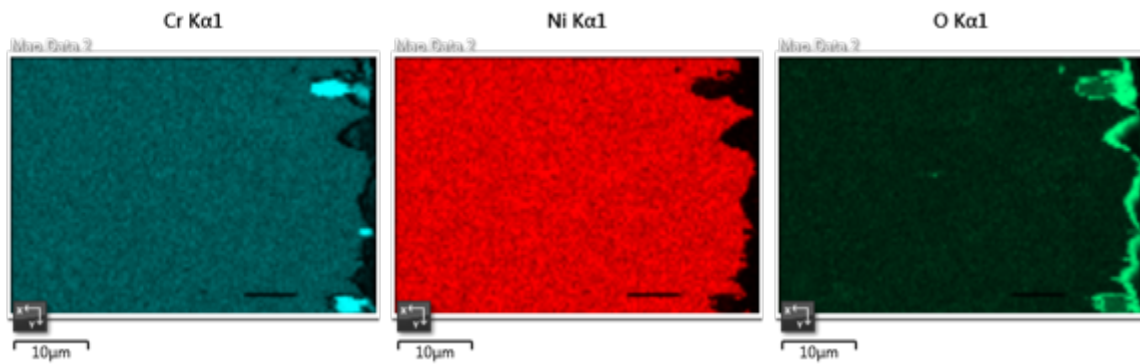


Figure 159: EBSD layered image of RA602CA exposed for 12 months at edge



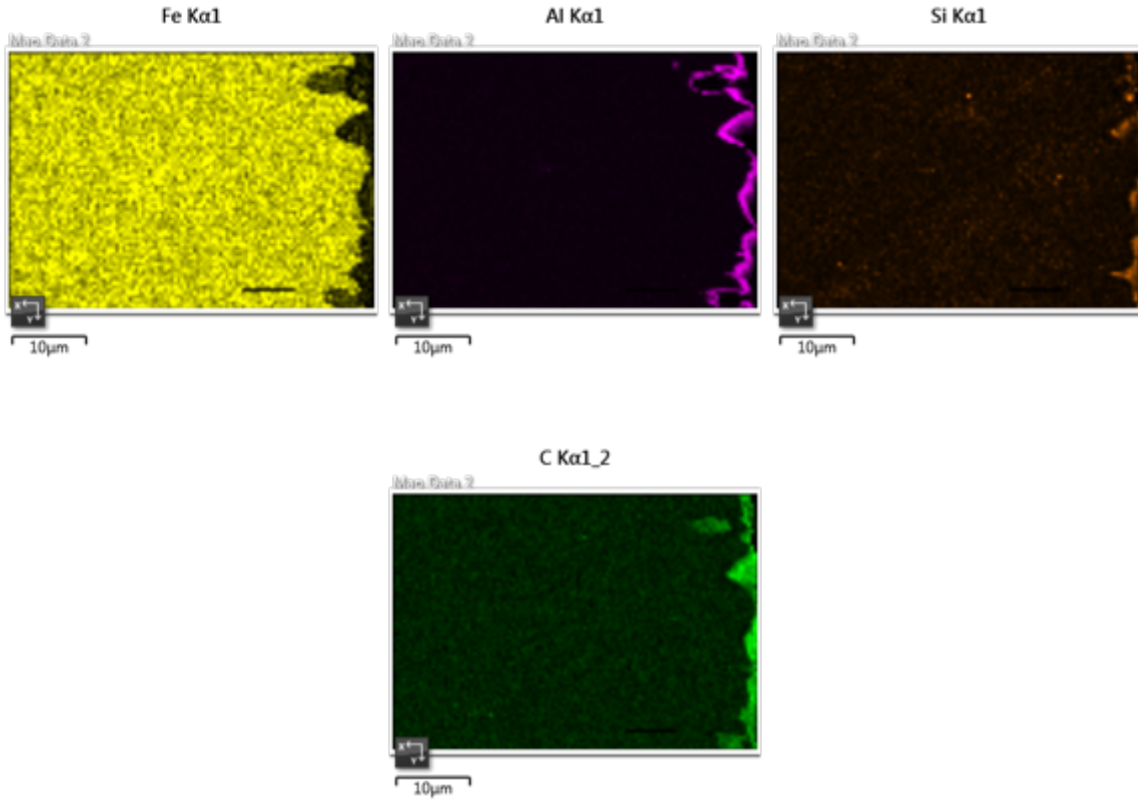
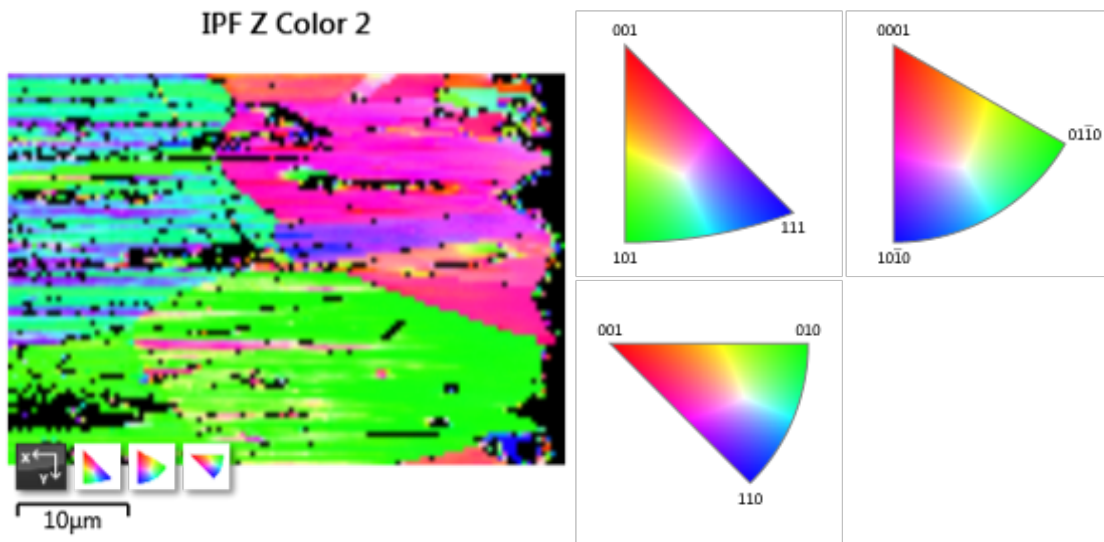


Figure 160: EDS mapping of RA602CA exposed for 12months



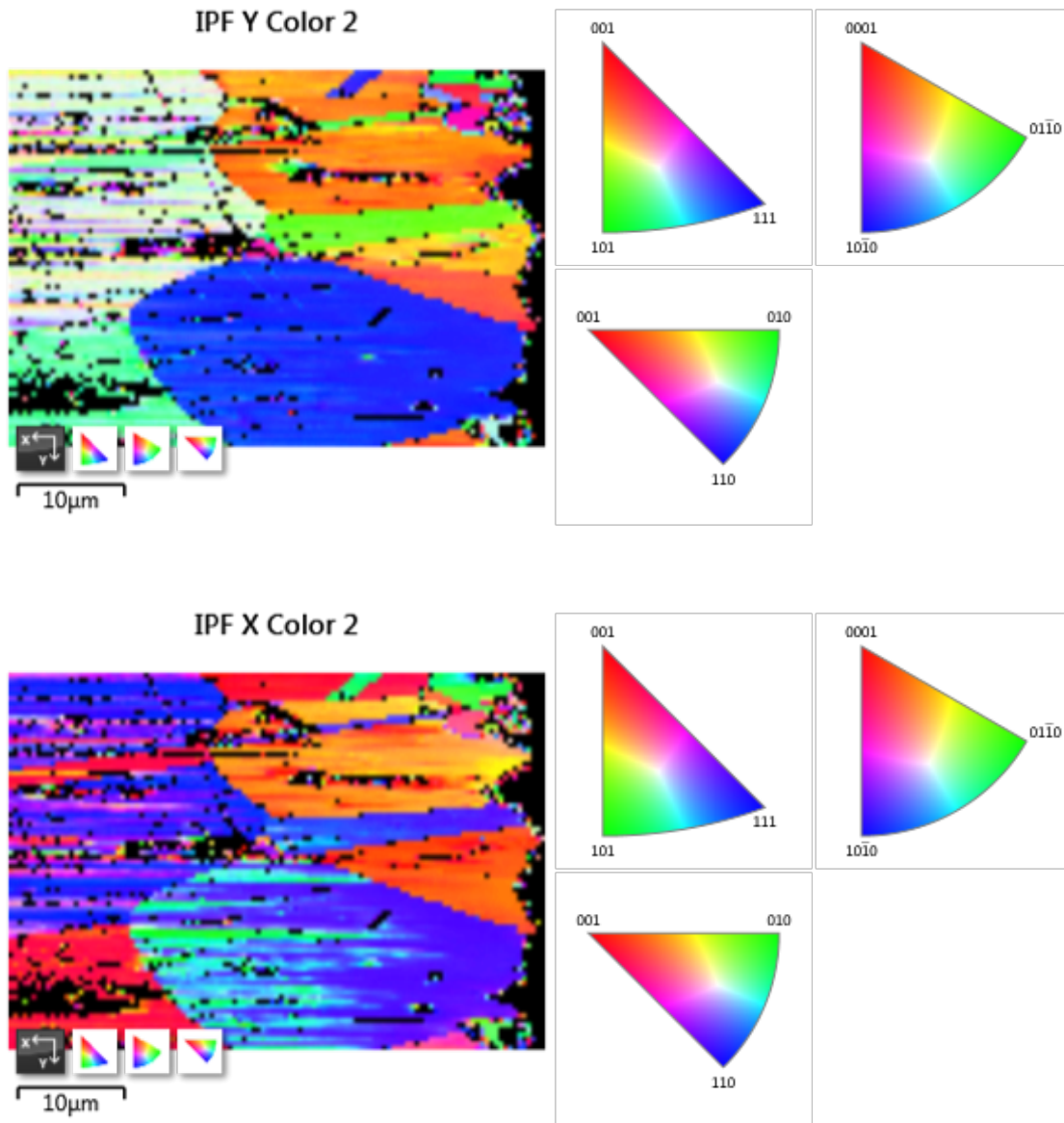


Figure 161: EBSD orientation of RA602CA exposed for 12 months

Phase Color 2

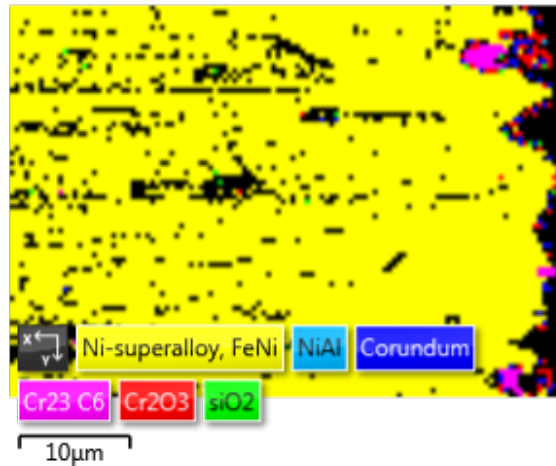


Figure 162: EBSD phase identification of RA602CA exposed for 12 months

EBSD analysis was conducted on RA602CA exposed for 12 months in gas carburization furnace. Cr_2O_3 , SiO_2 and Al_2O_3 oxides were identified on the surface as presented in Figure 162. The thickness of oxides was about $1\mu m$ on the surface as presented in Figure 161. The orientation images of RA602CA after exposure demonstrated the grain size as shown in

Figure 163. EDS mapping shows that $Cr_{23}C_6$ precipitated beneath the oxides layer. Sample has been exposed for 12 months, carbon diffuse through the defects of oxides to form $Cr_{23}C_6$ precipitates. The matrix of RA602CA exposed for 18 months is austenite.

The weight of each sample were measured by high accuracy electronic scales. After exposure in the carburizing batch furnace, the weight gains was measured again. Before each measurement, samples were ultrasonically cleaned by ethanol. The typical error range is within $\pm 0.005g$. Surface areas were also calculated for RA 330, INCONEL alloy 625, RA 602CA, individually. After 24 months service in the carburizing batch furnace, the weight gain per area were measured and the results are listed below.

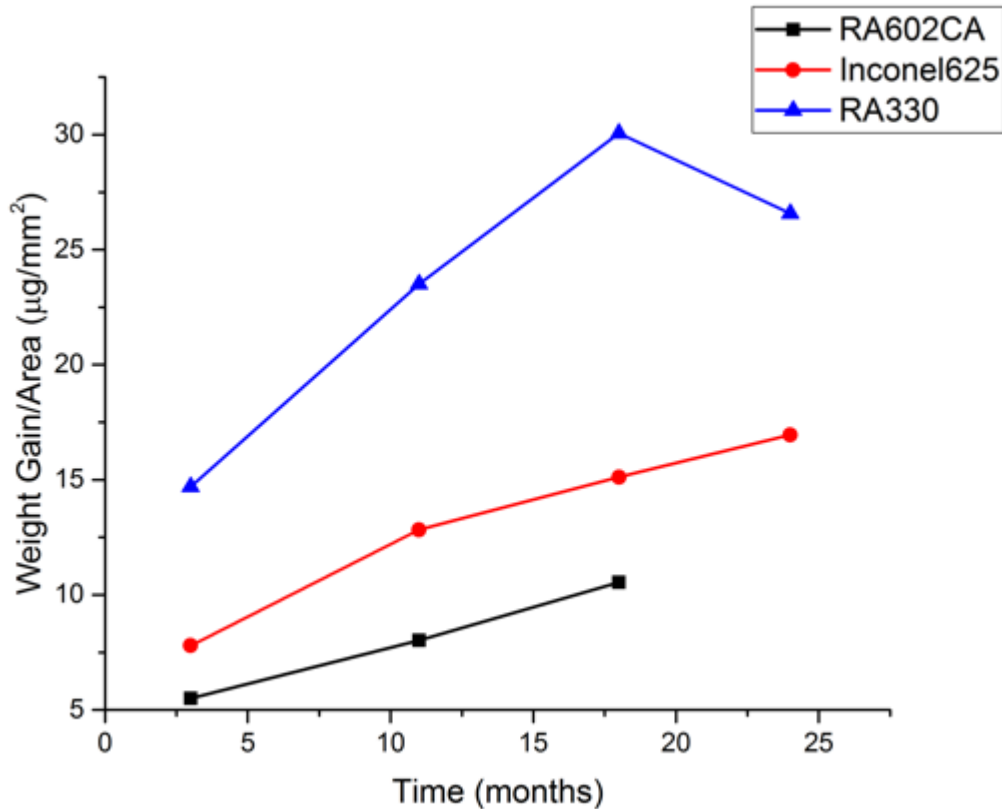


Table 30. Weight gain per area as a function of time for exposed RA602CA

As presented in *Table 30*, the weight gain is comprised of both oxidation and carburization. For alloys that have a reduced weight gain may be due to spalling of the oxides.

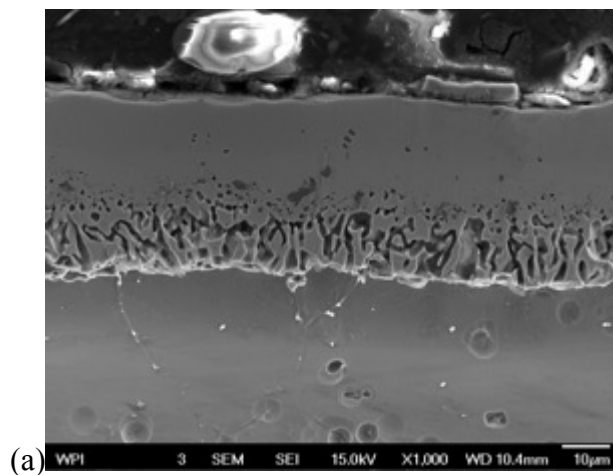
The alloys have been exposed in the carburization furnace for 24 months. Carbon continually diffuses through the oxide layer into the alloys substrate. Therefore, weight gain per area as a function of time shows that weight gain increased for RA330, Inconel625 and RA602CA during the exposure as the expose time increases.

According to *Table 30*, weight gain per area increases as a function of time increases. The blue triangle mark line represents the weight gain for RA330, it was found that RA330 lost weight after 24 months exposure compare to 18 months. That was because of decomposition of Cr_2O_3 layer. It was found that the weight gain per area for the RA602CA was uniformly less than the RA330 and Inconel 625 alloys. Besides, less chromium carbides were found at matrix of RA602CA compare to RA330. The reason for relatively better corrosion resistance for RA602CA was because of

oxides layer on the surface were combined of Cr_2O_3 , SiO_2 and Al_2O_3 . Due to the low solubility of carbon in SiO_2 and Al_2O_3 , carbon could not diffuse into the matrix of RA602CA during the carburizing. RA602CA has the best corrosion resistance amount the selected alloys in this project. The combination of Cr_2O_3 , SiO_2 and Al_2O_3 blocked the carbon uptakes for RA602CA which gave RA602CA an extended service lifetime.

II. Aluminized RA602CA

RA602CA was aluminized to increase the corrosion resistance in the gas carburization atmosphere. Aluminizing introduce extra aluminum into the matrix of RA602CA where $\beta - NiAl$ was form near the surface. An alumina layer less than a micron was formed on the surface of as aluminized sample. However, the thickness of Al_2O_3 layer has increased from submicron to $2\mu m$. Below the oxides layer, $\beta - NiAl$ provides Al content to the alumina layer on the surface. Al_2O_3 formed on top of $\beta - NiAl$ after exposure as presented in *Figure 163*. The thickness of Al_2O_3 for samples Exposed for 1 month is about $2\mu m$ as presented in *Figure 163*. After exposure for longer time, the thickness of Al_2O_3 is about $5\mu m$ as presented in *Figure 163*. The thickness of Al_2O_3 after 24 months exposure is about $10\mu m$. In this case, the thickness of Al_2O_3 increases with time.



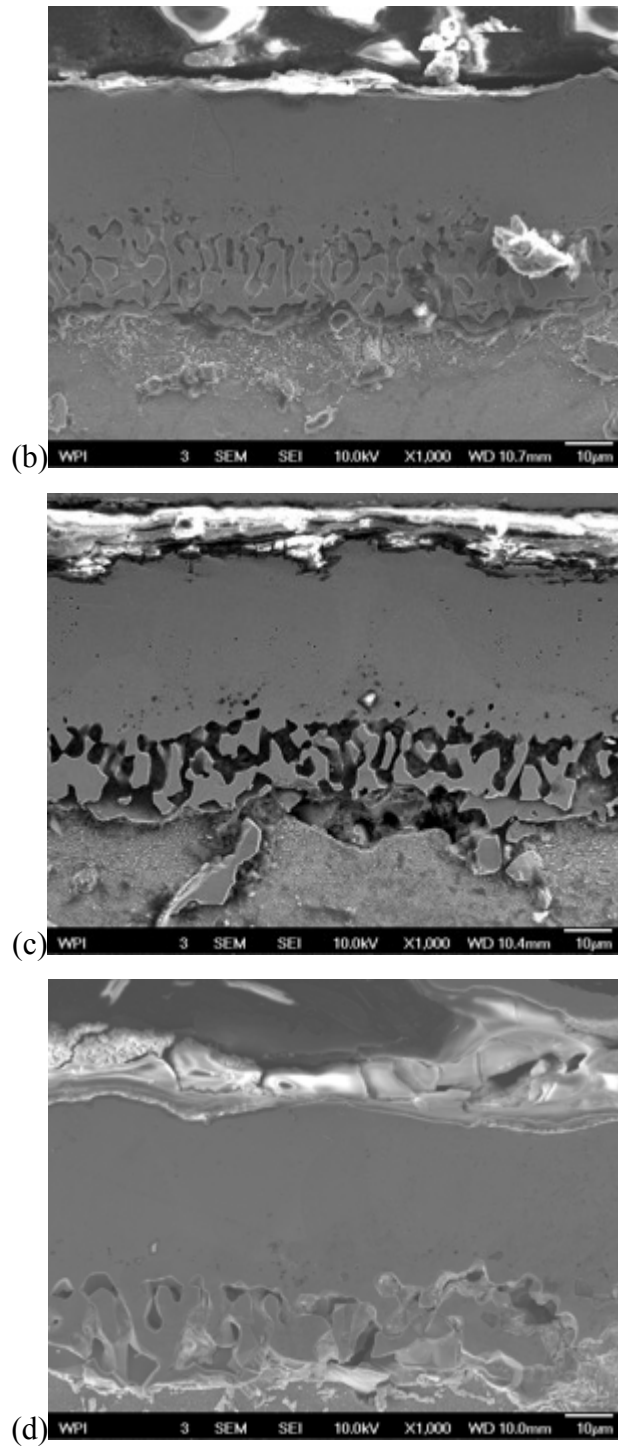


Figure 163: SEM photomicrographs of as fabricated aluminized RA602CA (a), aluminized RA602CA exposed for 3 months (b), aluminized RA602CA exposed for 12 months (c), aluminized RA602CA exposed for 24 months (d)

Figure 163(a) shows that unexposed aluminized RA602CA did not form continuous layer of alumina on the surface of RA602CA. About $2\mu\text{m}$ thickness of alumina layer was found at surface of RA602CA exposed for 3 months as presented in Figure 163. Figure 163 (c) shows the alumina layer on the surface after 12 months exposure, and the thickness of alumina was about $5\mu\text{m}$. $\beta - \text{NiAl}$ phase also formed during aluminizing process which act as the pool of aluminum content for Al_2O_3 layer on the surface.

No chromium carbides were found on the cross section of unexposed RA602CA beneath the $\beta - \text{NiAl}$ layer. However, chromium carbides were identified after 3 months exposure beneath the $\beta - \text{NiAl}$ layer. Carbides were also found at grain boundaries after exposed for 12 months. The carbides were primarily Cr_{23}C_6 due to the carbon up take and subsequent inward diffusion as presented by XRD analysis as shown in Figure 164.

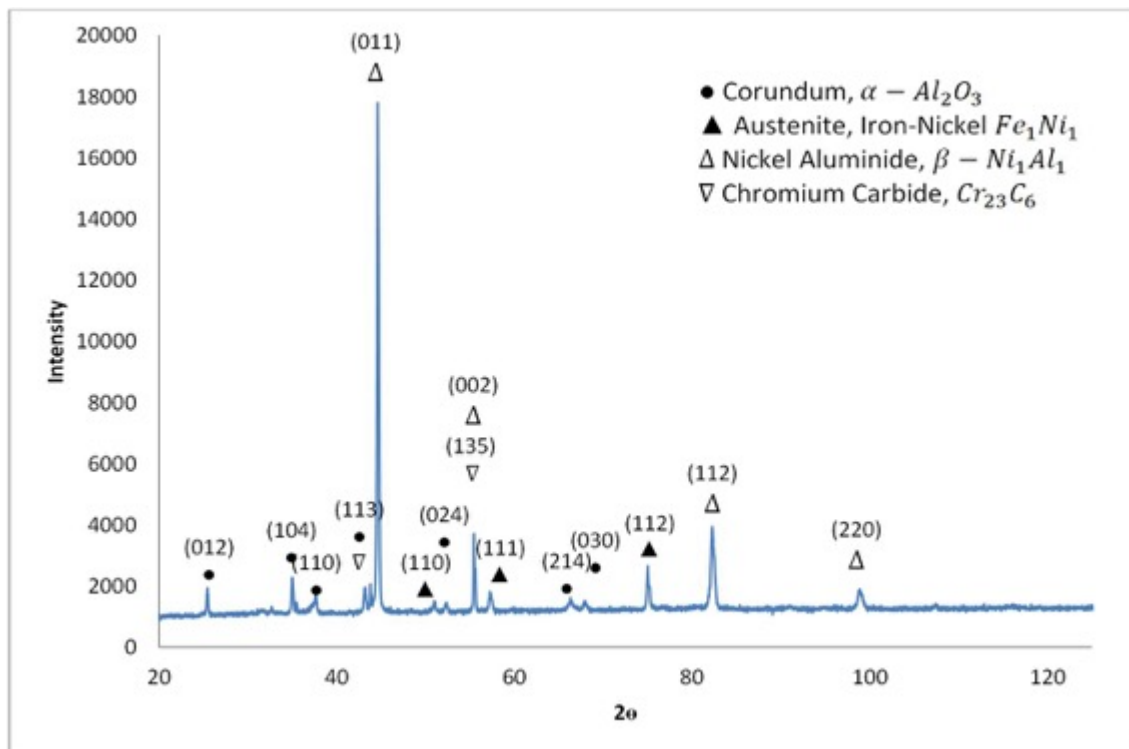
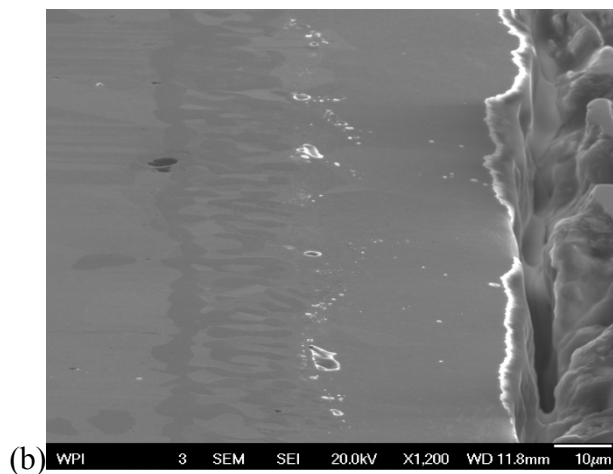
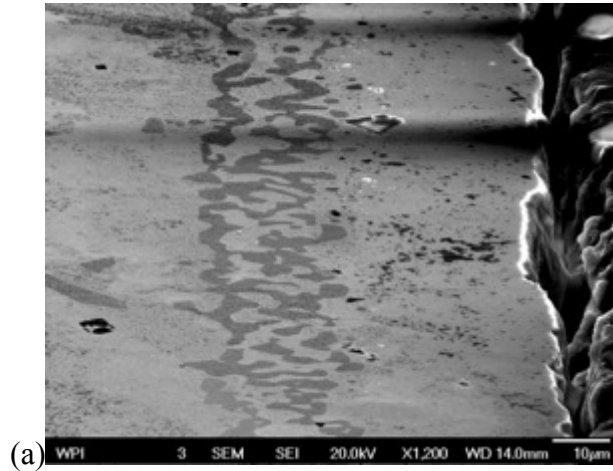


Figure 164. XRD analysis of Aluminized RA602CA exposed for 3 months

According to XRD analysis on *Figure 164*, the premier phase on the surface of aluminized RA602CA is nickel aluminide $\beta - NiAl$. The secondary phase is corundum Al_2O_3 on the surface. And small amount of $Cr_{23}C_6$ were also identified by XRD in *Figure 164*.



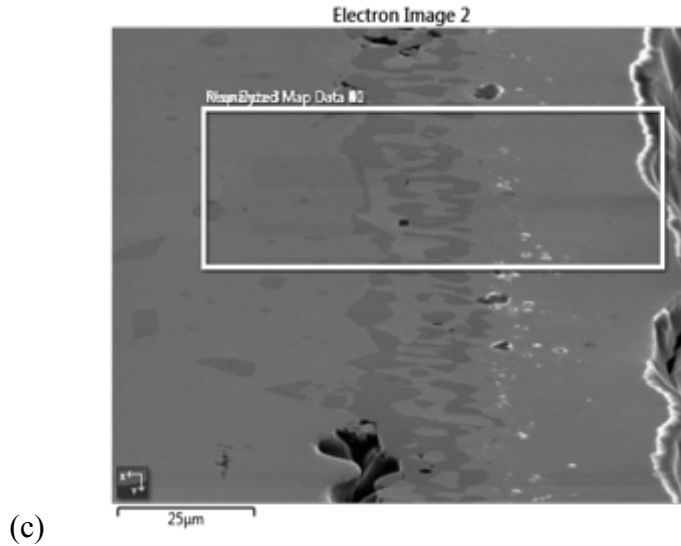


Figure 165: SEM photomicrographs of Aluminized RA602CA exposed for 12 months (a), SEM photomicrographs of Aluminized RA602CA exposed for 18 months (b) and SEM photomicrographs of Aluminized RA602CA exposed for 24 months (c)

$\beta - NiAl$ phase formed during aluminizing process which act as the pool of aluminum content for Al_2O_3 layer on the surface. According to *Figure 165*, the thickness of $\beta - NiAl$ layer remain approximately $30\mu m$ after exposure.

However, more chromium carbides were identified after 18 months exposure than 12 months exposure beneath the $\beta - NiAl$ layer as shown in EBSD *Figure 166* and *Figure 168*.

An EBSD investigation also conducted on the aluminized RA602CA samples. The RA602CA sample was exposed for 12 months in the gas carburization furnace.

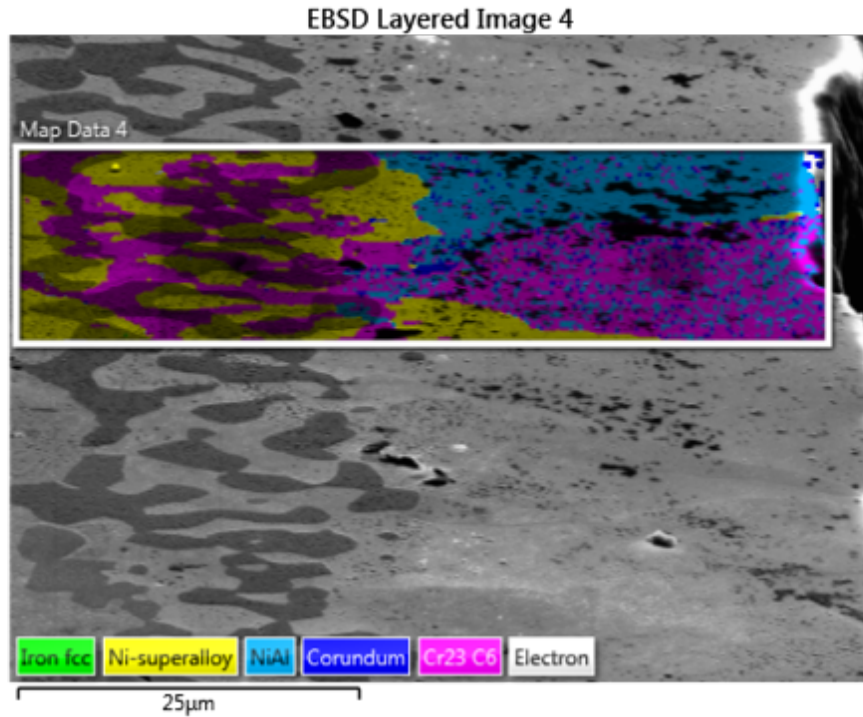


Figure 166: EBSD layered image of Aluminized RA602CA exposed for 12 months at edge

Figure 166 shows that chromium carbides precipitate on the $\beta - NiAl$ layer near the surface. According to EBSD image, chromium carbides clearly growth into the $\beta - NiAl$ layer after long term exposure, and each grains have different amount of carbides. The thickness of $\beta - NiAl$ layer is about $30\mu m$ as shown in *Figure 166*. In the interior, the darker phases are chromium carbides. The lighter grey phases are austenite. At the surface of alloys, corundum Al_2O_3 phases also identified by EBSD.

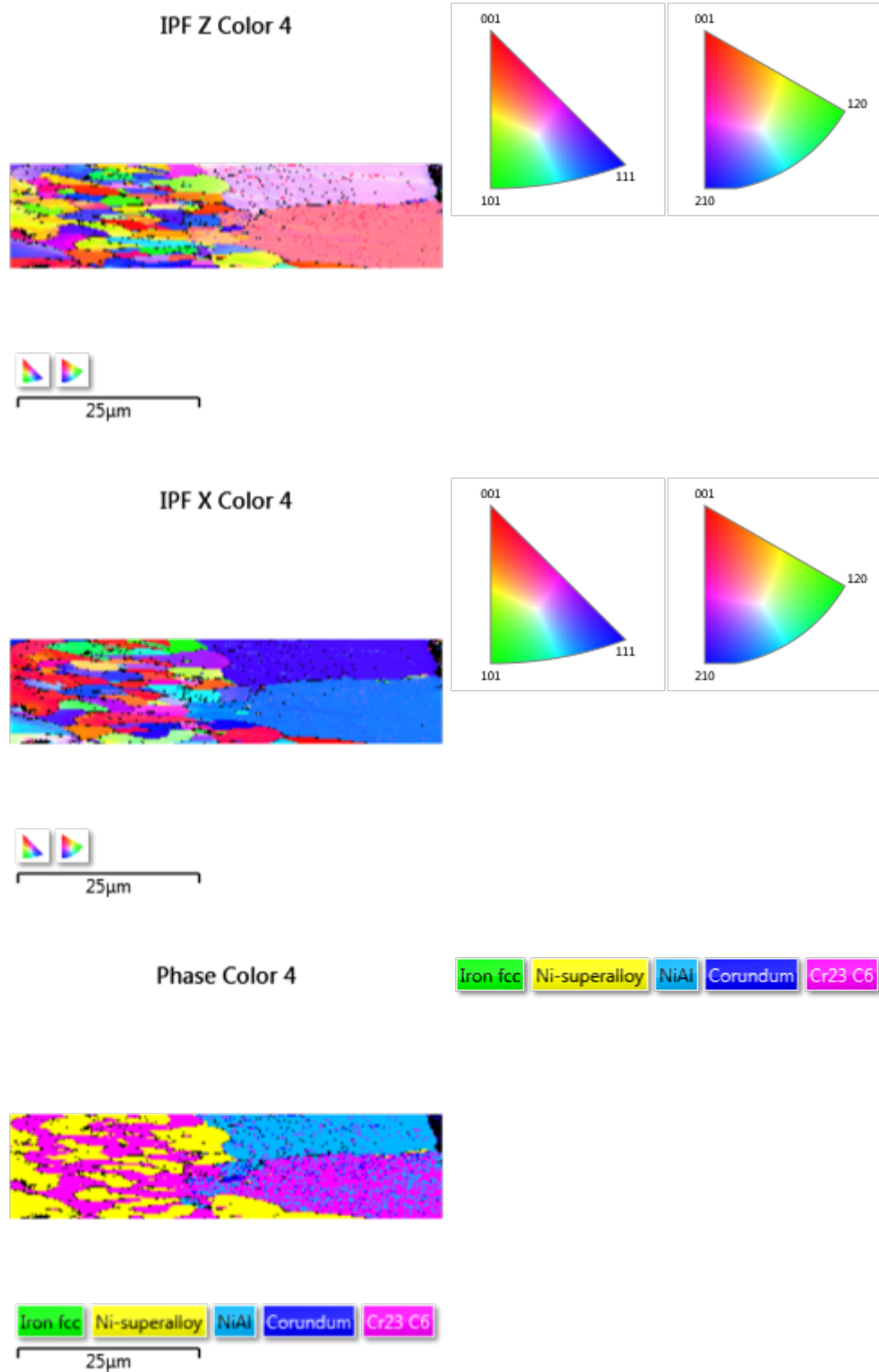


Figure 167: EBSD phase identification of aluminized RA602CA exposed for 12months

Figure 167 shows the phase distribution of sample, $Cr_{23}C_6$ and austenite phases were shown on the left side of picture. Two grain about $25\ \mu m$ in width were shown in Figure 167 near the surface of sample, the upper blue region was $\beta - NiAl$ phases with submicron $Cr_{23}C_6$ precipitates inside the grain. The lower pink region was $Cr_{23}C_6$ phase with small $\beta - NiAl$ inside the carbides as presented in Figure 167.

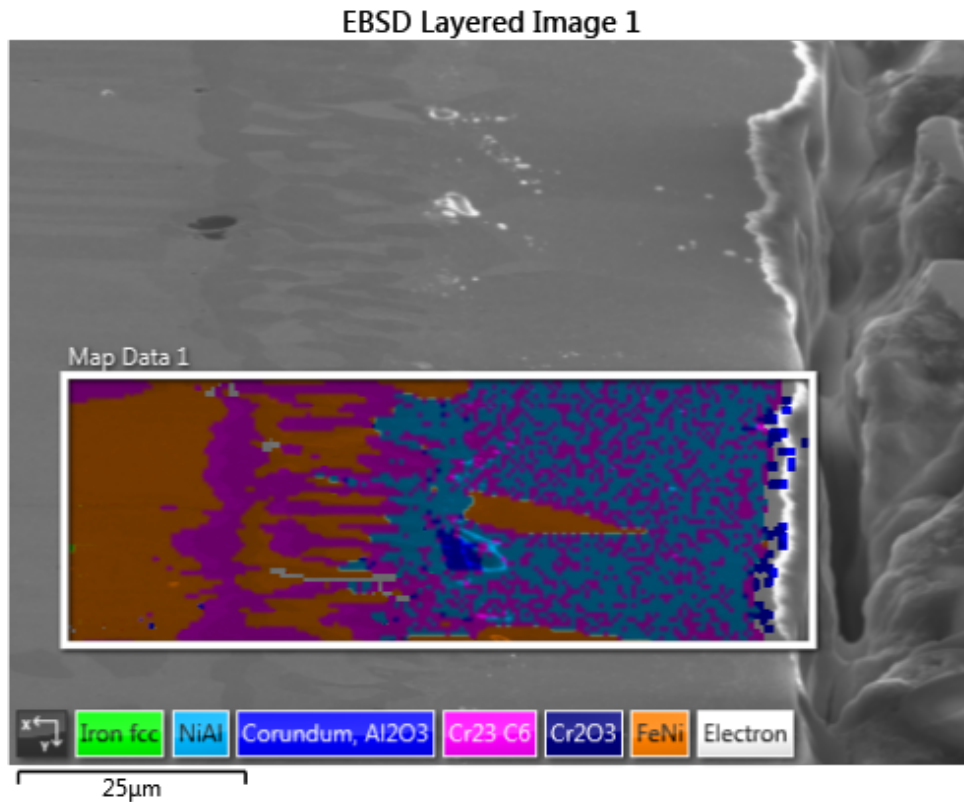


Figure 168: EBSD phase identification of aluminized RA602CA exposed for 18 months

EBSD phase images clearly shows a layer of Al_2O_3 on the surface of aluminized RA602CA exposed for 18 months. Beneath the $3\ \mu m$ alumina layer, $\beta - NiAl$ phase as well as $Cr_{23}C_6$ precipitates were identified near the surface of sample. Compare to aluminized RA602CA exposed for 12 months in Figure 166, there was only single grain was identified by EBSD. Chromium carbides precipitated at the $\beta - NiAl$ region, no grain that primarily occupied by $Cr_{23}C_6$ was found in cross-section EBSD phase identification as seen in Figure 167. The blue color in Figure 167 represented $\beta - NiAl$ phase, pink color represented $Cr_{23}C_6$, and orange color stands for austenite in the matrix. Notably, a large grain of austenite phase was identified in the

$\beta - NiAl$ region after aluminized RA602CA exposed for 18 months. According to EBSD analysis of aluminized RA602CA in *Figure 170*, the $\beta - NiAl$ region no longer exist after sample exposed for 24 months. Al content in $\beta - NiAl$ diffuse both inward into the matrix and outward to the surface to form Al_2O_3 . In this case, $\beta - NiAl$ phase may transfer to austenite phase due to significant lost of Al.

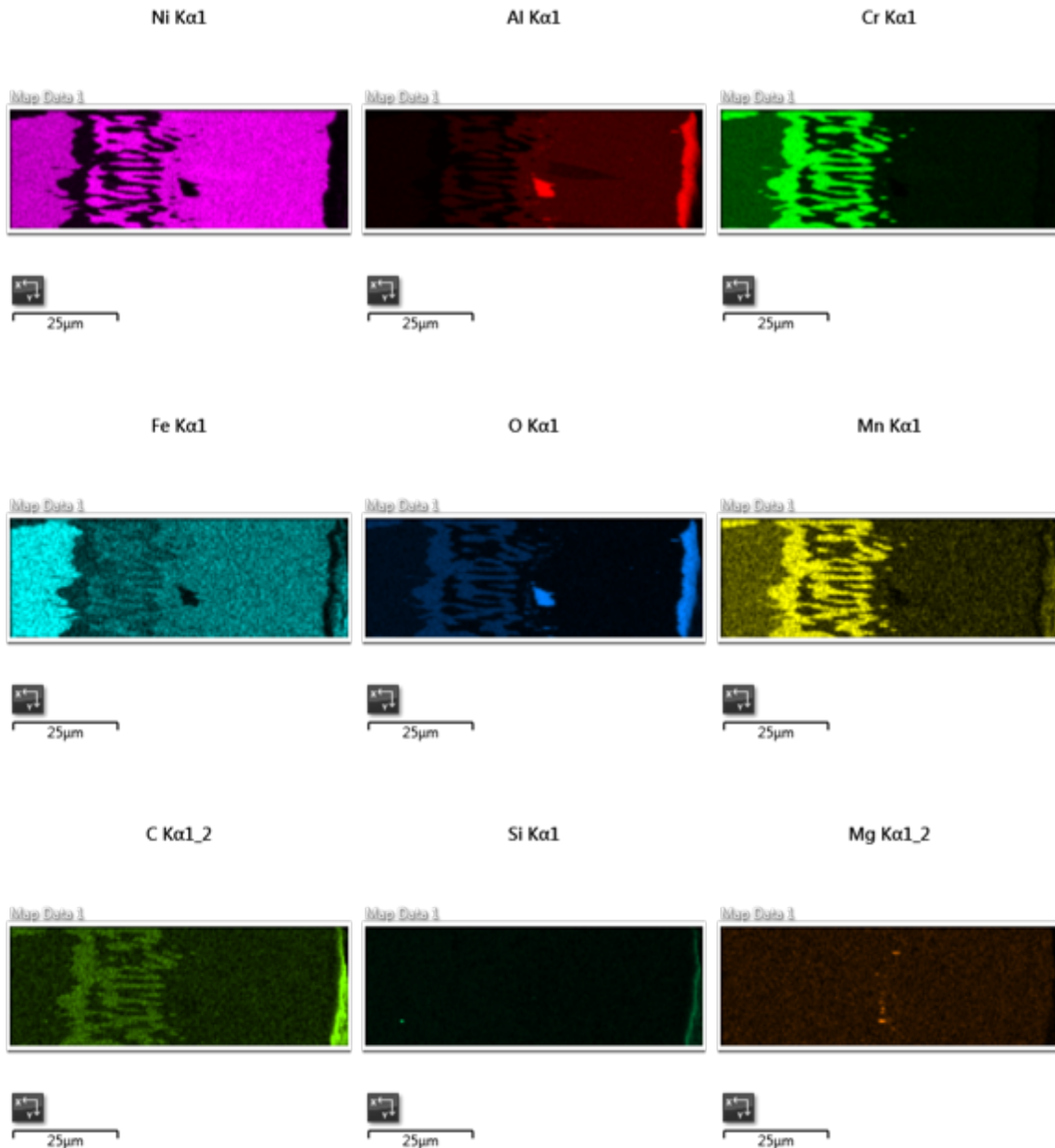
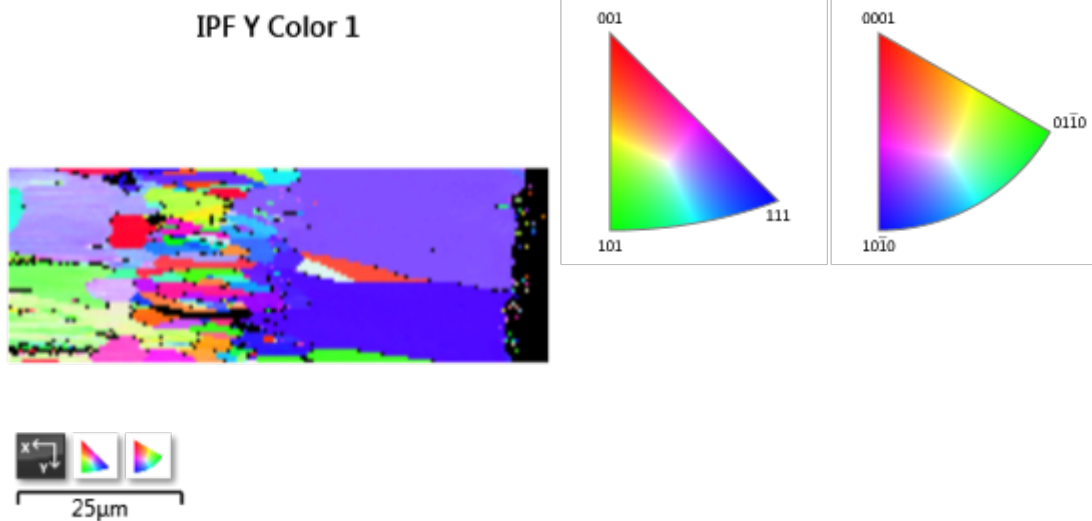
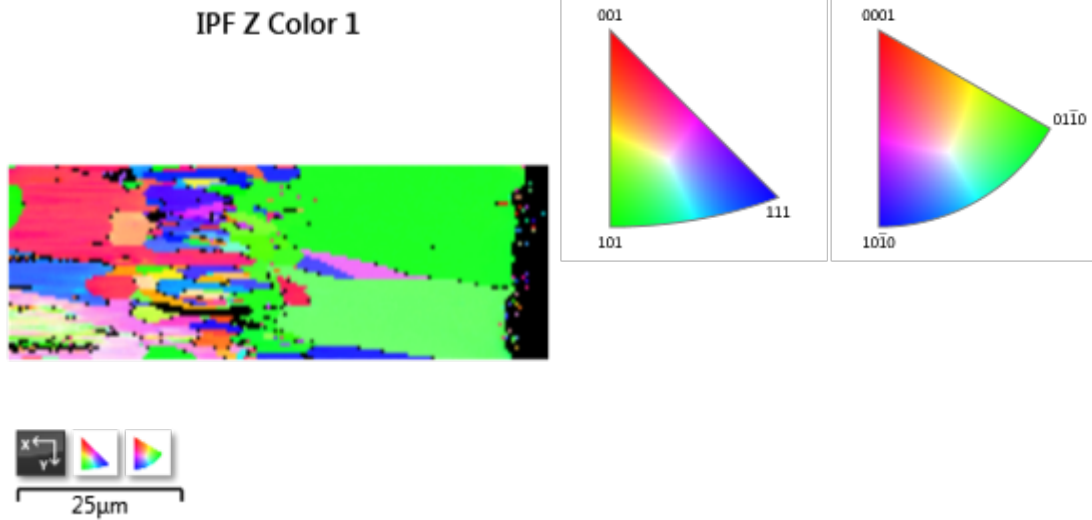


Figure 169: EDS mapping of Aluminized RA602CA exposed for 18 months

EDS mapping indicated that oxide layer on the surface was rich of Al and O. Limited percentage of Fe and Si identified at oxides layer due to the outward diffusion during exposure. The area under the oxides layer was rich of Nickel and Aluminum, which was in good agreement with EBSD analysis, $\beta - NiAl$ was premier phase in this region. Chromium carbides $Cr_{23}C_6$ and $\beta - NiAl$ mixed zone located beneath the $\beta - NiAl$ region. Austenite phase in the matrix of RA602CA.



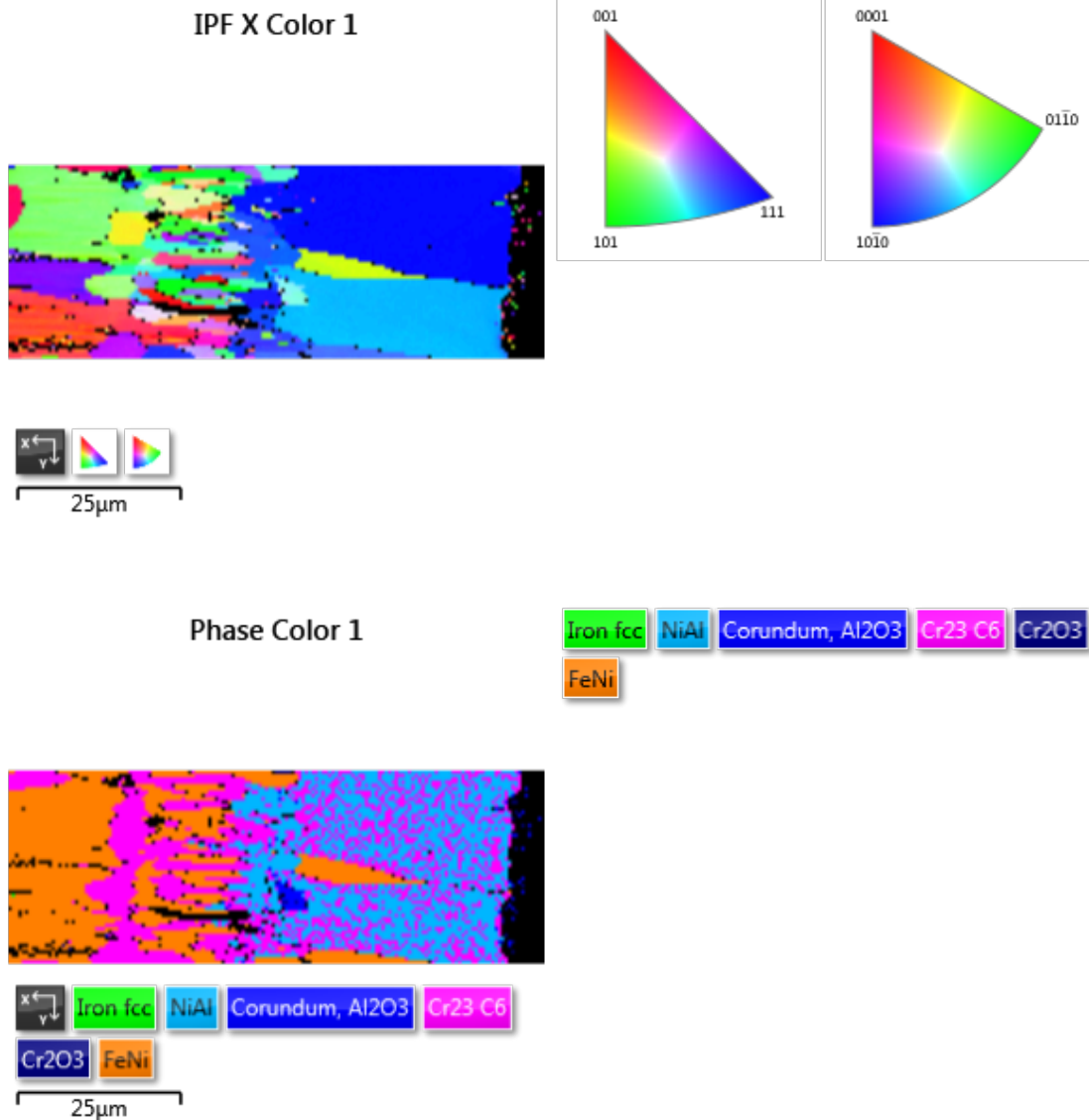


Figure 170: EBSD phase identification of aluminized RA602CA exposed for 18months

Carbides were also found at $\beta - NiAl$ region after exposed for 18 months. The orientation images of XYZ direction shows three grains in $\beta - NiAl$ region, austenite grain was identified between the two larger $\beta - NiAl$ grains as presented in *Figure 170*. The carbides were primarily $Cr_{23}C_6$ due to the carbon uptake. *Figure 170* shows the $Cr_{23}C_6$ near the alumina layer on the surface after 18 months exposure, and the thickness of $Cr_{23}C_6$ and $\beta - NiAl$ mixed zone was about $30 \mu m$ from the surface.

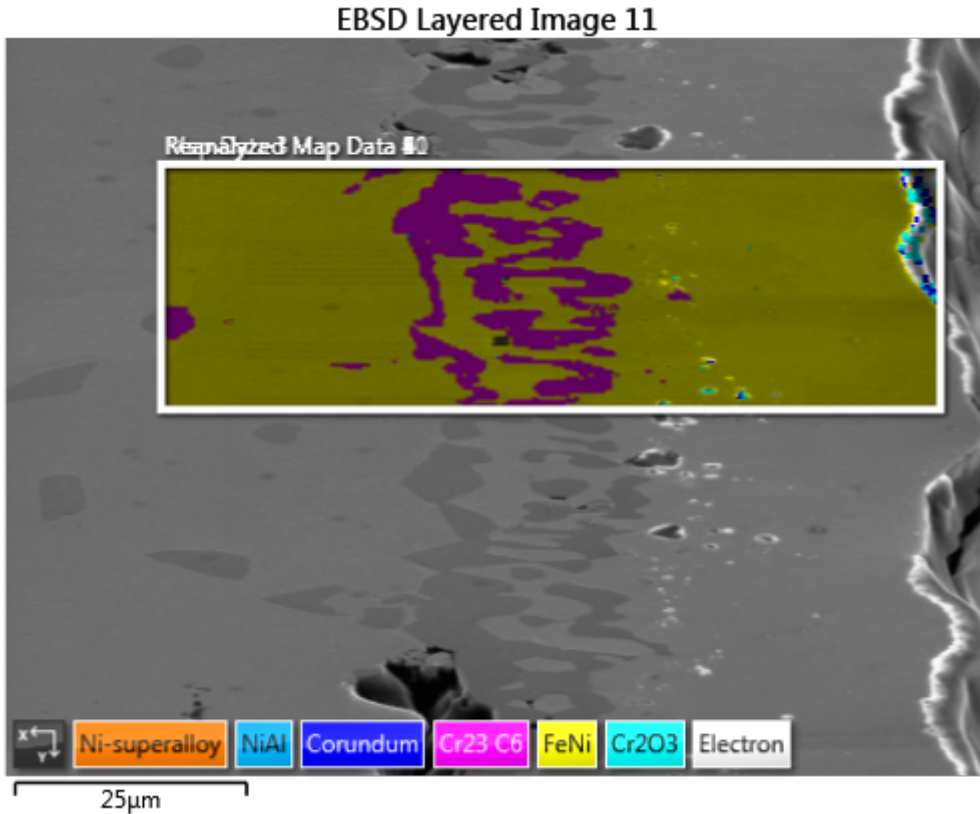


Figure 171: EBSD phase identification of aluminized RA602CA exposed for 24 months

An EBSD analysis also conducted on Aluminized RA602CA after 24 months exposure in gas carburization furnaces. In *Figure 171*, EBSD image clearly shows that nickel aluminide phases have already consumed after 2 years exposure. According to EBSD analysis, no $\beta - Ni_1Al_1$, $NiAl_3$ or Ni_3Al were identified at the cross section of aluminized RA602CA exposed for 2 years. On the left side of *Figure 172*, the thickness of $Cr_{23}C_6$ is about $10 \mu m$ for aluminized RA602CA exposed for 24 months. Aluminum atoms in the $\beta - Ni_1Al_1$ layer could be absorbed by the corundum Al_2O_3 layer on the surface. And there were not enough aluminum to form nickel aluminide phases. Due to the concentration gradient of Fe, Ni, and Al, the Fe continues diffuse outward to the surface and the Al content diffuse inward to the matrix. Therefore, no more $\beta - Ni_1Al_1$ phase precipitated beneath the oxide layer. Instead, FCC structure austenite was identified near the surface.

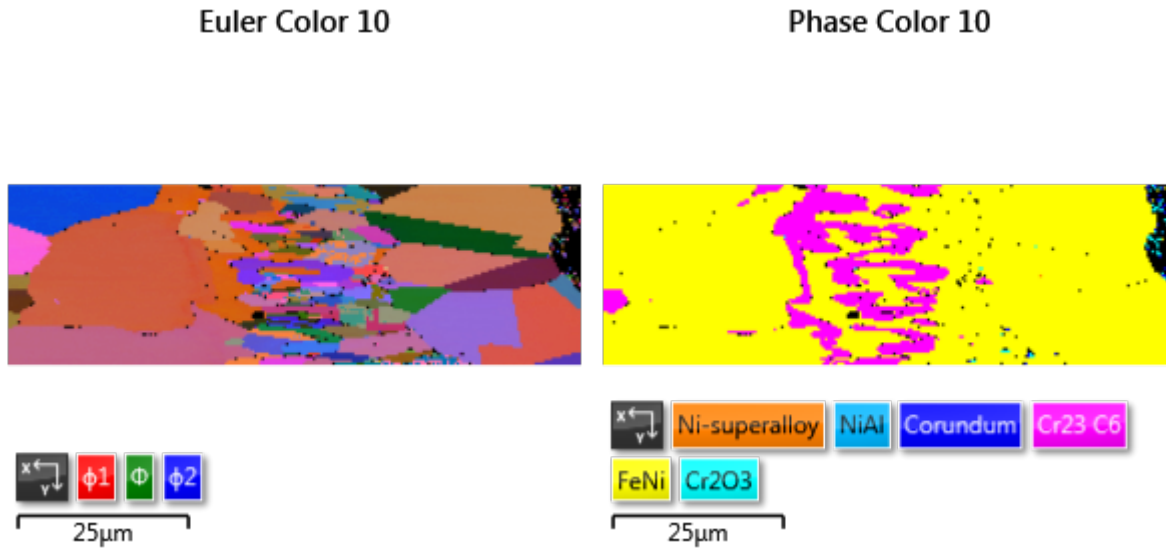


Figure 172: EBSD phase identification of aluminized RA602CA exposed for 24months

In Figure 172, Euler color images shows grain size of chromium carbides $Cr_{23}C_6$ was smaller than austenite. The orientation of chromium carbides was perpendicular to the surface along the diffusion path as shown in Figure 172. For austenite phases, the outer phase at right hand side of Figure 172 near surface shows smaller grain size than inner austenite phases at matrix.

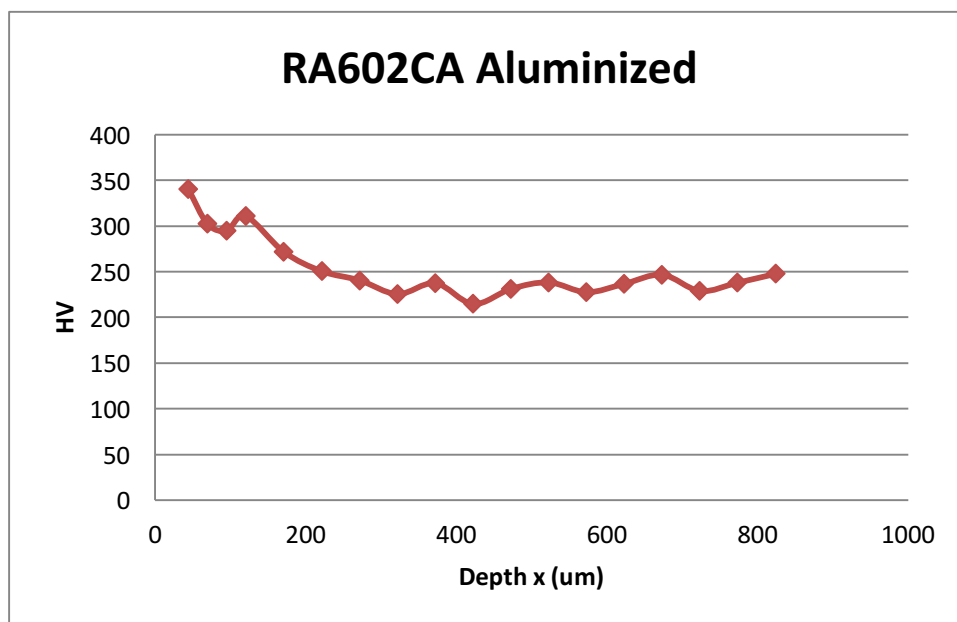


Figure 173. Micro-hardness profile of aluminized RA602CA exposed for 12 months

Within the 200 μm beneath the surface, hardness decreases as deeper from surface. Hardness profile of aluminized RA602CA in *Figure 173* shows Al_2O_3 scale and nickel aluminum intermetallic have relative higher hardness than austenite matrix.

Continuous $\alpha - \text{Al}_2\text{O}_3$ layer on the surface of aluminized RA602CA alloys was maintained after 24 months exposure in gas carburization furnace. $\beta - \text{NiAl}$ layer is important for maintaining effective protection for aluminized alloys or alloys that contain high aluminum content. The $\beta - \text{NiAl}$ layer was consumed after 24 months exposure. Cr_{23}C_6 precipitated at the $\beta - \text{NiAl}$ region due to the carbon uptake. However, the austenite phase in the matrix was not change after 24 months exposure.

The alloys were exposed in the carburization furnace for 24 months. Carbon continually diffuses through the oxide layer into the alloys substrate.

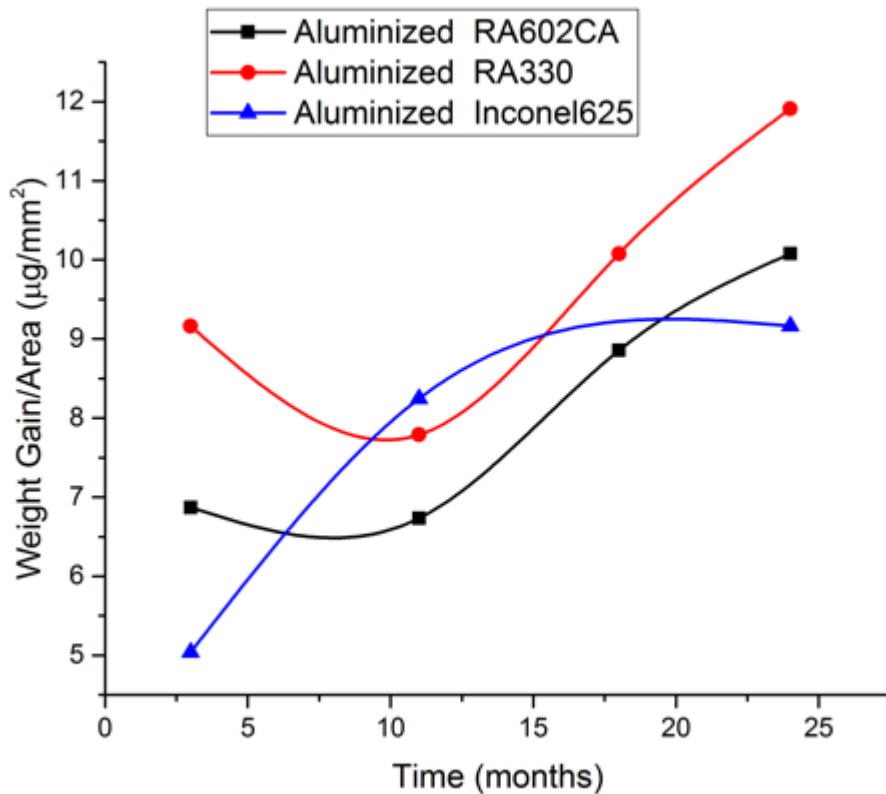


Table 31: Weight gain per area as a function of time for aluminized sample

According to *Table 31*, weight gain per area increases as a function of time. The black line with round mark represents the weight gain for RA602CA, it was found that RA602CA lost weight at first 12 months exposure. That was because of decomposition of oxide layer.

Conclusion

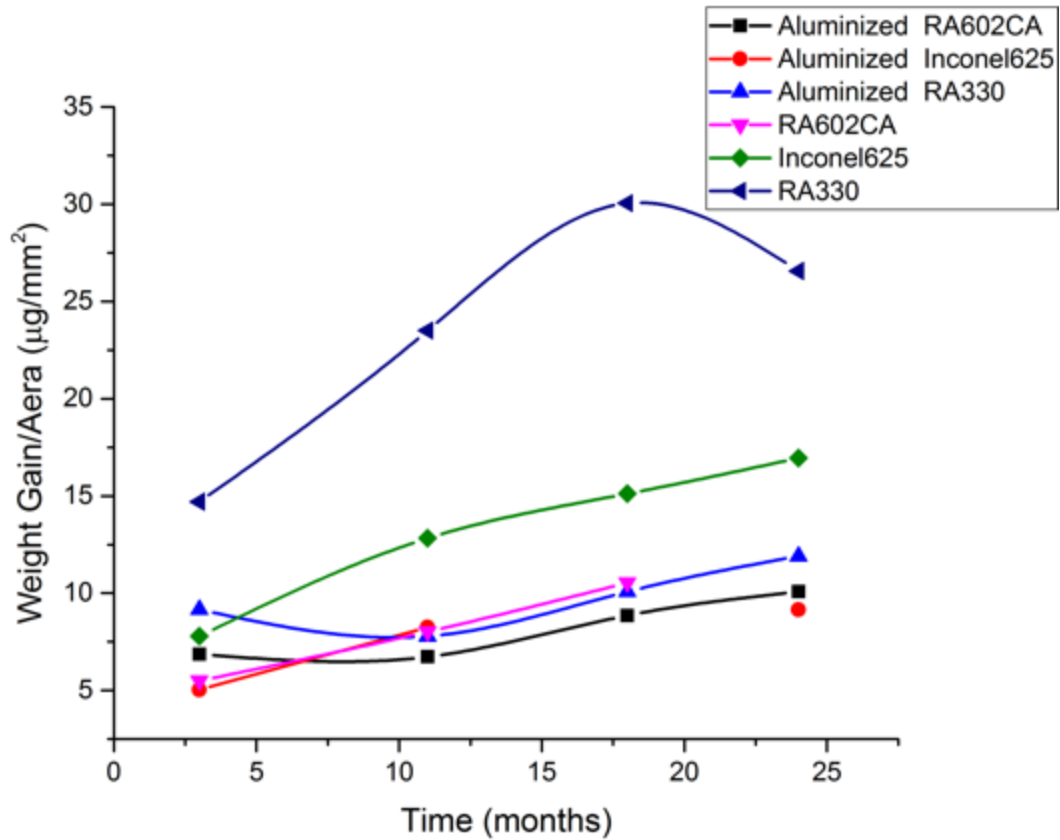


Table 32: *Weight gain per area as a function of time*

According our weight gain analysis, aluminized samples have lower weight gain per area as seen in Table 32. The alumina Al_2O_3 layers coated samples have less weight gain per area than uncoated samples, which means the weight gain for the aluminized alloys was uniformly less than the as-fabricated alloys. After aluminizing process, the anti-corrosion properties of RA602CA samples increased significantly.

Acknowledgements

This work was supported by Center for Heat-treating Excellence. The authors also want to acknowledge the kindly help offered by Dr. Craig Zimmerman from Bluewater Thermal Solution, and Marc Glasser from Rolled Alloys.

References

[1]. Marc Glasser, “RA602CA: [An Alloy for the Highest Temperature Processes](#)”, 28th ASM Heat Treating Society Conference, 2015

[2]. Rolled Alloys, RA602CA Data Sheet, Bulletin No. 1602USe 02/12

6. Conclusion

In this thesis, the performance of RA330, RA602CA, and Inconel 625 alloys in an industrial carburizing furnace were investigated.

These alloys were exposed in both the as fabricated and aluminized condition for times up to two years. Failure analysis were conducted on exposed alloys. For high chromium containing alloys like RA330, a protective Cr_2O_3 and SiO_2 layer was formed as mentioned above. Due to inhomogeneous oxidation, chromium oxide contains numerous pores and defects. Furthermore, due to disintegration of the chromium oxide protective layer, carbon diffuses into alloy forming chromium carbides. The main reason for failure is due to the excessive carburization that leads to formation of $M_{23}C_6$ and M_7C_3 carbides in the grain boundaries, and subsequent cracking because of embrittlement of carbides. In this case, the key to suppressing metal dusting is to stop the dissociation of the carbon source or subsequent carbon diffusion into the susceptible materials

The test samples were exposed to 0.7%C carburizing atmosphere at approximately 900°C for 3 months, 6months, 12months, 18 months and 24 months. In this paper the microstructural development of both aluminized and unaluminized alloys during the prolonged exposure in the carburizing environment were presented and discussed. It was found that the weight gain for the aluminized alloys was uniformly less than the as-fabricated alloys. Continuous $\alpha - Al_2O_3$ layer on the surface of aluminized RA330 and RA602CA alloys was maintained after 24 months exposure in gas carburization furnace. This alumina resulted is a reduced oxidation rate and decreased carbon absorption. $\beta - NiAl$ layer is important for maintaining effective protection for aluminized alloys or alloys that contain high aluminum content.

Aluminizing coating extended the life of alloys in gas carburizing atmosphere. The service lifetime of alloys in furnace and fixtures increased by at least two year because of $\beta - NiAl$ kept continues Al_2O_3 on the surface of alloys that eliminated the inward diffusion of carbon.

High temperature corrosion processes including carburization and oxidation that are two main causes of corrosion for the alloys used in gas carburizing furnaces. High temperature corrosion

resistance is provided by the presence of stable, fine, dense and adhering protective oxides. Pre-oxidation increased the thickness of oxides layer Cr_2O_3 and SiO_2 at surface of RA330. As a result, the pre-oxidation treatment enhanced the corrosion resistance of RA330 in gas carburizing furnaces.

7. Future work

- Follow up the performance of the aluminized racking poles that exposed in vacuum carburizing furnace (periodically take out of furnace and measure, sample, analyze)
 - a) *No metal dusting or excessive carburization was identified on aluminized racking poles after 7 months exposure in gas carburizing furnace. Longer exposure was needed.*
- Continue characterization on selected alloys RA330, Inconel 625, RA602CA, 316SS, 304SS, APMT, and RA253MA after exposure.
 - a) *A metallographic analysis using optical microscope, SEM with EDS, XRD, and EBSD was conducted on APMT alloys. It was found that APMT formed a continuous Al_2O_3 layer on the surface and it has the lowest weight gain among all the tested samples.*
 - b) *APMT is found to be resistant to oxidational carburization. APMT was designed with a high Al content that will form Al_2O_3 in oxidizing environments. Most of the other alloys in our work are chromia formers.*
- Continue characterization on Aluminized RA330, Inconel 625, RA602CA, 316SS, 304SS and RA253MA after exposure.
 - a) *Preliminary metallographic analysis indicated that continuous layer of intermetallic Nickel Aluminide on the surface of RA602CA alloys was consumed after 24 months exposure in gas carburization furnace.*
 - b) *Conduct modeling investigation of diffusion process of alloys during the carburizing*
- Bending tests will be conducted on selected samples to characterize the ductility of alloys and coated alloys.

8. Relevant presentations and publications

8.1. Publications

Paper #1: Microstructure and Failure Analysis of Austenitic Fe-Ni alloys and Ni-Cr-Fe alloys for Furnace Alloys and Fixtures (published in *Proc. ASM Heat Treating Society 2015*, 344-351)

Paper #2: Life Extension of Furnace and Fixture Alloys by Surface Engineering in Carburizing Atmospheres (published in *Proc. International Journal of Heat Treatment and Surface Engineering 2016*, 153-160)

Paper #3: The Performance of RA330 and Aluminized RA330 in an Industrial Gas Carburizing Furnace (submitted to *Journal of Surface and Coating Technology*)

Paper #4: Life Extension of High Temperature Structural Alloys RA602CA in Gas Carburizing Atmosphere (submitted to *Journal of Material Science and Engineering A*)

Paper #5: Life Extension of Furnace and Fixture Alloys by Aluminizing in Vacuum Carburizing Atmospheres (submitted to *Journal of Material Processing Technology*)

8.2. Presentation

[1]. A Wang, RD Sisson, Life Extension of Furnace and Fixture Alloys by Surface Engineering in Carburizing Atmospheres, International Federation of Heat Treatment and Surface Engineering 2016, Proceedings of the 23rd IFHTSE Congress

[2]. A Wang, RD Sisson, Microstructure and Failure Analysis of Austenitic Fe-Ni alloys and Ni-Cr-Fe alloys for furnace Alloys and Fixtures, An Alloy for the Highest Temperature Processes”, 28th ASM Heat Treating Society Conference, 2015

[3]. A Wang, RD Sisson, Life Extension of High Temperature Structural Alloys by Surface Engineering in Carburizing Atmospheres, *Materials Science & Technology* 2016, 2016

[4]. A Wang, RD Sisson, A Microstructural Study of RA330 and Aluminized RA330 in a Gas Carburizing Furnace, *Materials Science & Technology* 2016, 2016

8.3. List of future publications

- [1]. A Wang, RD Sisson, Microstructure and Failure Analysis of Austenitic Ni based alloys and Ni-Cr-Fe alloys for High Temperature Structural Alloys in Gas/Vacuum carburization furnace
- [2]. A Wang, RD Sisson, Life Extension of Furnace and Fixture Alloys by aluminizing in Vacuum Carburizing Atmospheres
- [3]. A Wang, RD Sisson, Life Extension of Furnace and Fixture Alloys by aluminizing in Gas Carburizing Atmospheres
- [4]. A Wang, RD Sisson, An Microstructural Development of RA330 and Aluminized RA330 in a Gas Carburizing Furnace
- [5]. A Wang, M Glasser, RD Sisson, An Microstructural Development of RA602CA and Aluminized RA602CA in a Gas Carburizing Furnace
- [6]. A Wang, H Yu, RD Sisson, An EBSD Investigation on RA330 and Aluminized RA330 in a Gas Carburizing Furnace